

RECENT ADVANCES in ELECTRICAL ENGINEERING and COMPUTER SCIENCE

**Proceedings of the 2014 International Conference on Circuits, Systems
and Signal Processing (CSSP '14)**

**Proceedings of the 2014 International Conference on Communications
and Computers (CC '14)**

**Saint Petersburg State Polytechnic University
Saint Petersburg, Russia
September 23-25, 2014**



RECENT ADVANCES in ELECTRICAL ENGINEERING and COMPUTER SCIENCE

**Proceedings of the 2014 International Conference on Circuits, Systems
and Signal Processing (CSSP '14)**

**Proceedings of the 2014 International Conference on Communications
and Computers (CC '14)**

**Saint Petersburg State Polytechnic University
Saint Petersburg, Russia
September 23-25, 2014**

Copyright © 2014, by the editors

All the copyright of the present book belongs to the editors. All rights reserved. No part of this publication may be reproduced, stored in a retrieval system, or transmitted in any form or by any means, electronic, mechanical, photocopying, recording, or otherwise, without the prior written permission of the editors.

All papers of the present volume were peer reviewed by no less than two independent reviewers. Acceptance was granted when both reviewers' recommendations were positive.

Series: Recent Advances in Electrical Engineering Series | 39

ISSN: 1790-5117

ISBN: 978-1-61804-249-1

RECENT ADVANCES in ELECTRICAL ENGINEERING and COMPUTER SCIENCE

**Proceedings of the 2014 International Conference on Circuits, Systems
and Signal Processing (CSSP '14)**

**Proceedings of the 2014 International Conference on Communications
and Computers (CC '14)**

**Saint Petersburg State Polytechnic University
Saint Petersburg, Russia
September 23-25, 2014**

Organizing Committee

Editors:

Prof. Yuri B. Senichenkov, St. Petersburg State Politechnical University, Saint Petersburg, Russia

Prof. V. Korablev, St. Petersburg State Politechnical University, Saint Petersburg, Russia

Prof. Klimis Ntalianis, Technological Educational Institute of Athens, Greece

Prof. Kleanthis Psarris, The City University of New York, USA

Prof. Pierre Borne, Ecole Centrale de Lille, France

Prof. Yuriy S. Shmaliy, The University of Guanajuato, Mexico

Senior Program Chair

Professor Imre Rudas,
Obuda University, Budapest,
Hungary

Program Chairs

Prof. Yuri B. Senichenkov,
St. Petersburg State Politechnical University,
Saint Petersburg, Russia

Prof. Constantin Udriste,
University Politehnica of Bucharest,
Bucharest
Romania

Professor Leon Chua,
IEEE Fellow,
University of Berkeley, USA

Tutorials Chair

Prof. Yury A. Rossikhin,
Voronezh State University of
Architecture and Civil Engineering,
Voronezh, Russia

Special Session Chair

Prof. Yuri B. Senichenkov,
St. Petersburg State Politechnical
University,
Saint Petersburg, Russia

Workshops Chair

Prof. Sehie Park,
The National Academy of Sciences,
Republic of Korea

Local Organizing Chair

Prof. Vadim Korablev,
St. Petersburg State Politechnical University,
Saint Petersburg, Russia

Publication Chair

Prof. Marina Shitikova,
Voronezh State University of Architecture and
Civil Engineering, Voronezh, Russia

Publicity Committee

Prof. Vjacheslav Yurko,
Saratov State University,
Astrakhanskaya, Russia
Professor Theodore B. Trafalis,
University of Oklahoma, USA

International Liaisons

Professor Jinhua Lu, IEEE Fellow
Institute of Systems Science
Academy of Mathematics and Systems Science
Chinese Academy of Sciences
Beijing 100190, P. R. China

Prof. Olga Martin
Applied Sciences Faculty
Politehnica University of Bucharest
Romania

Prof. H. M. Srivastava
University of Victoria
Victoria, British Columbia V8W 3R4
Canada

Prof. Eduardo Mario Dias
Electrical Energy and Automation
Engineering Department
Escola Politecnica da Universidade de Sao Paulo
Brazil

Steering Committee

Prof. Dr. H. M. Srivastava, University of Victoria, Canada
Prof. Stefan Siegmund, Technische Universitaet Dresden, Germany
Prof. Waler Caseri, ETH, Zurich, Switzerland
Prof. Narcisa C. Apreutesei, Technical University of Iasi, Iasi, Romania
Prof. Imre Rudas, Obuda University, Budapest, Hungary

Program Committee

Prof. Lotfi Zadeh (IEEE Fellow, University of Berkeley, USA)
Prof. Leon Chua (IEEE Fellow, University of Berkeley, USA)
Prof. Michio Sugeno (RIKEN Brain Science Institute (RIKEN BSI), Japan)
Prof. Dimitri Bertsekas (IEEE Fellow, MIT, USA)
Prof. Demetri Terzopoulos (IEEE Fellow, ACM Fellow, UCLA, USA)
Prof. Georgios B. Giannakis (IEEE Fellow, University of Minnesota, USA)
Prof. George Vachtsevanos (Georgia Institute of Technology, USA)

Prof. Abraham Bers (IEEE Fellow, MIT, USA)
Prof. Brian Barsky (IEEE Fellow, University of Berkeley, USA)
Prof. Aggelos Katsaggelos (IEEE Fellow, Northwestern University, USA)
Prof. Josef Sifakis (Turing Award 2007, CNRS/Verimag, France)
Prof. Hisashi Kobayashi (Princeton University, USA)
Prof. Kinshuk (Fellow IEEE, Massey Univ. New Zeland),
Prof. Leonid Kazovsky (Stanford University, USA)
Prof. Narsingh Deo (IEEE Fellow, ACM Fellow, University of Central Florida, USA)
Prof. Kamisetty Rao (Fellow IEEE, Univ. of Texas at Arlington, USA)
Prof. Anastassios Venetsanopoulos (Fellow IEEE, University of Toronto, Canada)
Prof. Steven Collicott (Purdue University, West Lafayette, IN, USA)
Prof. Nikolaos Paragios (Ecole Centrale Paris, France)
Prof. Nikolaos G. Bourbakis (IEEE Fellow, Wright State University, USA)
Prof. Stamatios Kartalopoulos (IEEE Fellow, University of Oklahoma, USA)
Prof. Irwin Sandberg (IEEE Fellow, University of Texas at Austin, USA),
Prof. Michael Sebek (IEEE Fellow, Czech Technical University in Prague, Czech Republic)
Prof. Hashem Akbari (University of California, Berkeley, USA)
Prof. Yuriy S. Shmaliy, (IEEE Fellow, The University of Guanajuato, Mexico)
Prof. Lei Xu (IEEE Fellow, Chinese University of Hong Kong, Hong Kong)
Prof. Paul E. Dimotakis (California Institute of Technology Pasadena, USA)
Prof. Martin Pelikan (UMSL, USA)
Prof. Patrick Wang (MIT, USA)
Prof. Wasfy B Mikhael (IEEE Fellow, University of Central Florida Orlando, USA)
Prof. Sunil Das (IEEE Fellow, University of Ottawa, Canada)
Prof. Panos Pardalos (University of Florida, USA)
Prof. Nikolaos D. Katopodes (University of Michigan, USA)
Prof. Bimal K. Bose (Life Fellow of IEEE, University of Tennessee, Knoxville, USA)
Prof. Janusz Kacprzyk (IEEE Fellow, Polish Academy of Sciences, Poland)
Prof. Sidney Burrus (IEEE Fellow, Rice University, USA)
Prof. Biswa N. Datta (IEEE Fellow, Northern Illinois University, USA)
Prof. Mihai Putinar (University of California at Santa Barbara, USA)
Prof. Wlodzislaw Duch (Nicolaus Copernicus University, Poland)
Prof. Tadeusz Kaczorek (IEEE Fellow, Warsaw University of Tehcnology, Poland)
Prof. Michael N. Katehakis (Rutgers, The State University of New Jersey, USA)
Prof. Pan Agathoklis (Univ. of Victoria, Canada)
Dr. Subhas C. Misra (Harvard University, USA)
Prof. Martin van den Toorn (Delft University of Technology, The Netherlands)
Prof. Malcolm J. Crocker (Distinguished University Prof., Auburn University, USA)
Prof. Urszula Ledzewicz, Southern Illinois University , USA.
Prof. Dimitri Kazakos, Dean, (Texas Southern University, USA)
Prof. Ronald Yager (Iona College, USA)
Prof. Athanassios Manikas (Imperial College, London, UK)
Prof. Keith L. Clark (Imperial College, London, UK)
Prof. Argyris Varonides (Univ. of Scranton, USA)
Prof. S. Furfari (Direction Generale Energie et Transports, Brussels, EU)
Prof. Constantin Udriste, University Politehnica of Bucharest , ROMANIA
Prof. Patrice Brault (Univ. Paris-sud, France)
Prof. Jim Cunningham (Imperial College London, UK)
Prof. Philippe Ben-Abdallah (Ecole Polytechnique de l'Universite de Nantes, France)
Prof. Ichiro Hagiwara, (Tokyo Institute of Technology, Japan)
Prof. Andris Buikis (Latvian Academy of Science. Latvia)
Prof. Akshai Aggarwal (University of Windsor, Canada)
Prof. George Vachtsevanos (Georgia Institute of Technology, USA)
Prof. Ulrich Albrecht (Auburn University, USA)

Prof. Imre J. Rudas (Obuda University, Hungary)
Prof. Alexey L Sadovskii (IEEE Fellow, Texas A&M University, USA)
Prof. Amedeo Andreotti (University of Naples, Italy)
Prof. Ryszard S. Choras (University of Technology and Life Sciences Bydgoszcz, Poland)
Prof. Remi Leandre (Universite de Bourgogne, Dijon, France)
Prof. Moustapha Diaby (University of Connecticut, USA)
Prof. Brian McCartin (New York University, USA)
Prof. Charles Long (Prof. Emeritus University of Wisconsin, USA)
Prof. Marvin Goldstein (NASA Glenn Research Center, USA)
Prof. Ron Goldman (Rice University, USA)
Prof. Milivoje M. Kostic (Northern Illinois University, USA)
Prof. Helmut Jaberg (University of Technology Graz, Austria)
Prof. Ardeshir Anjomani (The University of Texas at Arlington, USA)
Prof. Heinz Ulbrich (Technical University Munich, Germany)
Prof. Reinhard Leithner (Technical University Braunschweig, Germany)
Prof. Elbrous M. Jafarov (Istanbul Technical University, Turkey)
Prof. M. Ehsani (Texas A&M University, USA)
Prof. Sesh Commuri (University of Oklahoma, USA)
Prof. Nicolas Galanis (Universite de Sherbrooke, Canada)
Prof. S. H. Sohrab (Northwestern University, USA)
Prof. Rui J. P. de Figueiredo (University of California, USA)
Prof. Valeri Mladenov (Technical University of Sofia, Bulgaria)
Prof. Hiroshi Sakaki (Meisei University, Tokyo, Japan)
Prof. Zoran S. Bojkovic (Technical University of Belgrade, Serbia)
Prof. K. D. Klaes, (Head of the EPS Support Science Team in the MET Division at EUMETSAT, France)
Prof. Emira Maljevic (Technical University of Belgrade, Serbia)
Prof. Kazuhiko Tsuda (University of Tsukuba, Tokyo, Japan)
Prof. Milan Stork (University of West Bohemia , Czech Republic)
Prof. C. G. Helmis (University of Athens, Greece)
Prof. Lajos Barna (Budapest University of Technology and Economics, Hungary)
Prof. Nobuoki Mano (Meisei University, Tokyo, Japan)
Prof. Nobuo Nakajima (The University of Electro-Communications, Tokyo, Japan)
Prof. Victor-Emil Neagoe (Polytechnic University of Bucharest, Romania)
Prof. P. Vanderstraeten (Brussels Institute for Environmental Management, Belgium)
Prof. Annaliese Bischoff (University of Massachusetts, Amherst, USA)
Prof. Virgil Tiponut (Politehnica University of Timisoara, Romania)
Prof. Andrei Kolyshkin (Riga Technical University, Latvia)
Prof. Fumiaki Imado (Shinshu University, Japan)
Prof. Sotirios G. Ziavras (New Jersey Institute of Technology, USA)
Prof. Constantin Volosencu (Politehnica University of Timisoara, Romania)
Prof. Marc A. Rosen (University of Ontario Institute of Technology, Canada)
Prof. Thomas M. Gattton (National University, San Diego, USA)
Prof. Leonardo Pagnotta (University of Calabria, Italy)
Prof. Yan Wu (Georgia Southern University, USA)
Prof. Daniel N. Riahi (University of Texas-Pan American, USA)
Prof. Alexander Grebennikov (Autonomous University of Puebla, Mexico)
Prof. Bennie F. L. Ward (Baylor University, TX, USA)
Prof. Guennadi A. Kouzaev (Norwegian University of Science and Technology, Norway)
Prof. Geoff Skinner (The University of Newcastle, Australia)
Prof. Hamido Fujita (Iwate Prefectural University(IPU), Japan)
Prof. Francesco Muzi (University of L'Aquila, Italy)
Prof. Claudio Rossi (University of Siena, Italy)
Prof. Sergey B. Leonov (Joint Institute for High Temperature Russian Academy of Science, Russia)
Prof. Lili He (San Jose State University, USA)

Prof. M. Nasseh Tabrizi (East Carolina University, USA)
Prof. Alaa Eldin Fahmy (University Of Calgary, Canada)
Prof. Gh. Pascovici (University of Koeln, Germany)
Prof. Pier Paolo Delsanto (Politecnico of Torino, Italy)
Prof. Radu Munteanu (Rector of the Technical University of Cluj-Napoca, Romania)
Prof. Ioan Dumitrache (Politehnica University of Bucharest, Romania)
Prof. Miquel Salgot (University of Barcelona, Spain)
Prof. Amaury A. Caballero (Florida International University, USA)
Prof. Maria I. Garcia-Planas (Universitat Politecnica de Catalunya, Spain)
Prof. Petar Popivanov (Bulgarian Academy of Sciences, Bulgaria)
Prof. Alexander Gegov (University of Portsmouth, UK)
Prof. Lin Feng (Nanyang Technological University, Singapore)
Prof. Colin Fyfe (University of the West of Scotland, UK)
Prof. Zhaohui Luo (Univ of London, UK)
Prof. Wolfgang Wenzel (Institute for Nanotechnology, Germany)
Prof. Weilian Su (Naval Postgraduate School, USA)
Prof. Phillip G. Bradford (The University of Alabama, USA)
Prof. Ray Hefferlin (Southern Adventist University, TN, USA)
Prof. Hamid Abachi (Monash University, Australia)
Prof. Karlheinz Spindler (Fachhochschule Wiesbaden, Germany)
Prof. Josef Boercsoek (Universitat Kassel, Germany)
Prof. Eyad H. Abed (University of Maryland, Maryland, USA)
Prof. F. Castanie (TeSA, Toulouse, France)
Prof. Robert K. L. Gay (Nanyang Technological University, Singapore)
Prof. Andrzej Ordys (Kingston University, UK)
Prof. T Bott (The University of Birmingham, UK)
Prof. T.-W. Lee (Arizona State University, AZ, USA)
Prof. Le Yi Wang (Wayne State University, Detroit, USA)
Prof. Oleksander Markovskyy (National Technical University of Ukraine, Ukraine)
Prof. Suresh P. Sethi (University of Texas at Dallas, USA)
Prof. Hartmut Hillmer (University of Kassel, Germany)
Prof. Bram Van Putten (Wageningen University, The Netherlands)
Prof. Alexander Iomin (Technion - Israel Institute of Technology, Israel)
Prof. Roberto San Jose (Technical University of Madrid, Spain)
Prof. Minvydas Ragulskis (Kaunas University of Technology, Lithuania)
Prof. Arun Kulkarni (The University of Texas at Tyler, USA)
Prof. Joydeep Mitra (New Mexico State University, USA)
Prof. S. Y. Chen, (Zhejiang University of Technology, China and University of Hamburg, Germany)
Prof. Duc Nguyen (Old Dominion University, Norfolk, USA)
Prof. Tuan Pham (James Cook University, Townsville, Australia)
Prof. Jiri Klima (Technical Faculty of CZU in Prague, Czech Republic)
Prof. Rossella Cancelliere (University of Torino, Italy)
Prof. Christian Bouquegneau (Faculty Polytechnique de Mons, Belgium)
Prof. Wladyslaw Mielczarski (Technical University of Lodz, Poland)
Prof. Ibrahim Hassan (Concordia University, Montreal, Quebec, Canada)
Prof. James F. Frenzel (University of Idaho, USA)
Prof. Vilem Srovnal, (Technical University of Ostrava, Czech Republic)
Prof. J. M. Giron-Sierra (Universidad Complutense de Madrid, Spain)
Prof. Walter Dosch (University of Luebeck, Germany)
Prof. Rudolf Freund (Vienna University of Technology, Austria)
Prof. Erich Schmidt (Vienna University of Technology, Austria)
Prof. Alessandro Genco (University of Palermo, Italy)
Prof. Martin Lopez Morales (Technical University of Monterey, Mexico)
Prof. Vladimir Damgov (Bulgarian Academy of Sciences, Bulgaria)

Additional Reviewers

Bazil Taha Ahmed	Universidad Autonoma de Madrid, Spain
M. Javed Khan	Tuskegee University, AL, USA
James Vance	The University of Virginia's College at Wise, VA, USA
Minhui Yan	Shanghai Maritime University, China
Angel F. Tenorio	Universidad Pablo de Olavide, Spain
Jose Flores	The University of South Dakota, SD, USA
Francesco Zirilli	Sapienza Universita di Roma, Italy
Kei Eguchi	Fukuoka Institute of Technology, Japan
Jon Burley	Michigan State University, MI, USA
Imre Rudas	Obuda University, Budapest, Hungary
Philippe Dondon	Institut polytechnique de Bordeaux, France
Zhong-Jie Han	Tianjin University, China
George Barreto	Pontificia Universidad Javeriana, Colombia
Frederic Kuznik	National Institute of Applied Sciences, Lyon, France
Stavros Ponis	National Technical University of Athens, Greece
Lesley Farmer	California State University Long Beach, CA, USA
Francesco Rotondo	Polytechnic of Bari University, Italy
Genqi Xu	Tianjin University, China
Manoj K. Jha	Morgan State University in Baltimore, USA
Hessam Ghasemnejad	Kingston University London, UK
Ole Christian Boe	Norwegian Military Academy, Norway
Deolinda Rasteiro	Coimbra Institute of Engineering, Portugal
Masaji Tanaka	Okayama University of Science, Japan
Takuya Yamano	Kanagawa University, Japan
Konstantin Volkov	Kingston University London, UK
José Carlos Metrôlho	Instituto Politecnico de Castelo Branco, Portugal
Moran Wang	Tsinghua University, China
Santoso Wibowo	CQ University, Australia
Yamagishi Hiromitsu	Ehime University, Japan
Kazuhiko Natori	Toho University, Japan
Abelha Antonio	Universidade do Minho, Portugal
Matthias Buyle	Artesis Hogeschool Antwerpen, Belgium
Tetsuya Yoshida	Hokkaido University, Japan
Miguel Carriegos	Universidad de Leon, Spain
Andrey Dmitriev	Russian Academy of Sciences, Russia
Dmitrijs Serdjuks	Riga Technical University, Latvia
Shinji Osada	Gifu University School of Medicine, Japan
Tetsuya Shimamura	Saitama University, Japan
Valeri Mladenov	Technical University of Sofia, Bulgaria
João Bastos	Instituto Superior de Engenharia do Porto, Portugal
Sorinel Oprisan	College of Charleston, CA, USA
Alejandro Fuentes-Penna	Universidad Autónoma del Estado de Hidalgo, Mexico
Xiang Bai	Huazhong University of Science and Technology, China
Eleazar Jimenez Serrano	Kyushu University, Japan

Table of Contents

Plenary Lecture 1: Stiff Models and Gradient Methods with the Exponential Relaxation <i>Igor G. Chernorutskiy</i>	13
Plenary Lecture 2: EMG-Analysis for Enhancing Efficiency and Performance of Electric Power Systems by Using Smart Grid Technology <i>Nikolay V. Korovkin</i>	14
Plenary Lecture 3: Modeling of Mechanism of State and Private Partnership Development of the Social Infrastructure in the Regions <i>Vladimir V. Gluhov</i>	15
Plenary Lecture 4: On Complete Monotonicity of Some Functions of the Mittag-Leffler Type in Non-Debye Relaxation Processes <i>Francesco Mainardi</i>	17
Plenary Lecture 5: From Physical to Mathematical Circuits: Theoretical and Practical Issues <i>Massimo Ceraolo</i>	18
Statistical Linearization Based on the Mutual Quadratic Rényi Information <i>Kirill R. Chernyshov</i>	21
Causal Polynomial Pole Assignment for Linear Control Systems <i>Bernhard P. Lampe, Efim N. Rosenwasser</i>	27
New Way of Digital Processing of Short Noisy Signals <i>V. Tutygin</i>	32
Minimization of THD Using Evolutionary Optimization Methods for Photovoltaic Generation Systems <i>Jorge Luis Diaz Rodriguez, Luis David Pabon, Aldo Pardo Garcia</i>	38
Stochastic Model for Local Ice Loads Measured on the Vessel Hull <i>Petr N. Zvyagin</i>	45
Dynamic Optimization of Carbon Dioxide Enrichment for Tomato Crop in a Greenhouse <i>J. E. Moises Gutierrez, N. Iliá Ponce de Leon Puig, J. Eladio Flores, Ma. Monserrat Morin Castillo, Josefina Castaneda Camacho, Jose Italo Cortes, Pedro Garcia Juarez</i>	48
Access Control Model for Grid Calculations <i>Artem Konoplev, Maxim Kalinin, Dmitry Moskvín, Dmitry Zegzhda</i>	54
FPGA Based Omnidirectional Video Acquisition Device (OVAD) <i>Jan Kwiatkowski, Dawid Sobel, Karol Jędrasiak, Aleksander Nawrat</i>	58

Top-level Power Unit System and the Task “Calculation of Technical and Economical Indexes” for the “Kudankulam” NPP	62
<i>Elena Ph. Jharko</i>	
Shore-to-Sea Maritime Communication with Visible Light Transmission	68
<i>Hyeongji Kim, Atul Sewaiwar, Yeon-Ho Chung</i>	
Experimental Study of Influence of Orthogonal Magnetization on a Ferromagnetic Characteristic	72
<i>Yu. E. Adamian, S. I. Krivosheev</i>	
Continuous Health-Monitoring for Early Detection of Patient by Web Telemedicine System	76
<i>Hafez Fouad</i>	
The Electromagnetics Foundation of Circuits Revisited	84
<i>Massimo Ceraolo</i>	
Disturbances Applied to Axis of Telescope Installed on the Deck of a Ship	92
<i>S. A. Tushev, V. N. Drozdov</i>	
Voice Analysis for Detecting Persons with Parkinson’s Disease Using MFCC and VQ	96
<i>A. Benba, A. Jilbab, A. Hammouch</i>	
Hand Gesture Recognition Using 1\$ and Background Subtraction Algorithms	101
<i>Hazem Khaled, E. M. Saad, S. Sayed, Hossam Ali</i>	
In-circuit Emulation of Memory Fault Injection	105
<i>Olga V. Mamoutova, Oleg V. Nenashev, Alexey S. Filippov</i>	
Distress Situation Detection Based Data Fusion Analysis for HSH	108
<i>Mohamed Fezari, Leila Abdoune, Ali Al-Dahoud</i>	
New Method Based on a Speech Processing Algorithm for Cochlea Implants Using IIR Filters	114
<i>Hajer Rahali, Zied Hajaiej, Nouredine Ellouze</i>	
Management of a Standardized Platform of Unified Medical History from Health Interoperability - Case Study Colombian Caribbean Islands System	119
<i>Fernando Prieto Bustamante, Yaneth P. Caviativa, Yoan Manuel Guzmán</i>	
Authors Index	125

Plenary Lecture 1

Stiff Models and Gradient Methods with the Exponential Relaxation



Professor Igor G. Chernorutskiy

Saint Petersburg State Polytechnical University

Russia

E-mail: igcher@spbstu.ru

Abstract: 1. For a class of matrix gradient methods a new concept of the relaxation function is suggested. This concept allows to evaluate the effectiveness of each gradient optimization procedure, and to synthesize new methods for special classes of ill conditioned (stiff) non-convex optimization problems. According to the suggested formula , it is possible to build relevant search procedures for any given relaxation function.

2. The theorem about the relaxation conditions of each matrix gradient method is proven. Based on the concept of the relaxation functions it is given the geometric interpretation of relaxation properties of gradient methods. According to this interpretation it is possible to build a relaxation area, and to evaluate the speed of the objective function values decreasing.

3. The analysis of classical matrix gradient schemes such as simple gradient method, Newton's methods, Marquardt method is given. It is shown that the relaxation function and its geometric interpretation gives almost full information about the properties and capabilities of relevant gradient optimization methods.

4. A new class of matrix gradient methods with the exponential relaxation function (ERF) is suggested. It is shown that ERF-method summarizes the classical gradient methods including Newton methods, and Marquardt method. In contrast to these methods, ERF-methods have the relaxation functions, entirely located in the relaxation area, which significantly increases the computational efficiency of gradient methods.

5. The ERF-methods convergence for a wide class of non-convex objective functions is established.

Brief Biography of the Speaker: Dr. Chernorutskiy currently is a Professor of Saint-Petersburg State Polytechnical University (SPbSPU). Degrees (SPbSPU): Professor, 1990; Doctor of Technical Science, 1987; Associate Professor, 1982; Ph.D., 1978; M.S., 1970.

Professor Chernorutskiy is the Chair of Information & Control Systems Division of Computer Science and Engineering School (CSES).

Research Interests

Applied Software Engineering, Optimization Tools, Real - Time Systems Modeling and Simulation, Parameter Estimation, and Adaptive Optimization, Decision Support Systems, Artificial Intelligence and Expert Systems.

Plenary Lecture 2

Enhancing Efficiency and Performance of Electric Power Systems by Using Smart Grid Technology



Professor Nikolay V. Korovkin

Chef of Theoretical Electrical Engineering Department
Saint Petersburg State Polytechnical University
Russia

E-mail: nikolay.korovkin@gmail.com

Abstract: A new approach for optimization of power system states with Smart grid utilities will be proposed.

The development of electric power systems (EPS) goes to the construction of power plants, connection of new consumers to networks, introduction into service of new power transmission lines. The complication of electric power system structure and configuration results in reduction of their flexibility and has an adverse effect on the main indices of EPS performance: power distribution losses, power quality and power supply security. Actual conditions of operation and development of large EPS call for new control techniques to be introduced, that is why the elaboration of methods to control the power system operation and to optimize its states with respect to various criteria is now the trend of scientific researches of current concern.

Brief Biography of the Speaker: Education (degrees, dates, universities):

1978, Leningrad Polytechnic Institute, research engineer

1984, Leningrad State University, candidate of science (Phd)

1997, Saint Petersburg Polytechnic university, doctor of science

Career/Employment (employers, positions and dates):

1978, Leningrad State University, assistance professor

1984, Leningrad State University, docent

1997, Saint Petersburg Polytechnical university, professor

2010, Saint Petersburg Polytechnical university, head of Theoretical Electrical Engineering department

Plenary Lecture 3

Modeling of Mechanism of State and Private Partnership Development of the Social Infrastructure in the Regions



Professor, Doctor of Science, Vice Rector Vladimir V. Gluhov

Saint Petersburg State Polytechnical University
Polytechnicheskaja str., 29, 195251, St. Petersburg
Russia

E-mail: vicerektor.me@spbstu.ru

Abstract: 1. There are identified and analyzed the problems of development of social infrastructure in the regions of Russia. It is developed the mechanism and proposed the forms of cooperation for their solution on the basis of private and state partnership.
2. It is developed institutional framework for interaction between city administrations and business communities, aimed at creating an environment for effective development of the social infrastructure in the regions.
3. It is developed the game theory approach for modeling the interaction of city administrations and businesses considering the possible development of the institutional environment.
4. It is described a class of cooperative games simulating the interaction of businesses and city administration.
5. It is proposed a mechanism for solving the problems of social infrastructure development based on the analysis of game interaction models of city administrations and businesses.

Brief Biography of the Speaker: Vice-Rector for administrative and economic activity of St. Petersburg State Polytechnic University, Professor of Russian-German Center of Management and Marketing “Progress”, laureate of state prize “President of Russian Federation Prize in Higher Education”, laureate of St. Petersburg governor prize for excellence in higher education, laureate of V.V. Novozhilov prize (the Russian Academy of Sciences).

Member of following Academies:

- International Academy of Technological Cybernetics
- International Academy of Informational Support
- Baltic Academy of Informational Support
- International Academy of Ecology and Security Sciences
- Academy of Humanities
- International Academy of Higher School Science
- Academy of Municipal Sciences

The scholarly works of Vladimir V. Gloukhov develop the “effective management” research area.

Vladimir V. Gloukhov developed the full system of optimization mathematical models for iron and steel enterprises, which found their places in engineering practice and were described in “Mathematical methods and models in manufacturing planning and management” scientific work. These models formed a basis of new school of thought and applied research area – optimization models of iron and steel production.

Vladimir V. Gloukhov has also developed some methods of economic analysis of newest technological processes (in the fields of powder metallurgy, laser processing, ferrous and non-ferrous industry), which have later been implemented in many production enterprises of Russia. The theory of economic analysis of newest technological processes allowed to form the “economics and management of innovation technologies” educational direction.

Plenary Lecture 4

On Complete Monotonicity of Some Functions of the Mittag-Leffler Type in Non-Debye Relaxation Processes



Professor Francesco Mainardi

Department of Physics, University of Bologna, and INFN
Via Irnerio 46, I-40126 Bologna, Italy
E-mail: francesco.mainardi@bo.infn.it.it

Abstract: In this talk we discuss some interesting examples of relaxation occurring in viscoelastic and dielectric materials, which are described by special completely monotone functions of the Mittag-Leffler type. This means that these response functions are represented by continuous distributions of elementary (i.e. exponential) relaxation processes via non-negative spectra of relaxation in frequency or time. In addition to the well known functions of Mittag-Leffler type in one and two parameters, we revisit two more general kinds of Mittag-Leffler functions in three parameters, that is the Prabhakar and the Kilbas-Saigo functions. For all these functions we prove the conditions on the parameters to ensure the complete monotonicity and compute the corresponding frequency spectra. For some study-cases we present numerical results with illustrative plots for the field variable and for the corresponding spectral distribution. We hope that our results can be adopted when the field variable is the response function associated with non-Debye relaxation processes found e.g. in dielectrics. In particular we have derived as noteworthy particular cases the classical models of non-Debye relaxation phenomena referred to as Cole-Cole, Davidson-Cole, Havriliak-Negami along with the so-called Kohlrausch-Williams-Watts (KWW) law based on the stretched exponential function.

Brief Biography of the Speaker: For a full biography, list of references on author's papers and books see:

Home Page: <http://www.fracalmo.org/mainardi/index.htm>

and <http://scholar.google.com/citations?user=UYxWyEEAAA&hl=en&oi=ao>

Plenary Lecture 5

From Physical to Mathematical Circuits: Theoretical and Practical Issues



Professor Massimo Ceraolo

University of Pisa

Italy

E-mail: massimo.ceraolo@unipi.it

Abstract: Electrical engineers typically talk about “circuits”, without first defining what a circuit really is. If we mean circuits to be sets of elements containing insulating and conducting material, as well as magnetic material, nearly everything is a circuit.

If, instead, we mean circuits as “sets of elements in which some wires that connect components to each other are clearly distinguishable”, they constitute a set (the set of all possible circuits) that is a bit more limited, and maybe clear enough.

When talking about circuits, typically electrical engineers think of this latter definition. In addition, they typically assume that Kirchhoff’s equations are valid for all circuits.

This creates theoretical and practical issues that are normally underestimated. In particular:

- Kirchhoff’s laws are not valid in general. In the speech examples of “circuits” (according to the above definition) for which they are not valid are reported;
- the very concept of “potential” of points of the circuits is vague if not totally wrong.

The speech will discuss this inconsistency thoroughly and proposes a solution to the issues the following approach:

- Systems in which electric and magnetic phenomena occur are simply called electromagnetic systems; for them Maxwell’s equations are valid, where Kirchhoff’s laws not only are not valid, but even loose meaning
- Systems in which electric magnetic phenomena occur and have a circuital shape, i.e. are composed by lumped components connected to each other by means of insulated wires, are called physical circuits. For them Maxwell’s equations are still valid; they are susceptible to be abstracted in such a way that, under given conditions, mathematical circuits can be inferred from them
- Mathematical circuits, or simply circuits, are abstracted structures, that constitute under given conditions, approximations of actual physical circuits, for which Kirchhoff’s equations are valid, or better, are postulated to be valid. As such, Kirchhoff’s equations are just the version of the continuity (charge conservation) equation and energy conservation for mathematical circuits. Instead of the Maxwell’s equations, for circuits Kirchhoff’s and constitutive equations are valid.

Once circuits (the short name of mathematical circuits) are defined, not all problems are solved.

In the speech, the author shows that to obtain circuits from physical circuits containing transmission lines, for which Kirchhoff's laws are valid, is not always possible; however, a special version of them, that will be called metacircuit, will be introduced.

Again, it will be discussed that in circuits with ideal transformers do not allow Kirchhoff's laws to be written in their more common form, and special treatment is needed.

Circuits are lumped component systems: i.e., systems composed by components that are connected to each other through interfaces. Therefore their behavior over time can be computer-simulated using object-oriented tools and languages. The final part of the speech will show that the modern simulation language Modelica has an approach that is one perfectly in line with the analysis of this speech, and even the graphical tricks used to evidence lumped components and connections are in total agreement with the Modelica approach.

This gives additional usefulness to the approach proposed in the speech, and in its companion paper.

Brief Biography of the Speaker: Born in 1960, he took his Ms Degree in Electrical Engineering from the University of Pisa, with honours, in 1985. For some years he has worked in an Italian private research centre. Since 1992 he has been working in Electric Power Systems first as a researcher, then as a professor.

He is full professor of Electric Power Systems since 2002, and teaches Electric and Hybrid Vehicles at the University of Pisa and on-board Electrical Systems at the Naval Academy of Livorno.

He is author or co-author of more than one hundred National and International scientific papers, mainly regarding power systems, electrochemical energy storage, and electric and hybrid vehicles.

He is the chairman of the School of Engineering of the University of Pisa, that coordinates teaching activities of around 250 researchers and professors.

He is the main author of the IEEE-Wiley book "Fundamentals of Electric Power Engineering – from Electromagnetics to Power Systems".

Statistical Linearization Based on the Mutual Quadratic Rényi Information

Kirill R. Chernyshov

Abstract – The paper presents an approach to the statistical linearization of the input/output mapping of non-linear discrete-time stochastic systems driven by a white-noise Gaussian process. The approach is based on applying the quadratic mutual Rényi information. Within such an approach, the statistical linearization criterion is the condition of coincidence of the mathematical expectations of the output processes of the system under study and the derived model and the condition of coincidence of the quadratic mutual Rényi information of the input and output processes of the system and the quadratic mutual Rényi entropy of the input and output processes of the model. As a result, explicit analytical expressions to derive coefficients of the weight function of the target linearized model are obtained. The consideration is preceded with an analysis of applying consistent measures of dependence within the system identification.

Keywords – consistent measures of dependence, input/output model, quadratic mutual Rényi information, statistical linearization, system identification.

I. MEASURES OF DEPENDENCE AS A MATHEMATICAL GROUND OF THE IDENTIFICATION OF STOCHASTIC SYSTEMS

Solving identification problems within a stochastic framework is always based on applying measures of dependence of random values both within representation of the system under study either by use of an input/output mapping, or within state space approaches. Most frequently, conventional linear correlation/covariance measures of dependence are used within identification approaches. Their use directly follows from an identification problem statement itself, when it is based on applying the conventional mean square. The main advantage of these measures is convenience of their use, involving a possibility of deriving explicit analytical expressions to determine required characteristics of the system under study.

However, the main disadvantage of measures of dependence based on the linear correlation is the possibility of their vanishing even if there exists a deterministic dependence between a pair of investigated variables [1, 2]. Just to overcome such a disadvantage, the use of more complicated, non-linear, measures of dependence has been applied to the system identification (in accordance to the A.N. Kolmogorov terminology, a measure of dependence between a pair of two random values is referred as consistent if it vanishes if and only if these random values are stochastically independent).

The paper has been supported by a grant of the Russian Foundation for Basic Researches (RFBR): project 12-08-01205-a.

Kirill R. Chernyshov is with the Laboratory of System Identification of the V.A. Trapeznikov Institute of Control Sciences of the Russian Academy of Sciences, Moscow, Russia, e-mail: myau@ipu.ru.

In 1959, A. Rényi has formulated axioms that were finally commonly recognize to be the most natural conditions to define a measure of dependence $\mu(X, Y)$ between two random values X and Y .

A) $\mu(X, Y)$ is defined for any pair of random values X and Y , if no one of them is a constant with probability 1.

B) $\mu(X, Y) = \mu(Y, X)$.

C) $0 \leq \mu(X, Y) \leq 1$.

D) $\mu(X, Y) = 0$ if and only if X and Y stochastically independent.

E) $\mu(X, Y) = 1$ if there exists a strict dependence between X and Y , that is either $Y = \varphi(X)$, or $X = \psi(Y)$, where φ and ψ are some Borel-measurable functions.

F) Если φ и ψ некоторые взаимно однозначные борелевские функции, то $\mu(\varphi(X), \psi(Y)) = \mu(X, Y)$.

G) If the joint probability distribution of X and Y is normal, then $\mu(X, Y) = |r(X, Y)|$, where $r(X, Y)$ is the conventional correlation coefficient between X and Y .

Commonly used measures of dependence are the ordinary correlation coefficient $r(Y, X)$, the correlation ratio

$$\theta(X, Y) = \frac{\text{var}(\mathbf{E}\{Y/X\})}{\text{var}(Y)}, \text{var}(Y) > 0, \quad (1)$$

and the maximal correlation coefficient.

$$S(X, Y) = \sup_{\{B\}, \{C\}} \frac{\text{cov}(B(Y), C(X))}{\sqrt{\text{var}(B(Y))\text{var}(C(X))}}, \quad (2)$$

$$\text{var}(B(Y)) > 0, \text{var}(C(X)) > 0,$$

where here and below the supremum is taken over Borel-measurable functions $\{B\}$ and $\{C\}$, and $B \in \{B\}$, $C \in \{C\}$.

Throughout the paper the symbols $\mathbf{E}(\cdot)$, $\text{var}(\cdot)$, $\text{cov}(\cdot)$, and $\mathbf{E}\{Y/X\}$, respectively stand for the mathematical expectation, variance, covariance, and conditional expectation.

The value $S(Y, X)$ in (2) was originally proposed in [3] and investigated in [2, 4-7] and subsequent papers.

Let

$$\begin{aligned} (B^*, C^*) &= \\ &= \arg \sup_{\{B\}, \{C\}} \frac{\mathbf{E}(B(Y)C(X)) - \mathbf{E}(B(Y))\mathbf{E}(C(X))}{\sqrt{\text{var}(B(Y))\text{var}(C(X))}}. \end{aligned} \quad (3)$$

Then, as known the pair (B^*, C^*) meeting (3) exists if the stochastic kernel [2, 7]

$$K_{yx}(y, x) = \frac{p_{yx}(y, x)}{\sqrt{p_y(y)p_x(x)}} \quad (4)$$

is integrable with the square, i.e.

$$\int_{-\infty}^{\infty} \int_{-\infty}^{\infty} K_{yx}^2(y, x) dy dx < \infty, \quad (5)$$

what, in turn, holds if from the condition

$$B(Y) - C(X) \equiv 0 \text{ a.s.},$$

it follows that the B and C are identically zero. In (4) and in sequel, $p_{yx}(y, x)$, $p_y(y)$, $p_x(x)$ are the joint and marginal probability distribution densities of the random values Y and X .

Under condition (5), the bivariate density $p_{yx}(y, x)$ has the following bilinear expansion converging in mean [6-8]

$$p(y, x) = p(y)p(x) \times \left(1 + \sum_{i=1}^{\infty} S_i B_i(y) C_i(x) \right),$$

where S_i are eigenvalues of stochastic kernel (4), and $B_i(y), C_i(x)$ are its eigenfunctions corresponding to these eigenvalues, $i = 1, 2, \dots$, meanwhile

1) $S_1 = S(Y, X)$ in expression (2);

2) $B_i(y)$ and $C_i(x)$ are mutually orthonormal with the weights $\sqrt{p_y(y)}$ and $\sqrt{p_x(x)}$ correspondingly, i.e.

$$\int_{-\infty}^{\infty} p_y(y) B_i(y) B_j(y) dy = \begin{cases} 1, & i = j \\ 0, & i \neq j \end{cases},$$

$$\int_{-\infty}^{\infty} p_x(x) C_i(x) C_j(x) dx = \begin{cases} 1, & i = j \\ 0, & i \neq j \end{cases}.$$

Rényi [2] has shown that $S(X, Y)$ in (2) satisfies all the above axioms only, while ordinary correlation coefficient $r(X, Y)$ and the correlation ratio $\theta(X, Y)$ (1) do not, in particular, the correlation coefficient does not meet axioms D, E, F, and the correlation ratio does not meet axioms D and F.

Along with the maximal correlation coefficient, for example, the following measures are consistent (but do not meeting the Rényi's axioms [7]):

- The contingency coefficient

$$\Delta^2(Y, X) = \mathbf{E} \left\{ \frac{(p_{yx}(y, x) - p_x(x)p_y(y))^2}{p_{yx}(y, x)p_x(x)p_y(y)} \right\},$$

- The Shannon mutual information

$$I(Y, X) = \mathbf{E} \left\{ \ln \frac{p_{yx}(y, x)}{p_x(x)p_y(y)} \right\}. \quad (6)$$

Meanwhile, $I(Y, X) \leq \Delta^2(Y, X)$.

The class of consistent in the A.N. Kolmogorov's sense measures of dependence (i.e. not mandatory meeting the Rényi's axioms) is quite wide and new ones continue to appear, while the class of measures of dependence meeting the Rényi's axioms, measures of dependence in the Rényi's sense, is quite narrow.

Identification problems, solving which is considerably defined by characteristics of the dependence of the input and output processes of the system under study, involve the

statistical linearization of the input/output mapping. Meanwhile, approaches to the statistical linearization known are based on applying either conventional correlation functions, or dispersion functions [1] (that is based on correlation ratio (1)), what, due to the reasons pointed out above, may lead to deriving models, whose output will be identical zero. The approach proposed in the present paper is oriented to elimination of the disadvantages pointed out, concerned with applying the correlation and dispersion measures of dependence under system identification based on linearized representations of their input/output models.

In the literature, a methodologically close approach [9-11] is known to deriving equivalent models of nonlinear systems, based on the maximal correlation. However, the approach leads out of deriving the directly linear models, meanwhile to derive approximating models declarative relationships are used (that is not confirmed with a correct mathematical inference). Delusions concerned with the approach [9-11] are analyzed in details in [12-16].

Generically, regarding the application of the maximal correlation within system identification problems one should be mandatory note that deriving the maximal correlation coefficient requires solving a complex problem of finding the pair of the first eigenfunctions and the first (in modulo) eigenvalue of stochastic kernel (4) [6]. From this point of view, such an approach as the information-theoretic one, looks and is much more suitable within the system identification.

At the same time, along with the Shannon mutual information (6), some other ways of defining the mutual information are known. So, for a pair of random values Y, X , their Rényi mutual information of the order α is defined as [17-19]

$$I_{R_\alpha}(Y, X) = \frac{1}{\alpha - 1} \ln \mathbf{E} \left\{ \left(\frac{p_{yx}(y, x)}{p_y(y)p_x(x)} \right)^{\alpha - 1} \right\}, \quad \alpha > 0, \alpha \neq 1.$$

As known, if the parameter α tends to 1, the value $I_{R_\alpha}(Y, X)$ tends to the Shannon mutual information (6), and, thus the Shannon mutual information may be considered as the Rényi one of the "order 1".

From computational point of view, especially under necessity of estimation by use of sample date, the Rényi mutual information is recognized as more attractive than that of Shannon since the Rényi mutual information involves "logarithm of integral" what is computational simpler than "integral of logarithm" in the case of the Shannon mutual information. Meanwhile, selection of a particular value of the order α is of importance since the larger the order is, the more complicated a computational procedure becomes. These considerations of the computational and analytical issues of the value of the order α of the Rényi mutual information imply reasonability of achieving a "compromise", within which the parameter value $\alpha = 2$ looks most attractive. The value $\alpha = 2$ corresponds to the quadratic Rényi mutual information taking the form

$$I_{R_2}(Y, X) = \ln \mathbf{E} \left\{ \frac{p_{yx}(y, x)}{p_y(y)p_x(x)} \right\}.$$

In the case of the stationary and joint stationary in the strict sense random processes $y(t)$ and $x(s)$, $I_{R_2}(Y, X)$ is the corresponding function in the time:

$$I_{R_2}(Y, X; \tau) = \ln \mathbf{E} \left\{ \frac{p_{yx}(y, x; \tau)}{p_y(y)p_x(x)} \right\}, \quad \tau = t - s. \quad (7)$$

Just the function $I_{R_2}(Y, X; \tau)$ (7) will be used in sequel to derive a criterion of the statistical linearization.

II. THE STATISTICAL LINEARIZATION PROBLEM: STATEMENT AND SOLUTION

Let in a non-linear dynamic system $y(t)$ be output random process, being assumed to be stationary in the strict sense and ergodic,; $w(s)$ be input random process, being assumed within the process problem statement to be a white-noise Gaussian process, while the dependence of the input and output processes of the system is characterized by the probability distribution density (being of course not known to the researcher)

$$p_{y,w}(y, w, \tau), \quad \tau = 1, 2, \dots \quad (8)$$

For sake of simplicity, but without loss of generality, the processes $y(t)$ and $w(s)$ are assumed to be zero-mean and unit-variance, that is

$$\mathbf{E}\{y(t)\} = \mathbf{E}\{w(s)\} = 0, \quad \mathbf{var}\{y(t)\} = \mathbf{var}\{w(s)\} = 1. \quad (9)$$

The processes $y(t)$ and $w(s)$ are also assumed to be joint stationary in the strict sense.

The model of the system described by densities (8) is searched in the form

$$\hat{y}(t; G) = \sum_{k=1}^{\infty} g(k)w(t-k), \quad t = 1, 2, \dots, \quad (10)$$

where $\hat{y}(t; G)$ is the model output process, $G = \{g(k), k \in [1, \infty)\}$, $g(k), k = 1, 2, \dots$ are coefficients of the weight function of the linearized model, subject to identification in accordance to a criterion of the statistical linearization. Such a criterion is the condition of coincidence of the mathematical expectations of the output process of the system described by densities (8) and the output process of model (10), and the condition of coincidence of the quadratic mutual Renyi entropy (7) of the output and input processes of the system described by densities (8) and the output and input processes of model (10), or, mathematically,

$$\mathbf{E}\{y(t)\} = \mathbf{E}\{\hat{y}(t; G)\} = 0, \quad (11)$$

$$I_{R_2}(y(t), w(s); k) = I_{R_2}(\hat{y}(t; G), w(s); k), \quad k = 1, 2, \dots \quad (12)$$

In (12), it is accounted that, in accordance to the above assumptions on the input, $w(s)$, and output, $y(t)$, processes $t-s=k$.

In sequel, the following notations will be used. $p_{y,w}(y, w, k)$, $p_{\hat{y}(G), w}(\hat{y}(G), w, k)$ are correspondingly the joint probability distribution density of the output and input process of the system and the joint probability distribution density of the model, $p_y(y)$, $p_{\hat{y}(G)}(\hat{y}(G))$, and $p_w(w)$ are correspondingly the marginal probability distribution densities of the output process of the system $y(t)$, output process of the

model $\hat{y}(t; G)$, and the input process of the system (as well as of the model) $w(s)$, $k = t - s$.

Again, in accordance to conditions of normalization (9), model (10) is restricted with the condition

$$\mathbf{var}\{\hat{y}(t; G)\} = 1,$$

and, correspondingly, the weight coefficients of the model meet the condition

$$\sum_{k=1}^{\infty} g^2(k) = 1. \quad (13)$$

Thus, expressions (11) and (12) are the criterion of the statistical linearization of the system described by probability distribution densities (8).

Let

$$v_t \langle -k \rangle = \sum_{j=1}^{k-1} g(j)w(t-j) + \sum_{j=k+1}^{\infty} g(j)w(t-j), \quad k = 1, 2, \dots$$

be a sequence of random values that are obviously Gaussian, zero-mean, and having the variance

$$\mathbf{var}\{v_t \langle -k \rangle\} = \sum_{j=1}^{k-1} g^2(j) + \sum_{j=k+1}^{\infty} g^2(j) = 1 - g^2(k), \quad k = 1, 2, \dots$$

Then within the notations introduced and by virtue of model (10) description, one may write the following matrix equalities

$$\begin{pmatrix} \hat{y}(t; G) \\ w(t-k) \end{pmatrix} = \begin{pmatrix} 1 & g(k) \\ 0 & 1 \end{pmatrix} \begin{pmatrix} v_t \langle -k \rangle \\ w(t-k) \end{pmatrix}, \quad (14)$$

$$\begin{pmatrix} v_t \langle -k \rangle \\ w(t-k) \end{pmatrix} = \begin{pmatrix} 1 & -g(k) \\ 0 & 1 \end{pmatrix} \begin{pmatrix} \hat{y}(t; G) \\ w(t-k) \end{pmatrix}. \quad (15)$$

As well known, if two n -dimensional random vectors \mathbf{z} and \mathbf{x} , having the marginal probability distribution densities $p_z(\mathbf{z})$ and $p_x(\mathbf{x})$ correspondingly, are functionally connected by a one-to-one relationship, $\mathbf{z} = \varphi(\mathbf{x})$, then

$$p_z(\mathbf{z}) = p_x(\varphi^{-1}(\mathbf{z})) \left| \frac{D(\varphi^{-1}(\mathbf{z}))}{D(\mathbf{z})} \right|,$$

where $\frac{D(\varphi^{-1}(\mathbf{z}))}{D(\mathbf{z})}$ is the Jacobian of the inverse transformation

$\mathbf{x} = \varphi^{-1}(\mathbf{z})$.

In accordance to this relationship, the joint probability distribution density $p_{\hat{y}(G), w}(\hat{y}(G), w, k)$ of the random values $\hat{y}(t; G)$ and $w(t-k)$ may be expressed via the joint probability distribution density $p_{v_t \langle -k \rangle, w}(v_t \langle -k \rangle, w, k)$ of the random values $v_t \langle -k \rangle$ and $w(t-k)$. In turn, the density $p_{v_t \langle -k \rangle, w}(v_t \langle -k \rangle, w, k)$ is evidently of the form

$$p_{v_t \langle -k \rangle, w}(v_t \langle -k \rangle, w, k) = p_{v_t \langle -k \rangle}(v_t \langle -k \rangle) p_w(w),$$

where $p_{v_t \langle -k \rangle}(v_t \langle -k \rangle)$, $p_w(w)$ are the marginal probability distribution densities of the random values $v_t \langle -k \rangle$ and $w(t-k)$ correspondingly. Hence, by virtue of relationships

(14) and (15), and applying relationship (13), for the density $p_{\hat{y}(G),w}(\hat{y}(G),w,k)$ one may write:

$$p_{\hat{y}(G),w}(\hat{y}(G),w,k) = p_{v_i(-k)}(\hat{y}(G) - g(k)w)p_w(w) = \frac{1}{2\pi\sqrt{1-g^2(k)}} e^{-\frac{1}{2} \begin{bmatrix} \hat{y}(G) \\ w \end{bmatrix}^T \begin{bmatrix} 1 & -g(k) \\ -g(k) & 1 \end{bmatrix}^{-1} \begin{bmatrix} \hat{y}(G) \\ w \end{bmatrix}}$$

that is this density is Gaussian. Hence, expression for the quadratic mutual Rényi information (7) directly implies

$$\sqrt{1 - e^{-I_{R_2}(y(t),w(s);k)}} = |g(k)|, \quad k = 1, 2, \dots \quad (16)$$

Meanwhile, the measure of dependence $I_{R_2}(y(t),w(s);k) = \sqrt{1 - e^{-I_{R_2}(y(t),w(s);k)}}$ defined by expression (7) and formula (16) meets all the Rényi axioms [2] for measures of dependence of random values, however, its computation is much more simpler in comparison to the computation of the maximal correlation coefficient mentioned in the preceding Section.

To “open” the modulo in (16), one should apply the sign of the regression of the output process of the system onto the input one, that is

$$\text{sign}[reg_{yw}(k)] = \begin{cases} 1, & reg_{yw}(k) \geq 0 \\ -1, & reg_{yw}(k) < 0 \end{cases}$$

where

$$reg_{yw}(k) = \mathbf{E} \left\{ \frac{y(t)}{w(t-k)} \right\}.$$

Thus, finally,

$$g(k) = \text{sign}[reg_{yw}(k)] \sqrt{1 - e^{-I_{R_2}(y(t),w(s);k)}}, \quad k = 1, 2, \dots$$

The latter expression determines the coefficients of the weight function of linearized model (10).

III. EXAMPLE: ZERO CORRELATION OF INPUT AND OUTPUT VARIABLES

As it was pointed out in Section 1, there exist many examples when applying conventional correlation methods under deriving models does not provide suitable results. Among these systems, one may indicate those ones, the dependence of input and output processes of which is described by probability distribution densities related to the class of distributions of O.V. Sarmanov [20, 21] and having the form

$$p_{S:\alpha,\lambda}(y,x) = \frac{1}{2\pi} e^{-\frac{x^2+y^2}{2}} \times \left(1 + \frac{\lambda}{\kappa_\alpha^2} \left(e^{-(\alpha x)^2} - \frac{1}{\sqrt{1+2\alpha^2}} \right) \left(e^{-(\alpha y)^2} - \frac{1}{\sqrt{1+2\alpha^2}} \right) \right), \quad (17)$$

where $0 \leq \lambda \leq 1$, $\alpha \in R$, and

$$\kappa_\alpha = \sup_x \left| e^{-(\alpha x)^2} - \frac{1}{\sqrt{1+2\alpha^2}} \right|.$$

The marginal distributions of the density $p_{S:\alpha,\lambda}(y,x)$ are the Laplace ones, while the correlation coefficient and correlation ratio (1) corresponding to this density are zero for all $0 \leq \lambda \leq 1$ and $\alpha \in R$.

The maximal correlation coefficient (2) $S_{\alpha,\lambda}(Y,X)$ for density (17) is of the form

$$S_{\alpha,\lambda}(Y,X) = \frac{\sigma_\alpha^2}{\kappa_\alpha^2} \lambda,$$

where

$$\sigma_\alpha^2 = \frac{1}{\sqrt{2\pi}} \int_{-\infty}^{\infty} e^{-\frac{x^2}{2}} \left(e^{-(\alpha x)^2} - \frac{1}{\sqrt{1+2\alpha^2}} \right) dx.$$

One may be easily be shown that the maximal (in modulo) magnitude of $S_{\alpha,\lambda}(Y,X)$ is achieved (under a fixed λ) under

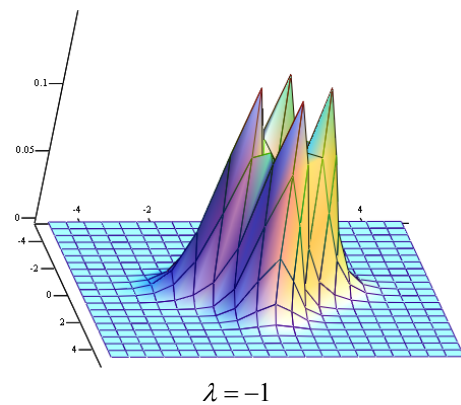
$\alpha = \sqrt{\frac{3}{2}}$. For this magnitude of the parameter α , bivariate probability distribution density (17) takes the form

$$p_{S:\sqrt{3/2},\lambda}(y,x) = \frac{e^{-\frac{x^2+y^2}{2}}}{2\pi} \times \left(1 + \lambda \left(2e^{-\frac{3}{2}x^2} - 1 \right) \left(2e^{-\frac{3}{2}y^2} - 1 \right) \right), \quad -1 \leq \lambda \leq 1, \quad (18)$$

with corresponding maximal correlation coefficient $S_{\sqrt{3/2},\lambda}(Y,X)$:

$$S_{\sqrt{3/2},\lambda}(Y,X) = \left(\frac{4}{\sqrt{7}} - 1 \right) \lambda.$$

Magnitudes of the parameter λ considerably influence the shape of bivariate probability distribution density (18). Fig. 1 displays its shape for magnitudes of $\lambda = -1; -1/2; 1/2; 1$.



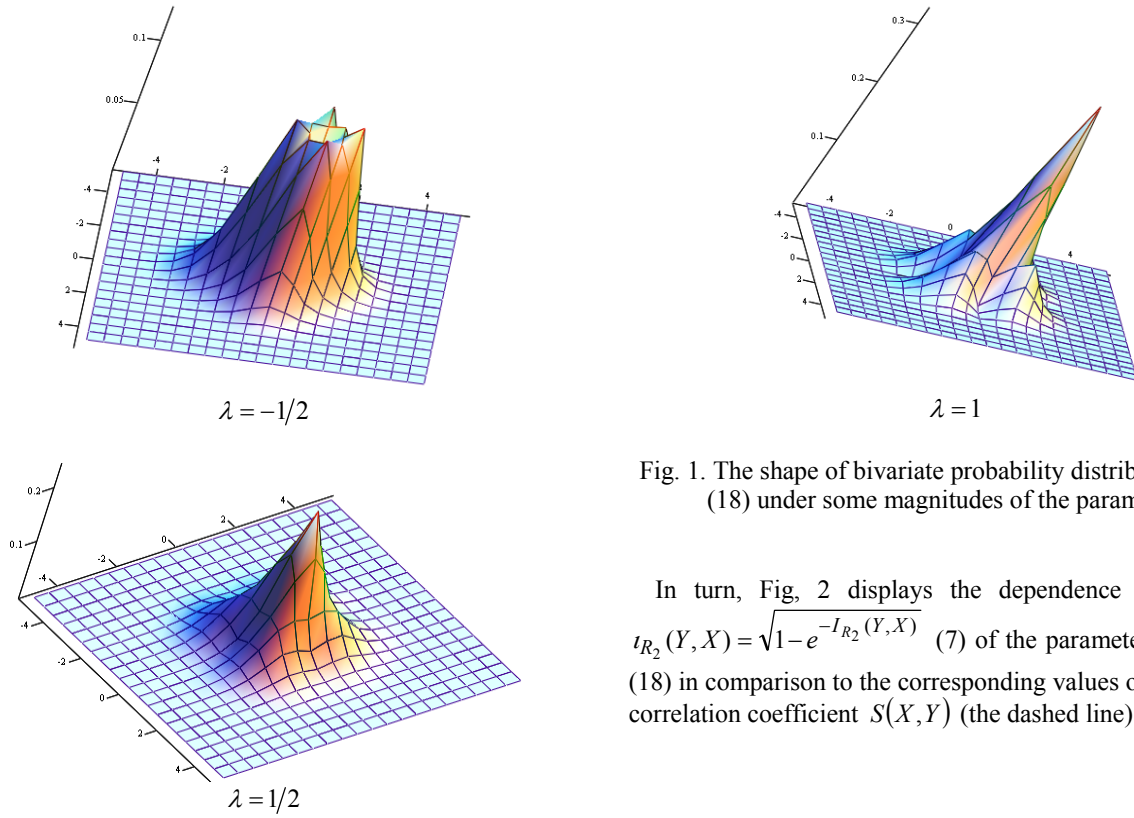


Fig. 1. The shape of bivariate probability distribution density (18) under some magnitudes of the parameter λ .

In turn, Fig. 2 displays the dependence of values of $\iota_{R_2}(Y, X) = \sqrt{1 - e^{-I_{R_2}(Y, X)}}$ (7) of the parameter λ in density (18) in comparison to the corresponding values of the maximal correlation coefficient $S(X, Y)$ (the dashed line).

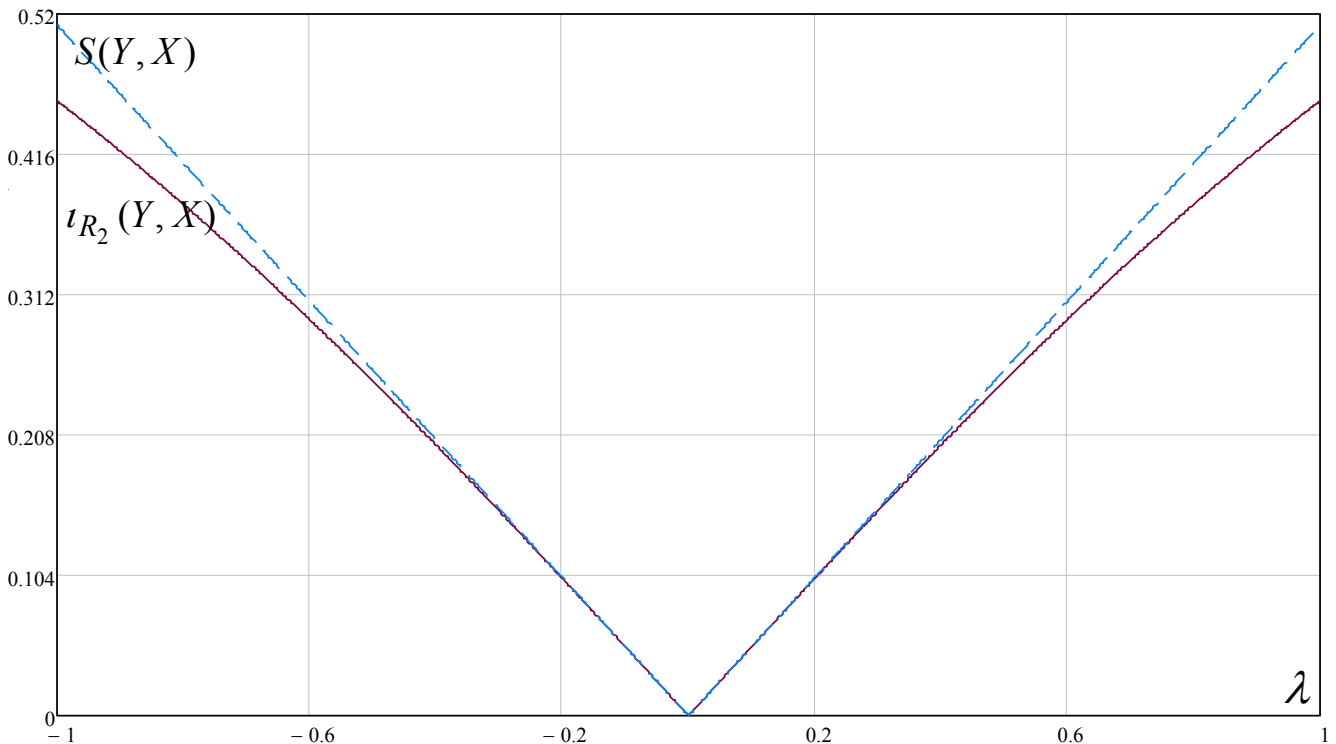


Fig. 2. The closeness of values of $\iota_{R_2}(Y, X)$ and $S(X, Y)$ under various magnitudes of the parameter λ in probability distribution density (18).

Thus, for instance, if stochastic dependence (8) between the output process, $y(t)$, and the input process, $w(s)$, of a nonlinear system is defined by probability distribution density (being assumed, of course, to be not known to the researcher) of form (17) with the parameter $\lambda = \lambda(k)$, $k = t - s$, then applying both conventional and dispersion methods of the statistical linearization would lead, under identification of model (10), to representation of the output process as identical zero, what is eliminated under applying the presented approach based on the quadratic mutual Rényi information.

IV. CONCLUSIONS

An approach to the statistical linearization of input/output mappings of non-linear discrete-time stochastic systems driven by a white-noise Gaussian process has been considered. The approach is based on applying quadratic mutual Rényi information (7) to construct a criterion of the statistical linearization. Within the approach proposed, the criterion of the statistical linearization is the condition of coincidence of mathematical expectations of the output processes of the system and model, and the condition of coincidence of the quadratic mutual Rényi information of the output and input processes of the system and the quadratic mutual Rényi information of the output and input processes of the model. Explicit analytical expressions to determine coefficients of the weight function of the linearized model have been obtained. Meanwhile, the expressions are based on the quadratic mutual Rényi information and define a measure of stochastic dependence of random values, meeting all the Rényi axioms [2].

REFERENCES

- [1] Rajbman, N.S. "Extensions to nonlinear and minimax approaches", *Trends and Progress in System Identification*, ed. P. Eykhoff, Pergamon Press, Oxford, 1981, pp. 185-237.
- [2] Rényi, A. "On measures of dependence", *Acta Math. Hung.*, 1959, vol. 10, no. 3-4, pp. 441-451.
- [3] Gebelein, H. „Das statistische Problem der Korrelation als Variations- und Eigenwertproblem und sein Zusammenhang mit der Ausgleichsrechnung“, *Zeitschrift für Angewandte Mathematik und Mechanik*, 1941, vol. 21, no. 6, pp. 364-379.
- [4] Rényi, A. "New version of the probabilistic generalization of the large sieve", *Acta Math. Hung.*, 1959, vol. 10, no. 1-2, pp. 217-226.
- [5] Sarmanov, O.V. "Maximum correlation coefficient (symmetric case). *Select. Transl. Math. Stat. Probab.* 1963, vol. 4, pp. 271-275.
- [6] Sarmanov, O.V. "The maximum correlation coefficient (nonsymmetric case)", *Sel. Trans. Math. Statist. Probability*, 1963, vol. 4, pp. 207-210.
- [7] Sarmanov, O.V and E.K. Zakharov "Measures of dependence between random variables and spectra of stochastic kernels and matrices", *Matematicheskiiy Sbornik*, 1960, vol. 52(94), pp. 953-990. (in Russian)
- [8] Chesson, P.L. "The canonical decomposition of bivariate distributions", *J. Multivariate Analysis*, 1976, vol. 6, pp. 526-537.
- [9] Pashchenko, F.F. "Determining and modeling regularities via experimental data", In: *System Laws and Regularities in Electrodynamics, Nature, and Society*. Chapter 7, Nauka Publ., Moscow, 2001, 411-521. (in Russian) ISBN 5-02-013088-5
- [10] Pashchenko, F.F. *Introduction to consistent methods of systems modeling. Identification of non-linear systems*. Finans i statistika Publ., Moscow, 288 p. ISBN 978-5-279-03042-2 (in Russian)
- [11] Pashchenko, A.F. and F.F. Pashchenko. "Application of the method of statistical linearization in problems of identification of nonlinear systems", *Industrial Electronics and Applications (ICIEA), 2012 7th IEEE Conference*, DOI: 10.1109/ICIEA.2012.6360966, pp. 1529-1532.
- [12] Chernyshov, K.R. "An essay on some delusions in system identification", In: *Proceedings of the II International conference "System Identification and Control Problems" SICPRO '03. Moscow, 29-31 January 2003*. Moscow: V.A. Trapeznikov Institute of Control Sciences, 2003, pp. 2660-2698. (in Russian)
- [13] Chernyshov, K.R. *Questions of identification: consistent measures of dependence*, Moscow, V.A. Trapeznikov Institute of Control Sciences, 60 p. (in Russian)
- [14] Chernyshov, K.R. "Towards the educational process support in the stochastic modeling (the essay no. 2)", In: *Proceedings of the VI International Conference "System Identification and Control Problems" SICPRO '07. Moscow, January 29 - February 1, 2007*. Moscow: V.A. Trapeznikov Institute of Control Sciences, 2007, pp. 1632-1671. (in Russian)
- [15] Chernyshov, K.R. "Stochastic systems and information-theoretic methods: an analysis of some approaches", In: *Proceedings of the 9th International Conference "System Identification and Control Problems" SICPRO '12. Moscow, January 30 - February 2, 2012* (Moscow, V.A. Trapeznikov Institute of Control Sciences, 2012), pp. 1140-1164. (in Russian)
- [16] Chernyshov, K.R. "Delusions in System Identification: Professor Pashchenko's School", *IFAC-PapersOnLine*. ISSN: 1474-6670, 2003, vol. 7, part 1, pp. 939-944.
- [17] Rényi, A. "On measures of information and entropy", in: *Proceedings of the 4th Berkeley Symposium on Mathematics, Statistics and Probability*, 1960, pp. 547-561.
- [18] Rényi, A. "Some Fundamental Questions of Information Theory", *Selected Papers of Alfred Rényi, Akademiai Kiado*, Budapest, vol. 2, 1976, pp. 526-552.
- [19] Rényi, A. "On Measures of Entropy and Information", *Selected Papers of Alfréd Rényi, Akademiai Kiado*, Budapest, vol. 2, 1976, pp. 565-580.
- [20] Sarmanov, O.V. "Remarks on uncorrelated Gaussian dependent random variables", *Theory Probab. Appl.*, 1967, vol. 12, issue 1, pp. 124-126.
- [21] Kotz, S., Balakrishnan, N., and N.L. Johnson. *Continuous Multivariate Distributions. Volume 1. Models and Applications* / Second Edition, Wiley, New York, 2000, 752 p. ISBN 978-0-471-18387-7

Causal polynomial pole assignment for linear control systems

Bernhard P. Lampe and Efim N. Rosenwasser,

Abstract—The paper considers the pole assignment problem under the practically important constraint that the designed controller has to be causal, i.e. realizable. It is shown that in case of a strictly proper process, when the set of solutions of the pole assignment problem is not empty, then it always contains a nonempty subset of noncausal controllers. Moreover, according to the set of causal solutions we have one of the three situations: 1) the set is empty, 2) the set has only one element, 3) there exists a subset of causal solutions.

Index Terms—Controller design, Polynomial methods, Characteristic polynomials, Pole assignment, Causality conditions

I. INTRODUCTION

The paper considers the pole assignment problem for SISO linear processes, which are described by operational equations in the differential operator $p = \frac{d}{dt}$ or the forward shift operator q .

As is well known, [2], [1], two approaches are used for its solution.

In the first approach, the solution is searched in state space and is based on the application of state observers and controllers.

The second approach is associated with the solution of Diophantine polynomial equations and does not require observers. The first contribution in this direction was presented by L. N. Volgin in [6]. Further development was performed by V. Kucera [3]. Here it emerges, that the application of the polynomial method for the solution of practical problems encounters honest difficulties, which are connected with the demand that the designed controllers have to be causal. Methods for the solution of this problem in a number of special cases are provided in [1], [4].

The monograph [5] provides the general solution of the problem for the MIMO case, based on the transfer to the associated model of the process. The paper at hand presents a direct solution of the problem for SISO strictly causal processes - a transfer to the associated model is not necessary, and the solution is directly expressed by the process parameters.

II. PROBLEM

1) Let the dynamics of the SISO linear process with input $u(t)$ and output $y(t)$ be described by the linear operator equation

$$a(\lambda)y = b(\lambda)u, \quad (1)$$

where λ is the differential operator $p = \frac{d}{dt}$ or the right shift operator q , [1]. Moreover, in (1) the quantities $a(\lambda), b(\lambda)$ are coprime polynomials. Below, equation (1) is called process equation, and the polynomial pair $(a(\lambda), b(\lambda))$ is called process. The process $(a(\lambda), b(\lambda))$ is called strictly causal, if

$$\deg a(\lambda) > \deg b(\lambda), \quad (2)$$

where the notation \deg means the degree of a polynomial.

2) Let us have in addition to process (1) an object described by the equation

$$\alpha(\lambda)u = \beta(\lambda)y, \quad (3)$$

where $\alpha(\lambda), \beta(\lambda)$ are polynomials. Below, equation (3) is called controller equation, and the pair $(\alpha(\lambda), \beta(\lambda))$ is called controller. The controller $(\alpha(\lambda), \beta(\lambda))$ is called causal, if the condition

$$\deg \alpha(\lambda) \geq \deg \beta(\lambda) \quad (4)$$

is fulfilled.

3) Together, equations (1) and (3) define the operational equation of the closed loop

$$\begin{aligned} a(\lambda)y - b(\lambda)u &= 0, \\ -\beta(\lambda)y + \alpha(\lambda)u &= 0. \end{aligned} \quad (5)$$

The dynamical properties of the closed loop are substantially determined by the properties of the characteristic polynomial

$$\Delta_0(\lambda) \triangleq \det \begin{bmatrix} a(\lambda) & -b(\lambda) \\ -\beta(\lambda) & \alpha(\lambda) \end{bmatrix}. \quad (6)$$

The roots of the polynomial $\Delta_0(\lambda)$ are normally called the poles of the closed loop.

Let $\Delta(\lambda)$ be a certain desired characteristic polynomial. Then the causal pole assignment problem consists in constructing the set of all causal controller $(\alpha(\lambda), \beta(\lambda))$ satisfying the equation

$$\det \begin{bmatrix} a(\lambda) & -b(\lambda) \\ -\beta(\lambda) & \alpha(\lambda) \end{bmatrix} = \Delta(\lambda). \quad (7)$$

Relation (7) for given process $(a(\lambda), b(\lambda))$ can be considered as equation depending on the polynomials $\alpha(\lambda)$, $\beta(\lambda)$ and satisfying condition (4).

4) Calculating the determinant in (7), we arrive at the Diophantine polynomial equation

$$a(\lambda)\alpha(\lambda) - b(\lambda)\beta(\lambda) = \Delta(\lambda) \quad (8)$$

and the considered causal pole assignment problem can be formulated as follows:

For a given strictly causal process $(a(\lambda), b(\lambda))$ and polynomial $\Delta(\lambda)$, find the set of solutions of equation (8) satisfying condition (4).

Let $\alpha_0(\lambda), \beta_0(\lambda)$ be an arbitrary solution of equation (8). Then the set of all solutions of this equation is defined by the relations [6], [3]

$$\begin{aligned} \alpha(\lambda) &= \alpha_0(\lambda) + b(\lambda)\xi(\lambda), \\ \beta(\lambda) &= \beta_0(\lambda) + a(\lambda)\xi(\lambda), \end{aligned} \quad (9)$$

where $\xi(\lambda) = 0$ or any polynomial.

However, the considered problem needs to select from set of controllers (9) the subset of controllers, which satisfy causality condition (4).

We will show that set of controllers (9) always contains noncausal controllers. Indeed, from (9) it follows that

$$\begin{aligned} \deg \alpha(\lambda) &= \deg(\alpha_0(\lambda) + b(\lambda)\xi(\lambda)), \\ \deg \beta(\lambda) &= \deg(\beta_0(\lambda) + a(\lambda)\xi(\lambda)). \end{aligned} \quad (10)$$

For sufficiently high values of $\deg \xi(\lambda)$, we obtain

$$\begin{aligned} \deg[b(\lambda)\xi(\lambda)] &> \deg \alpha_0(\lambda), \\ \deg[a(\lambda)\xi(\lambda)] &> \deg \beta_0(\lambda) \end{aligned} \quad (11)$$

and, thus

$$\begin{aligned} \deg \alpha(\lambda) &= \deg[b(\lambda)\xi(\lambda)] \\ &= \deg b(\lambda) + \deg \xi(\lambda), \\ \deg \beta(\lambda) &= \deg[a(\lambda)\xi(\lambda)] \\ &= \deg a(\lambda) + \deg \xi(\lambda). \end{aligned} \quad (12)$$

Hence, due to (2) and (12), we find $\deg \alpha(\lambda) < \deg \beta(\lambda)$, i.e. for sufficiently large $\deg \xi(\lambda)$ all controllers (9) are noncausal.

III. β -MINIMAL CONTROLLERS

1) Consider the rational function

$$W(\lambda) = \frac{\Delta(\lambda)}{a(\lambda)b(\lambda)}. \quad (13)$$

Since the polynomials $a(\lambda), b(\lambda)$ are coprime, there exists a set of separations

$$W(\lambda) = \frac{\Delta(\lambda)}{a(\lambda)b(\lambda)} = \frac{\alpha(\lambda)}{b(\lambda)} - \frac{\beta(\lambda)}{a(\lambda)}, \quad (14)$$

where $\alpha(\lambda), \beta(\lambda)$ are polynomials. We can immediately verify that any pair of polynomials $\alpha(\lambda), \beta(\lambda)$, configured in (14), defines a solution of equation (11). The reverse is also true: any polynomial pair establishing a solution of equation (11), corresponds to a separation of form (14). Among all possible separations (14), there exists a single one, in which the polynomials $\alpha(\lambda) = \alpha^*(\lambda), \beta(\lambda) = \beta^*(\lambda)$ fulfill the condition

$$W(\lambda) = \frac{\alpha^*(\lambda)}{b(\lambda)} - \frac{\beta^*(\lambda)}{a(\lambda)} \quad (15)$$

and in addition

$$\deg \beta^*(\lambda) < \deg a(\lambda). \quad (16)$$

The in this way constructed solution of equation (11) is called β -minimal controller, and it is denoted by $(\alpha^*(\lambda), \beta^*(\lambda))$.

2) Introduce

$$\begin{aligned} D_1 &= \deg \Delta(\lambda) - \deg a(\lambda), \\ D_2 &= \deg \Delta(\lambda) - \deg a(\lambda) - \deg b(\lambda), \\ D_3 &= \deg \Delta(\lambda) - 2 \deg a(\lambda). \end{aligned} \quad (17)$$

Using these notations, we can formulate a statement characterizing the β -minimal solution.

Theorem 1 *The following statements hold:*

i) For

$$D_1 < 0 \quad (18)$$

the β -minimal controller is noncausal.

ii) For

$$D_1 \geq 0, \quad D_3 < 0 \quad (19)$$

the β -minimal controller can be causal or noncausal depending on the choice of the polynomial $\Delta(\lambda)$.

iii) For

$$D_3 \geq 0 \quad (20)$$

the β -minimal controller is causal.

Proof

- i) Let $(\alpha(\lambda), \beta(\lambda))$ be any causal solution of equation (11). Since $\deg a(\lambda) > \deg b(\lambda)$ and $\deg \alpha(\lambda) \geq \deg \beta(\lambda)$, we obtain

$$\deg[a(\lambda)\alpha(\lambda)] > \deg[b(\lambda)\beta(\lambda)] \quad (21)$$

and from (11) we find

$$\deg[a(\lambda)\alpha(\lambda)] = \deg a(\lambda) + \deg \alpha(\lambda) = \deg \Delta(\lambda). \quad (22)$$

Hence, for any causal controller $(\alpha(\lambda), \beta(\lambda))$ we obtain $D_1 = \deg \Delta(\lambda) - \deg a(\lambda) \geq 0$, because $\deg \alpha(\lambda) \geq 0$. Therefore, under condition (18), equation (11) does not possess causal solutions. However, the β -minimal controller is a solution of equation (11), so it must be noncausal.

- ii) For the proof of this claim we consider the two cases

$$D_1 \geq 0, \quad D_2 < 0 \quad (23)$$

or

$$D_2 \geq 0, \quad D_3 < 0. \quad (24)$$

To avoid unwieldy constructions, we show the validity of claim ii) at an example.

For case (23) consider the equation

$$\begin{aligned} (\lambda + 1)^5 \alpha(\lambda) - (\lambda - 2)^2 \beta(\lambda) \\ = (\lambda + 1)^5 \lambda - (\lambda - 2)^2 (\lambda + 2)^k \end{aligned} \quad (25)$$

where $k \geq 0$ is an integer. For $0 \leq k \leq 3$ we obtain $\deg \Delta(\lambda) = 6$, $\deg a(\lambda) = 5$, $\deg b(\lambda) = 2$ and, thus $D_1 = 1$, $D_2 = -1$. Under this conditions the β -minimal solution of equation (25) takes the form

$$\alpha^*(\lambda) = \lambda, \quad \beta^*(\lambda) = (\lambda + 2)^k. \quad (26)$$

From this we realize that for $0 \leq k \leq 1$ the constructed β -minimal controller is causal, and for $2 \leq k \leq 3$ it is noncausal.

Analogously, for the illustration of case (24) consider the equation

$$\begin{aligned} (\lambda - 1)^7 \alpha(\lambda) - (\lambda - 2)^2 \beta(\lambda) \\ = (\lambda - 1)^7 \lambda^3 - (\lambda - 2)^2 (\lambda + 1)^k \end{aligned} \quad (27)$$

where k is a nonnegative integer.

For $0 \leq k \leq 6$ we obtain $\deg \Delta(\lambda) = 10$, $\deg a(\lambda) = 7$, $\deg b(\lambda) = 2$, and thus $D_2 = 1$, $D_3 = -4$. Then the β -minimal controller takes the form

$$\alpha^*(\lambda) = \lambda^3, \quad \beta^*(\lambda) = (\lambda + 1)^k.$$

This controller is causal for $0 \leq k \leq 3$, and noncausal for $4 \leq k \leq 6$.

- iii) For the proof of this claim, at first notice that for $D_3 \geq 0$, we have

$$D_2 > 0. \quad (28)$$

Hence,

$$\deg \alpha^*(\lambda) = \deg \Delta(\lambda) - \deg a(\lambda) = D_1. \quad (29)$$

Indeed, since the second term on the right side of (15) is strictly proper, so due to (13), we obtain

$$\begin{aligned} \deg \Delta(\lambda) - \deg a(\lambda) - \deg b(\lambda) \\ = \deg \alpha^*(\lambda) - \deg b(\lambda), \end{aligned}$$

which is equivalent to (29). At the same time, owing to the definition of the β -minimal controller,

$$\deg \beta^*(\lambda) = \deg a(\lambda) - \rho, \quad (30)$$

where ρ is a positive integer. From (29) and (30), we find

$$\deg \alpha^*(\lambda) - \deg \beta^*(\lambda) = D_3 + \rho > 0,$$

that completes the proof. \blacksquare

IV. MAIN RESULT

The next theorem yields the complete solution of the construction problem for the set of causal solutions of equation (11).

Theorem 2 *The following statements are true:*

- i) *When condition (18) takes place, equation (11) does not possess causal solutions.*
- ii) *When condition (19) holds, the set of causal solutions of equation (11) consists of the β -minimal controller, if this controller is causal, and it is empty, if this controller is noncausal.*
- iii) *When condition (20) is true, then there exists a set of causal solutions of equation (11), which is determined by the relations*

$$\begin{aligned} \alpha(\lambda) &= \alpha^*(\lambda) + b(\lambda)\xi(\lambda), \\ \beta(\lambda) &= \beta^*(\lambda) + a(\lambda)\xi(\lambda), \end{aligned} \quad (31)$$

where $(\alpha^*(\lambda), \beta^*(\lambda))$ is the β -minimal controller and $\xi(\lambda)$ is zero or any polynomial satisfying the condition

$$0 \leq \deg \xi(\lambda) \leq D_3. \quad (32)$$

Proof

- i) This fact follows from the proof of statement i) in Theorem 1.
- ii) Assume (23). Then fraction (13) is strictly proper. In this case both fractions on the right side of (15) are strictly proper, and so we obtain

$$\begin{aligned} \deg \alpha^*(\lambda) &\leq \deg b(\lambda) - 1 \\ \deg \beta^*(\lambda) &\leq \deg a(\lambda) - 1. \end{aligned} \quad (33)$$

Choose $\alpha_0(\lambda) = \alpha^*(\lambda)$, $\beta_0(\lambda) = \beta^*(\lambda)$, and write general solution (22) in the form

$$\begin{aligned} \alpha(\lambda) &= \alpha^*(\lambda) + b(\lambda)\xi(\lambda), \\ \beta(\lambda) &= \beta^*(\lambda) + a(\lambda)\xi(\lambda). \end{aligned} \quad (34)$$

Then, using (33), we obtain for $\xi(\lambda) \neq 0$

$$\begin{aligned} \deg \alpha(\lambda) &= \deg b(\lambda) + \deg \xi(\lambda), \\ \deg \beta(\lambda) &= \deg a(\lambda) + \deg \xi(\lambda). \end{aligned} \quad (35)$$

Since $\deg a(\lambda) > \deg b(\lambda)$, we realize that for $\xi(\lambda) \neq 0$ all controllers (34) are noncausal. For $\xi(\lambda) = 0$ formula (34) yields the β -minimal controller, which, as follows from Theorem 1 in the actual case can be causal or noncausal.

For the investigation of case (24), we construct the dependence of the quantity $\deg \alpha(\lambda)$ from the value of $\deg \xi(\lambda)$. For this task notice, that from the first equation in (34), we obtain

$$\deg \alpha(\lambda) = \deg[\alpha^*(\lambda) + b(\lambda)\xi(\lambda)]. \quad (36)$$

In the actual case, relation (29) is valid

$$\deg \alpha^*(\lambda) = \deg \Delta(\lambda) - \deg a(\lambda). \quad (37)$$

Applying this formula, we find

$$\begin{aligned} \deg \alpha^*(\lambda) - \deg[b(\lambda)\xi(\lambda)] \\ = \deg \Delta(\lambda) - \deg a(\lambda) - \deg b(\lambda) - \deg \xi(\lambda). \end{aligned} \quad (38)$$

Hence, for

$$\begin{aligned} 0 \leq \deg \xi(\lambda) < D_2 \\ = \deg \Delta(\lambda) - \deg a(\lambda) - \deg b(\lambda) \end{aligned} \quad (39)$$

we obtain

$$\deg \alpha^*(\lambda) > \deg[b(\lambda)\xi(\lambda)], \quad (40)$$

and thus, owing to (37)

$$\begin{aligned} \deg \alpha(\lambda) &= \deg \alpha^*(\lambda) = \deg \Delta(\lambda) - \deg a(\lambda) \\ &= D_1. \end{aligned} \quad (41)$$

For

$$\deg \xi(\lambda) = \deg \Delta(\lambda) - \deg a(\lambda) - \deg b(\lambda) = D_2, \quad (42)$$

from the first equation in (35), again formula (41) is achieved. Consequently, we find that formula (41) is valid for

$$0 \leq \deg \xi(\lambda) \leq D_2. \quad (43)$$

For

$$\deg \xi(\lambda) > D_2 \quad (44)$$

it follows from (38) that

$$\deg \alpha^*(\lambda) < \deg[b(\lambda)\xi(\lambda)] \quad (45)$$

and from (36), we realize that

$$\deg \alpha(\lambda) = \deg b(\lambda) + \deg \xi(\lambda). \quad (46)$$

Using (41), (43) and (44), (46) we are able to construct the dependence of the quantity $\deg \alpha(\lambda)$ on the quantity $\deg \xi(\lambda)$ for arbitrary solution (34) under assumption $\xi(\lambda) \neq 0$

$$\begin{aligned} \deg \alpha(\lambda) \\ = \begin{cases} D_1, & 0 \leq \deg \xi(\lambda) \leq D_2, \\ \deg b(\lambda) + \deg \xi(\lambda), & \deg \xi(\lambda) > D_2. \end{cases} \end{aligned} \quad (47)$$

The dependence of $\deg \beta(\lambda)$ on $\deg \xi(\lambda)$ is the straight line

$$\deg \beta(\lambda) = \deg a(\lambda) + \deg \xi(\lambda). \quad (48)$$

When condition (24) is true, we obtain

$$D_3 = \deg \Delta - 2 \deg a < 0, \quad (49)$$

i.e.

$$D_1 = \deg \Delta - \deg a < \deg a. \quad (50)$$

The last inequality means that for $\xi(\lambda) \neq 0$, straight line (48) is located over broken line (47). This fact signifies that in case (24) for $\xi(\lambda) \neq 0$, set of controllers (31) does not contain causal ones. This completes the proof of statement ii).

Fig. 1 shows broken line (47) for the case $\deg \Delta(\lambda) = 7$, $\deg a(\lambda) = 4$, $\deg b(\lambda) = 2$. Here $D_1 = 3$, $D_2 = 1$, $D_3 = -1$. Moreover, Fig. 1 presents straight line (48), which for the above concrete values has the form $\deg \beta(\lambda) = 4 + \deg \xi(\lambda)$.

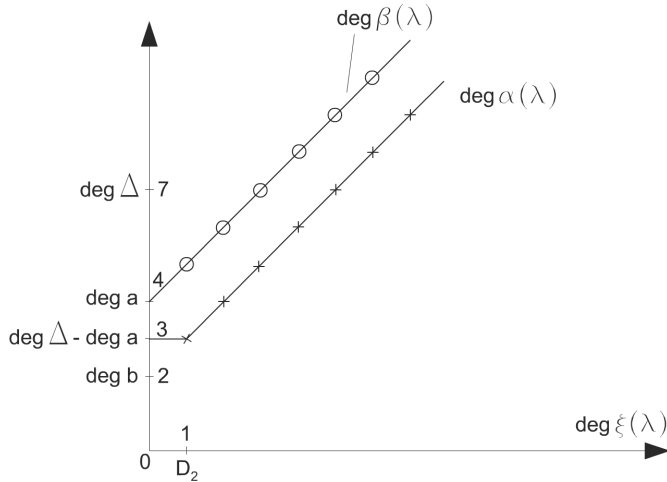


Fig. 1. Controller numerator and denominator degrees in dependence on the degree of the parameter $\xi(\lambda)$ in case ii) and (24)

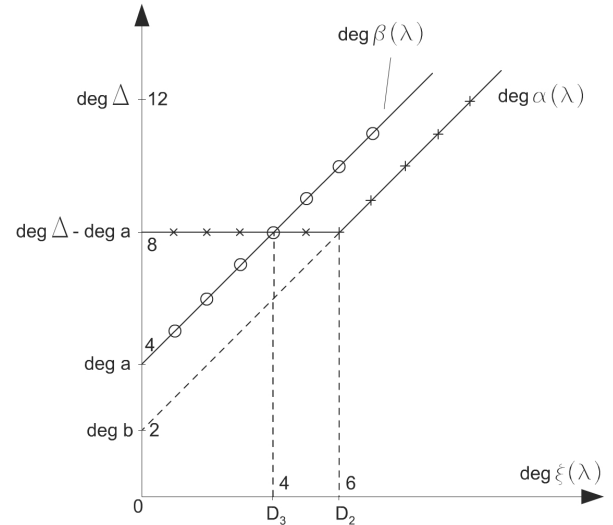


Fig. 2. Controller numerator and denominator degrees in dependence on the degree of the parameter $\xi(\lambda)$ in case iii)

iii) Under condition (20), straight line (45) intersects broken line (47) for

$$\deg a + \deg \xi(\lambda) = D_1 = \deg \Delta(\lambda) - \deg a(\lambda). \quad (51)$$

Hence, in the intersection point, we have

$$\deg \xi(\lambda) = \deg \Delta(\lambda) - 2 \deg a(\lambda) = D_3. \quad (52)$$

Hereby, for $0 \leq \deg \xi(\lambda) \leq D_3$, we obtain

$$\deg \beta(\lambda) \leq \deg \alpha(\lambda), \quad (53)$$

i.e. solution (31) is causal. At the same time, for $\deg \xi(\lambda) > D_3$

$$\deg \beta(\lambda) > \deg \alpha(\lambda) \quad (54)$$

and corresponding controller (31) is noncausal. If we finally respect that, owing to Theorem 1, under condition (24) and for $\xi(\lambda) = 0$, the corresponding β -minimal controller $(\alpha^*(\lambda), \beta^*(\lambda))$ is causal, so statement iii) is completely proven.

Fig. 2 shows the situation according to case iii) for $\deg \Delta(\lambda) = 12$, $\deg a(\lambda) = 4$, $\deg b(\lambda) = 2$, i.e. $D_1 = 8$, $D_2 = 6$, $D_3 = 4$. ■

The following consequence of the main result is convenient for the solution of practical problems.

Corollary 1 Equation (11) has a causal solution, if and only if the β -minimal controller is causal.

REFERENCES

- [1] K. J. Åström and B. Wittenmark. *Computer Controlled Systems: Theory and Design*. Prentice-Hall, Englewood Cliffs, NJ, 3rd edition, 1997.
- [2] M. J. Grimble. *Industrial Control Systems Design*. John Wiley & Sons, Inc., Chichester, 2001.
- [3] V. Kučera. *Analysis and Design of Discrete Linear Control Systems*. Prentice Hall, New York, 1991.
- [4] A. A. Pervozvanskii. *Course on Automatic Control Theory*. Nauka, Moscow, 1986. (in Russian).
- [5] E. N. Rosenwasser and B. P. Lampe. *Multivariable computer-controlled systems – a transfer function approach*. Springer, London, 2006.
- [6] L. N. Volgin. *Optimal discrete control of dynamic systems*. Nauka, Moscow, 1986. (in Russian).

New way of digital processing of short noisy signals

V.Tutygin

Abstract—Classic mathematical analyses of the noisy signals is designed for “long” signals and for the case where the noise level is significantly less than the level of the signal, whereas the solution of many problem, for example, when the processing of satellite chirp signals, echo signals spectrometers, radar signals of electromagnetic acoustic thickness meter the number of periods of the signals is very small and the noise level be compared with the level of the signal and even exceed it. The paper, based on published works and inventions of the author, considered new ways of digital processing of short noisy signals.

Keywords—Short noisy signals, digital signal processing, multi-stage algorithm, anti-noise power of digital signal processing algorithm, covariance, correlation, rediscritization, spline-approximation .

I. INTRODUCTION

The problem of processing noisy short signals occur in digital processing of satellite radar signals, echo-signals of nuclear magnetic resonance spectrometers, radio pulses of electromagnetic-pulse thickness gauges (thicknessmeters). These system can be classified as a variety of radio , radar , sonar , command and control systems , telecommunications , telephony. Methods proposed in the paper digital short signal processing can be used in the equipment receiving , analyzing and transmitting signals and oscillations of different nature : radio, sound , ultrasound , sonar , speech .

Characteristic features of *short noisy signals* are:

- A small amount of signal periods.
- Noise level of signal can be compared with the signal level and even exceed it.
- Signal can takes only part of a time domain.
- Number of signal periods can be nonintegral.
- Signal can be modulated on amplitude.

In many cases informative parameter must be calculated on *only one realization* of the signal.

II. DIGITAL SIGNAL PROCESSING ALGORITHM FOR SIGNIFICANTLY NOISY SIGNALS

Digital signal processing (DSP) algorithm for significantly noisy signals should be different from one for slightly noisy signals. Informative parameter must be calculate with given accuracy, but if original signal contains noise then calculated informative parameter also will be noisy. It is desirable that noise level of informative parameter will be less then noise level of original signal. All DSP algorithm (for example, Fast Fourier Transform) have anti-noise properties. For significantly noised signals this characteristic of algorithm is especially relevant. We offer new characteristic of DSP algorithms – power or anti-noise *power of algorithm* that means ratio of random mean square error (RMSE) of original signal to RMSE of calculated informative parameter.

DSP algorithms are based on the several basic algorithm: Fast Fourier Transform, covariance, correlation, autocorrelation and others. Each of them are characterized with anti-noise *power*. For calculation of informative parameter you use one or many basic algorithms in the complex base. We offer to name them *single-stage* and *multi-stage algorithms* respectively. In last case anti-noise power of algorithm will be greater. It is obviously, that for digital processing of significantly noised signal more effective to use multi-stage algorithms instead of single-stage algorithms.

III. TRADITIONAL ALGORITHMS FOR DSP OF NOISY SIGNALS

To measure the thickness of metal in hard to reach places, such as in the measurement of the thickness of oil and gas pipes in the course of their operation developed devices (thickness meter) using a variety of physical phenomena. Greatest precision measurements provide electromagnetic-acoustic (EMA) thickness meter, using the principle of measuring the time of the ultrasonic pulse generated by the radio pulse through the metal. Radio pulse source with converter radio pulse in the acoustic pulse is placed in a one surface, and recorder with converter acoustic pulse in the radio pulse the signal repeatedly reflected from the other surface (Fig. 1). The thickness of the metal can determine the time delay of the first reflected signal, or a time interval between two neighboring echoes.

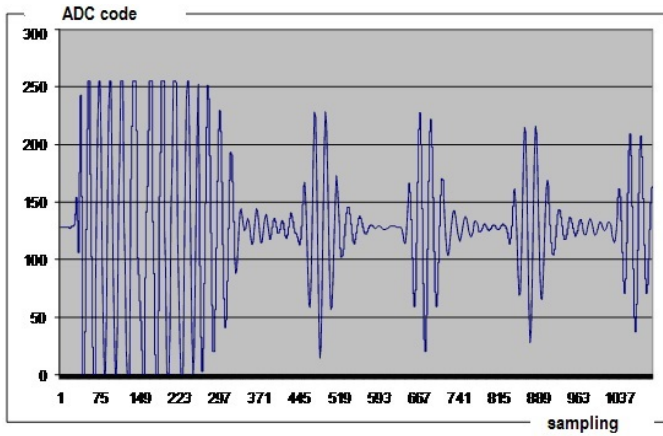


Fig. 1. Echo-signal of EMA-thicknessmeter, registered by the ADC

If metal is corroded the reflected signal is noised (Fig. 2), accuracy of timing and accuracy of thickness measurement is reduces.

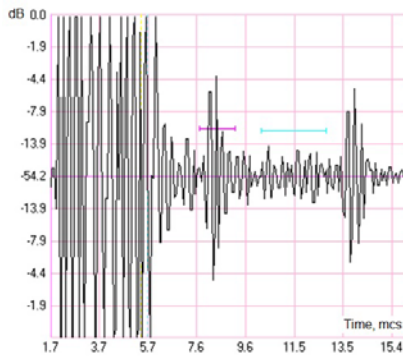


Fig. 2. Echo-signal of EMA-thicknessmeter when metal is corroded.

An alternative known method of determining the time intervals between radio pulses that provides greater accuracy of measurement is based on the using of the autocorrelation function (ACF) of the reflected signal (Fig. 3).

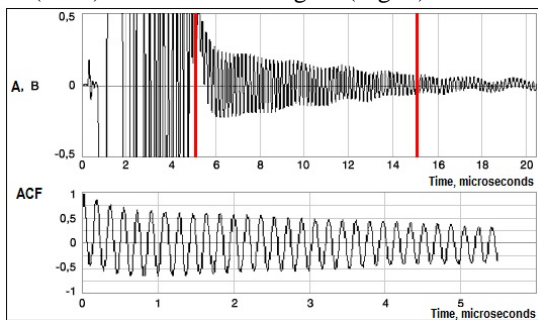


Fig. 3. Typical implementation of informative signal and its autocorrelation function.

The using of ACF allows greatly improve the signal / noise ratio, and the ACF of a periodic function is also a periodic function having the same period. In this case, the measured parameter is the duration of the period of ACF. To calculate the length of the period conventionally used one of two methods: counting the number of periods of the signal in a time window of fixed duration or a fast Fourier transform (FFT).

Using the traditional approach based on determining the number of periods ACF fixed time window or determining the FFT does not provide a accurate value of the interval between the autocorrelation peaks and, therefore, between two adjacent reflected signals as the number of cycles can not be taken sufficiently large (maximum 30, as shown on Fig. 3) because reflected signals amplitudes are decreases and number of periods in the fixed time window may be non-integral. This generates an error in determining the number of periods. General error in determining the number of periods occurs because the presence of fluctuating and quantization noise.

Since waveforms ACF is known , it gives the opportunity to create reference signals in a neighborhood of the expected frequency of ACF . In the absence of noise you can find the length of the period or frequency of ACF, producing a correlation comparison with the reference signal, the frequency of the reference signal to pick up the condition, when the maximum of the correlation function is equal to unity. However, a maximum of the correlation function decreases both the frequency difference of ACF and the reference signal and at the coincidence frequency , but because the presence of noise. Therefore, in such a way it's impossible precisely determine the frequency of a noisy ACF.

IV. NEW MULTI-STAGE ALGORITHMS FOR DSP OF NOISY SIGNALS

We propose new *approximation-correlation multi-stage* (ACM) methods of digital short noisy signals processing developed by the author of the paper, and described in [2-4]. ACM method represent an unconventional combination of cross-correlation, autocorrelation, the approximations, oversampling in the iterative process of calculations provide a significant increase in the accuracy of determining the parameters of noisy short signals. ACM provides several times higher accuracy of the frequency and time offset determination of short signals.

The idea of the ACM of digital processing in this case is in calculation of correlation coefficients with several reference signals in a small neighborhood of the estimated time shift signal, spline-approximation and oversampling, finding the maximum of correlation coefficients function. Position of the maximum of the correlation coefficient function is taken as the corrected value of time shift signal. Function, constructed in this way, has the form of a parabola for not-noisy (Fig. 4a) and noisy signal (Fig. 4b).

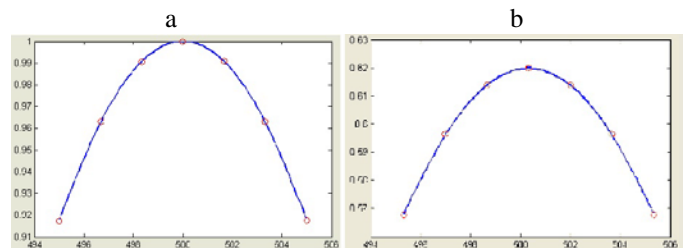


Fig. 4. The dependence of the correlation coefficient of the time shift for signal without noise (a) and when a signal / noise ratio of 2/1 (b).

The precise value of the shift in Fig. 4 is 500. The calculated value of the time shift is 499.998 (a) and 500.327 (b). Approximation is made in MATLAB using the spline approximation function *spaps*.

It allows to determine the time shift more exactly. For noised signal correlation coefficient function is maintained, the absolute value of the maximum reduces only.

Accuracy of calculating the value of the time shift of the echo signal will be higher if the initial approximation will be closer to the true value. Therefore, the proposed algorithm uses iterative calculation, at each stage of iteration as the initial approximation used refined value of the time shift obtained in the previous step. As a first approximation takes time shift determined by the maximum of amplitude of signal.

Brief description of the algorithm are:

1) Getting a numeric array of the reflected signal $X [i]$, $i = 0, \dots n$.

2) Identification of the item number j_{max} a numerical array, corresponding to the maximum value of X . Value found j_{max} corresponds to the approximate value of the center of the reflected signal;

3) Creating $2k + 1$ standard numeric arrays in the form of appropriate probing signals j_{max} by the amount $j_{max} * (s/k-1) * b$, where $s = 0, 1, 2, \dots 2k$, $b = 0 \dots 1$, the value b is set in view of possible error in the approximate value of the time shift. For example, $b = 0.1$, when the estimation error of the approximate value of the time shift does not exceed 10%.

4) Calculation of correlation coefficients numeric array of the reflected signal with all the reference and the formation of a numeric array of correlation coefficients $R [m]$, where $m = j_{max} + j_{max} * (s/k-1) * b$.

5) Approximation for the array $R [m]$ (Finding continuous functional dependence $F(m)$, corresponding to an array $R [m]$).

6) Oversampling, based on the found the functional relationship $F (m)$ for the array $R [m]$ with the number of elements in array r times, i.e. formation $Rl [m_l]$, where $m_l = j_{max} + j_{max} * (s_l / (k * r) - 1) * b$, $s_l = 0, 1, 2, \dots 2k * r$, r - oversampling ratio.

7) Finding the value of m_{lmax} is equivalent to the maximum value of R_l . M_{lmax} value will represent a real number to be determined (in general non-integral) value of the reflected signal center (or, equivalently, the time delay of the reflected signal from the center of the center of the probe signal)

8) Calculation of the difference $err = m_{lmax} - j_{max}$.

9) If $err < err_{acceptable}$, then $j_{max} = m_{lmax}$, $b = b/2$ and go to step 3, else go to step 10.

10) The output value found time shift of the reflected signal relative to the probe $T = m_{lmax} * dt$ where dt - discrete step in time in the measurement of the reflected signal.

Accuracy of the calculation of frequency using the proposed algorithm depends on the values of k and r , and the higher than they are. However, if the analyzed signal is noisy, its significant increase occurs during the growth of k and r only up to a certain limit. In particular, if the signal / noise ratio $> 2/1$, best choice for precision / time analysis criteria is $k = 3$

and $r = 10$. The number of iterations to calculate the time delay at a predetermined accuracy by the above algorithm depends on how close to the actual delay will be an initial approximation.

V. THEORETICAL EVALUATION OF ACCURACY OF NEW MULTI-STAGE ALGORITHMS

Known mathematical expression for the correlation coefficient of two signals, one of which is noised, given in [1] and obtained in some constraints on the properties of the signal and noise.

Specifically, when the solution detection signal from the noise background using autocorrelations suggest that the signal $p (t)$ and noise $b (t)$ are centered, i.e. their average value is zero. Autocorrelation function is computed as:

$$C_{xx}(\tau) = \lim_{T \rightarrow \infty} \frac{1}{T} \int_0^T [p(t) + b(t)][p(t-\tau) + b(t-\tau)] dt, \quad (t \rightarrow \infty)$$

By the distributive property of the correlation operator

$$C_{xx}(\tau) = C_{pp}(\tau) + C_{bb}(\tau) + C_{pb}(\tau) + C_{bp}(\tau)$$

It is believed that the noise $b (t)$ and the signal $p (t)$ are independent. Under this condition, the correlation function $C_{pb}(\tau)$ and $C_{bp}(\tau)$ identically zero (up error estimates due to the finite time integration). The autocorrelation function of the

noise $C_{bb}(\tau)$ tends to zero with increasing τ , Therefore, for sufficiently large values of τ value $C_{bb}(\tau)$ practically zero and the final expression can be written as:

$$C_{xx}(\tau) = C_{pp}(\tau)$$

or more precisely

$$C_{xx}(\tau) = C_{pp}(\tau) + \varepsilon(\tau)$$

However, for the short signals modulated in amplitude and having a non-integer number of periods, these expressions are not sufficiently accurate due to the finite time of integration. Calculation error given by the expressions will be greater, the smaller the integration time, and it is this characteristic of short signals.

When considering the problem of detection of a periodic noisy signal with a known period proceed as follows.

It is suggested that the main period T_l of signal is known. Considered the cross-correlation signal $x (t) = p (t) + b (t)$ an auxiliary signal $P (t)$, the main period of which is also equal to T_l

$$C_{xP}(\tau) = \lim_{T \rightarrow \infty} \frac{1}{T} \int_0^T [p(t) + b(t)]P(t-\tau) dt$$

or

$$C_{xP}(\tau) = C_{pP}(\tau) + C_{bP}(\tau)$$

Since the function $P (t)$ and $b (t)$ independent, then the function $C_{bP}(\tau)$ zero (up to estimation error), and hence arrive at the expression:

$$C_{xP}(\tau) = C_{pP}(\tau)$$

The cross-correlation function $C_{pP}(\tau)$ of two periodic signals with the same period T_l is also periodic with the same

fundamental period. Error estimates for this dependence depends on the integration time and will increase with time decreases.

However, these limitations and assumptions are often impractical, especially in digital short signals processing such as spectrometers signals, electromagnetic acoustic signals of thickness meters, satellite radar signals. For the correlation analysis of the signals are required to obtain other analytical descriptions, derivation of which is made by the author of the paper and is provided below.

Covariance coefficient k_{cov} and correlation coefficient k_{cor} of two harmonic signals having the same frequency and duration but different time shift are:

$$k_{cov} = \frac{1}{T} \int_0^T x(t) * y(t - \Delta t) dt = \frac{1}{T} \int_0^T \sin\left(\frac{2\pi m t}{T}\right) * \sin\left(\frac{2\pi m(t - \Delta t)}{T}\right) dt$$

$$k_{cor} = \frac{k_{cov}}{\sqrt{\sigma_x^2 * \sigma_y^2}},$$

where

$$\sigma_x^2 = \frac{1}{T} \int_0^T \sin^2\left(\frac{2\pi m t}{T}\right) dt; \quad \sigma_y^2 = \frac{1}{T} \int_0^T \sin^2\left(\frac{2\pi m(t - \Delta t)}{T}\right) dt.$$

Function

$$k_{cor} = k_{cor}\left(\frac{\Delta t}{T}\right)$$

can be adequately approximated by a parabola of order 6, facing top up and its maximum value is equal to 1 (Fig. 4a). If the second signal is noisy, the kind of cross-correlation functions of the coefficients will be the same (Fig. 4b) and can be calculated as:

$$k_{cov2} = \frac{1}{T} \int_0^T x(t)(y(t - \Delta t) + \xi(t)) dt = \frac{1}{T} \int_0^T \sin\left(\frac{2\pi m t}{T}\right) \left(\sin\left(\frac{2\pi m(t - \Delta t)}{T}\right) + \xi(t)\right) dt =$$

$$= k_{cov} + \frac{1}{T} \int_0^T \sin\left(\frac{2\pi m t}{T}\right) \xi(t) dt = k_{cov} + \xi(\theta) \frac{1}{T} \int_0^T \sin\left(\frac{2\pi m t}{T}\right) dt, \quad \text{где } 0 < \theta < T$$

because by the mean value theorem

$$\int_a^b f(x)g(x)dx = f(\theta) \int_a^b g(x)dx \quad a < \theta < b$$

If n is integer, then

$$\int_0^T \sin\left(\frac{2\pi m t}{T}\right) dt = -\frac{T}{2\pi m} \cos\left(\frac{2\pi m t}{T}\right) \Big|_0^T = -\frac{T}{2\pi m} (1 - 1) = 0$$

hence $k_{cov2} = k_{cov}$.

Cross-correlation function will be:

$$k_{cor2} = \frac{k_{cov2}}{\sqrt{\sigma_{x2}^2 * \sigma_{y2}^2}} = \frac{k_{cov}}{\sqrt{\sigma_x^2 * \sigma_y^2}}$$

$$\sigma_{y2}^2 = \frac{1}{T} \int_0^T \left(\sin^2\left(\frac{2\pi m(t - \Delta t)}{T}\right) + \xi^2(t)\right) dt =$$

$$= \frac{1}{T} \left\{ \int_0^T \left[\sin^2\left(\frac{2\pi m(t - \Delta t)}{T}\right) + 2\sin\left(\frac{2\pi m(t - \Delta t)}{T}\right) * \xi(t) + \xi^2(t)\right] dt \right\} =$$

$$= \sigma_y^2 + \frac{2}{T} \int_0^T \sin\left(\frac{2\pi m(t - \Delta t)}{T}\right) * \xi(t) dt + \frac{1}{T} \int_0^T \xi^2(t) dt$$

Applying the mean value theorem to the second term, we find that for the case when n - integer, the second term is zero.

We define $\xi_1(t)$ as the part of a standard deviation (std) equal to 1 and $\xi(t) = A\xi_1(t)$, then obtain

$$\frac{1}{T} \int_0^T \xi^2(t) dt = A^2$$

wherein A - noise deviation expressed as a fraction, i.e. $A = \sigma_{noise}$.

More precisely, the integral of the square of the noise or, equivalently, the auto covariance function of the noise is random and is characterized by the expectation, standard deviation and confidence interval for a given confidence level.

Below are the results of the quantitative calculation of these characteristics at a confidence level of 0.95 and the histogram distributions.

In [2] shows that:

$$MO_{k_{cov noise}} = \sigma_{noise}^2; \quad \sigma_{k_{cov noise}} = 0.02\sigma_{noise}^2$$

As a result, we obtain

$$k_{corr2} = \frac{k_{cov}}{\sqrt{\sigma_x^2 * (\sigma_y^2 + \sigma_{noise}^2)}} = \frac{k_{cov}}{\sqrt{\sigma_x^2 \sigma_y^2 + \sigma_x^2 \sigma_{noise}^2}}$$

And from here:

$$\frac{k_{corr}}{k_{corr2}} = \sqrt{\frac{\sigma_x^2 \sigma_y^2 + \sigma_x^2 \sigma_{noise}^2}{\sigma_x^2 \sigma_y^2}} = \sqrt{1 + \frac{\sigma_{noise}^2}{\sigma_y^2}}$$

and

$$k_{corr2} = \frac{k_{corr}}{\sqrt{1 + \frac{\sigma_{noise}^2}{\sigma_y^2}}}$$

It is shows that the maximum correlation coefficient of two harmonic signals, one of which is noisy with the same frequency and duration of the absence of a shift in time is less than unity and would decrease with increasing noise.

If the number of signal periods is not an integer, and the time shift is not zero, then the coefficient of cross-covariance k_{cov2} of noisy signal with not noisy signal will be different from zero:

$$k_{cov2} = k_{cov} + \xi(\theta) \frac{1}{T} \int_0^T \sin\left(\frac{2\pi m t}{T}\right) dt, \quad \text{где } 0 < \theta < T$$

$$\frac{1}{T} \int_0^T \sin\left(\frac{2\pi m t}{T}\right) dt = -\frac{1}{T} * \frac{T}{2\pi m} \cos\left(\frac{2\pi m t}{T}\right) \Big|_0^T =$$

$$= -\frac{1}{2\pi m} [\cos(2\pi m) - \cos(0)] = \frac{1}{2\pi m} [1 - \cos(2\pi m)]$$

Hence

$$k_{cov2} = k_{cov} + \xi(\theta) * \frac{1 - \cos(2\pi m)}{2\pi m}, \quad \text{где } 0 < \theta < T$$

The normalization divider $\sqrt{\sigma_{x2}^2 * \sigma_{y2}^2}$ will not be equal $\sqrt{\sigma_x^2 * (\sigma_y^2 + \sigma_{noise}^2)}$ as in the previous case, when the n - an integer, because expression σ_{y2}^2 will be:

$$\sigma_{y2}^2 = \sigma_y^2 + \frac{2}{T} \int_0^T \sin\left(\frac{2\pi m(t - \Delta t)}{T}\right) * \xi(t) dt + \frac{1}{T} \int_0^T \xi^2(t) dt$$

wherein the second member is not equal to zero:

$$\begin{aligned} & \frac{2}{T} \int_0^T \sin\left(\frac{2\pi m(t-\Delta t)}{T}\right) * \xi(t) dt = \xi(\theta) \frac{2}{T} \int_0^T \sin\left(\frac{2\pi m(t-\Delta t)}{T}\right) dt = \\ & = \xi(\theta) \frac{2}{T} \left[-\frac{T}{2\pi m} \cos\left(\frac{2\pi m(t-\Delta t)}{T}\right) \right] \Big|_0^T = \\ & = -\xi(\theta) * \frac{1}{\pi m} \left[\cos\left(\frac{2\pi m(T-\Delta t)}{T}\right) - \cos\left(\frac{2\pi m(-\Delta t)}{T}\right) \right] \end{aligned}$$

Using trigonometric transformations, we obtain:

$$\begin{aligned} \sigma_{y2}^2 &= \sigma_y^2 - \xi(\theta) * \frac{1}{\pi m} \left[\cos\left(\frac{2\pi m\Delta t}{T}\right) - \cos\left(\frac{2\pi m(-\Delta t)}{T}\right) \right] + \sigma_{noise}^2 = \\ &= \sigma_y^2 + \xi(\theta) * \frac{2}{\pi m} \cos\left(\frac{2\pi m\Delta t}{T}\right) + \sigma_{noise}^2 \end{aligned}$$

and

$$k_{cor2} = \frac{k_{cov} + \xi(\theta) \frac{1 - \cos(2\pi m)}{2\pi m}}{\sqrt{\sigma_x^2 * (\sigma_y^2 + \xi(\theta) * \frac{2}{\pi m} \cos\left(\frac{2\pi m\Delta t}{T}\right) + \sigma_{noise}^2)}}$$

This is based on the correlation of comparison in the simulation to calculate the final amounts corresponding integrals:

- the product of a harmonic signal and noise (computation of the cross-covariance of the harmonic signal and noise);
- harmonic signal with integral and non-integral number of periods;
- square of noise.

We introduce the notation:

$$I_1 = k_{cov} = \frac{1}{T} \int_0^T \sin\left(\frac{2\pi m t}{T}\right) * \sin\left(\frac{2\pi m(t-\Delta t)}{T}\right) dt,$$

$$I_2 = \frac{1}{T} \int_0^T \sin\left(\frac{2\pi m t}{T}\right) dt, \quad I_3 = \sigma_{x2}^2 = \sigma_x^2 = \frac{1}{T} \int_0^T \sin^2\left(\frac{2\pi m t}{T}\right) dt,$$

$$I_4 = \sigma_y^2 = \frac{1}{T} \int_0^T \sin^2\left(\frac{2\pi m(t-\Delta t)}{T}\right) dt,$$

$$I_5 = \frac{1}{T} \int_0^T \sin\left(\frac{2\pi m(t-\Delta t)}{T}\right) dt, \quad I_6 = \frac{1}{T} \int_0^T \xi^2(t) dt.$$

In this notation, the final expression for the correlation coefficient of two time-shifted harmonic signals, one of which is noisy, can be written as:

$$k_{cor2} = \frac{I_1 + \xi(\theta_1) I_2}{\sqrt{I_3 * (I_4 + 2\xi(\theta_2) * I_5 + I_6)}},$$

where $\theta_1 \in [0, T]$, $\theta_2 \in [0, T]$.

The numerator of this expression, as mentioned earlier, represents a coefficient of the covariance of two harmonic signals, one of which is shifted in time and noisy. It is of interest to investigate the level of the random component of the error in determining the coefficient covariance. Obviously, the ratio I_2 / I_1 represents the attenuation (or amplification) as a function of the noise covariance coefficients compared to noise in the original signal.

The I_2 / I_1 depends on the number of signal periods from the time shift does not depend on the noise level. Below in Fig. 5 shows graphs of these dependencies.

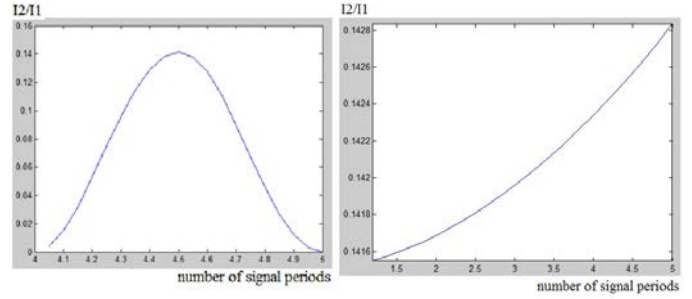


Fig. 5. The dependence of I_2 / I_1 from the number of signal periods, the noise level $A=0.1$.

From these results it follows that the maximum value of the ratio I_2 / I_1 is 0.2. We now show that the maximum value of covariance and correlation coefficient of the two harmonic signals one of which is shifted in time and noised and will be achieved when the value of the time shift is zero.

The dependence of the correlation coefficient on the mismatch between the harmonic signals in time and position of the maximum score of this dependence we obtained analytically in a continuous form for the original signal x and the reference signal y :

$$x = \sin\left(\frac{2\pi m t}{T}\right) \quad u \quad y = \sin\left(\frac{2\pi m(t-\Delta t)}{T}\right),$$

having the same number of periods n in the observation interval T and different time offset.

Correlation coefficient r , as it is known, is calculated as the ratio of the covariance k_{xy} to the normalizing factor:

$$r = \frac{k_{xy}}{\sqrt{\sigma_x^2 * \sigma_y^2}}.$$

The final expression for the correlation coefficient r will be:

$$r = \frac{\frac{1}{2} (\cos(2\pi m \delta) - \frac{\sin(2\pi m(2-\delta))}{4\pi m} - \frac{\sin(2\pi m \delta)}{4\pi m})}{\sqrt{\frac{1}{2} (1 - \frac{\sin(4\pi m)}{4\pi m}) * \frac{1}{2} (1 - \frac{\sin(4\pi m(1-\delta))}{4\pi m} + \frac{\sin(4\pi m \delta)}{4\pi m})}}.$$

It is this dependence as a result of the approximation has the form of a parabola of order 6, facing top up receiving the maximum value for $\delta=0$ for any (integer and non-integer) values of n .

At $|\delta| < 0.1$ the denominator is approximately equal to $1/2$ and expression can be written as

$$r = \cos(2\pi m \delta) - \frac{\sin(2\pi m(2-\delta))}{4\pi m} - \frac{\sin(2\pi m \delta)}{4\pi m}.$$

In order to find analytically the position of the maximum, it is necessary to calculate the first derivative of the last expression and equate it to zero:

$$\begin{aligned} \frac{dr}{d\delta} &= -\sin(2\pi m \delta) * 2\pi m - \frac{1}{4\pi m} \cos(2\pi m(2-\delta)) * (-2\pi m) - \frac{1}{4\pi m} \cos(2\pi m \delta) * 2\pi m = \\ &= -2\pi m * \sin(2\pi m \delta) + \frac{1}{2} \cos(2\pi m(2-\delta)) - \frac{1}{2} \cos(2\pi m \delta) = 0. \end{aligned}$$

The solution of a trigonometric equation also leads to $\delta=0$ for any (integer and non-integer) values of n , which proves obtain the exact value of the time shift of radar echoes the proposed method.

The above analytical expressions allow to quantify the expected error in determining the time delay of the reflected radar signal by the proposed method.

We have developed and registered in the Patent Office of the Russian Federation a few programs implementing the proposed method in the environment of MATLAB. For the practical use of the new method we have developed a program in C++, as described in [5]. Implementation in C++ makes it possible to transfer the program to the microcontroller or digital signal processor that allows you to create portable digital EMA-precision thickness meter.

Function of the correlation coefficients and spline approximation required in the software implementation method of measuring the time delay of the radio pulse in the standard C++ libraries are missing, so the correlation coefficients are calculated in the program on the above formulas, spline-interpolation (that we used instead of spline approximation) is implemented according to [6].

Work program has been tested using normalized to the maximum amplitude of the signal model, similar in form to the real signal EMA-thickness meter. To simulate normally distributed noise we used Mersenne Twister [7] - a pseudorandom number generator, from the library of random standard C++11, the compiler supports Microsoft Visual C++ 11.0.

The proposed method has been implemented in Visual Studio 2012 as a dynamic library in C++. To implement a GUI application type has been selected Windows Store Application, available in Windows 8, and the language C#. This allows you to use application designed for different types of devices (desktop, laptop, tablet, etc.) and for different processor architectures (x86, x64, ARM) without changing the source code. Software of ACM method we have published in Internet:

- <http://apps.microsoft.com/windows/ru-RU/app/delaymeter/d9dc0b12-b88f-4000-985a-1b9856b149e0>
- <http://apps.microsoft.com/windows/ru-RU/app/freqmeter/de835b11-ea5e-429e-bba6-28939fa3dc1b>

To estimate the measurement uncertainty and delay with the proposed traditional methods was conducted 100 tests for each RMS noise from 0.0 to 0.2 in increments of 0.04. The results of evaluation of the relative error given in Table 1 and in Fig. 6.

1. Estimates of errors in determining the time delay of the reflected radar signal and the proposed ACM methods and traditional method.

RMSE of original signal	Sample mean of relative error, %		Sample variance of relative error, %	
	Traditional method	ACM method	Traditional method	ACM method
0.00	0.000	0.000	0.000	0.000
0.04	0.094	0.019	0.062	0.004
0.08	0.186	0.024	0.175	0.005
0.12	0.276	0.041	0.274	0.013
0.16	0.312	0.054	0.389	0.016
0.20	0.326	0.060	0.500	0.019

Using this program in EMA-thickness meter will greatly increase the accuracy of measuring the thickness of the metal,

and the use of Windows 8 operating system - to create a graphical interface, that allows you to create a compact low-cost systems for measuring the thickness of the metal-based tablet PCs, and USB - data acquisition and digital processing devices, suitable for use in the field conditions.

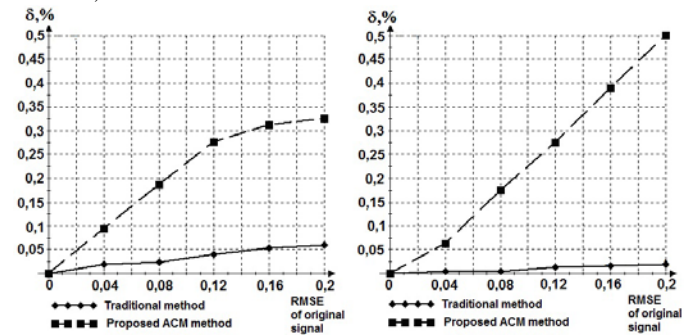


Fig. 6. Sample mean relative error (A) and the sample variance of the relative error (B) measuring the time delay of the radar signals.

We have also developed a hardware implementation of the proposed methods based on a digital signal processor. To simplify the hardware implementation instead of FFT is used the DFT, instead of spline approximation is used Lagrange interpolation polynomial, as a criterion of proximity of two harmonic signals is factor covariance, instead of harmonic reference signals, the signals of rectangular shape.

VI. CONCLUSION

1. New classification level for DSP algorithms: single-stage and *multi-stage algorithms*.
2. New characteristics of DSP algorithms: anti-noise *power of DSP algorithm*.
3. A new approach to the theoretical analysis of the achievable accuracy of determining the parameters of short noisy signals.
4. A new multi-stage methods for precise determination of the frequency and time delay of short noisy signals, that improve the accuracy in comparison with the traditional approaches several times. The methods are protected by Russian Federation patents.
5. Software and hardware realization of our new multi-stage methods.

REFERENCES

- [1] J. Max, "Methodes et techniques de traitement du signal et applications aux mesures physiques," Tome 1, Masson, Paris, 1981.
- [2] V. S. Tutygin, Digital processing of short signals (Monography style). Polytechnical university publisher, SPb, 2012.
- [3] V. S. Tutygin, Method of measuring of time interval between radiopulses. Russian Federation Patent No.2456632, 2011.
- [4] V. S. Tutygin, Method of measuring of signal frequency. Russian Federation Patent No. 2478213, 2012.
- [5] V. S. Tutygin, I. A. Pelkonen, K.S. Kirilenko "Method and software implementation of precision measuring the time delay radio impulse," Scientific and technical sheets *SPbSTU*, Series Informatics. Telecommunications. Control. Vol 3(174), 2013.
- [6] J. Forsythe, M. Malcolm, C. Moler. Computer methods of mathematical calculations. Moscow: Publishing House "Mir", 1980.
- [7] Mersenne Twister Engine - C++ Reference http://www.cplusplus.com/reference/random/mersenne_twister_engine/

Minimization of THD using evolutionary optimization methods for photovoltaic generation systems

Jorge Luis Diaz Rodriguez

Faculty of Engineering.
University of Pamplona.
Pamplona, Colombia.

E-mail: jdiazcu@gmail.com

Luis David Pabon

Faculty of Engineering.
University of Pamplona.
Pamplona, Colombia.

E-mail: davidpabon@hotmail.com

Aldo Pardo Garcia

Faculty of Engineering.
University of Pamplona.
Pamplona, Colombia.

E-mail: aapardo13@hotmail.com

Abstract— This paper presents an optimization of the electric power quality by designing a 9 steps multilevel power inverter, which adopts a multi-PWM optimized using genetic algorithms (GA), and minimizing Total Harmonic Distortion (THD) of the first 50 harmonics to about 0%. This optimization is considered an alternative technique because it reduces the expression used to quantify TDH numerically. Particularly for the 9 steps multilevel wave form, it reduces the number of power on-and-off angles as well as the position within the levels of the first quarter-wave modulation. The research involved developing a prototype for experimental verification.

Keywords— *Multilevel inverter, total harmonic distortion, genetic algorithm, PWM.*

I. INTRODUCTION

Power quality in photovoltaic (PV) systems depends on the power inverter [1], which is responsible for making a DC / AC conversion, and solar panels generate DC voltage component and conversion is needed to ac for use energy or connect to the network [2]. However, conventional power inverters have some quality problems due to harmonic distortion [3], [4]. To be able to solve this problem, it has been suggested to use multilevel inverters [5], [6] which have lower harmonic content than conventional inverters regarding the output voltage [7], [8]. This research found harmonic content optimization of PV systems through evolutionary techniques using a two-steps multilevel power inverter -for economic reasons- and with the highest number of steps in the output, for this case the number of steps will be nine using cascaded H bridge multilevel inverter with common source topology [9], [10].

II. STATE OF THE ART

The first multilevel inverter was presented by Baker and Lawrence in 1975 [11], called the serial inverter cascade H-bridge topology, in the year 1981 the first multilevel inverter was implemented in three steps through clamping diodes [12], based on this patent and this work it has been generated a variety of researches seeking to optimize and improve the multilevel inverter system [13], one of these proposals is to

use a single voltage source directly accompanied by transformers at the output of the H bridge, this topology is the cascaded multilevel inverter H bridge with common source [14]. This configuration is very suitable due to its low cost, renewable energy applications because there is a single power supply for the entire system, however, using output transformers can create problems such as disruption of the waveform and the system becomes more complex [14], [15]. In this research a prototype has been designed based on a methodology proposed by the authors to improve the transformers response in this application [16]; the improvement was shown in the results.

Regarding multilevel inverters modulation, specifically talking about harmonic content optimization, it has been suggested several techniques depending on the topology being used, the specific objective and the way of searching the best point [8], [17]-[22], nevertheless, there are promising strategies in the field of evolutionary algorithms such as *Particles Swarm Optimization* (PSO), [23], [24] and *Genetic Algorithms* (GA) [9], [20], [25], for which it has been compared with the common techniques, some of this research has concluded that genetic algorithms gets better results [26], this way, the technique used in this research are genetic algorithms justified in the numeric character of the optimization.

III. CASCADE MULTILEVEL INVERTER

In figure 1 it shown the general scheme of a *Cascade H bridges Multilevel Inverter* (CMLI) is shown, where the basic performance is presented and in which the output waveform is constructed by adding the outputs of each H-bridge [12]. The CMLI topologies can be divided into two categories depending on the voltages that supply each bridge; therefore these can be symmetrical or asymmetrical. CMLI is symmetrical when all of them are equal; and asymmetric if the voltages are different, they are common relations 1:2 or 1:3.

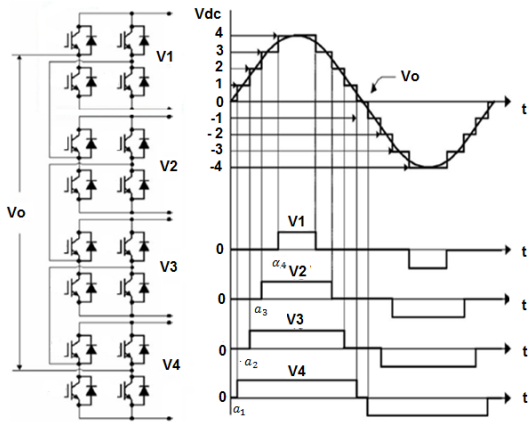


Fig. 1. Cascaded H bridge multilevel inverter, voltage output on the bridges and inverter.

In order to obtain the voltages for each bridge two topologies will be described, first, the independent sources in which all the bridges are powered autonomously (see Figure 2a) and second the common source topology, in the all bridges are powered by a single source where the potential difference and the electrical galvanic isolation is achieved by transformers (see figure 2.b). The figure 2 shows an example of asymmetric form topology with a ratio of 1:2. Both get the same output voltage waveform [10].

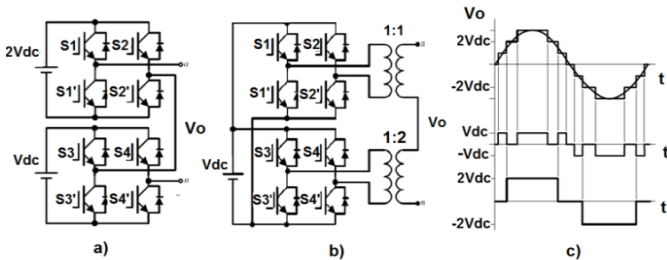


Fig. 2: Topologies of asymmetric cascade H bridges multilevel inverter. a) Independent source. b) Common Source. c) Output voltage.

A. Multilevel Inverter common source of three stages

The multilevel inverter topology selected for this work is the cascade multilevel H bridge inverter asymmetrical common source with 1:3 ratios of 2 steps, which generate 9 levels of output voltage.

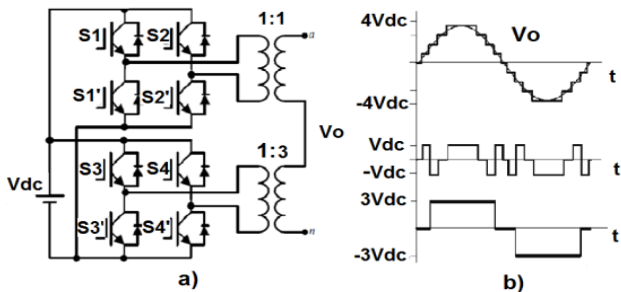


Fig. 3. Asymmetric Cascade Multilevel Inverter common source, two stages with 9 levels at the output, asymmetry 1:3. a) Topology. b) Output voltage.

This inverter allows with minimal H bridge stages (2 steps) to reach the maximum number of steps in the output voltage (9 steps). In fig. 3 shows how the selected topology and the generated voltage is observed.

IV. MATHEMATICAL MODELING

The waveform of a multi-modulation PWM to 9 steps is shown in Figure. 4.

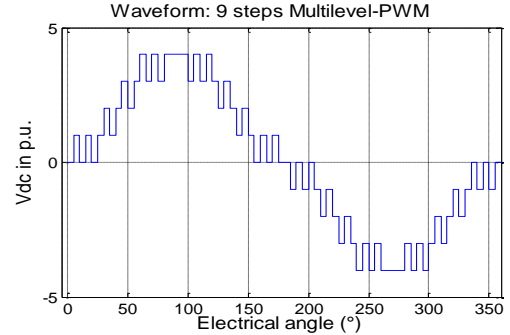


Fig. 4. Waveform output voltage PWM 9 steps.

In this research it was obtained an expression that quantifies the total harmonic distortion with reference to the number of switch angles on and off (firing angles) for each step. The modulation form has a 1/4 wave symmetry so it is necessary to define these angles in the first quarter-wave only (fig. 5); the remaining modulation was constructed by using trigonometric relationships. Thus, a vector $L = [x \ y \ z \ w]$ which represents the total number of firing angle is defined at each step. The Fourier series for periodic wave forms provides:

$$v(t) = \frac{a_0}{2} + \sum_{n=1}^{\alpha} (a_n \cos n\omega_0 t + b_n \sin n\omega_0 t) \tag{1}$$

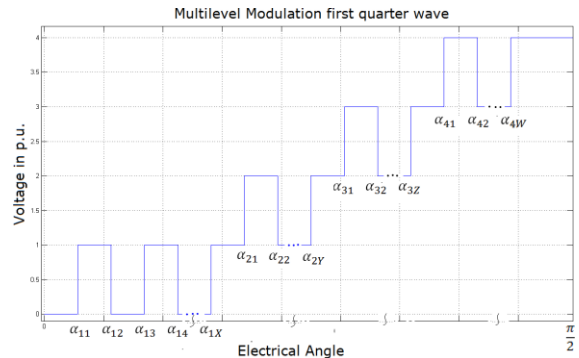


Fig. 5. Graphic of one quarter wave modulation regarding switch-on-and-off firing angles for each step.

Where, n is the harmonic number, ω the fundamental wave frequency, t the time, $a_0/2$ is the DC component, which is calculated by the expression:

$$a_0 = \frac{1}{2\pi} \int_0^{2\pi} v(\omega t) d(\omega t) \tag{2}$$

a_n coefficient of the Fourier series is calculated using (3):

$$a_n = \frac{1}{\pi} \int_0^{2\pi} v(\omega t) \cos n(\omega_0 t) d(\omega t) \quad (3)$$

b_n coefficient of the Fourier series, calculated by :

$$b_n = \frac{1}{\pi} \int_0^{2\pi} v(\omega t) \sin n(\omega_0 t) d(\omega t) \quad (4)$$

The waveform (Fig. 4) has odd symmetry and positive wave is equal to the negative, thus applying the symmetries of the theory of Fourier series.

$$a_0 = 0 \text{ y } a_n = 0 \quad (5)$$

Only be related coefficient with sinus, therefore, waveform in terms of the Fourier series will be expressed as follows:

$$v(t) = \sum_{n=1}^{\alpha} b_n \sin n\omega_0 t \quad (6)$$

b_n in terms of the vector L to the waveform :

$$b_n = \frac{4v_{cd}}{n\pi} \left[\sum_{i=1}^4 \sum_{j=1}^{L_i} (-1)^{j-1} \cos n\alpha_{ij} \right] \text{ for } n \text{ odd}; \quad (7)$$

and $b_n = 0$ for n pairs.

Where i is the number of stage (hence the summation is from 1 to 4), L_i component i of vector L and α_{ij} the angle j of stage i , and this can be on or off. To obtain a ladder components vector L must be odd. If the peak magnitude of the harmonic n , in the Fourier series is defined as:

$$h_n = \sqrt{a_n^2 + b_n^2} \quad (8)$$

Substituting (5) and (7) to (8) the peak magnitude of each harmonic n is obtained, when only exist odd harmonic because $b_n = 0$ if n is pair, so:

$$h_n = \frac{4v_{cd}}{n\pi} \left[\sum_{i=1}^4 \sum_{j=1}^{L_i} (-1)^{j-1} \cos n\alpha_{ij} \right] \text{ for } n = 1, 3, \dots, \quad (9)$$

The standard IEEE 519 in 1992 [27], defines the total harmonic distortion as using (10):

$$THD = \frac{\sqrt{\sum_{n=2}^{50} h_n^2}}{h_1} \cdot 100 \quad (10)$$

Where h_1 is the fundamental harmonic component and h_n peak harmonic n . Replacing (9) to (10):

$$THD = \frac{\sqrt{\sum_{n=2}^{50} \left[\frac{1}{n} \left(\sum_{i=1}^4 \sum_{j=1}^{L_i} (-1)^{j-1} \cos n\alpha_{ij} \right) \right]^2}}{\left(\sum_{i=1}^4 \sum_{j=1}^{L_i} (-1)^{j-1} \cos n\alpha_{ij} \right)} \cdot 100 \quad (11)$$

Where n takes only odd values and L_i components vector L = [x y z w]. Thus (11) defines the objective function to be minimized by the optimization algorithm.

V. OPTIMAZATION ALGORITHM

Using Matlab® and *Genetic Algorithm Toolbox* (GA), algorithms for the mathematical model of the fitness function (equation 11) and the corresponding optimization using genetic algorithms [28] were scheduled. The population size for the algorithm is taken from 20 individuals, each individual (X) formed by the total angle shot in the first quarter output voltage wave form:

$$X = [\alpha_{11} \alpha_{12} \dots \alpha_{1x} \alpha_{21} \alpha_{22} \dots \alpha_{2y} \alpha_{31} \dots \alpha_{3z} \alpha_{41} \dots \alpha_{4w}] \quad (12)$$

The vector L, program to evaluate the fitness function angles corresponding to each step (flowchart shown in Figure 6).

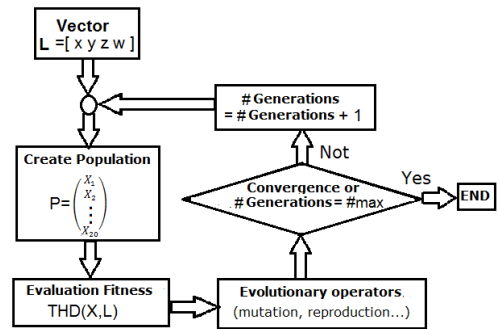


Fig. 6. Flowchart of the optimization genetic algorithm (GA).

The condition of algorithm was finished when the values of the population converge or because the number of generations reaches the maximum assigned.

A. Results

Figure 7 shows the evolution of the algorithm is shown below:

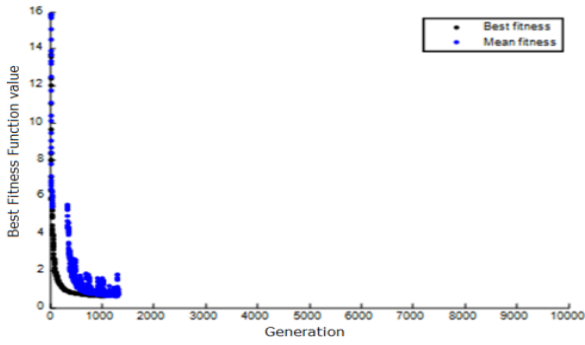


Fig. 7. Evolution of the genetic algorithm.

The modulation has found the following number vector angles in steps $L = [3 \ 5 \ 5 \ 11]$. The individual with better fitness is presented in Table I, corresponding to the vector L defined above.

TABLE I. ANGLES IN DEGREES OF THE BEST INDIVIDUALS.

x=3	y=5	z=5	w=11	
4.73702	19.02595	31.53636	53.98341	69.30872
7.04851	21.24552	33.92124	55.63071	70.78062
9.43937	23.98322	38.16271	59.44358	75.93116
	29.94251	41.60589	62.51731	76.61193
	31.53636	43.39352	65.04481	82.19461
				82.38271

The fitness for this individual, its THD, was calculated equal 0.2207 %. The output voltage waveforms of the modulation with these angles are shown in Fig. 8.

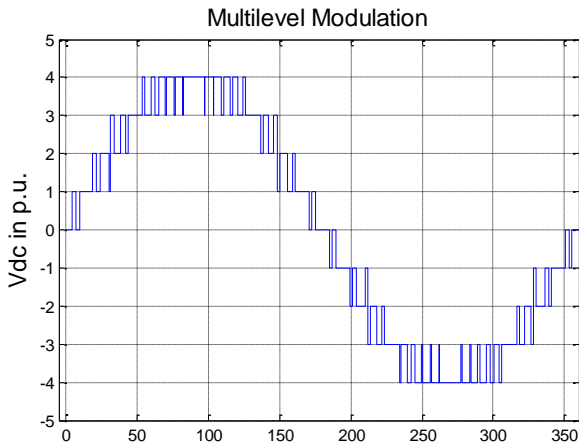


Fig. 8. The output voltage waveform optimized modulation.

VI. SIMULATION

The topology MLICH Bridge with common source described in Section III adopting found modulation was simulation using Simulink® Matlab® and using block Fast Fourier Transform (FFT) was obtained spectrum and the values of total harmonic content for different bands. The scheme of the simulation (Figure 9).

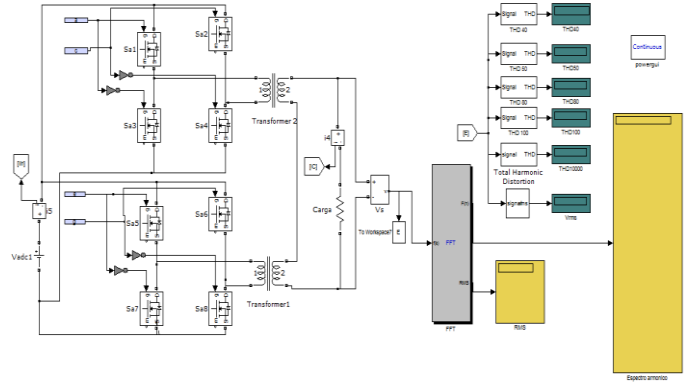


Fig 9. Simulink block diagram of the simulation inverter.

Figure 10 shows the waveform of the output voltage of the inverter and figure 11 the harmonic spectrum peak value, in this displacement of harmonic content is clearly observed at the higher harmonic frequencies 50, just as the y-axis (peak voltage) was expanded to observe the small presence at low frequencies, the maximum value the 15 harmonic (h15) contribution to 0.21V, insignificant value when compared to the 180 V of the fundamental component (h1).

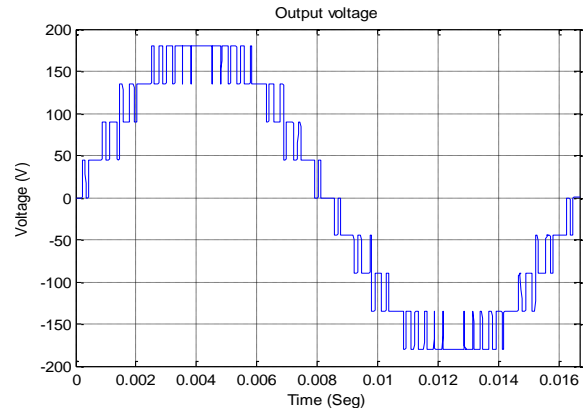


Fig. 10. Waveform output voltage inverter in the simulation.

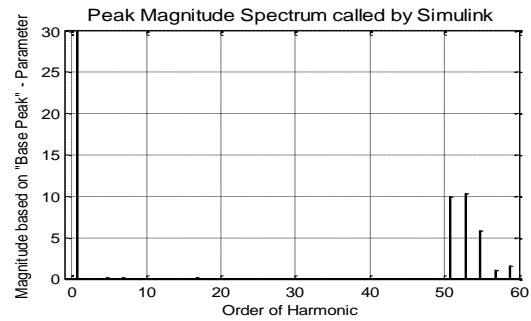


Fig. 11. Extending the spectrum of the output waveform (simulation).

The total harmonic distortion in the bands THDxx assessment (the number next to it indicates the harmonic THDv is evaluated), with the band THD50 defined for total harmonic distortion by the IEEE -519 1992, are summarized in table II.

TABLE II. THDV IN DIFFERENT BANDS EVALUATION.

%THD40	%THD50	%THD80
0.0	0.2207	11.16

Similarly values current were measured when the inverter fed a resistive load, the harmonic content to the component evaluated was $THDi\ 10\ 000 = 0.3\ \%$, when assessed in the side THD50i the value is zero.

VII. IMPLEMENTACION

To validate results was implemented a low-power prototype, based on the use of MOSFETs as switching devices topology. Inverter output is 120 VA nominal input voltage 24 Vdc, so they apply to low cost photovoltaic systems, in which only a battery block is accumulator has the nominal frequency 60 Hz, and nominal output voltage of 120 V rms. Drive control is performed only four signals necessary to control the upper MOSFETs of the bridges, the lower mosfet are controlled by the denial of the 4 signs of control and assigned died time was performed with hardware. The prototype was based on the use of FPGAXUPV5 - LX110T and final prototype in the dsPIC 30F4013. The transformer design, device critical in achieving waveform, it is raised according to an optimization proposed by the authors [16] that is to replace, in conventional methodologies transformer design , the equation:

$$\frac{N}{V_{rms}} = \frac{10^8}{2\pi \cdot f \cdot A [cm^2] \cdot B_{max} [Gauss]} \quad (13)$$

For equation

$$\frac{N}{V_p} = \frac{(\alpha_2 - \alpha_1) \cdot 10^8}{2\pi \cdot B_{max} [Gauss] \cdot A [cm^2]} \quad (14)$$

Where α_1 and α_2 are the angles that define the longer pulse input at transformer, or in the case because the initial and final angles of a pulse train that could saturate the transformer core. This improves the output waveform and reduces the load current of the transformer. In figure 12 shows the experimental prototype with FPGA.

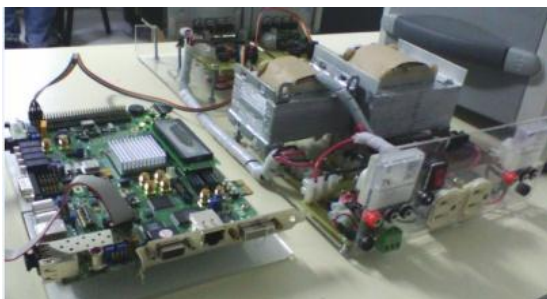


Fig. 12. Experimental prototype with FPGA.

VIII. EXPERIMENTAL TEST

In figure 16 assemblies was performed, shown equipment used in the tests. The output voltage and current of the inverter is evaluated through a system of acquisition and evaluation of power quality based on the acquisition card NI 6009 of the National Instruments with a sampling rate of 48Ks/s, evaluation software is programmed in Labview®, just as the data acquired voltage and current were processed in Matlab® Simulink® with FFT blocks. In both programs were evaluated harmonic contents, calculating the THD spectrum in the bands of 40, 50 , 80 and 100 first harmonics; THD50 being the most representative shown standardized by IEEE -519, 1992.

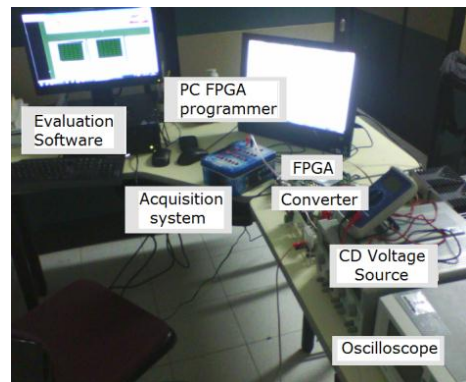


Fig. 13. Workstation with FPGA experimental tests.

Waveforms on the oscilloscope were observed and the rms values of current and voltage output test without load, with resistive load and inductive load is measured. In figure 14 a photograph of the shape of waves and Labview shown on the oscilloscope.



Fig. 14. Voltage on the oscilloscope and the evaluation system.

IX. RESULTS

The captured waveform Labview® for a test without load is shown in figure 15.

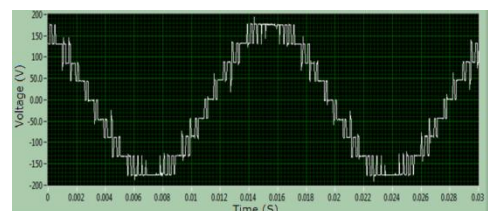


Fig. 15. Voltage to the inverter output in Labview®.

The value calculated by the peak magnitude in Labview® (until the component 80) with the captured data, to a fundamental frequency of 60Hz spectrum is shown in figure16 and the evaluation by the Matlab® given captured data as results the voltage waveform of figure 17.

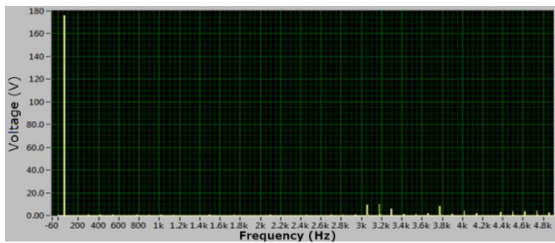


Fig. 16. Spectrum of the output voltage (Labview®).

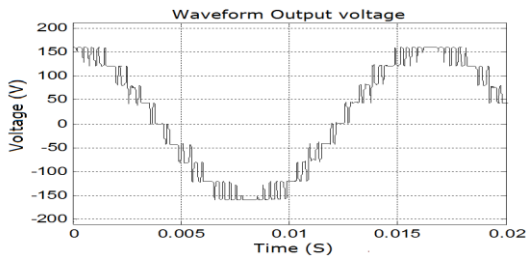


Fig. 17. Output voltage waveform of the inverter (Matlab®).

With the FFT block of Matlab® Simulink® for resistive load test the following spectrum was obtained.

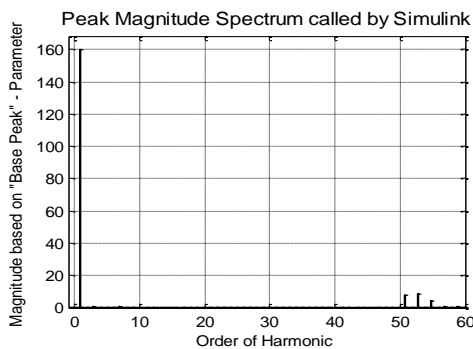


Fig 18. Spectrum of the output voltage in Matlab®.

Comparing the results of the two softwares used to assess the characteristics of harmonic content, it was observed that the behaviors are almost identical appearing on small differences, less 0.9%. Usually the harmonic content was always lower in Matlab® evaluation, and the minimum difference from Labview®. The result of the tests and evaluations in the different bands of THDs is shown in table III. The highest values that are delivered by the evaluation system were taken.

TABLE III. BANDS IN DIFFERENT EXPERIMENTAL THD.

Test	Vrms(V)	%THD40	%THD50	%THD80	%THD100
1	125.85	0.64	0.7062	11.26	12.17
2	115.89	0.925	0.96	10.49	11.2245
3	117.47	0.915	0.9448	11.3368	12.2567

Where: 1- Without load. 2 - with resistive load. 3- with inductive load.

The results validate the optimization performed in the range of 50 harmonics, appearing a THD = 0.96 % for the output voltage waveform. Similarly one can show that the behavior of the inverter is satisfactory, because although the calculated level is not reached, the THD is below 1 %, provided wide the standards proposed by the IEEE -519 standard 1992 set a limit

of 5 %. Finally in figure 19 inverter operation is evidenced in its finished prototype, with an accumulator block of a photovoltaic power low system.



Fig. 19. Inverter operating with the photovoltaic system.

X. CONCLUSIONS

Simulations validated that the calculated TDH expression defined by the IEEE 519, for a multi - modulation PWM nine steps, is correct, since the spectra and THD values match with those values in the simulation algorithm.

The optimization algorithm developed will be able to void all harmonic content defined between 2 and 50 if given a sufficient number of shooting angles, however, it may be possible to find modulations that are not likely to implement.

The optimized theoretical THD for this project is defined as 0.2207 % which is the harmonic content of the modulation harmonic, optimized up to the 50 harmonic, this being the upper bound of assessment established by the IEEE 519.

The inverter performance shows the presence of voltage waveforms corresponding to those calculated in the optimization algorithm, it validates the transformer design proposed for such applications, as well as the proposal to control the two-stages inverter with only four signals (2 for bridges), this was achieved by negating and allocation dead time for hardware, so it was possible to test, decreasing the software complexity and increasing performance.

From the experimental point of view the optimized THD, specifically for the voltage wave is defined as 0.96 % because this is the largest THD in the voltage waveform present in the harmonic modulation optimized up to the 50 harmonic.

To supply the in CHBMI with a photovoltaic power source system can significantly improve the power quality of these systems.

REFERENCES

- [1] Spertino, F.; Di Leo, P.; Corona, F.; Papandrea, F. "Inverters for grid connection of photovoltaic systems and power quality: Case studies" Power Electronics for Distributed Generation Systems (PEDG), 3rd IEEE Int. Symposium on Aalborg, June 2012, pp. 564 – 569.
- [2] Hassan, A. and Mohamed, C. "Robust Controller for Interleaved DC-DC Converters and Buck Inverter in Grid-Connected Photovoltaic Systems" (APPEEC), WSEAS Transactions on Power Systems Vol. 6, 2011. pp. 21-30.

- [3] Mohammad, S. Z.; Omar, A. N.; Andrahim, I. R. "A Review of Single-Phase Single Stage Inverter Topologies for Photovoltaic System". 4th Control and System Graduate Research Colloquium, Shah Alam, Malaysia, Vol. 19, N. 20, Aug. 2013, pp. 69-75.
- [4] Mehmet, Y.; Seydi, V.; Seci, V. and Hasan, C. "Comparison of Output Current Harmonics of Voltage Source Inverter used Different PWM Control Techniques". WSEAS Transactions on Power Systems Volume 3, 2008. pp. 696-703.
- [5] Karuppanan P. and Kamalakanta M. "PI, PID and Fuzzy Logic Controlled Cascaded Voltage Source Inverter based Active Filter for Power Line Conditioners" WSEAS Transactions on Power Systems Vol. 6, 2011 pp. 100-109.
- [6] Longhua, Z.; Qing, F.; Xiangfeng, L.; y Changshu L. "A novel photovoltaic grid-connected power conditioner employing hybrid multilevel inverter" Sustainable Power Generation and Supply, SUPERGEN '09. International Conference on Nanjing, 2009, pp. 1-7.
- [7] Rodriguez, J.; Jih-Sheng Lai; Fang ZhengPeng. "Multilevel inverters: a survey of topologies, controls, and applications". IEEE Trans. on Ind. Elect., Vol. 49, N. 4, 2002, pp. 724- 738.
- [8] Rahim N.; Krismadinata; Wooi, H.; Selvaraj, J. "Elimination of Harmonics in Photovoltaic Seven-level Inverter with Newton-Raphson Optimization", Procedia Environmental Sciences, Volume 17, 2013, pp. 519-528.
- [9] Debnath, S and Narayan, R. "THD Optimization in 13 level photovoltaic inverter using Genetic Algorithm". International Journal of Engineering Research and Applications. Vol. 2, Issue 3, May-Jun 2012, pp. 385-389.
- [10] Ríos, F. and Dixon J. Diseño y construcción de un inversor trifásico multinivel. Trabajo de Grado, Pontificia Universidad Católica de Chile, Santiago de Chile, 2003.
- [11] Baker R. H. and Lawrence H. B. Electric Power Converter, US. Patent Number: 3,867,643, 1975.
- [12] Nabae, A. , Takahashi, I. y H. Akagi. "A new neutral point clamped PWM inverter", IEEE Trans. Ins. Appl., vol. IA-17, N. 5, pp.518-523, Sep-Oct 1981.
- [13] Malinowski, M.; Gopakumar, K.; Rodriguez, J. and Pérez, M. "A Survey on Cascaded Multilevel Inverters", IEEE Trans. on Ind. Elect., Vol. 57, N. 7, July 2010, pp. 2197-2206.
- [14] Panda, A. K. and Suresh, Y. "Research on cascade multilevel inverter with single DC source by using three-phase transformers". Int. Journal of Electrical Power & Energy Systems, Vol. 40, N. 1, 2012, pp. 9-20.
- [15] Banaei, M. R.; Khounjahan H. y Salary, E. "Single-source cascaded transformers multilevel inverter with reduced number of switches". IET Power Electron, Vol. 5, N. 9., 2012, pp. 1748- 1753.
- [16] Diaz R., J. L.; Pabón, L. D.; and Caicedo, A. "Optimization to improve power quality in the design of transformers for power multilevel inverters". Universidad de Pamplona, 2014.
- [17] Govindaraju, C. and Baskaran, K. "Performance Improvement of Multiphase multilevel Inverter Using Hybrid Carrier Based Space Vector Modulation". International Journal on Electrical Engineering and Informatics - Vol. 2, N. 2, 2010.
- [18] Karuppanan, P. and Mahapatra, K. "FPGA based cascaded multilevel pulse width modulation for single phase inverter," Environment and Electrical Engineering (EEEEIC), 2010 9th International Conference on, Vol. 16, N. 19, Mayo 2010, pp. 273-276.
- [19] Al-Judi, A.; Bierk, H. and Nowicki, E., "Selective harmonic power optimization in multilevel inverter output" Vehicle Power and Propulsion Conference (VPPC), Vol. 6, N. 9, Sept. 2011, pp. 1-5.
- [20] Periasamy, M. and Shankar, M. "Harmonic optimization of cascade multilevel Inverter with unequal DC sources using genetic algorithm". International Journal of Engineering Research & Technology, Vol. 1, N. 6, August, 2012.
- [21] Mathew, M. "THD Reduction in Multilevel Inverters Using Real-Time Algorithm". Journal of Computer Engineering, Vol. 8, N. 2, Nov.-Dec. 2012, pp. 1-12.
- [22] Yousefpoor, N.; Fathi, S.H.; Farokhnia, N. and Abyaneh, H.A., "THD Minimization Applied Directly on the Line-to-Line Voltage of Multilevel Inverters," IEEE Transactions on Ind. Elect., Vol. 59, No.1, Jan. 2012, pp. 373-380.
- [23] Narayan, R.; Chatterjee, D. and Kumar, S. "A PSO based optimal switching technique for voltage harmonic reduction of multilevel inverter", Expert Systems with Applications, Vol. 37, N. 12, Dec. 2010, pp. 7796-7801.
- [24] Papriwal, A. and Mahor, A. "Review of mitigation of harmonics in multilevel inverters using PSO" International Journal of Electrical and Electronics, Vol. 2, N. 4, Dec. 2012, pp. 65-72.
- [25] Araque G., J. A.; Diaz R., J. L. and Pardo G., A. "Optimization of the THD in a Multi-Level Single-Phase Converter using Genetic Algorithms". Advances in Automatic Control, Modelling & Simulation WSEAS Conference Brasov 2013, pp. 326-331.
- [26] Debnath, S. Narayan, R. and Ghosh, T. "Comparison of Different Soft Techniques applicable to Multilevel Inverter for Harmonic Elimination". International Journal of Computer Application, Vol. 6, N. 2, Dec., 2012.
- [27] IEEE Std. 519-1992 - IEEE Recommended Practices and Requirements for Harmonic Control in Electrical Power Systems. IEEE, 1992.
- [28] Goldberg, D. E. "Genetic Algorithms in Search, Optimization and Machine Learning". Addison-Wesley Publishing Company, 1989.

Stochastic model for local ice loads measured on the vessel hull

Petr N. Zvyagin

Abstract—In the paper the raw signals of strain gauge transducers mounted on the vessel’s hull, and registered while vessel was heading through the solid ice, are investigated. It was shown that the model of stationary stochastic lognormal process can be applied to the data mentioned above. The theorem of ice loads process stationarity in specific conditions was proved. The formula for covariance function of ice loads process, recalculated from strain gauge transducer observations process characteristics, was evaluated.

Keywords—Ice loads, strain gauge transducers signal, lognormal stationary process.

I. INTRODUCTION

INVESTIGATION of ice loads on the vessel’s hull is now very promising, and at the same time it turns to be a rather difficult problem of Arctic Science. It is due to the fact that the process of ice crushing is rather complicated and can be considered stochastic. Physical ice parameters, such as ice thickness, ice strength and others, significantly vary in the course of time. To measure them, the special equipment is of necessity, on the other hand measurements now usually can not be carried out with the proper precision.

In addition there is now no univocal opinion about how exactly ice regime parameters relate to ice loads and ice pressure. To estimate these relations, a number of design formulas were offered by different investigators. An overview of such formulas was made by Loset et al. [5].

All of this provides an opportunity to use the assumption about the stochastic nature of ice loads. It is usual now, that ice loads are presented as observations of a random variable (for instance, [1]), but more recent investigations use the model of a stochastic process for ice loads and ice pressure [2], [3], [7]. To estimate stochastic variable parameters or stochastic process parameters, one needs appropriate statistics.

Strain gauge transducers mounted on the various locations of the hull from inside are used to measure local ice forces. Such locations can be the frame or the side panel of the bow, or the ice belt. Measurements of strain gauge transducers should be recalculated to local ice loads using special relations [4].

Petr N. Zvyagin is with the Higher Mathematics Department, St. Petersburg State Polytechnical University, ul. Politechnicheskaya, 29, St. Petersburg, 195251, Russia, and with Krylov State Research Center, Moskovskoe sh., 44, St. Petersburg, 196158, Russia (e-mail: p_zvyagin@bk.ru).

II. ICE LOADS MEASUREMENTS DISTRIBUTION

We will consider signals of strain gauge transducers mounted on the front part of the hull of the vessel “Academic Fyodorov” during its voyage to the North Pole in 2005. Types and positions of strain gauge transducers to be scrutinized are presented in the Table 1. Raw data of these strain gauge transducers without any preprocessing will be used.

We shall take into consideration only those parts of time series, when the vessel headed through the plain solid ice without ridges, i.e. external conditions should be regarded as “stationary”. This will allow us to deal with time series that could be considered as observations of stationary, in sense, stochastic processes. In any case, the fact of stationarity for specific time series should be proved statistically. This fact was proved for some ice loads time series measured in experimental conditions in ice basin earlier [8].

Strain gauge transducer’s number	Type	Position
1	Bending deformations	Frame face, height 7,5-9,5 m
2	Bending deformations	Frame face, height 4,5-6 m
3	Shifting deformations	Frame, height 4,5-6 m

Table 1 Types and positions of strain gauge transducers

As estimators for mean, variance and correlation function we shall use those, given by the method of moments. These estimators are consistent, but in general they are biased.

Let us to assume that the absolute value of correlation between two observations with time lag greater than l is rather small, for example, less than 0.05. Then we take every l -th observation in time series, and compose a set of these observations. The next step is correction of the set by removing outliers with the use of the algorithm described in the next section. For the corrected set of uncorrelated strain gauge transducers measurements of ice loads, obtained this way, the next hypothesis H_0 can be put forward: “the distribution law is lognormal”. This hypothesis can be tested,

for example, by Chi-square test. Results of such testing are provided in the Table 2.

Strain gauge transducer	l	Number of observations in the set (outliers are removed)	Number of intervals	Value of Chi square estimator	Critical Chi-square level for 0.95 confidence probability
1	70	170	13	15,61	19,68
2	50	239	13	5,42	19,68
3	50	239	15	12,41	22,36

Table 2. Results of Chi-square test

The value of Chi-square estimator can vary in dependence on number of intervals and their position. The values presented in the Table 2 allow us to accept the hypothesis H_0 .

III. ICE LOADS OUTLIER VALUES

Strain gauge transducers mounted on the vessel hull measure not only the results of direct impacts in the place where these transducers are mounted, but also echoes and influences of loads appeared to be in other locations of the hull. The lognormal distribution of ice loads is very useful for the analysis and modeling, but registered values in the case of heavy direct ice impact can contradict with lognormal model. To find out if there are outliers in the set about which the hypothesis of the lognormal distribution was accepted, we shall use the next reasoning.

Let us assume that the set, taken from lognormally distributed general population with parameters a and σ , consist of n independent observations. And we consider next event E: "The magnitude of strain gauge transducer observation will exceed critical level cr in at least of one of n independent observations". Then we denote p_0 the probability of not exceeding critical level cr in one observation. Then

$$P(E) = 1 - p_0^n \quad (1)$$

Here in fact $P(E)$ is a statistical significance level. We can take the value of $P(E)$ less than 0.1. Hence, p_0 can be expressed from (1) as

$$p_0 = \exp\left(\frac{\ln(1 - P(E))}{n}\right) \quad (2)$$

The critical level cr can be found as p_0 -quantile of a lognormally distributed random variable with parameters a and σ :

$$cr = \exp(\sigma\Phi^{-1}(p_0 - 0.5) + a), \quad (3)$$

where $\Phi^{-1}(z)$ is a reverse Laplace function. Here we take in account that two uncorrelated observations are independent as well for lognormal distribution.

All observations in the set that exceed critical level cr , should be considered as outliers, removed from the data and investigated separately. Results of such set testing for outliers are presented in the Table 3.

Place of strain gauge transducer	Number of observations in the set	$P(E)$	p_0 , found by (2)	Critical level cr , found by (3)	Number of outliers
1	172	0.1	0.9993	0.1425	2
2	240	0.1	0.9995	0.11	1
3	240	0.1	0.9995	0.379	1

Table 3. Outliers in the set of independent strain gauge transducers measurements

Thus we can see that in the set of 172 or 240 uncorrelated observations, which is $1/70$ or $1/50$ part of entire time series, there are 1-2 outliers that are unlikely to take place if the hypothesis about lognormal distribution is valid. If we estimate distribution parameters a and σ without these outliers, $P(E)$ can be even less than 0.1. That happens because after outliers removal, estimator of parameter σ can be significantly decreasing.

IV. AUTOCORRELATION FUNCTIONS OF ICE LOADS AND REGISTERED SIGNAL

If we denote strain gauge transducer signal process $\eta(t)$, and ice loads process $F(t)$, the relation between these two processes, according to [4], should be:

$$F(t) = c \cdot \eta(t),$$

where $c = const$. We shall consider a more general relation

$$F(t) = c \cdot \eta^\alpha(t), \quad (4)$$

where $\alpha = const$. Then we shall derive autocorrelation function for ice loads $F(t)$, in the case when process $\eta(t)$ is lognormal and we know autocorrelation function of it, that is

$$\eta(t) = e^{\xi(t)} \quad (5)$$

where $\xi(t)$ is a normal process. We have the next theorem:

Theorem 1. [7] If $\eta(t)$ is a process, stationary in wide sense, then $\xi(t)$ is also stationary wide sense, and vice versa.

That means that we can denote mean and standard deviation of the process $\xi(t)$ with constants a and σ .

Theorem 2. If the lognormal process $\eta(t)$ in (4) is stationary in wide sense, then the $F(t)$ is also stationary in wide sense, and vice versa.

Proof. If the process $\eta(t)$ is stationary in wide sense then, according to the Theorem 1, process $\xi(t)$ is also stationary in

wide sense. That means that $\xi(t)$ has constant mean a and constant variance σ^2 , as well as autocorrelation function $r_\xi(t_1, t_2)$ depends only on time lag $\tau = t_2 - t_1$, that is $r_\xi(t_1, t_2) = r(\tau)$. For mean of the process $F(t)$ we have:

$$MF(t) = c \cdot \exp\left(\alpha a + \frac{(\alpha\sigma)^2}{2}\right) = \text{const}$$

$$M(F(t_1)F(t_2)) = c^2 \exp(2\alpha a + \alpha^2 \sigma^2 (1 + r(\tau))),$$

Hence, covariance function for $F(t)$ is

$$K_F(t_1, t_2) = c^2 \exp(2\alpha a + \alpha^2 \sigma^2) (\exp(\alpha^2 \sigma^2 r(\tau)) - 1) = K_F(\tau)$$

And it means that covariance function depends only on time lag τ , and with $MF(t) = \text{const}$, $\sigma^2(F(t)) = \text{const}$, that proves the theorem.

Remark. According to [7] we have

$$r(\tau) = \frac{1}{\sigma^2} \ln\left(\frac{K_\eta(\tau)}{\exp(2a + \sigma^2)} + 1\right),$$

and hence

$$K_F(\tau) = c^2 \exp(2\alpha a + \alpha^2 \sigma^2) \cdot \left(\left(\frac{K_\eta(\tau)}{\exp(2a + \sigma^2)} + 1 \right)^{\alpha^2} - 1 \right) \quad (6)$$

When dealing with strain gauge transducer measurements time series, the method of moments can be used to estimate the covariance function $K_\eta(\tau)$ or autocorrelation function

$$\frac{K_\eta(\tau)}{\sigma^2(\eta)}$$

for specific values of τ , where $\sigma^2(\eta)$ is a constant.

In the Figure 1 such estimations are presented for strain gauge transducers described in the Table 1.

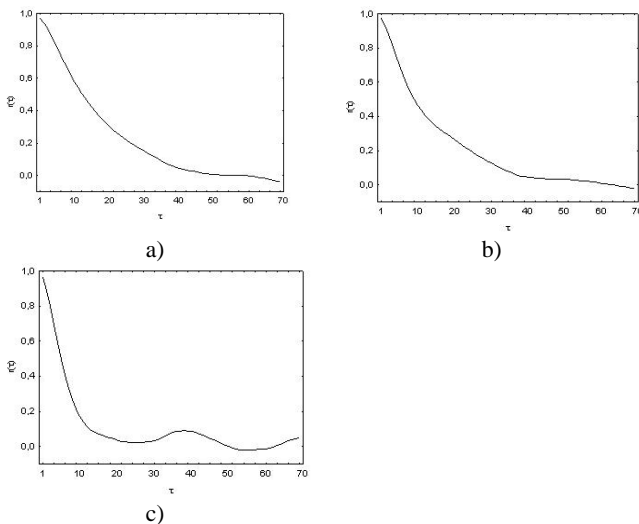


Figure 1. Estimations for the autocorrelation function $K_\eta(\tau)/\sigma^2(\eta)$ of strain gauge transducers time series, given by the method of moments, for time series of a) transducer 1; b) transducer 2; c) transducer 3 from the Table 1

For the covariance function $K_\eta(\tau)$ the simple function of the type $e^{-\beta\tau}$ can be taken, for which it is easy to estimate the value of β using, for example, LSQ method. After that, $K_F(\tau)$ can be found by relation (6). Spectral densities of strain gauge transducers time series measured in the expedition of the vessel “Academic Fyodorov” in 2005 were investigated in the paper [6].

V. CONCLUSION

Strain gauge transducers, mounted from the inside of the vessel hull, are usually used to investigate local ice loads. As soon as such measurements can be considered as correlated in time, the problem of evaluation of ice loads correlation function arises.

In the paper it was shown, that lognormal distribution is applicable for description of uncorrelated strain gauge transducers measurements. The technique of outliers remove in the case of lognormal data distribution was used.

According to the proved Theorem 2, the important statement can be formulated: if a signal, registered by strain gauge transducer is lognormally distributed and related to local ice loads in the way, given by (4), and this signal can be considered as stationary in wide sense, then loads are also a process, stationary in wide sense. As a result, the relation (6) between ice loads covariance function and strain gauge transducers covariance function was evaluated.

REFERENCES

- [1] L. Fransson, and T. Olofsson, “On Scaling of the Maximum Ice Pressure on the vertical foundation,” in *Proc. 18th POAC Conf.*, Potsdam, USA, 2005, pp 341-351.
- [2] F. Guo, “A Spectral Model for Simulating Continuous Crushing Ice Load,” in *Proc. 21st IAHR International Symposium on Ice*, Dalian, China, 2012, pp.1035-1045.
- [3] T. Karna, Y. Qu, W. Kuhnlein, Q. Yue and X. Bi, “A Spectral Model of Ice Forces due to Ice Crushing,” in *Journal of Offshore Mechanics and Arctic Engineering*, 129, 2007, pp. 138-145.
- [4] I.A. Kozlov, V.G. Bazhenov and V.V. Matveev, *Investigation of machine parts strength using strain gauge transducers* (in Russian), Kiev, Technika, 1967, 203 p.
- [5] S. Loset, K. Shkhinek and E. Uvarova, “An overview of the influence of structure width and ice thickness on the global ice load,” in *Proceedings of 15th POAC Conf.* Espoo, Finland, 1999, pp.425-434.
- [6] P. Zvyagin, “Application of Fuzzy Neural Networks for the Data Clusterization Problem,” in *Optical Memory and Neural Networks Journal (Information Optics)*, Vol. 16, No. 2, 2007, pp. 104-110.
- [7] P. Zvyagin and K. Sazonov “Analysis and Probabilistic Modeling of the Stationary Ice Loads Stochastic Process with Lognormal Distribution”, in *Proceedings of 33th OMAE Conf.*, San Francisco, USA, 2014, OMAE2014-24713 paper, 7pp.
- [8] P. Zvyagin and K. Sazonov, “Statistically Based Method of Representing Ice Loads Signal as a Sum of Several Uncorrelated and Stationary Processes,” in *Proceedings of 22th POAC Conf.*, Espoo, Finland, 2013, 7pp

Dynamic Optimization of Carbon Dioxide Enrichment for Tomato Crop in a Greenhouse.

J. E. Moisés Gutiérrez , *Research fellow, BUAP*

N. Iliá Ponce de León Puig, *Student researcher, BUAP*, J. Eladio Flores, *Research fellow, BUAP* Ma. Monserrat Morín Castillo, *Research fellow, BUAP* Josefina Castañeda Camacho, *Research fellow, BUAP* José Italo Cortés, *Research fellow, BUAP* Pedro García Juárez, *Research fellow, BUAP*

Abstract—An optimal control for the carbon dioxide enrichment in a greenhouse can be obtained from a mathematical model of the crop and the greenhouse. We consider a model with four states: the structural biomass of leaves and fruit, the non-structural biomass (nutrients) and the carbon dioxide, also, we select a cost functional in order to increase the benefit for the farmer, it means the farmer will get a saving in the energy consumption expenses. The control law is deduced from optimal control theory and is simulated in a two week period and compared with the ramp function as control input.

Index Terms—Greenhouse, carbon dioxide, structural biomass of leaves, structural biomass of fruit, optimal control, functional, state space.

I. INTRODUCTION

In the last two decades researchers have done many efforts to develop advanced climate control systems in greenhouses [Aikman(1996)], [Ioslovich, Seginer(1995, 1998)], [Seginer, Ioslovich(1998)], [Tchamitchian, Ioslovich(1998)], [Van Straten et al.(2000)], [Van Henten(1994)]. They have proposed different optimal control methods although it has not been applied in the practice because this methods are difficult for the application [Van Straten et al.(2000)].

The growth in a crop is based in different variables, all of them are very important, but in this research the variable that has our interest is the carbon dioxide. The carbon dioxide enrichment is practised in the crops of greenhouse in order to increase the yield and the benefit. There are studies that show the CO₂ enrichment improves the net photosynthesis in the plants, it makes the total weight, height, and the number of leaves and branches increase [Mortensen(1987)]. Other research has demonstrated the CO₂ enrichment makes physic-chemical changes in the crop, like color and firmness [Md. Shahidul et al.(1996)].

Optimal strategies for CO₂ enrichment can be deduced experimentally or analytically. Experimentation is not able to produce a valid result for all condition set. The analysis as a tool gives us a mathematical idea for an optimal strategy, this method is based on ventilation, photosynthesis, dry matter and production rate models. The method used for calculate the optimal enrichment level is valid for different models which describe the production rate, dry matter, photosynthesis and ventilation.

There are develops about optimal strategies for the CO₂ enrichment [Challa, Schapendonk(1984)], [Nederhoff(1988)],

which are supported in reduction of expenses for energy consumption, reduction of CO₂ consumption and increase in the production, which results in a higher net gain for the crop. Figure (1) shows three different types of control for the crop, the first one is a traditional method for the farmer, the second one and the last one are optimal controllers, note the two last have a better impact for energy save, production and total gain.

One of the main objectives is to contribute with the optimal control problem, and its implementation in real time. Having control over CO₂ we have an extra advantage talking about production. The tomato crop has been chosen because it is one of the most important crop in our country and is the second farm product consumed on the world. To achieve the objective, we part from the tomato and greenhouse mathematical set model considering the variable of plant and fruit dry weight, the availability of nutrients and the quantity of carbon dioxide.

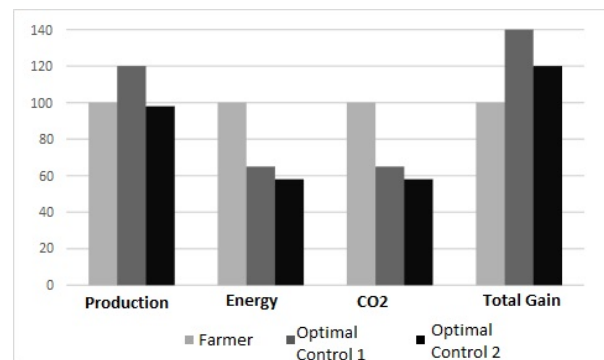


Fig. 1. Energy and CO₂ consumption, total production and gain with different control strategies.

II. GENERAL FORMULATION OF THE OPTIMAL CONTROL PROBLEM

The optimal control of any system, has to be based on three concepts: the dynamic model of the system, a functional and the system restrictions. In matrix notation the equation of state is represented as follow:

$$\dot{x} = f(x(t), u(t), t). \quad (1)$$

Where $x(t)$ is the states vector, $u(t)$ is the control signal and t is the time. A criterion is required to help to evaluate the

performance of the system, normally, the functional is defined by:

$$J = \phi(x(t_f), t_f) + \int_{t_0}^{t_f} L(x(t), u(t), t) dt, \quad (2)$$

where t_0 and t_f are the initial and final time, ϕ and L are scalar functions, t_f can be fixed or free. Starting at the initial state $x(t_0) = x_0$ and applying the control signal $u(t)$ for $t \in [t_0, t_f]$, it makes that system follows some trajectory of states, then the performance index assigns a unique real number for each trajectory of the system.

The fundamental problem of optimal control is reduced to determinate an admissible control u^* which makes that equation (1) follows one admissible trajectory x^* that minimize the performance measure showed in the equation (2). Then, u^* is called optimal control and x^* is an optimal trajectory.

Necessary conditions for a stationary solution.

The restrictions (1) are added to the functional (2) with a Lagrange multipliers vector time variant $\Psi(t)$,

$$J = \phi(x(t_f)) + \int_{t_0}^{t_f} [L(x(t), u(t), t) - \Psi^T f(x(t), u(t), t) - \dot{x}] dt, \quad (3)$$

Then, we define the Hamiltonian scalar function:

$$\begin{aligned} H(x(t), u(t), \Psi(t), t) &= \\ &= L(x(t), u(t), t) + \Psi(t) f(x(t), u(t), t) \end{aligned} \quad (4)$$

An infinitesimal variation in $u(t)$ is considerate and it is denominated like $\delta u(t)$, this variation produces a change in the functional. If $x(t_0)$ is specified then $\delta x(t_0)$ also is specified. This variation can be calculated as follow:

$$\delta J = \Psi^T(t_0) \delta x(t_0) + \int_{t_0}^{t_f} \left[\frac{\partial H}{\partial u} \delta u \right] dt$$

We choose the multiplier $\Psi(t)$, from this, the auxiliary system equations is formed:

$$\dot{\Psi}^T = -\frac{\partial H}{\partial x} = -\frac{\partial L}{\partial x} - \Psi^T \frac{\partial f}{\partial x} \quad (5)$$

With final conditions

$$\Psi^T(t_f) = \frac{\partial \phi}{\partial x}(t_f) \quad (6)$$

For a stationary solution it is required that the functional with an arbitrary variation must be equal to zero, $\delta J = 0$. This is true when:

$$\frac{\partial H}{\partial u} = \frac{\partial L}{\partial u} + \Psi^T \frac{\partial f}{\partial u} = 0 \quad (7)$$

To find the vector function of control $u(t)$ that produce a stationary value of the functional we must solve the following differential equation system:

$$\begin{cases} \dot{x}(t) = f(x(t), u(t), t), \\ \dot{\Psi}(t) = -\frac{\partial H^T}{\partial x}, \end{cases} \quad (8)$$

The boundary conditions for this differential equations are separated, it means, some of them are defined in $t = t_0$ and the others in $t = t_f$. This is a *problem with boundary values of two points*. Note that the equations that describe the states $x(t)$ and the auxiliary states $\psi(t)$ in the equation (8) are coupled, for this reason $u(t)$ depends on $\psi(t)$ through the stationary condition and the attachment states depend on $x(t)$ and $u(t)$.

III. MATHEMATICAL MODEL OF THE CROP

The model in space states of the tomato crop has three principles states (Van Straten et al., 2011):

- Nonstructural Biomass (Assimilates).
- Leaves Structural Biomass.
- Fruits Structural Biomass.

The basic mass balances are as follow.

- Assimilates:

$$\frac{dW_B}{dt} = P - G_V - \theta_V G_V - G_F - \theta_F G_F - R_{B,V} - R_{B,F}, \quad (9)$$

- Leaves:

$$\frac{dW_V}{dt} = G_V - R_{V,V} - H_L, \quad (10)$$

- Fruits:

$$\frac{dW_F}{dt} = G_F - R_{F,F} - H_F, \quad (11)$$

where:

+ Production of assimilates by photosynthesis (P).

- Conversion of assimilates to vegetative biomass by growth (G_V).

- Use of assimilates as energy to drive vegetative growth ($\theta_V G_V$).

- Conversion of assimilates to generative (fruit) biomass by growth (G_F).

- Use of assimilates as energy to drive generative (fruit) growth ($\theta_F G_F$).

- Drain of assimilates for maintenance of vegetative parts ($R_{B,V}$).

- Drain of assimilates for maintenance of generative parts ($R_{B,F}$). - Use of biomass for maintenance there is lack of assimilates ($R_{V,V}$).

- Leaf picking rate (H_L).

- Use of biomass for maintenance when there is a lack of assimilates ($R_{F,F}$).

- Fruit harvest rate (H_F).

All biomass and rates are expressed in dry weight per unit greenhouse projected area.

A. Biomass balance of nutrients

We denote W_B like total nutrients in the plant, it is expressed like dry weight per area unit, the biomass balance equation of nutrients is the follow:

$$\begin{aligned} \frac{dW_B}{dt} = P - h\{\cdot\} \left(\frac{(1+\theta_V)}{z} G_L^{dem} + (1+\theta_F) G_F^{dem} \right) - \\ - h\{\cdot\} \left(\frac{R_L}{z} + R_F \right). \end{aligned} \quad (12)$$

The biomass balance equation of nutrients (12) can take two values depending on the nutrients abundance $h\{\cdot\}$ where the first expression is taken when $h\{\cdot\} = 1$ (abundance of nutrients) and the second one is taken when $h\{\cdot\} = 0$ (lack of nutrients).

$$\frac{dW_B}{dt} = \begin{cases} P - \frac{(1+\theta_V)}{z} G_L^{dem} - (1 + \theta_F) G_F^{dem} - \\ - \frac{R_L}{z} - R_F, \\ P, \end{cases} \quad (13)$$

where

R_F .- Respiration needs of fruits

θ_V .- Additional amount of assimilates needs for one unit of structural vegetative parts.

G_L^{dem} .- Unit area growth demand of leaves.

θ_F .- Additional amount of assimilates needs for one unit of structural fruit parts.

G_F^{dem} .- Unit area growth demand of fruit.

z .- Total vegetative parts.

$h\{\cdot\}$.- Nutrients abundance.

B. Biomass balance of leaves

The leaf growth is equal to the amount of assimilates converted to structural leaf biomass in the plant and it is given by $h\{\cdot\}G_L^{dem}$. The model does not incorporate an extra state for stem and roots, but the factor z assumes that each increment in leaf will be accompanied by an increment in stem and roots. If there are no sufficient assimilates (nutrients), growth stops, normally the assimilates are used for the maintenance, but in lack of assimilates, maintenance in the model goes at the expense of structural parts (leaves and fruit). The biomass balance of leaves is expressed like:

$$\frac{dW_L}{dt} = h\{\cdot\}G_L^{dem} - (1 - h\{\cdot\})R_L - H_L, \quad (14)$$

Depending on the abundance of nutrients $h\{\cdot\}$, the biomass leaf balance equation (14) can take two values:

$$\frac{dW_L}{dt} = \begin{cases} G_L^{dem} - H_L, & \text{si } h\{\cdot\} = 1, \\ -R_L - H_L, & \text{si } h\{\cdot\} = 0. \end{cases} \quad (15)$$

where

H_L is the leaf picking rate.

The term G_L^{dem} depends principally on the pivotal temperature, cultivation temperature level and the reference temperature.

C. Biomass balance of fruit

Similarly to the biomass of leaf case, the growth of fruits in the plant from the nutrients is given by $h\{\cdot\}G_F^{dem}$. The term G_F^{dem} depends principally on the pivotal temperature, cultivation temperature level and the reference temperature.

$$\frac{dW_F}{dt} = h\{\cdot\}G_F^{dem} - (1 - h\{\cdot\})R_F - H_F, \quad (16)$$

Finally, the equation (16) of biomass balance of fruits can take two different values depending on nutrient abundance $h\{\cdot\}$ where H_F is the fruit harvest rate.

$$\frac{dW_F}{dt} = \begin{cases} G_F^{dem} - H_F, & \text{si } h\{\cdot\} = 1, \\ -R_F - H_F, & \text{si } h\{\cdot\} = 0. \end{cases} \quad (17)$$

IV. GREENHOUSE MATHEMATICAL MODEL

A. Balance of carbon dioxide energy in the greenhouse

The balance of carbon dioxide energy within greenhouse is given by the equation [Van Straten et al.(2011)]:

$$\frac{V_g}{A_g} \frac{dC_{CO_2}}{dt} = -\eta_{CO_2/dw} P + \eta_{CO_2/dw} R - \varphi_{CO_2,g-o}^{vent} + u_{CO_2}, \quad (18)$$

Then each term is described

* Carbon dioxide taken from the greenhouse air for plant photosynthesis:

$$\eta_{CO_2/dw} P,$$

* Carbon dioxide returned to the greenhouse air for plant respiration:

$$\eta_{CO_2/dw} R,$$

The term $\frac{V_g}{A_g}$ is the reason of the volume of greenhouse per unit of area.

R is the respiration total plant per unit of time.

* Lost of carbon dioxide mass by ventilation:

$$\varphi_{CO_2,g-o}^{vent} = u_V (C_{CO_2} - C_{CO_2-o}),$$

where: u_V ventilation flow rate per unit of area.

C_{CO_2} (kgm^{-3}), is the carbon dioxide concentration within greenhouse.

C_{CO_2-o} (kgm^{-3}), is the carbon dioxide concentration on the outside greenhouse.

* Carbon dioxide supply:

$$u_{CO_2} = u_{CO_2}^{Vp} \varphi_{CO_2,in-g}^{max},$$

where: $u_{CO_2}^{Vp}$ is the opening supply valve.

$\varphi_{CO_2,in-g}^{max}$ ($kg[CO_2]m^{-2}[gh]s^{-1}$), is the maximum flow rate of carbon dioxide.

In this greenhouse model, the position of the carbon dioxide supply valve is the control input. For this reason, the valve relates directly to the actuator that is present on a physic way in the greenhouse.

V. SYNTHESIS OF OPTIMAL CONTROL

We considerate the system formed by the state equations (13, 15, 17, 18), the first three of them are relative to the crop and the last one is relative to the greenhouse. We suppose there is nutrients abundance for the three equations relative to the crop. The terms for the equation systems (19) and (22) have been substituted using the equation table of the mathematical model (table 1) and the values have been substituted using the table of physical parameters (table 2).

$$\begin{cases} \dot{W}_L = 2.2996 \times 10^{-6} W_L, \\ \dot{W}_F = 4.3925 \times 10^{-6} W_F, \\ \dot{W}_B = P - 5.39 \times 10^{-6} W_L - 5.92 \times 10^{-6} W_F, \\ 3C_{CO_2} = 1.0266(R - P) + 0.155 \times 10^{-10} u_{CO_2}^{Vp}, \end{cases} \quad (19)$$

P and R are as show following:

$$P = \frac{3.7192 \times 10^{-11} W_L^{2.511}}{1.6353 \times 10^{-9} + 4.0439 \times 10^{-5} W_L^{2.511}},$$

TABLE I
GREENHOUSE AND CROP MATHEMATICAL MODEL EQUATIONS

Term	Description
$P = P^{max} \left(\frac{I^{PAR}}{I^{PAR} + K_I} \right) \left(\frac{C_{CO_2}}{C_{CO_2} + K_C} \right) f_m \{ \cdot \}$	Production of assimilates by photosynthesis.
$R = h \{ \cdot \} \left(\frac{\theta_L G_L^{dem}}{z} + \theta_F G_F^{dem} \right) + \frac{R_L}{z} + R_F$	Total amount breathed plant per unit of time.
$I^{PAR} = f_{PAR} / I \tau_r I_0$	The PAR light intensity at the crop level.
$f_m \{ \cdot \} = \frac{(W_L / p_m)^m}{1 + (W_L / p_m)^m}$	Maturity factor.
$G_L^{dem} = f_{L/F}(T) k_{GF}^{ref} f_{TG}(T) f_D \{ \cdot \} W_L$	Growth leaves demand.
$G_F^{dem} = k_{GF}^{ref} f_{TG}(T) f_D \{ \cdot \} W_F$	Growth fruits demand.
$f_{L/F}(T) = \int_{L/F}^{ref} e^{v_2(T - T_{L/F}^{ref})}$	Temperature-dependent ratio.
$f_{TG}(T) = Q_{10R}^{T - T_G^{ref} / 10}$	Temperature dependent with a Q_{10G} relation.
$f_{TR}(T) = Q_{10B}^{T - T_R^{ref}}$	Function of temperature with a Q_{10G} relation.
$f_D \{ \cdot \} = \frac{c_{f1} - c_{f2} D}{c_{f1} - c_{f2}}$	Correction factor for the fruit growth rate.
$R_L = k_{RL}^{ref} f_{TR}(T) W_L$	Respiration demand of the leaves.
$R_F = k_{RF}^{ref} f_{TR}(T) W_F$	Respiration demand of the fruits.
$H_L = k_{HL} W_L$	Leaf picking rate.
$H_F = k_{HF} W_F$	Harvest rate.
$K_{HL} = C_{yL} K_H$	Coefficient of harvest.
$K_{HF} = C_{yF} K_H$	Coefficient of harvest.
$K_H = Cd1 + Cd2 \ln(T / Cd3) - Cd3 - Cd4 e_D$	Harvest rate.
$u_V = \left(\frac{p_{V1} u_V^{A_{plsd}}}{1 + p_{V2} u_V^{A_{plsd}}} + p_{V3} + p_{V4} u_V^{A_{pwsd}} \right) v + p_{V5}$	Ventilation flow rate.

$$R = 1.5942 \times 10^{-6} W_F + 0.4856 \times 10^{-6} W_L + 1.668 \times 10^{-7}.$$

We considerate the following performance functional:

$$J = \frac{1}{2} [W_L^2(t_f) + W_F^2(t_f) + W_B^2(t_f) + C_{CO_2}^2(t_f) + \int_{t_0}^{t_f} [W_L^2 + W_F^2 + W_B^2 + C_{CO_2}^2 + (u_{CO_2}^{vp})^2] dt], \quad (20)$$

The first term of performance index involves the three first variables at the end time, they are related to the final production and the nutrients, and the integral contains the control input in order to avoid the risk for big control inputs. The idea is minimize the functional (20), related with the equations system (19).

A. Method solution description

The Hamiltonian scalar function is obtained considering the relation (4) of this function with the Lagrange multipliers and the functional (20).

$$\begin{aligned} H(\mathbf{x}, \mathbf{u}, \Psi, t) = & \\ = & \frac{1}{2} [W_L^2(t) + W_F^2(t) + W_B^2(t) + C_{CO_2}^2(t) + (u_{CO_2}^{vp})^2(t)] + \\ & + 2.2996 \times 10^{-6} W_L(t) \Psi_1(t) + 4.3925 \times 10^{-6} W_F(t) \Psi_2(t) + \\ & + [P - 5.39 \times 10^{-6} W_L(t) - 5.92 \times 10^{-6} W_F(t)] \Psi_3(t) + \\ & + \frac{1}{3} [1.0266(R - P) + 0.1554 \times 10^{-10} u_{CO_2}^{vp}] \Psi_4(t). \quad (21) \end{aligned}$$

The system of auxiliary variables has the following form:

$$\begin{cases} \dot{\Psi}_1 = W_L + 2.2996 \times 10^{-6} \Psi_1 + \frac{\partial P}{\partial W_L} \Psi_3 - \\ \quad - 5.39 \times 10^{-6} \Psi_3 + \frac{1}{3} \frac{\partial (R-P)}{\partial W_L} \Psi_4 (1.0266) \\ \dot{\Psi}_2 = W_F + 4.3925 \times 10^{-6} \Psi_2 - \\ \quad - 5.92 \times 10^{-6} \Psi_3 + \frac{1}{3} \frac{\partial R}{\partial W_F} \Psi_4 (1.0266), \\ \dot{\Psi}_3 = W_B, \\ \dot{\Psi}_4 = C_{CO_2}, \end{cases} \quad (22)$$

The stationary condition give us the following control form, which was obtained from equation (7) and depends on fourth appended state:

$$u_{CO_2}^{vp} = -\frac{1}{3} 0.1554 \times 10^{-10} \Psi_4(t). \quad (23)$$

It is necessary to solve the equation systems (19) and (22), in this way we can know the Ψ_4 value and finally we will get the control form. The system (19) has initial condition and the system (22) has final conditions. The systems are coupled, because the control form (23) has been substituted. To solve the complete system like a system with initial conditions, the appended equations are considerate in reverse time, then the behaviour of the appended variables is returned to the direct time. When we solve the appended equation system in reverse time the system becomes in a system with initial conditions. It is important to note that the equation (23) depends on fourth state but this state depends on the other three states. Using MatLab tools we solve the equation systems (19) and (22) and then, we can get the state Ψ_4 in reverse time and finally return it to the direct time. The MatLab tools were used to elaborate the program that solve the differential equations system.

VI. SIMULATION AND RESULTS

A. Analysis with a ramp input

A ramp control signal is introduced to the system (19), and the simulation is for a two weeks period. The behaviour is described in the figure 2. The graphic shows how assimilates decrease with the time, and fruits, leaves and carbon dioxide grow with the time.

The dry matter of fruits grows more than dry matter of leaves, which is very acceptable. However it is important to note the carbon dioxide cost that is used.

TABLE II
PHYSIC PARAMETERS.

Variable	Value	Description
z	0.6081	Fraction leaf of total vegetative mass
θ_v	0.23	Surplus assimilate requirement factor per unit fruit increment.
θ_F	0.2	Surplus assimilate requirement factor per unit vegetative increment.
p_h	2.7×10^{-3}	Parameter of switching function, $[m^2 kg^{-1}]$
p_m	1.8×10^{-2}	Parameter in maturity factor, $[kg m^{-2}]$
m	2.511	Parameter in maturity factor
p^{max}	2.2×10^{-6}	Maximum gross canopy photosynthesis rate, $[kg m^{-2} s^{-1}]$
K_1	577	Monod constant for PAR, $[W m^{-2}]$
K_c	0.211	Monod constant for CO_2 , $[kg m^{-3}]$
$f_{PAR/I}$	0.475	PAR fraction of global radiation
τ_r	0.7	Transmittance of the roof
k_{GF}^{ref}	3.8×10^{-6}	Reference fruit growth rate coefficient, $[s^{-1}]$
T_{GF}^{ref}	20	Reference temperature, $[^{\circ}C]$
Q_{10G}	1.6	Temperature function parameter growth
$f_{L/F}^{ref}$	1.38	Reference leaf-fruit partitioning factor
v_2	-0.168	Parámetro de partición de fruta-hoja, $[K^{-1}]$
$T_{L/F}^{ref}$	19	Fruit-leaf partitioning reference temperature, $[^{\circ}C]$
k_{RL}^{ref}	2.9×10^{-7}	Maintenance respiration coefficient leaf, $[s^{-1}]$
Q_{10R}	2	Temperature function parameter respiration
T_R^{ref}	25	Reference temperature for respiration, $[^{\circ}C]$
k_{RF}^{ref}	1.2×10^{-7}	Maintenance respiration coefficient leaf, $[s^{-1}]$
η	0.7	Absorbed in relation to the total energy of the net radiation heat received.
$Cd1$	2.13×10^{-7}	Parameter in development rate function, s^{-1}
$Cd2$	2.47×10^{-7}	Parameter in development rate function, s^{-1}
$Cd3$	20	Parameter in development rate function, C
$Cd4$	7.50×10^{-11}	Parameter in development rate function, s^{-1}
C_{yL}	1.636	Parameter in harvest function (fruit)
C_{yF}	0.4805	Parameter in harvest function (leaf)
$CCO_{2,0}$	1.6637	
$CCO_{2/dw}$	1.4667	Ratio CO_2 per unit dry weight, $Kg[CO_2]Kg^{-1}[dw]$
$CCO_{2,ing}$	2.10×10^{-6}	Ratio CO_2 per unit dry weight, $Kg[CO_2]m^{-2}[gh]s^{-1}$
$\frac{V_g}{A_g}$	3	Volume per unit greenhouse area
p_{v1}	7.17×10^{-5}	Parameter.
p_{v2}	0.0156	Parameter.
p_{v3}	2.71×10^{-5}	Parameter.
p_{v4}	6.32×10^{-5}	Parameter.
p_{v5}	7.40×10^{-5}	Parameter.

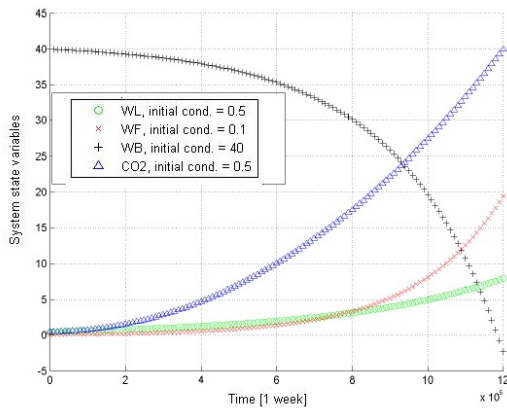


Fig. 2. Behavior of fruits and leaves dry matter, assimilates and carbon dioxide flux with an input ramp.

B. Analysis of the synthesized control

Simulation for two weeks, considering the control law determinate in this paper is presented in the figure 3. The figure 3 shows like dry matter of fruits, leaves and nutrients is a similar case in where the ramp was simulated

for the system. It is important to note the fact that in the control law obtained in this research the carbon dioxide flux was significantly reduce, and it give benefits to the farmers.

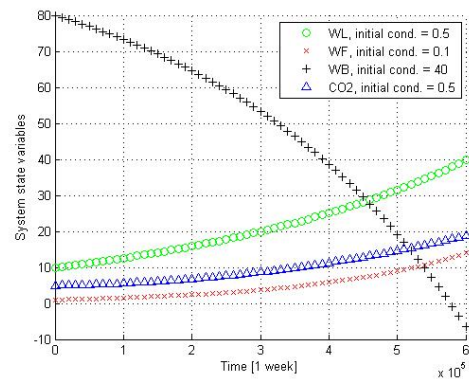


Fig. 3. Behaviour of fruits and leaves dry matter, assimilates and carbon dioxide flux with control law deduced. $u_{CO_2}^{vp}$.

The figure 4 shows the behaviour of the auxiliary variable Ψ_4 , note the variable was solve in reverse time and in the figure 4 the variable is represented in real time. The behaviour

is important because the control expression depends on it for each time instant.

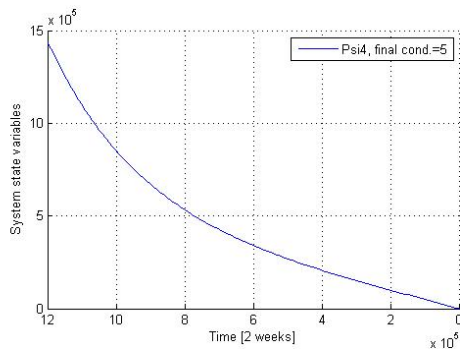


Fig. 4. Behavior of auxiliary variable Ψ_4 .

In agreement with expression (23), the behaviour in each instant time of the appended state variable $\Psi_4(t)$ must be multiplied by the value $(-\frac{1}{3}0.1554 \times 10^{-10})$, this gives us the control behaviour.

VII. CONCLUSION

The tomato and greenhouse model was analysed and we obtained the synthesized control law that give benefits to the farmers, because it is possible to having the same growth for the dry matter of fruits, but the consumption of carbon dioxide is reduced significantly. The analysis of matrix in the functional can make the dry matter growth of fruits is bigger than the showed in this paper. The work that is making in this moment is get the control law with temperature and solar radiation variables, because both of them are variables with the time but in this paper this parameters are constants. On the other hand, the next short-term work is the design and construction of the electronic system which will control the carbon dioxide flux and its application in a greenhouse.

ACKNOWLEDGMENT

This work is supported by *Consejo Nacional de Ciencia y Tecnología* (CONACYT), the *Benemrita Universidad Autnoma de Puebla* (BUAP).

REFERENCES

- [Aikman(1996)] Aikman D. P., 1996. A procedure for optimizing carbon dioxide enrichment of a glasshouse tomato crop. *Journal of agricultural engineering research* 63, No. 2, 171–183.
- [Ioslovich et al.(2009)] Ioslovich I., Gutman P. and Linker R., 2009. Hamilton-Jacobi-Bellman formalism for optimal climate control of greenhouse crop. *Automatica*, 1227–1231.
- [Ioslovich, Seginer(1995, 1998)] Ioslovich I. and Seginer I., 1995. Normalized co-state variable for seasonal optimization of greenhouse tomato production. *Acta horticulturae* 417, 87–94.
- [Ioslovich, Seginer(1998)] Ioslovich I. and Seginer I., 1998. Approximate seasonal optimization of the greenhouse environment for a multi-state-variable tomato model. *Transactions of the ASAE* 41, No. 4, 1139–1149.
- [Md. Shahidul et al.(1996)] Md. Shahidul I., Toshiyuki M., Yuichi Y., 1996. Effect of carbon dioxide enrichment on physico-chemical and enzymatic changes in tomato fruits at various stages of maturity. *Scientia horticulturae* 65, 137–149.

- [Mortensen(1987)] Mortensen M. L., 1987. CO₂ enrichment in greenhouse. *Sci. Horticulturae* 33, 1–25.
- [Seginer, Ioslovich(1998)] Seginer I. and Ioslovich I., 1998. Seasonal optimization of the greenhouse environment for a simple two-stage crop growth model. *Journal of agricultural engineering research* 70, 145–155.
- [Tchamitchian, Ioslovich(1998)] Tchamitchian M. and Ioslovich I., 1998. Equivalence of the temperature integral and the carbon dynamics concepts in plants: Utility for controll. *Acta horticulturae* 519, 171–180.
- [Van Straten et al.(2000)] Van Straten G., Challa H. and Buwalda F., 2000. Towards user accepted optimal control of greenhouse climate. *Computers and electronics in agriculture* 26, No. 3, 221–238.
- [Van Straten et al.(2011)] Van Straten G., van Willigenburg L. G., van Henten E. and van Ooteghem R., 2011. *Optimal control of greenhouse cultivation*. CRC. Press, United States of America.
- [Van Henten(1994)] Van Henten E. J., 1994. *Greenhouse climate management: An optimal control approach*. Doctorate dissertation. Agricultural University, Wageningen.
- [Challa, Schapendonk(1984)] Challa H. and Schapendonk A. H. C. M., 1984. Dynamic optimization of CO₂ concentration in relation to climate control in greenhouses. In: *Carbon dioxide enrichment for greenhouse crops*. CRG Press, Boca Raton, FL, 147–160.
- [Nederhoff(1988)] Nederhoff E.M., 1988. Dynamic optimization of the CO₂ concentration in greenhouses: an experiment with cucumber (*Cucumis sativus* L.). *Acta horticulturae* 229, 341–348.

Nubia Iliá Ponce de León Puig Born on July 23, 1989 in Puebla, Mexico. Graduate in *Mecatronics Engineer* from the *Autonomous University of Puebla (BUAP)*. Student in *Master of Electronic Engineering (MIE)* of the *Autonomous University of Puebla (BUAP)*.



J. E. Moisés Gutiérrez Arias He received the titles of the *Bachelor of Mathematics* and the *Master of Sciences Mathematics* in 1997 from the *Autonomous University of Puebla*, the *Doctorate in Mathematical Sciences* also he received from the same institution in 2003.



Jos E. Flores Research fellow in *Faculty of Science of the Electronics (FCE)* of the *Benemérita Universidad Autónoma de Puebla (BUAP)*

Ma. Monserrat Morí Catillo Research fellow in *Faculty of Science of the Electronics (FCE)* of the *Benemérita Universidad Autnoma de Puebla (BUAP)*

Josefina Castañeda Camacho Research fellow in *Faculty of Science of the Electronics (FCE)* of the *Benemérita Universidad Autnoma de Puebla (BUAP)*

Access control model for Grid calculations

Artem Konoplev, Maxim Kalinin, Dmitry Moskvina, Dmitry Zegzhda

Abstract—The paper discusses security problem with Grid systems, the systems which provide high performance distributed computing. It points to Grid security features, provides common security threat model of Grid, and proposes the Petri net model of access control in Grid. That model allows us to implement Grid security mechanism using job submission in accordance with security policy rules.

Keywords—access, Grid, model, security.

I. INTRODUCTION

GRID systems is a kind of distributed computing systems which are applied to solve intensive and massive calculations mostly in scientific fields (e.g. modeling, prognosis, big data processing). Grid systems are focused on aspects of high performance and job distribution not as well as on information security, especially concerning protection of calculating and storage resources. At the same time the security problem becomes extremely actual for Grid systems because of sensitivity and importance of data being processed. This problem is caused by specific nature of Grid, which is built according to the principles of common ownership of job processing infrastructure, high dynamics of system states, and decentralized calculations.

In Grid, every job runs remotely on multiple host systems, but due to specific nature of Grid there is no unified access control check-point which could allow the security requirements to be defined for each entity involved in job processing. This paper proposes a technology targeted to solve this security problem.

Grid resources are divided into few classes: computing resources, storage resources, software resources, network resources. Grid infrastructure is implemented in virtual organization (VO) — the dynamic community of users that share resources of Grid to solve common tasks and in accordance with predefined access rules [1]. Each user may be involved in few VO at once and VO content changes extremely high for intensive job distribution.

Artem Konoplev is with St. Petersburg State Polytechnical University, St. Petersburg, Russia (e-mail: artem.konoplev@ibks.ftk.spbstu.ru).

Maxim Kalinin is with St. Petersburg State Polytechnical University, St. Petersburg, Russia (phone: +78125527632, fax: +78125527632, e-mail: maxim.kalinin@ibks.ftk.spbstu.ru).

Dmitry Moskvina is with St. Petersburg State Polytechnical University, St. Petersburg, Russia (e-mail: dmitry.moskvina@ibks.ftk.spbstu.ru).

Dmitry Zegzhda is with St. Petersburg State Polytechnical University, St. Petersburg, Russia (e-mail: dmitry.zegzhda@ibks.ftk.spbstu.ru).

The following classes of computer attacks are mostly typical for Grid (Fig. 1):

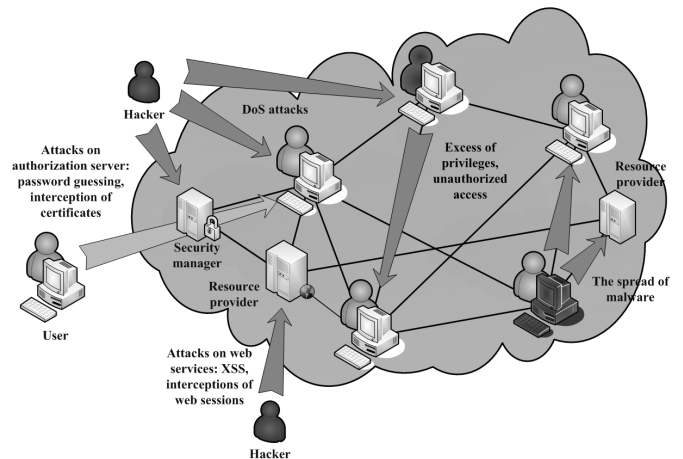


Fig. 1. Security threat model of Grid

- **Denial of service:** network attacks targeted at basic services of Grid, forcing an authorized component to disconnect from Grid, overloading of Grid with jobs.
- **Unauthorized access to resources:** connection of an unauthorized user to the system; attempt to access user data by different user processes; attempt to exceed user privileges to get full access to systems or data.

In the next sections we review our approach to solve these security issues in Grid systems using method of Petri nets modeling. The paper is structured as follows: Section 2 observed the related works, Section 3 suggests mathematical apparatus of Petri nets for modeling of job distribution and access control, Section 4 summarizes our work results.

II. THE RELATED WORKS

Since Grid platform is a set of personal computers, an important task for Grid is to ensure data confidentiality. Data protection and access control are required for local host users including 'root' user (superuser). For this purpose, the trusted software and hardware platform is used on the hosts. User data are protected in a special encrypted repository at host environment.

Special hardware and software components are used to provide protection against denial of service attacks and against

malicious software. These components are also known as security managers. Security managers include Intrusion Detection Systems (IDS), firewalls and antivirus agents [2]. There are also several works targeted at anomaly detection in distributed computing systems [3][4].

In addition, in some Grid, fuzzy trust logic is used [5]. Each host is initially labeled. This label shows the trustworthy level assigned to it by other components of Grid. If attack from that host is fixed, the trustworthy level is decreased. While search for a suitable host for a user-defined task, the hosts with the highest trustworthy level are chosen for running this task.

In existing products, such as Grid Resource Allocation and Management (GRAM) in Globus Toolkit [6] and Community Authorization Service (CAS) in gLite [7], there are authentication and authorization mechanisms implemented to control user tasks access to Grid resources.

Definition and realization of security policies in these solutions are based on a set of Virtual Organizations (VOs) and fixed states of the Grid [8].

All above mentioned works do not take into account high dynamics and access rights distribution at the level of user jobs. Therefore, it might cause unauthorized access from job to data being processed in Grid, and local user may access to job which is running on Grid node. Both types of access violations can influent on valuable results.

This paper refers to development of Grid system model, taking into account high dynamics of user tasks distribution, and suggests secure user tasks distribution method based on this model. In [9], an algorithmic behavior model of multi-agent distributed system is proposed. This model is based on adaptive random graphs mathematical apparatus and takes into account sufficiently high frequency of the number of nodes and links between nodes changing. There is high frequency of node status and user tasks distribution between nodes in Grid systems that can be observed. Whereas to add or delete a node in the Grid, you must pass the verification procedure which means that the number of nodes in such distributed network changes quite rarely.

In [10][11], an unfolding technique is formally described and applied to colored Petri nets to describe branching processes whose behavior close to the Grid. Branching process is a Markov process [10] that models a population in which each individual in generation n produces some random number of individuals in generation $n + 1$. They propose a model of branching processes for describing behavior of general Petri net [11]. In this paper we extend the results of this work with reference to Grid security.

III. MODELING OF JOB DISTRIBUTION AND GRID SECURITY

Grid is described with Petri net $N = (RP, T, F, M)$, where $RP = \{rp\}$ is a finite set of vertices that represent Grid nodes (hosts, resource providers, etc.), $T = \{t_i\}$ is a set of transitions between the vertices. $F = RP \times T \cup T \times RP$ is a set of arcs [12]. Markers $\{m\}$ denote user jobs in set J (i.e., requests for a particular type of Grid resource).

T-transition of Petri net (N, M_0) is a simplest transition and it is defined as a transition $t_{ij} \in T$. Mark M' is directly accessible from mark M : $M' = (m_1, \dots, m_i - 1, \dots, m_j + 1, \dots, m_n)$. T-transition is presented in Fig. 2.

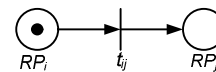


Fig.2 T-transition graph

F-transition of Petri net (N, M_0) is a branching, and it is defined as a transition $t_{ijk} \in T$, where mark M' directly accessible from marking M : $M' = (m_1, \dots, m_i - 1, \dots, m_j + 1, \dots, m_k + 1, \dots, m_n)$. F-transition is drawn on Fig. 3.

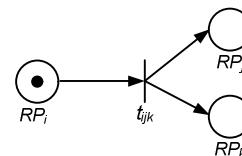


Fig. 3 F-transition graph.

The branching Petri net is a colored functional unlimited Petri net which includes just T-transactions and F-transitions.

Grid can be represented as a graph of branching Petri net. T-transition means the simple migration of user job from one node to another. There are no new markers to appear in that case, and it means that summary marker accounts taken before and after transition activation are the same.

F-transition means situation in which computing power of multiple Grid nodes is required to cope with user job. Total account of markers is increased according to the number of nodes involved for running this job.

Any user job migration in Grid keeps arcs multiplicity at the level of one. Taking into account specified definition, there are only T- and F-transitions can exist in the Grid.

Modeling of Grid meets the problem of state explosion: number of states grows exponentially with increasing the number of nodes. For example, an initial marking of any Petri net representing the Grid has the following form: $M_0 = (m_1, \dots, m_n)$. Each marker of this marking set assumes a value between 0 and n_A , where n_A is a number of active Grid nodes. Let's there is no user job which can be produced on any node before previous one would have been finished ($n_A \leq n$), than total number of states describing that Grid is n_A^n (e.g., if n equals to 1000 nodes, then power of states set is 10^{3000}).

We suggest a partial order method to solve this problem. Let's define the partial order on the set of markings of Petri net. M_1 and M_2 are the markings of Petri net (N, M_0) . We

assume that $M_1 \leq M_2$ being in a partial order relationship, if for every marker m of marking M_1 situated in p position there is a marker m' of marking M_2 in the same position p , $m \leq m'$.

M_1 is less than M_2 relatively to order \leq , if marking M_1 can be obtained from marking M_2 by sequential markers removing from Petri net vertices.

Therefore, minimal partial order of marking M of Petri net is a natural number D such that for any marking M' being in partial order with M : $M' \leq M$ there is no marker m' of marking M' , where $m' < D$. Minimal partial order of the branching Petri net marking is equal to 1.

Theorem of reachability: any marking of the branched Petri net N reachable from marking M is also reachable from marking $M' = (m'_1, \dots, m'_n)$, $m'_i = \{0, 1\}$ which is obtained from N by applying to it the partial order equal to 1.

Proof. Consider the simple case when the branched Petri net is 2-limited. Common case can be proved in induction. For every $m \in M$: $m \leq 2$. By the definition the branching Petri net consists of aggregate of T- and F-transitions. Consecutively, consider all possible ways of such Petri net fragment aggregation.

- **T-transition—T-transition.** Branched Petri net fragment of such kind has 1 of 2 forms, as shown in Fig. 4.

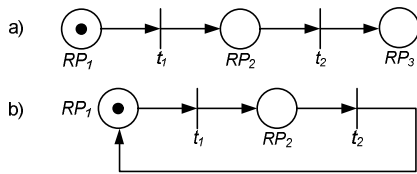


Fig. 4. The branched Petri net fragment of T-transition—T-transition type.

In that case, amount of markers at each position can be large. Find the set of reachable states for each form of branched Petri net fragment, taking into account deterministic form of transition function which means that *ceteris paribus* transitions are triggered simultaneously. For simplicity we also agree that all markers have the same type.

In induction $R(M_1) = R(M'_1)$ for $\forall D \in \mathbb{N}$: $M'_1 \leq M_1$. According to the Lemma 1 the minimal partial order of branching Petri net marking $D_{min}=1$. In addition, $\forall m' \in M'$: $m' = \{0, 1\}$, and we get $M' = (m'_1, \dots, m'_n)$, $m'_i = \{0, 1\}$.

- **F-transition—F-transition.** Branched Petri net fragment of such kind has 1 of 2 forms, as shown in Fig. 5.

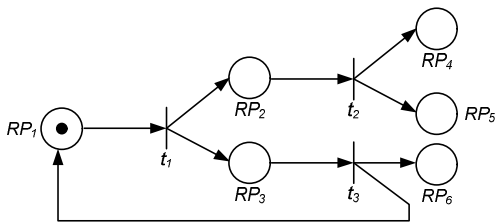


Fig. 5. The branched Petri net fragment of F-transition—F-transition type.

In induction $R(M_2)=R(M'_2)$ for $\forall D \in \mathbb{N}$: $M'_2 \leq M_2$. Minimal partial order of branching Petri net marking $D_{min} = 1$. Thus, we have $\forall m' \in M'$: $M' = (m'_1, \dots, m'_n)$, $m'_i = \{0, 1\}$.

- **F-transition—T-transition.** Branched Petri net fragment of such kind has 1 of 2 forms, as shown in Fig. 6.

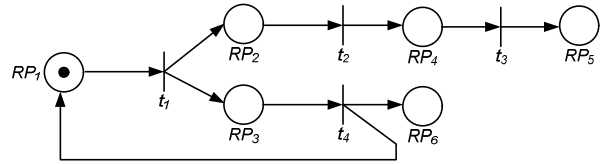


Fig. 6. The branched Petri net fragment of F-transition—T-transition type.

Following the induction, we get $R(M_3)=R(M'_3)$ for $\forall D \in \mathbb{N}$: $M'_3 \leq M_3$, where M_3 — marking of specified Petri net fragment. Thus, we get $\forall m' \in M'$: $M' = (m'_1, \dots, m'_n)$, $m'_i = \{0, 1\}$. The provisions of this theorem allows us to reduce a set of the states which describe the Grid from to n_A^n to 2^n .

Current security-based solutions referenced to describing and enforcement of security policies operate with a set of virtual organizations and fixed Grid states. These solutions do not take into account real access rights distribution at the level of user jobs running on Grid nodes. They also miss the fact of high intensity of job migration among Grid nodes.

The proposed method of secure user tasks distribution is based on the solution of a reachability problem in terms of Petri net describing the Grid. There is a reachability graph suggested to create for the specified Petri net $N=(RP, T, F, M)$ with initial marking $M_0 = (m_1, \dots, m_n)$, where vertices are the marking with minimum partial order equal to 1. According to Theorem if reachability, that tree must be a finite one. Vertices of this graph organize a set of the states which that system may reach. For every state from the set, a formalized transition function is used to determine compliance with security policy constraints. Verification is performed by comparison of security policy requirements with the current state.

As a result, there is the set of Grid nodes user jobs transition to which is permitted by security policy rules. After that, the rules of user tasks distribution are transmitted to such nodes (Fig. 7).

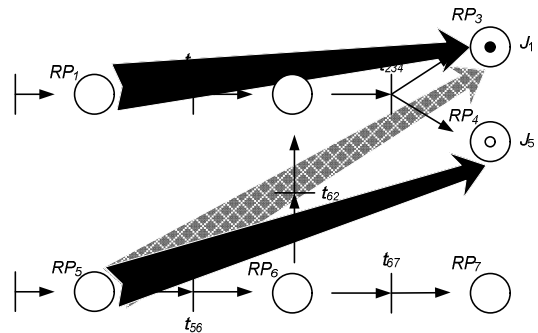


Fig. 7. Sample schema of secure user job distribution

Implementation of secure user job distribution system in the Grid allows us to protect data from computer attacks.

IV. CONCLUSION AND FUTURE WORK

A new approach of Grid security modeling is proposed. Subclass of colored Petri nets named 'branched Petri nets' is used to represent behavior of Grid. Extremely large size of models representing real high distributed systems causes the problem of state explosion for which partial order method has been applied.

We have proposed the secure user jobs distribution method based on reachability tree building.

The future works involves access control system integration to Grid commercial platforms.

REFERENCES

- [1] I. Foster, C. Kesselman. *The Grid: Blueprint for a New Computing Infrastructure* (2nd Edition), 2004.
- [2] S. Naqvi and M. Riguidel, "Threat model for grid security services", *Lecture Notes in Computer Science*, vol. 3470, 2005, pp. 1048-1055, doi:10.1007/11508380_107.
- [3] H. Lohr, H. V. Ramasamy, A. Sadeghi, S. Schulz, M. Schunter, and C. Stuble, "Enhancing grid security using trusted virtualization", *Lecture Notes in Computer Science*, vol. 4610, 2007, pp. 372-384, doi: 10.1007/978-3-540-73547-2_39.
- [4] T. Stepanova, D. Zegzhda, M. Kalinin, and P. Baranov, "Mobile anomaly detector module based on power consumption analysis", *Proc. International Conference on Information Security and Privacy (ISP-10)*, Jul. 2010, pp. 85-89.
- [5] M. Burgess, "Probabilistic anomaly detection in distributed computer networks", *Science of Computer Programming*, vol. 60, Mar. 2006, pp. 1-26, doi:10.1016/j.scico.2005.06.001.
- [6] S. Song, K. Hwang and M. Macwan, "Fuzzy trust integration for security enforcement in grid computing", *Lecture Notes in Computer Science*, vol. 3222, 2004, pp. 9-21, doi: 10.1007/978-3-540-30141-7_6.
- [7] D. Gomez, "Secure collaborative grid computing", Johns Hopkins Whiting School of Engineering, Spring 2008.
- [8] L. Pearlman, C. Kesselman, V. Welch, I. Foster, and S. Tuecke, "The community authorization service: status and future", *Proc. of Computing in High Energy Physics 03 (CHEP '03)*, 2003, pp. 44-52.
- [9] A. Chakrabarti, "Grid computing security", Berlin: Springer, 2007.
- [10] T. Stepanova and D. Zegzhda, "Stochastic model of interaction between botnets and distributed computer defense systems", *Computer Network Security, Lecture Notes in Computer Science*, vol. 7531, 2012, pp. 218-225, doi: 10.1007/978-3-642-33704-8_19.
- [11] V. Kozura, "Unfoldings of coloured Petri nets", *Lecture Notes in Computer Science*, vol. 2244, 2001, pp. 268-278, doi:10.1007/3-540-45575-2_27.
- [12] J. Couvreur, D. Poitrenaud and P. Weil, "Branching processes of general Petri nets", *Lecture Notes in Computer Science*, vol. 6709, 2011, pp. 129-148, doi: 10.1007/978-3-642-21834-7_8.

FPGA based Omnidirectional Video Acquisition Device (OVAD)

Jan Kwiatkowski, Dawid Sobel, Karol Jędrasiak and Aleksander Nawrat
Silesian University of Technology, Institute of Automatic Control, Gliwice, Poland

Abstract Nowadays, together with development of technology, and thus utilization of unmanned systems such as UAVs, providing wide field of view constantly becomes more and more important. One of solutions designed to solve that problem is OVAD (Omnidirectional Video Acquisition Device). A device, which was implemented using analog cameras and STM32 microcontroller, has proven its validity during testing process. The device may be found as useful in many applications, both civilian and military. However, size and weight of the device made it difficult to implement OVAD on small unmanned vehicles. Proposed solution is FPGA based OVAD, which is result of OVAD further development.

Keywords—omnidirectional camera, image processing, FPGA.

I. INTRODUCTION

The problem of omnidirectional video acquisition is an issue, which has been considered for many years, by engineers throughout the world. The need for providing 360 degrees of horizontal or vertical field of view is present among many branches of contemporary industry, such as surveillance systems, military, robotics, etc. In example, cameras, providing half-spherical field of view are widely used in military applications such as unmanned vehicles, where a necessity of observing all of vehicle surroundings is inevitable. Moreover, most of the time, success of a mission depends on information provided by vision system.

Nowadays, there are many devices, which can be a solution of the problem of omnidirectional video acquisition. One of them is a camera equipped with fisheye lens (Fig. 1, section c). Utilization of this particular type of lens creates a possibility to acquire video from a very wide angle. One of its greatest advantages is that this device does not include moving parts, which is associated with low susceptibility to external factors, such as shocks or adverse weather conditions. However, the image acquired by the device is significantly distorted [1]. Lens distortion, the fifth of the Seidel aberrations, is manifested by distortion of acquired image, which depends on the distance from its optical centre [2]. The occurrence of distortion always results in corruption of information carried by the image, while software elimination of distortion is always connected to loss of the information.

This work has been supported by Applied Research Programme of the National Centre for Research and Development as a project ID 178438 path A - Costume for acquisition of human movement based on IMU sensors with collection, visualization and data analysis software

Another, often utilized solution is PTZ camera (pan-tilt-zoom camera) (Fig. 1, section a). This device is based on utilization of one or more servomotors, which rotate the camera. Such a solution may prove imperfect in situations, when moving parts are exposed to dusty or pollinated environment. In this environment moving parts may become blocked, which may result in permanent damage of servomotor. If that situation occurs, the camera loses all of its original functionality, allowing only one direction of video acquisition [1].

The device, which combines advantages and eliminates disadvantages of both PTZ cameras and devices utilizing fisheye lenses is OVAD (Omnidirectional Video Acquisition Device) [1], presented in Fig. 1, section b. OVAD is made of multiple cameras, which are positioned statically in a way that provides 360 degrees of horizontal field of view. Video streams, acquired by adjacent cameras are combined into panorama. Thanks to that solution OVAD provides 360 degree of horizontal field of view without utilization of any moving elements, while preventing image from being significantly distorted. It is possible to immediately change the direction of video acquisition. Furthermore, failure of one cameras results only in losing part of field of view, while it does not cause a total loss of information, as in solutions based on single camera. Unfortunately, this solution has one major disadvantage. It is caused by utilization of analog cameras, which are too large and heavy to be able to be used on small vehicles, such as UAV (Unmanned Aerial Vehicle) [18-20].

Solution to the problems mentioned is utilization of digital cameras, which may have significantly smaller dimensions than analog cameras, while preserving similar quality of acquired video stream. However, the solution requires a system capable of real-time collecting and processing data acquired from multiple cameras. That problem is solved by utilization of FPGA, which are capable of parallel processing.

Utilization of FPGA in vision processing is not a new concept. Among present implementations, known are many solutions, such as using FPGA to process video data acquired from thermal [11], hyperspectral [12] and conventional cameras [16]. Another example of using FPGA in modern concepts is implementation of image processing algorithms, low-level, operating individual pixels, intermediate-level, converting pixels to a different representations (e.g. histogram, DFT, etc.), as well as high-level algorithms, designed to extract meaning from an image, [13, 17, 21] such as optical

flow extraction [15] or analysis of an image using neural networks, basing on FPGA allowance to access a number of subroutines in parallel [12].

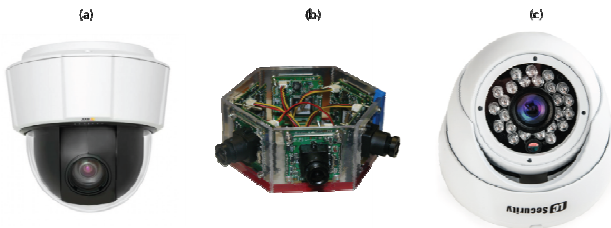


Fig. 1 PTZ camera AXIS P5532-E (a), OVAD (b), LC-1120 FISHEYE Premium (c) [1].

II. HARDWARE

Selection of appropriate equipment used to create FPGA based OVAD is very important task. Utilized parts have to be capable of real-time video acquisition, which involves collecting and processing data acquired from multiple cameras. Implementation of hardware required selection of cameras, FPGA and RAM used to store one frame obtained by each camera.

A. Cameras

Utilized cameras are OmniVision OVM7690 (Fig. 2). Maximum resolution of video acquired by that devices is 640x480. Their biggest advantage is small size and weight. Selected parameters of the cameras are presented in Table 1 [8].



Fig. 2 OVM7690 camera [10].

Before starting an acquisition every camera has to be properly configured. Configuration of OmniVision devices is being carried through SCCB (Serial Camera Control Bus), 2-wire interface similar to I²C. 2-wire SCCB consists of two master-slave connections: SCL and SDA. SCL line is used to transmit clock signal, while SDA is a bidirectional data line. Each subsequent byte is transmitted in 9 clock cycles. During the first 8 cycles data byte is transmitted, from MSB to LSB. The last, 9th cycle is used to determine whether information sent was acknowledged by destined device. During that cycle, when receiver acknowledges received byte, it forces low state on SDA line [3]. Operation of writing value to camera register requires sending three consecutive bytes. The first one contains 7-bit word containing slave device ID and one bit which carries information whether an incoming operation will be write register value or read register value. Second byte, called sub-address byte, contains 8-bit address of chosen

register, to which configuration data (sent in third telegram) is supposed to be written.

Parameter	Value
Active array size	640 x 480
operating temp. range	-30°C to 70°C
stable image temp. range	0°C to 50°C
output formats	YUV422 / YCbCr422, RGB565, CCIR656, raw RGB
input clock frequency	6 ~ 27 MHz
maximum image transfer rate	VGA (640x480): 30 FPS QVGA (320x240): 60FPS
package dimensions	2517μm x 2967μm x 2465μm

Table 1. Cameras specifications given by manufacturer.

B. Field-programmable Gate Array (FPGA)

Acquisition of data from multiple cameras means, that, in every second, huge amount of data will flow through the system. Maintaining real-time processing of the data means, that the device must be based on either CPU with relatively high computing abilities or CPU capable of parallel processing, when the same performance can be achieved at much lower clock frequencies. Parallel processing can be achieved through utilization of FPGA, which, along with pipelining is intrinsic resource of FPGA.

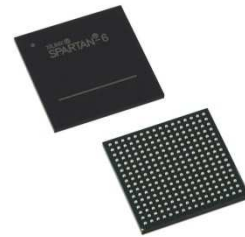


Fig. 3 Xilinx Spartan-6 XC6SLX16 [10].

FPGAs are composed of an array of independent components, called CLB (Configurable Logic Block). These elements can perform complex or simple logic functions such as logic gates, multiplexers, flip-flops, etc. They are connected to each other via configurable bus network, managed by interconnect blocks. Thanks to that feature, it is possible to configure FPGA in a way that two or more independent tasks can be executed in parallel to each other.

Configurable logic blocks are configured through filling LUT (Look-up table), a table, where all ready-made solutions, for every possible combination of inputs, are stored. Utilization of LUTs makes complex logical functions extremely simplified, every calculation can be performed in one clock cycle. Moreover, execution of parallel, independent components implemented in FPGA, does not require to be synchronized with a single clock signal [14]. Components can be triggered from any input, which means that FPGAs are capable of asynchronous processing.

Field-programmable Gate Array used in the device is Xilinx Spartan-6 XC6SLX16 [4] (Fig. 3.), available on Digilent

Nexys™ 3 Spartan-6 FPGA Board [9]. The board is equipped with 100MHz oscillator, however, according to datasheet [9], via utilization of DCM (Digital Clock Manager) and PLL (Phase-Locked Loop), clocking frequency can be increased to a value greater than 500MHz. FPGA based OVAD does not use that feature, because memory used in that device can be clocked at maximum frequency of 80MHz [7].

C. Memory

Maintaining independence between displaying and collecting of data acquired by multiple cameras requires storing a single frame from each camera. FPGAs, despite their incredible computing capability, proves very inefficient in terms of storing large amount of data. Every modern FPGA is backed up by dedicated memory blocks, called BlockRAM. However, BlockRAM capacity is not sufficient to store one frame obtained even by single camera. In consequence, use of external memory was necessary.

Used FPGA is placed on Digilent Nexys™ 3 Spartan-6 FPGA Board (Fig. 5.). The same board includes three components designed for memory storage: 16Mbyte Micron Cellular RAM, 16Mbyte Micron Parallel PCM and 16Mbyte Micron Quad-mode SPI PCM [9]. From the perspective of FPGA based OVAD, the best solution turned out to be Micron MT45W8MW16 [7] (Fig. 4.), which has 16bit parallel data bus and 23bit address bus. When working at maximum possible clock frequency equal to 80MHz, chosen memory can perform operation of write and read fast enough to store data acquired from several cameras. The memory can operate in two modes – asynchronous and burst. The most convenient option would be using asynchronous mode, however, in that mode, required time interval between two data operations is 100ns, which means maximum clocking speed equal to 10MHz. This maximum frequency is insufficient for real-time data acquisition. Therefore, it was necessary to use burst mode. Disadvantages of the mode are delay associated with the initialization of read or write operation, and inability of interspersing of read and write operations during single burst. However, after proper read/write burst initialization, memory can store up to 128 16bit words at a frequency of up to 80MHz (in a single burst), which is advantageous from the point of view of the described problem.



Fig. 4 Digilent Nexys 3 Spartan-6 FPGA Board [9].

III. IMPLEMENTATION

FPGA program has been written in VHDL language. Due to compatibility of the selected FPGA with the software provided by manufacturer, used development tool is Xilinx ISE Design Suite 14.7.

One of assumptions made during implementation planning was full application modularity. Required elements (defined in VHDL as components), which had to be implemented on FPGA are: component which handles data acquisition from camera, component which configures all cameras, component responsible for handling memory, and component responsible for handling the output. The output of FPGA based OVAD is a D-Sub connector, via which video is transmitted to receiver. Video standard used by the device is VGA (Video Graphics Array) . Main advantage of modular approach is that parts, such as cameras or memory, can be easily replaced with different types. Exchange would mean updating or replacing of only single component, but should not affect the rest of program implemented on FPGA.

The implemented solution uses asynchronous processing, supported by FPGA, due to the need of connecting components triggered by clock signals running at different frequencies. Each camera transmits its own, independent PCLK (Pixel CLock) signal, indicating, that pixel is ready to receive, while external memory works at frequency of 80 MHz. Subsequent components of camera-memory-display path are connected via asynchronous FIFO (First In First Out) buffers. This solution supports memory working in burst mode, when during single burst write and read operations cannot intersperse. By utilization of FIFO buffers, pixels ready to be written into memory are not lost when read operation is performed, but are stored in adequate buffers. FIFO buffers have been generated by IP Core Generator, and provide asynchronous work at frequency of read/write operation up to 500MHz [5]. IP Core Generator is an integral part of Xilinx ISE Design Suite and was also used to generate component providing all necessary clock signals (prescaler) [6].

Schematic, which describes the program implemented in FPGA is shown in Fig.6. The first step is to configure cameras via SCCB interface. At the same time memory configuration is performed. When configuration of all cameras ends, component responsible of configuration of cameras sets *acq_en* output, which triggers start of video acquisition. Data acquired by each camera is stored in adequate FIFO buffer. When FIFO buffer, used to store incoming data, is half-full, a signal is sent to memory management module, which stores write requests in its own operation queue. After executing all previous requests, write burst operation is performed. A similar situation occurs during processing data acquired to the display control module. When FIFO, used to store output data, is half-empty, request to read more data from memory is sent to memory management module, and stored in operation queue. Therefore, when memory is working at frequency, that provides appropriate read and write speed, FIFO used to store incoming pixels will never overflow, and FIFO used to store output data will never become empty.

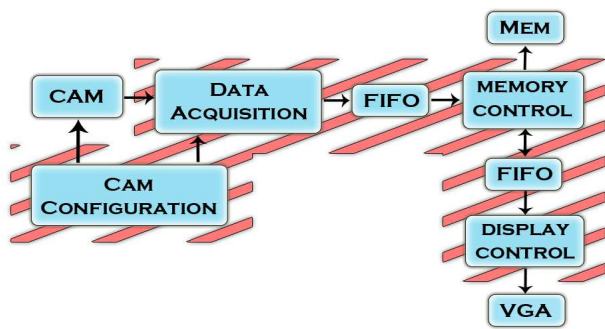


Fig. 5 Simplified schematic presenting interconnections between modules. Modules marked with red stripes are implemented using FPGA.

IV. SUMMARY

Use The implemented solution has proven to be the right approach in further development of OVAD. In the age of digital technology, utilization of digital cameras, backed up by FPGA and external memory, resulted in significant improvement in comparison with the previous version of the device. Main advantages, which should be distinguished, are:

- reducing size of device, while maintaining quality of acquired image – use of cameras, which dimensions are $2517\mu\text{m} \times 2967\mu\text{m} \times 2465\mu\text{m}$ resulted in significant reduction of size and weight of the device,
- ease of processing and analysis of digital image – transfer of an digital image is less vulnerable to transmission disturbances; moreover, flexibility in choosing transmission interface is evident. It is possible to use widely-used interfaces, such as Ethernet, USB, etc.,
- extended prospects for further development – utilization of respectively advanced FPGA creates a possibility to use cameras able to acquire higher resolution video, moreover, creates a flexibility of choosing the way of presenting and storing of data acquired, as well as possibility to implement additional modules designed for analysis and processing the acquired data, without changing the physical structure of the device.

In conclusion, similarly to OVAD, FPGA based OVAD can be found useful in many branches of technology, both civilian and military. Resistance to weather condition (in comparison to PTZ camera), as well as insignificant optical distortion (in comparison to camera equipped with fisheye lens), makes the device competitive option among existing solutions. In addition, costs of the device may still be several times less than the price of PTZ cameras.

REFERENCES

- [1] G. O. Young, "Synthetic structure of industrial plastics (Book style with paper title and editor)," in *Plastics*, 2nd ed. vol. 3, J. Peters, Ed. New York: McGraw-Hill, 1964, pp. 15–64.
- [2] Fraś, S., Jędrasiak, K., Kwiatkowski, J., Nawrat, A., & Sobel, D. (2013). Omnidirectional Video Acquisition Device (OVAD). In *Vision Based Systems for UAV Applications* (pp. 123-136). Springer International Publishing.
- [3] Jenkins, F. A., & White, H. E. (1957). *Fundamentals of optics*. New York: McGraw-Hill, 1957, 3rd ed., 1.

- [4] OmniVision, OmniVision Serial Camera Control Bus (SCCB) Functional Specification [online], [access: March 2014], access via Internet: <http://www.ovt.com/>,
- [5] Official Xilinx website, [access: March 2014], access via Internet: <http://www.xilinx.com/>,
- [6] Xilinx, LogiCORE IP FIFO Generator v8.1 [online], [access: March 2014], access via Internet: <http://www.xilinx.com/>,
- [7] Xilinx, LogiCORE IP Clock Generator (v4.01a) [online], [access: March 2014], access via Internet: <http://www.xilinx.com/>,
- [8] Micron, MT45W8MW16BGX datasheet [online], [access: March 2014], access via Internet: <http://www.micron.com/>,
- [9] OmniVision, OVM7690 product [online], [access: March 2014], access via Internet: <http://www.ovt.com/>,
- [10] Official Digikey website, [access: March 2014], access via Internet: <http://www.digilentinc.com/>,
- [11] Official Digi-Key website, [access: March 2014], access via Internet: <http://www.digkey.com/>
- [12] Bieszczak, G., Krupiński, M., Madura, H., & Sosnowski, T. (2013). Thermal Camera for Autonomous Mobile Platforms. In *Vision Based Systems for UAV Applications* (pp. 95-114). Springer International Publishing.
- [13] Nordin, A., Hsu, C. C., & Szu, H. H. (2001, March). Design of FPGA ICA for hyperspectral imaging processing. In *Aerospace/Defense Sensing, Simulation, and Controls* (pp. 444-454). International Society for Optics and Photonics.
- [14] Johnston, C. T., Gribbon, K. T., & Bailey, D. G. (2004, November). Implementing image processing algorithms on FPGAs. In *Proceedings of the Eleventh Electronics New Zealand Conference, ENZCon'04* (pp. 118-123),
- [15] Bailey, D. G. (2011). *Design for embedded image processing on FPGAs*. John Wiley & Sons.
- [16] Díaz, J., Ros, E., Pelayo, F., Ortigosa, E. M., & Mota, S. (2006). FPGA-based real-time optical-flow system. *Circuits and Systems for Video Technology, IEEE Transactions on*, 16(2), 274-279.
- [17] Jin, S., Cho, J., Dai Pham, X., Lee, K. M., Park, S. K., Kim, M., & Jeon, J. W. (2010). FPGA design and implementation of a real-time stereo vision system. *Circuits and Systems for Video Technology, IEEE Transactions on*, 20(1), 15-26.
- [18] Grzejszczak, T., Mikulski, M., Szkodny, T., Jedrasiak, K., *Gesture Based Robot Control, Computer Vision and Graphics, Lecture Notes in Computer Science*, vol. 7594, pp. 407-413, Springer-Verlag, 2013.
- [19] Jedrasiak, K., Nawrat, A., *Image Recognition Technique for Unmanned Aerial Vehicles, Computer Vision and Graphics, Lecture Notes in Computer Science*, vol. 5337, pp. 391-399, Springer-Verlag, 2009.
- [20] Iwaneczko, P., Jedrasiak, K., Daniec, K., Nawrat, A., *A Prototype of Unmanned Aerial Vehicle for Image Acquisition, Computer Vision and Graphics, Lecture Notes in Computer Science*, vol. 7594, pp. 87-94, Springer-Verlag, 2013.
- [21] Nawrat, A., Jedrasiak, K., *SETh system spatio-temporal object tracking using combined color and motion features, 9th WSEAS International Conference on Robotics, Control and Manufacturing Technology, Hangzhou, China, 2009.*
- [22] Jedrasiak, K., Nawrat, A., Daniec, K., Koteras, R., Mikulski, M., Grzejszczak, T., *A Prototype Device for Concealed Weapon Detection Using IR and CMOS Cameras Fast Image Fusion, Computer Vision and Graphics, Lecture Notes in Computer Science*, vol. 7594, pp. 423-432, Springer-Verlag, 2013.

Top-level Power Unit System and the task “Calculation of Technical and Economical Indexes” for the “Kudankulam” NPP

Elena. Ph. Jharko

Abstract— In the nuclear power engineering, methods of detection faults and diagnostics, as well as systems of information support of human-operators in order to increase the safety and reliability of the operation play the increasing role. One of tasks solved within the information support is the task of calculating technical and economical indexes. The problem of calculation of technical and economical indexes and its place in the make-up of the application software of the unit level control system of the automated process control system of the nuclear power plant “Kudankulam” is considered.

Keywords— efficiency, nuclear power plant, technical and economical indexes, upper level control system.

I. INTRODUCTION

Under development of systems for power engineering, where the operation period of the main equipment is dozens of years, one should apply such solutions in the automated process control system (APCS), which would enable one to operate, repair, and update the installed equipment without stopping the technological process. Besides this requirement, providing high reliability, survivorship, and safety are the key requirements.

Analysis of advanced requirements, present status of hardware and software, tendencies of development enabled one to formulate a common approach to constructing systems for the power engineering: the systems are to be constructed either by use of own technologies, or by use of imported technologies. Meanwhile, the technologies imported are to be subject to an adaptation process that is to make them transparent and controllable to such a degree so as a supplier could expand his/her warranty obligations of duration of several dozens of years to them.

The nuclear power engineering is increasingly interested in utilizing techniques of fault detection and diagnostics to increase the safety and reliability of nuclear power plants (NPP) [1].

At present, a clear tendency was found to solve the problem of control of nuclear power plants by use of the problem statement implying the necessity of implementation at the upper level of the NPP APCS of a system providing a powerful information support of operator performance. Such an information support involves:

- Providing a possibility of fast analysis of current situation, by use of which the operator makes a decision on various control actions;
- Initiating (as an advise) actions needed for correct control of the technological process;
- Monitoring actions of the operator himself.

At present, V.A. Trapeznikov Institute of Control Sciences implements the development of the software of the upper level control system (ULCS) of the “Kudankulam” NPP APCS [2-8]. The ULCS is a system of automatic sampling, storing, displaying information on a current status of technological plants subject to control (TPSC) and automated remote forming commands of control of TPSC mechanisms by use of the APCS algorithms.

The purpose of creating the ULCS is providing centralization of monitoring and control of the technological process for:

- Economically efficient manufacturing the electrical power;
- Observing the operation margins;
- Observing the margins and conditions of safe operation of the equipment;
- Improving characteristics of technological processes and performance of the technological equipment;
- Decreasing the labor-output ration of the equipment performance, improving hardware repair ability, decreasing the number of service personnel, improving consumer characteristics of APCS elements;
- Improving personnel labor conditions and decreasing the number and reducing the consequences of error actions of operators.

The ULCS is a complex software and hardware system, supported by a computer aided design and tuning system, and intended to unite in a unique system all subsystems of the APCS. The ULCS implements information, control, service, and auxiliary functions of the NPP APCS (see Table I).

The information task “Calculation of technical and economical indexes” (“IT-TEI”) is a computational application and is involved into the make-up of the application software of the “Kudankulam” APCS ULCS developed by the V.A. Trapeznikov Institute of Control Sciences. The IT-TEI task performs in the automatic mode.

Since there exist no two equivalent power units of an NPP, a problem of creating a software oriented to a particularity of a specific power unit of the NPP only, both in the part of hardware and accounting available monitoring points of technological parameters. But in spite of available distinctions of nuclear power units, applying a unified methodology is possible under implementation of the information task of calculating technical and economical indexes [5, 9].

Elena Ph. Jharko (IEC expert) is with the Laboratory of System Identification of the V.A. Trapeznikov Institute of Control Sciences of the Russian Academy of Sciences, Moscow, Russia, e-mail: zharko@ipu.ru.

Calculating TEI is the technological basis of automated receiving information characterizing the heat efficiency of the power unit and equipment involved into its make-up. Meanwhile, the heat efficiency (hereinafter, as just, “efficiency”) is understood as the efficiency of using the heat extracted in the reactor by the nuclear fuel to produce the electric power.

TABLE I. ULCS TASKS

№	Tasks
1.	Information tasks
1.1	Acquisition of data on the commands of the personnel
1.2	Analysis of messages arrival and events protocol formation
1.3	Reference information presentation
1.4	Presentation of recommendations for controlling energy-release fields formed in Monitoring, Control and Diagnostics System (MCDS)
1.5	Safety parameters presentation
1.6	Presentation of information on safety system channels readiness
1.7	Presentation of diagnostic information about process equipment operation coming from MCDS
1.8	Analysis of remote control commands nonpassage
1.9	Displaying the results of analysis on conformance of the controlled objects location to the given commands
1.10	Calculation of TEI and displaying of its results
1.11	Displaying mimic circuits and videogramms on videomonitors, indication of the controlled objects current state on videomonitors
1.12	Displaying the information for control on videomonitors
1.13	Emergency and preventative signaling on videomonitors
1.14	Presenting the information on calculation tasks and tasks of the analysis of TPSC operative state and diagnostics
1.15	Presenting the information about operation modes of the equipment and automatics
1.16	Registration and archiving of TPSC current state and process events, transition processes
1.17	Registration of receiving, issuing and processing of control actions inputted from ULCS
1.18	Registration of receiving, issuing and processing of control actions inputted by using the keys of individual control
1.19	Archiving the equipment work resource and its operation diagnostics
1.20	Registration and archiving of information on the process equipment state, repairs and process equipment replacements
1.21	Registration and archiving operator records
1.22	Print out of data and periodical reports per a shift
2.	Control Task
2.1	Normal operation and important for safety equipment remote control from workstation videomonitors
2.2	Automatic control
3.	Auxiliary Tasks
3.1	Acquisition and processing of the information about Automated process control system (APCS) means and system state
3.2	ULCS soft-and-hardware diagnostics
3.3	Universal time-keeping and marks assignment at diagnostics data collection
3.4	Informational support of system standard operation control
3.5	ULCS functioning control
3.6	Automatic control of ULCS SHC automated reserved elements reconfiguring, system restart after its failure due to common cause (power shutdown)
3.7	Data exchange with TLPS
3.8	Protection against unauthorized access

The purpose of the TEI calculation is providing information on mostly efficient use of the equipment, prediction of its service and repair, as well as preparation reports on the power unit efficiency.

II. THE INFORMATION TASK “IT-TEI”

The prospect of having performance measures that are useful in gauging the economic and financial success of business enterprises is certainly not new. It is well recognized that there are a plethora of commonly used standard measures that have been successfully employed by the business and financial community, as well as by electric utilities, throughout the world for a very long time. Clearly, when it comes to the safety and reliability of nuclear plants, there is no question as to the industry’s achievements in developing and implementing superlative nuclear performance indicators and the processes to engage them, on a worldwide basis. Over the years, the world nuclear industry’s development and application of WANO and PRIS performance indicators have contributed significantly to substantial improvements in the operating and safety performance of nuclear power plants. Although many nuclear plants have traditionally embraced simple economic measures of resource utilization and budget performance, little has been achieved to date to standardize and implement economic and financial performance measures that help to assure economic competitiveness and financial success at the nuclear plant generating level. Theoretically, the performance associated with any aspect of constructing or operating a nuclear power plant affords some degree of economic consequence [10].

The functional intention of the information task “IT-TEI” is implementation of processes of sampling, preliminary processing, determining, and analysis of the TEI for operative and reporting intervals, displaying and registering results of the calculation, preparing and re-setting the software (SW) within the operation process.

The operation intention of the information task “IT-TEI” is providing operative and production and technical personnel of the “Kudankulam” NPP with operative and reporting information of the efficiency of operation of the technological equipment.

The information task “IT-TEI” is solved for the main equipment influencing the efficiency of the power unit, as well as for the equipment, which status defines the mode of the power unit performance.

The make-up of the first group involves equipment whose status is assessed on the basis of results of performance of a complex of tasks. This equipment involves the turbine compartment, high pressure heaters, low pressure heaters, separator-steam-superheater, condenser, deaerator, etc.

The make-up of the second group involves equipment (pumps, valves) in dependence on the status and position the mode of performance of technological systems of the primary and secondary circuits is changed, and accordingly the algorithm of the TEI calculation is changed. This equipment involves feeding and condensing pumps, valves at feeding and condensing lines, main circulation pumps, etc.

Output IT-TEI information is displayed at the automated workplaces (AWP) of the senior engineer on reactor control, AWP of the senior engineer on turbine control, and AWP of the shift supervisor of the power unit.

III. THE SCHEME OF IMPLEMENTATION OF THE TASK "IT-TEI"

The software developed of the information task "IT-TEI" is separated in the type solved problems and consist of the following main parts:

- providing the calculation itself, analysis and displaying of the calculation at the automated work places of the results of the TEI calculation (it performs on-line);
- providing preparation of forms of reports (it performs in the interactive mode);
- providing service functions (it performs in the interactive mode).

The software application of the calculation of the TEI performs jointly with the ULCS SW and is developed accounting the requirements to the:

- fault-tolerance;
- software application reliability;
- providing temporal characteristics.

The TEI calculation is implemented within the range 5-100% of the electric power, the calculation is considered as authentic under the generator power being more than 30%. Under the generator power being lower than 30%, values obtained as a result of the calculation are assigned with the sign of unauthenticity.

The TEI calculation is a technological basis of automatic receiving information characterizing the heat efficiency of the power unit and equipment involved in its make-up. Meanwhile, the heat efficiency (hereinafter, the "efficiency") is understood the efficiency of use of the heat extracted by the nuclear fuel in the reactor to produce the electric power.

The TEI calculation is implemented by use of mutually coordinated complex of tasks, which involves:

- primary processing of initial information (input data enter the task with the period of 1 minute), which involves:
 - ordering current values;
 - gathering and forming arrays of analog and discrete information;
 - determining current values of discrete indicators characterizing the status of technological pieces of equipment, and forming analog values with accounting the current magnitude of discrete signal (for values measured at elements of equipment that may be turned off);
- implementing at the operative interval subsequently the following operations:
 - checking the authenticity of all analog values with preliminary calculation of auxiliary values intended to monitoring;
 - processing initial information (determining absolute pressures, thermodynamic functions, average values of parameters over several parallel flows, weight values of the coolant);
 - forming array of input information for the TEI calculation;
 - determining auxiliary calculation values;
 - calculating gathered values;
 - calculating the technical and economical indexes at the operative interval;

- preparations of forms of representation fo information;
- forming arrays of the shift, day, and month intervals;
- calculating the TEI at the shift, day, and month intervals by use of corresponding arrays of gathered values.

All calculated technical and economical indexes are separated onto three main groups:

- Actual indexes that characterize the level of efficiency of the equipment under operation conditions;
- Normative indexes that characterize a rated level of the equipment efficiency;
- Indexes of the change of the efficiency of the power unit due to deviation of the actual indexes from the normative ones.

The initial time period (sampling period) is a time segment between the beginnings of two cycles of sensor sampling, following one after another. The duration of the sampling period is accepted unique with other APCS functions. To calculate the TEI, the mostly rational duration of the sampling period 1 minute is.

To calculate the TEI, the following time intervals are envisaged, for which the calculation is implemented:

- Operative interval accepted being equal to 15 minutes;
- Shift, an interval being equal to the duration of one working shift;
- Day, a time interval being equal to 24 hours;
- Month, an interval being equal to the number of hours in a calendar month.

In dependence on an interval, within which the indexes are calculated, these are referred as operative, shift, day, and month intervals. Besides these indexes, obtaining integral indexes as progressive total is envisioned from the beginning of a month till the time instant of a request within this month.

Upon completion of the calculation of the technical and economical indexes, in accordance to templates forms of reports are generated (where xx is interval indicator: 01 is an indicator of the operative interval; 02 is an indicator of the shift report; 03 is an indicator of the day report; 04 is an indicator of the month report):

- TEI01_xx General characteristics;
- TEI02_xx NSSS;
- TEI03_xx Steam Parameters and HPC seal conditions;
- TEI04_xx NSSS parameters;
- TEI05_xx SRH Parameters Analysis;
- TEI06_xx HPR Analysis;
- TEI07_xx LPR Analysis;
- TEI08_xx Turbine condenser analysis;
- TEI09_xx Feedwater pump analysis;
- TEI10_xx General Operation parameters of the power unit;
- TEI11_xx Turbine parameters;
- TEI12_xx Efficiency analysis of the Unit;
- TEI13_xx Unit performance during the month.

In Figure 1, the cycle of the performance of the information task of the TEI is presented.

In the archive of report files (the file `tep_date_time.log`), in dependence on a mode of the power unit performance, as well as in dependence on the authenticity of signals, records of the following types may be available:

- in the case if the active generator power is less than 300 MW (30% NAT), but more than 50 MW (5% NAT):

```
The TEI calculation reliability - BAD: Nat
(10CHE02CE043_XQ03)=<value> MW < 300 MW
```

meanwhile, the task of calculating the TEI is not blocked, but the calculation results are unauthentic.

- in the case of appearance of unauthentic:

```
Insufficient data to calculate TEI
Unreliable of input signals
<List of the signal>
```

- in case of authenticity of all input signals and active generator power is less than 50 MW:

```
The TEI task is blocked: Nat
(10CHE02CE043_XQ03)= <value> MW < 50 MW
```

meanwhile, the task of calculating the TEI is blocked.

- in the case of invalidation of at least one signal from the set of the most important parameters:

```
The TEI task is blocked due to invalidation of
the major power unit indexes:
<List of the signal>
```

meanwhile, the task of calculating the TEI is blocked.

- in case of authenticity of all input signals and active generator power is more than 300 MW:

```
Input signals - OK
The TEI calculation reliability - OK
```

Output information is displayed to the operative personnel to the video monitors of the workstation of the shift supervisor of the power unit in the form of special formats and/or on printing devices. Figures 3 and 4 present examples of a reporting form the "IT-TEI" and a video frame correspondingly: "Generalized indexes of the power unit". In the ULCS, a possibility of call of "IT-TEI" information to video monitors of workstations of the automated work places of the senior engineer on reactor control and senior engineer on turbine control.

IV. PROBLEMS OF THE TASK "IT-TEI"

For the task "IT-TEI", more than 400 analog and discrete signals are input parameters and, in the event if at least one of these signals is inauthentic, then receiving an authentic complete calculation of technical and economical parameters of the power unit becomes impossible; and displaying the operative information in video monitors of workstations of the automated work places of the senior engineer on reactor control and senior engineer on turbine control is not implemented. But during the start and adjustment works, a necessity of at least partial displaying information on the task has appeared in order:

- Diagnosing both equipment faults and non-conformities of the equipment to ranges of changes of analog signals;
- Determining the efficiency of use of the equipment.

Thus, the problem of implementing a decomposition of the task over input signals and eliciting influence of these signals onto output parameters has arisen (see Fig. 4). As a result, those output parameters will be calculated and outputted to

video monitors only, for which a complete set of required authentic input signals will be available.

But the task of calculating the technical and economical indexes is strongly connected, and individual input signals (both discrete and analog ones) participate in the calculation of enough large number of output parameters, and their inauthenticity (for instance, the flow of chemical desalted water to the turbine condensers) may gives rise to the exclusion from the calculation of up to 30% of output task parameters connected with this inauthentic signal.

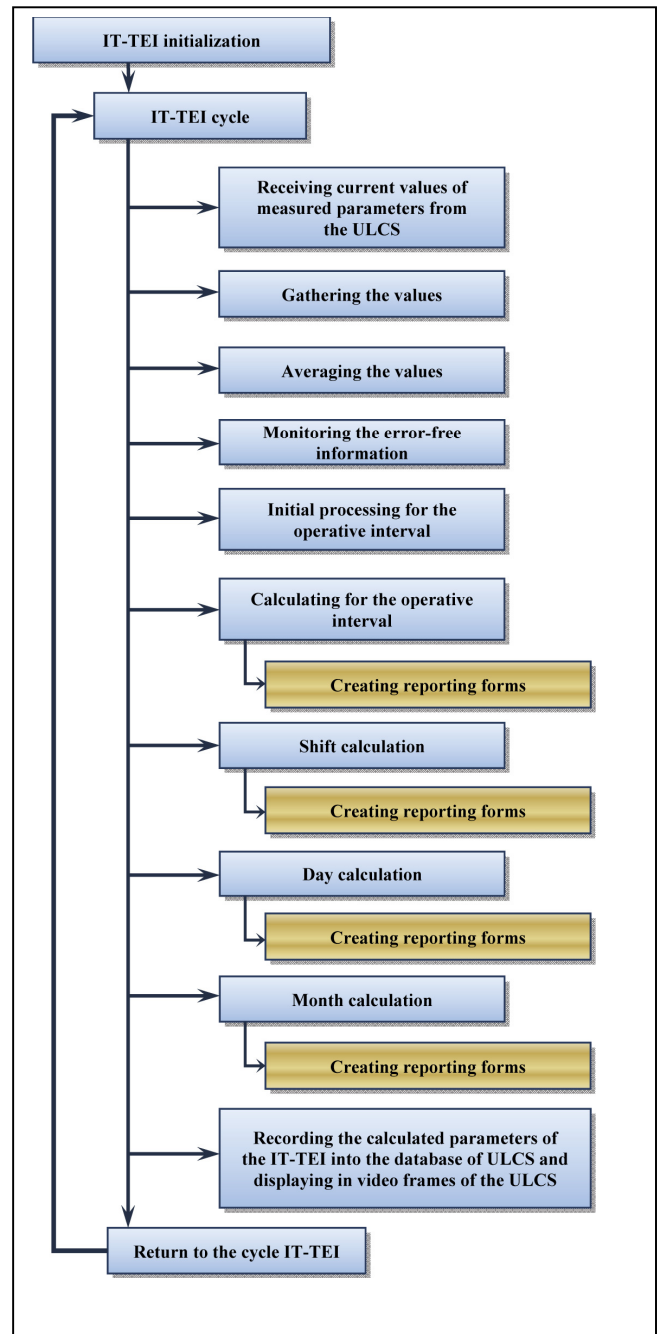


Figure 1. The cycle of the information task "IT-TEI".

TEI01_01 - General characteristics

N	Parameter	Changes in efficiency	
		kJ/kW	%
	Power average, MW	1000.00	
1	Specific consumption of heat for sold electricity, standard	37054.82	
Sources of change in economy:			
2	NSSS	29.54	
3	The parameters of steam and HPC turbine seals	-0.50	
4	Superheaters	1283.63	
5	HPR	-51.59	
6	LPR	-127.53	
7	Condensers	4570.67	
8	FWP	-19.51	
9	In-house electric supplies		17.02
10	Turbine	-629.73	
11	Summary changes	-25276.58	
12	Specific consumption of heat for sold electricity, actual	11778.23	

Figure 2. The reporting form "General characteristics"

GENERAL CHARACTERISTICS

No	Parameter	Changes in efficiency kJ/kWh	Changes in efficiency %
1	Specific consumption of heat for sold electricity, standard	100_0	
Sources of change in economy			
2	NSSS	100_00	
3	The parameters of steam and HPC turbine seals	100_0	
4	Superheaters	100_0	
5	HPR	100_0	
6	LPR	100_0	
7	Condensers	100_00	
8	FWP	100_0	
9	In-house electric supplies		100_0
10	Turbine	100_00	
11	Summary changes	100_00	
12	Specific consumption of heat for sold electricity, actual	100_00	

200WD108PF201

Figure 3. An example of the video frame "General characteristics"

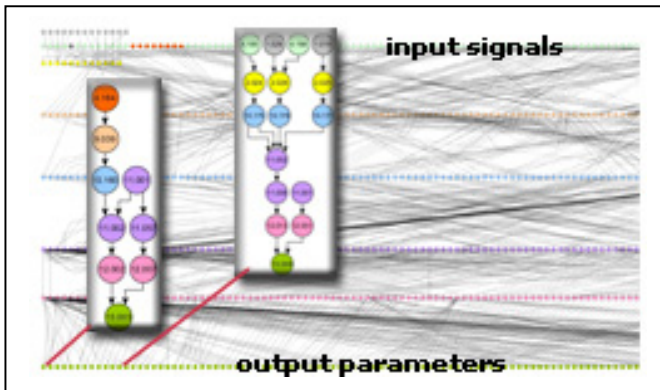


Figure 4. An example of the decomposition of the calculation

V. CONCLUSIONS

Under developing the software of the information task “IT-TEI”, unified approaches and solutions were used, being analogous to the ULCS SW in the part:

- Unification of components of the mathematical support by use of the module principle of constructing algorithms and unification of algorithmic modules;
- Unification of the functional structure and modules involved in it;
- Tools of implementation of the system functions and unique operator interface in the system;
- Using methods of the structure programming, module principle of constructing software components, and unification of the connections between the software modules by use of the unified software interfaces;
- Utilizing unique ways of structuring data and constructing data bases, data base control, access to data bases, and methods of connecting computer software applications and data.

The information task “IT-TEI” is solved for the main equipment influencing the power unit efficiency, as well as equipment whose status (state) defines the mode of the power unit performance.

The information task “IT-TEI” is implemented in the amount of organization structure, design solutions of the tools of automation of the “Kudankulam” NPP equipment, providing receiving information by the ULCS with a set periodicity. The calculation of the technical and economical indexes of the “Kudankulam” NPP is implemented with high accuracy that is expressed quantitatively in the accuracy of calculation of the reactor heat power:

- Under the nominal load (100%), inaccuracy of calculation of the heat power is to be not higher than 0,5% of the nominal power;
- Under the load of 30%, inaccuracy of calculation of the heat power is to be not higher than 1,5% of the nominal power.

The accuracy of the evaluation of the efficiency of performance of individual equipment is determined by the accuracy of regular channels of measurement of technological parameters. Since the complex of tasks presented is not concerned with providing or monitoring the power unit safety, requirements on an increased reliability are not imposed on the task “IT-TEI”.

REFERENCES

- [1] Ma, J. and J. Jiang, “Applications of fault detection and diagnosis methods in nuclear power plants: A review”, *Progress in Nuclear Energy*, 2011, vol. 53, no 3, pp. 255-266.
- [2] Byvaikov, M.E., Zharko, E.F., Mengazetdinov, N.E., Poletykin, A.G., Prangishvili, I.V. and V.G. Promyslov. “Experience from design and application of the top-level system of the process control system of nuclear power-plant”, *Automation and Remote Control*, 2006, vol. 67, no 5. pp. 735-747.
- [3] Zharko, E.F. “Flexible modeling complex for the operator support systems of UPP's with VVER-1000 reactor”, *Automation and Remote Control*, 2006, vol. 67, no 5. pp. 748-758.
- [4] Poletykin, A.G., Jharko, E.Ph., Zuenkova, I.N., Promyslov, V.G., Byvaikov, M.E., and N.E. Mengazetdinov. “Software for nuclear power engineering”, *Automation in industry*, 2006, no. 8, pp. 52-56. (in Russian)
- [5] Jharko, E.Ph. “Information task “Calculation of technical and economical indexes for the “Bushehr” NPP”, *Proceedings of the 6th Scientific Conference “Control and Information Technologies” UIT-2010*. St. Petersburg, Russia, October 12-14, 2010. Pp. 266-271. (in Russian)
- [6] Jharko, E.Ph. “Design of Intelligent Information Support Systems for Human-Operators of Complex Plants”, *Proceedings of the 17th IFAC World Congress*. Seoul, Korea, July 6-11, 2008. Pp. 2162-2167.
- [7] Jharko, E.Ph., O. Zaikin. “The Flexible Modeling Complex for an NPP Operator Support System”, *Proceedings of the 18th IFAC World Congress*. Milano, Italy, August 28 - September 2, 2011. Pp. 12156-12161.
- [8] Poletykin, A.G., Jharko, E.Ph., Zuenkova, I.N., Promyslov, V.G., Byvaikov, M.E., and N.E. Mengazetdinov. “Software for nuclear power engineering”, *Automation in industry*, 2006, no. 8, pp. 52-56. (in Russian)
- [9] Jharko, E.Ph. “Development of a software for the task “Calculation of technical and economical indexes” for the “Kudankulam” NPP”, *Proceedings of the 7th International Conference “Management of Large-Scale Systems Development” MLSD '2013*, V.A. Trapeznikov Institute of Control Sciences, Moscow, 2013. Vol. 2, pp. 270-272. (in Russian)
- [10] Technical Reports Series No. 437 (2006). Economic Performance Indicators for Nuclear Power Plants. IAEA. Vienna, 2006.

Shore-to-Sea Maritime Communication with Visible Light Transmission

Hyeongji Kim, Atul Sewaiwar and Yeon-Ho Chung

Abstract—Shore-to-sea maritime communication using visible light transmission is proposed. As it is based on LEDs for data transmission, it offers a low-cost, high-speed and low power consumption communication for maritime users. The proposed transmission considers unique properties of maritime environments where wave height, wind speed, etc. exist. Computer simulation results show that the proposed scheme can deliver a reliable performance up to approximately 120m under various sea states.

Keywords—Maritime communication, VLC, LEDs, e-Navigation

I. INTRODUCTION

Conventional maritime wireless communication is based on voice communication and usually operates with radio devices of various radio frequency bands, e.g. Very High Frequency (VHF). For remote environments, satellite systems are in use for broad coverage. Maritime wireless communication is, however, differentiated from its terrestrial counterpart, because service environments are distinctly different. Global maritime communication between sea users and the rest of the world is technically developed and provided, but at a high cost.

The radio devices loaded to a vessel are determined according to the size and sailing area of the vessel. The radio types for sailing vessels are defined by International Maritime Organization (IMO) and International Telecommunication Union (ITU) [1]. Further, IMO defined the maritime wireless communication according to technology and communication coverage as in Table I. A1 and A2 are massive complex areas of each country where small ships are sailing. A3 and A4 areas are ocean region where large ships are sailing [2].

Table I. IMO definition of sea area

Sea Area	Technology	Communication Coverage
A1	VHF	Coast (20~30 miles)
A2	MF	Offshore (about 100 miles)
A3	INMARSAT/HF	70° N and 70° S
A4	HF, MF, VHF	The remaining sea areas

This work was supported by the Research Grant of BB (Brain Busan) 21 Project of 2014.

Hyeongji Kim, Atul Sewaiwar and Yeon-Ho Chung are with Information and Communications Engineering, Pukyong National University, Korea (corresponding author is Yeon-Ho Chung, phone: +82 51 629-6236; e-mail: yhchung@pknpu.ac.kr)

e-Navigation is a concept of maritime safety and security formulated and launched by IMO [3]. It is based on the electronically collected maritime data information onboard and ashore to enhance berth to berth navigation and related services at sea and also to protect the marine environment. Sea users need a high-speed and low-cost maritime wireless communication like on land. However, current wireless communications at sea mainly rely on satellite links that are relatively slow than HF and VHF or on expensive Inmarsat.

In Singapore, a project called TRI-media Telematic Oceanographic Network (TRITON) based on IEEE 802.16 and IEEE 802.16e implemented a mesh network for maritime communication using a ship, lighthouse and buoys as communication nodes with the objective to develop a system for high-speed and low-cost maritime communications in narrow water channels and shipping lanes close to the shore [4].

European Space Agency (ESA) introduced Wired Ocean Project [5]. The intent of this project is to establish, on a commercial basis, cost-effective broadband IP-based communications services to ships. But the cost is still expensive and size of the terminal, especially stabilized Ku-band equipment, both receive-only and VSATs (Very Small Aperture Terminal).

To solve the problems of cost and efficiency, an improved maritime communication is needed to entrance new technology.

In this paper, we propose a scheme to overcome the issues in maritime communication with maritime wireless communication based on Visible Light Communication (VLC), termed as Maritime VLC (MVLC). VLC is a communication method using LEDs, operating in wavelength range of 380~780 nm. The blinking of a LED is used for communication and illumination simultaneously.

As a maritime network suffers from insufficient dedicated operation spectra, which is more likely in the future due to congested RF bands, VLC is a promising candidate with a vast spectrum, i.e. 10,000 times more than RF. Furthermore, the widespread use of visible light could provide necessary infrastructure, e.g. lighthouse, beacon. Thus, the VLC-based maritime wireless communication can be considered attractive technologies. Maritime VLC system can support shore-to-ship, ship-to-ship communication without requiring the change of frequency channel.

The rest of this paper is organized as follows. Section II introduces the maritime VLC system together with channel model. Performance analysis and simulation results are

presented in Section III. Finally, Section IV shows conclusions drawn from the investigation.

II. SYSTEM CONFIGURATION

A. Maritime VLC System

Maritime environments divide coast and offshore. We propose a VLC based maritime system that covers short-to-sea communication services. Fig. 1 shows the proposed system in which communication coverage area can be increased at low-cost implementation. The mesh network is formed by neighboring ships, marine beacons and buoys, and is connected to the terrestrial networks via base stations (lighthouses) that are regularly placed along the coastlines. The base station consists of power LEDs that provide coverage to a very large area, while sea transceivers (marine beacons, buoys, oil/gas platforms, sea farms) consist of an LED array and photo diodes.

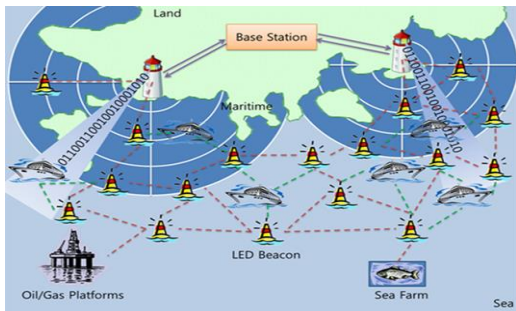


Fig. 1 High-level architecture of maritime VLC network

B. Maritime Channel Modeling

Maritime communication environments have unique property where sea surface movement is usually observed and subsequently periodic degradation exists. If long sea wave period occurs, the communication link may exhibit poor quality,

Table II. Sea state parameters

Sea state	Wind speed		Average wave period (sec)	Significant wave height (m)	Average wave length (m)
	(knots)	(m/s)			
4	18	9.26	5	1.83	24.1
5	21	10.8	5.5	2.4	32
6	27	13.89	7.5	4.3	56.1
7	36.5	18.9	10	7.62	100.13
8	43.75	22.5	13	13.72	180.1

thus causing data retransmission. Therefore, the maritime communication environment is mainly characterized by this sea surface movement, together with radio propagation and Fresnel effect [6].

Since the real-time data is not available for the present simulations in this study, we employ sea state data from Pierson-Moskowitz (PM) spectrum model [7], as it was developed from measurements of various sea parameters. Table

II shows the PM model. This model is based on new theory of sea behavior assuming that if the wind blew for a long time over a large sea area, the waves would come into equilibrium with the wind. This is the concept of a fully developed sea.

The sea waves are often portrayed as having a normal sine wave nature, however, by actual experiments they are described as a Trochoid [8]. The sea state conditions mentioned in Table II are reflected as a result of reflective nature of sea surface and wave height, which is measure of roughness of sea parameters. At lower sea states, i.e. state 1 to 4, the sea conditions are mild, and hence the signal distortion is negligible at the receiver. While at higher states, sea conditions are hostile with relatively high waves and rapid moving winds. These would result in scattering of incoming signals, thus causing the signals to be extremely damaged at receiver [9].

Sea surface moves all the time and thus renders link quality unstable. The sea wave movement continuously changes the marine beacon orientation and height, thus changing the marine beacon gain and received signal power. Fig. 2 shows the present maritime channel model under consideration. It consists of base station and maritime transceivers (beacons) placed over the sea.

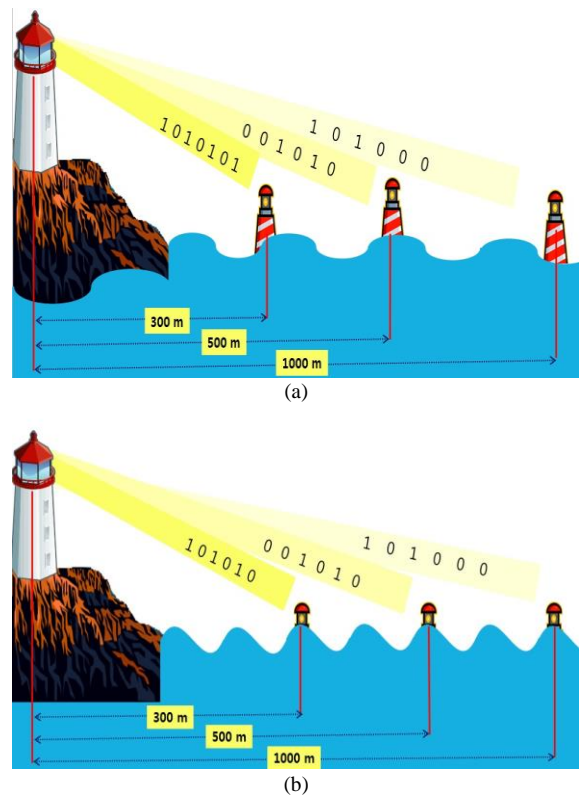


Fig. 2 Maritime channel model: (a) Sea state 4 (b) Sea state 8

III. SIMULATION RESULTS

Simulation has been carried out to investigate the link performance for the proposed shore-to-sea maritime VLC system. Performance is evaluated in terms of Bit Error Rate (BER) against Signal to Noise Ratio (SNR) values with respect

to distance between base station and beacons. We used the parameters shown in Table III and obtained the BERs for the proposed maritime VLC system. Further, we employed On-Off Keying (OOK) modulation technique for the VLC transmission

Table III. Parameters of the simulation

Parameters	Values
Transmitted optical power (1 LED)	300 W
Detector physical area	9 cm ²
Bit rate	1 Mbps
Channel	Maritime channel
Number LED	100
Field of view	50
Distance between lighthouse and receiver	[100 200 300 400 500 1000] m
Refractive index of a lens at receiver	1.5
LED half angle	60°
Receiving plane dimension	10m x 10m

For the simulations, we use the sea state data from PM spectrum. For example, Fig. 3 shows sea surface of the sea state 7 PM spectrum.

In Line of Sight (LOS) channel, the light from transmitter is directed towards the receiver where we measured SNRs and BERs. The receiving plane is assumed to be 10m x 10m over a

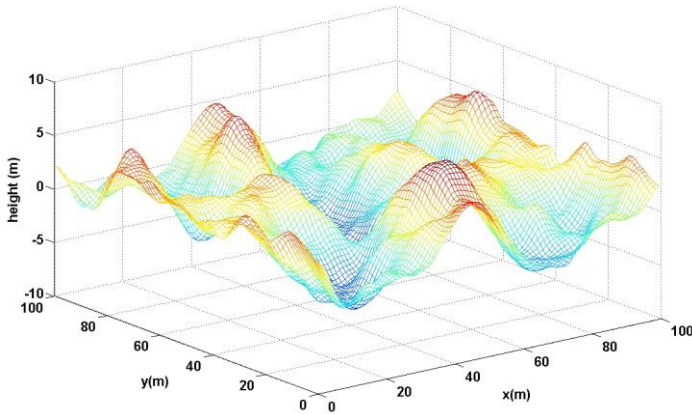


Fig. 3 Sea surface of the sea state 7 from the PM spectrum

beacon (maritime transceiver) as shown in Fig.4. Also, all subsequent analyses in terms of BERs and SNRs were conducted at the sea state 7.

Fig. 5 and 6 show the performance of the proposed channel model, where transmitter and receiver are separated with the distance of 100m. Fig. 7 and 8 show the performance of the channel between the transmitter and the receiver at the distance of 1000m apart.

Fig.9 shows the analysis of the maritime VLC system under various sea state conditions. It is apparent from the simulation results that the sea states 4 through 8 appear appropriate for communication up to approximately 120m. However, the BER performances at a larger distance between the transmitter and the receiver are poor, thus requiring further measures to be used.

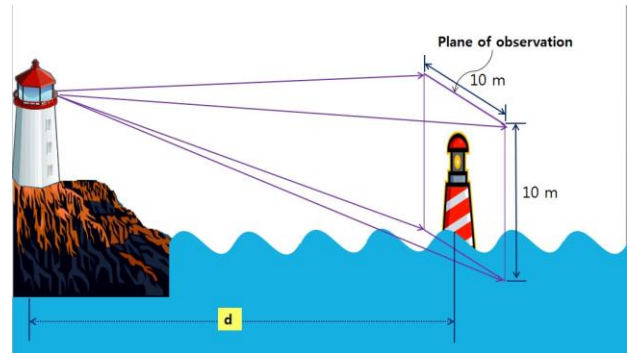


Fig. 4 The receiving plane (10m x 10m)

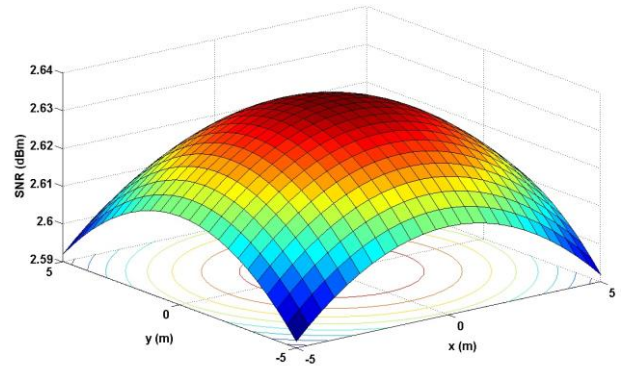


Fig. 5 Simulated maritime channel SNR (100m)

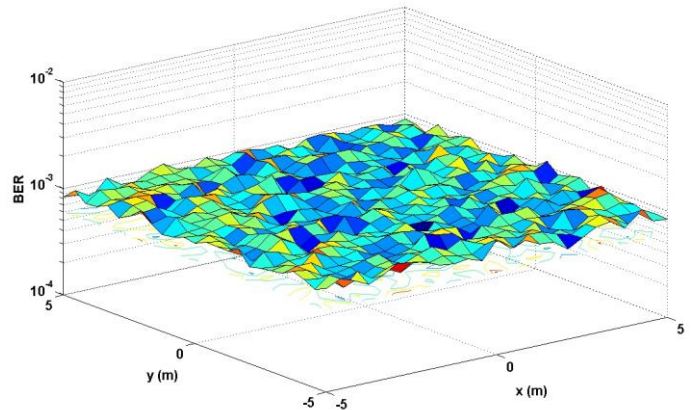


Fig. 6 Simulated maritime channel BER (100m)

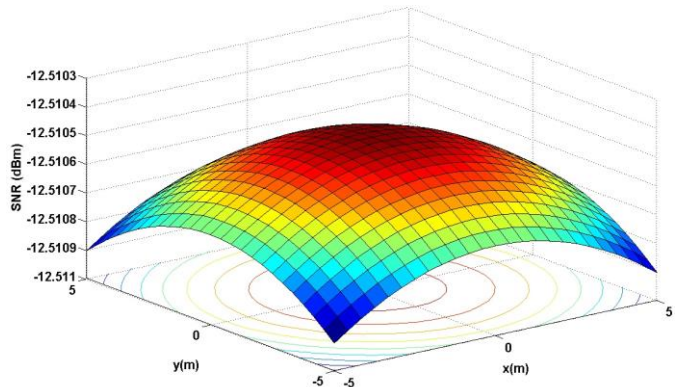


Fig. 7 Simulated maritime channel SNR (1000m)

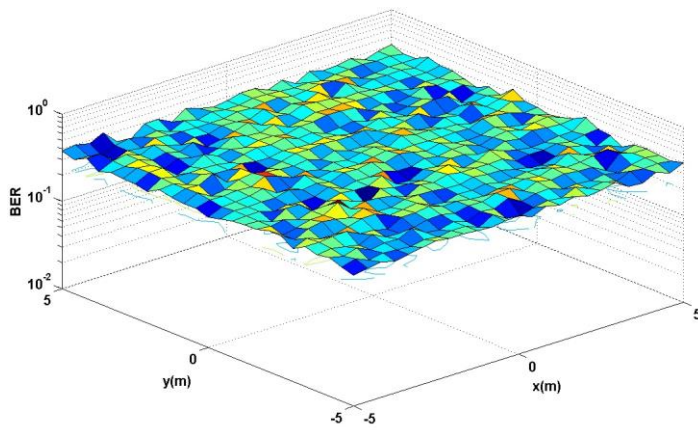


Fig. 8 Simulated maritime channel BER (1000m)

- [4] J. S. Pathmasuntharam, P. Y. Kong, M. T. Zhou, Y. Ge, H. Wang, C. W. Ang, W. Su, and H. Harada, "TRITON: High Speed Maritime Mesh Networks", *IEEE 19th International Symposium on Personal, Indoor and Mobile Radio Communications*, 2008 (PIMRC 2008), 15-18 Sept. 2008.
- [5] ESA telecommunication & integrated applications website. Available: telecom.esa.int/telecom/www/object/index.cfm?fobjectid=9121
- [6] ITU-R, "Maritime broadband wireless mesh networks," ITU-R M.2202, Nov. 2010.
- [7] Pierson-Moskowitz Sea Spectrum, Available: <http://www.sygwestinc.com/support/Sea%20State%20Table.htm>
- [8] Su Wen, Peng-Yong Kong, J. Shankar, H. Wang, Y. Ge, C.W. Ang, "A Novel Framework to Simulate Maritime Wireless Communication Networks," *IEEE/MTS OCEANS*, 2007.
- [9] K. D. Ward, C. J. Baker and S. Watts, "Maritime Surveillance Radar Part 1: Radar Scattering from the Ocean Surface," *IEE Proceedings*, Vol. 137, Part F, No.2, April 1990.

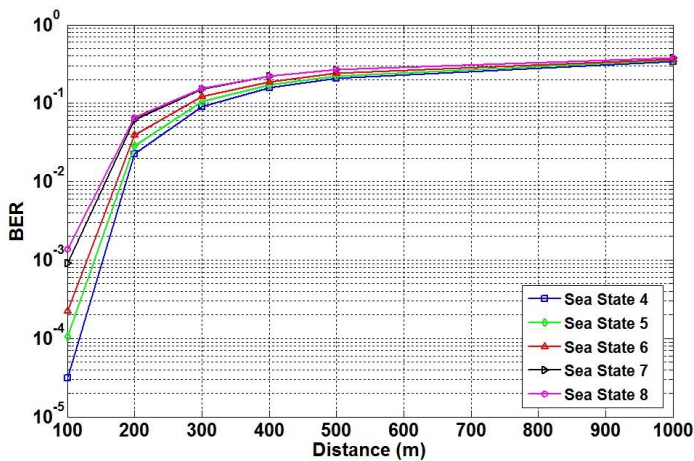


Fig. 9 Performance analysis of the maritime VLC system under sea state conditions

IV. CONCLUSION

In this paper, we presented the performance of the maritime VLC system in various maritime environments. The proposed system encompasses visible light transmission using LEDs and photo diodes for the transmission between shore and sea. The heavy reliance on RF communication networks would create bandwidth insufficiency for high-resolution sensors and equipment and also would be unable to provide capability for jamming. Therefore, the proposed maritime VLC can be an attractive candidate for advanced maritime broadband communications. Performance evaluation has been conducted using the PM model and shows that the performance relative to the sea states varies in terms of distance. It is also shown that at high sea states, a more rigorous transmission scheme needs to be employed.

REFERENCES

- [1] IMO COMSAR, Harmonization of GMDSS Requirements for Radio Installations on Board Solas Ships, August 2004
- [2] IMO website. Available: http://www.imo.org/blast/mainframe.asp?topic_id=69&doc_id=581#dsc
- [3] IALA, The IALA definition and vision for e-Navigation, March 2007.

Experimental study of influence of orthogonal magnetization on a ferromagnetic characteristic

Yu.E. Adamian, S.I. Krivosheev

Abstract — The experimental investigation of a reciprocally orthogonal fields interaction in a ferromagnetic is conducted. Specially designed tubular toroidal ferrite core is used for measurements of the magnetic permeability dependence on collinear and orthogonal components of the magnetic field tension. It is shown that the degree of the orthogonal field influence on the measured magnetic permeability in given direction substantially differs from the influence of the collinear field. Using measured permeability dependence on the field tension components the **H-B** loci corresponding to **B**-vector rotation are reconstructed. Obtained curves are qualitatively similar to published ferromagnetics vector testing data.

Keywords — collinear field, loci, magnetic permeability, orthogonal field, ferromagnetic.

I. INTRODUCTION

MAGNETIC field structure in ferromagnetics can have a complex spatial character. Typical examples where it is necessary to take into account the joint action of different spatial magnetic field components are ferrite antennas [1], elements of electric machines magnetic circuits, ferromagnetic elements of electric power converters etc. Such situations take place at a development of non-destructive testing magnetic methods [2] and at determination of magnetically induced mechanical force fields in ferromagnetics [3]. Areas with complex spatial magnetic fields geometry can appear as sources of additional energy losses. Also the situation can occur when the magnetic core is influenced by strong external magnetic field due to lightning currents, shorts in the circuit and other electromagnetic troubles. In these cases it is not enough to use B-H curves obtained by standard magnetic material testing. It is shown in a number of works [4,5,6] that for correct computation of electromagnetic processes in ferromagnetics it is necessary to take into account the tensor character of a material magnetic permeability (reluctance) both in isotropic and laminated materials. In this regard it seems to be useful to arrange experiments in relatively simple geometry for obtaining reliable and easily interpretable data.

This work is done by the authors on their own initiative.

The author Yu.E. Adamian is with Saint-Petersburg State Polytechnical University, Russia, yuriadamian@gmail.com

The author S.I. Krivosheev is with Saint-Petersburg State Polytechnical University, Russia, ksi.mgd@gmail.com

II. EXPERIMENT DESCRIPTION

The experimental investigation of a reciprocally orthogonal fields interaction in a ferromagnetic is conducted using tubular toroidal ferrite core (fig.1). The core that is manufactured specifically for this task is composed of two sections (1,2) in order to provide access to the internal area. Core material is ferrite 2000HM. Sections are separated by the air gap that is minimized by polishing of the halves edges. Windings inside (3) and outside (4) the core have excitation (5) and measuring (6) sections. Excitation windings and their currents are further referred respectively as internal and external. In contradiction to the core used in [3] there is no problem of the magnetic field components intensity measurement in such a type of core because both components distribution along field lines is close to uniform and field intensities can be easily calculated as $H_\varphi = i_z W_z / l_\varphi$ and $H_z = i_\varphi W_\varphi / l_z$, where i_z and i_φ are currents in the internal and external excitation windings, W_z and W_φ - corresponding numbers of turns, l_z - field line effective length along toroid, l_φ - field line effective length in toroid orthogonal section.

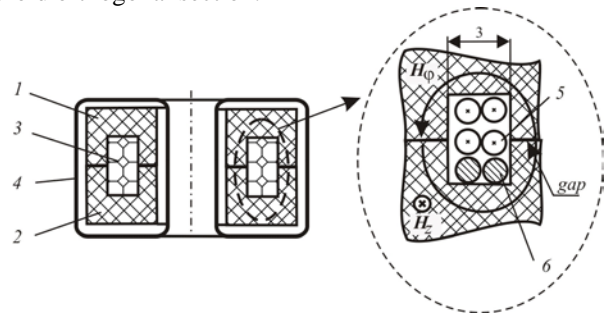


Fig. 1. Magnetic core and windings design.

The test circuit is presented on Fig.2. The circuit consists of two parallel branches fed by storage capacitor C_s through the mechanical switch. The first branch includes the resistor R , internal excitation winding and internal current measuring shunt. The second branch includes pulse forming capacitor C_{pt} and inductor L_{pt} connected in series, external excitation winding and external current measuring shunt. The storage capacitor C_s has big enough capacity for keeping voltage almost constant during oscillation process in the internal

winding branch ($C_s=20$ mF). The series inductor L_{pt} has much higher inductance than the internal winding that is nonlinear. So, the current in the internal winding has the shape close to damping sinusoid. The values of inductances L_e and L_i are determined by the internal and external windings parameters (Fig.1, items 3 and 4) and the core material magnetic state. At the currents i_z and i_ϕ flowing through the windings the orthogonal magnetic flux densities B_{Le} and B_{Li} are formed in the core material. At constant charging voltage of the capacitor C_s there is one variable circuit parameter – resistance R of the branch determining internal winding current. The resistance minimal value is limited by the time constant RC_s that must be substantially longer than the internal winding current oscillations period mainly determined by L_{pt} and C_{pt} . In the test circuit $L_{pt}=25$ mH, $C_{pt}=100$ μ F and R is stepwise varied from 6 to 100 Ohm. Current shunts R_s are similar and have resistance $R_s=20$ mOhm.

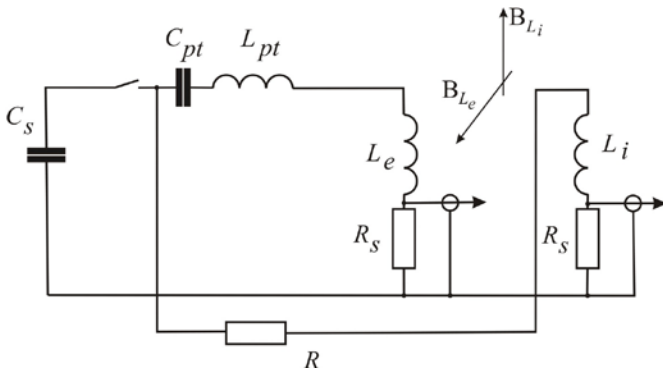


Fig. 2. Test circuit schematic

In order to determine the dependence of the core material magnetic permeability on collinear and orthogonal field components currents in both excitation windings and induced voltage of the external winding measuring section are registered by the oscilloscope Tektronix DPO3014. Toroidal magnetic flux density is measured by integration of signal from the external winding measuring section. In combination with excitation current signal it brings B_z vs H_z curve evolution at the current i_ϕ dumping and approximately constant orthogonal field intensity H_ϕ .

On Fig.3 B-H loops obtained during one period of i_ϕ are displayed at different values of H_ϕ . Orthogonal field H_ϕ was changed by varying of the resistor R value at constant charging voltage. Loop 1 corresponds to zero orthogonal field, 2 - 260 A/m, and 3 - 950 A/m. As it can be seen from the picture, application of the orthogonal field results in the hysteresis loop incline change. It should be highlighted that although the loop change is substantial at relatively low

orthogonal field, even at very strong orthogonal field (950 A/m) the change is not dramatic.

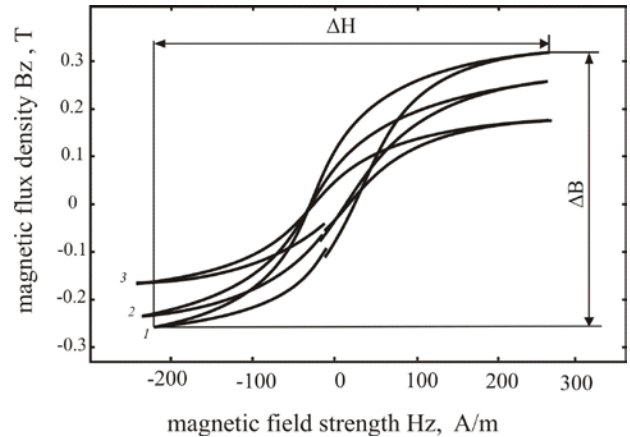


Fig.3 Hysteresis loops at the orthogonal field variation.

For characterizing of the orthogonal field influence on the material properties the magnetic permeability in Z-direction is determined using maximal and minimal values of the fields intensity and magnetic flux density at local hysteresis loops as $\mu_z = \Delta B_z / \Delta H_z$, where $\Delta B_z = B_{zmax} - B_{zmin}$; $\Delta H_z = H_{zmax} - H_{zmin}$ as it is shown on fig.3. In fact this permeability dependence characterizes the anhysteretic magnetization curve. The graph on Fig. 4 presents the experimental data as set of equal magnetic permeability μ_z lines in coordinates (H_z, H_ϕ) . The scales on axes are fitted to the experimental data and not equal.

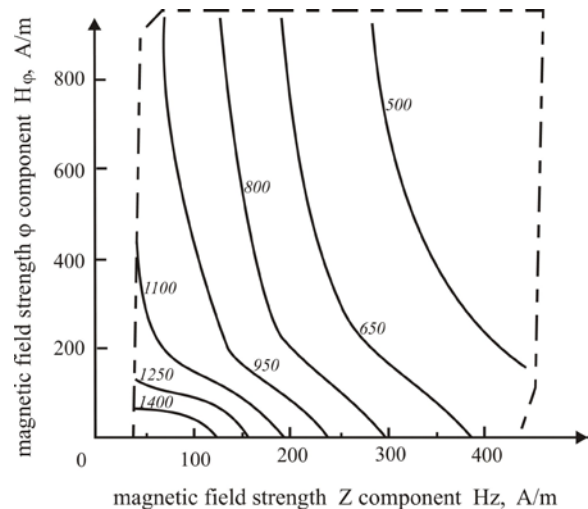


Fig. 4. Magnetic permeability as the function of collinear (H_z) and orthogonal (H_ϕ) field strength

III. DISCUSSION

It can be clearly seen from Fig. 3 that the degree of the orthogonal (H_ϕ) field influence on the measured magnetic permeability in Z-direction substantially differs from the influence of the collinear field (H_z). The difference is most conspicuous at H_ϕ higher than 150-200 A/m that corresponds to saturation area at standard hysteresis loop of the ferrite. This fact must be taken into account at design of ferromagnetic devices with orthogonal fields. It is especially important for ones operating under high magnetic fields intensities such as [7].

In order to compare our results with published data we transformed our results for constructing \mathbf{H} and \mathbf{B} loci at rotating vector of the magnetic flux density using experimental dependence μ_z vs H_z and H_ϕ for both coordinates. In other words, supposing that dependences $\mu_z(H_z, H_\phi)$ and $\mu_\phi(H_\phi, H_z)$ in isotropic material are similar we constructed the \mathbf{H} - loci shape corresponding to circular \mathbf{B} -loci.

At given $B_z = B_m \cdot \sin(\omega t)$, $B_\phi = B_m \cdot \cos(\omega t)$ the system of equations

$$\begin{cases} B_\phi = \mu_\phi(H_\phi, H_z) \cdot H_\phi \\ B_z = \mu_z(H_z, H_\phi) \cdot H_z \end{cases} \quad (1)$$

is numerically solved for H_z and H_ϕ using polynomial approximation of the dependences $\mu_z(H_z, H_\phi)$ and $\mu_\phi(H_\phi, H_z)$. Here B_m is \mathbf{B} -vector length.

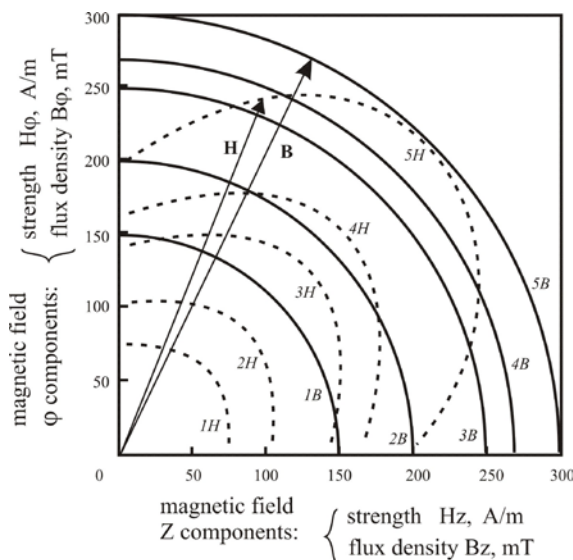


Fig. 5. Field strength \mathbf{H} loci corresponding to circular \mathbf{B} loci.

On Fig. 5 \mathbf{H} - loci corresponding to rotating vector \mathbf{B} with constant length are presented. Curves marked as 1B - 5B represent loci of vector \mathbf{B} with length from 0.15 to 0.3 T. Corresponding \mathbf{H} -loci are marked as 1H - 5H. The picture is qualitatively similar to curves [8] obtained in 3-D testing of isotropic soft magnetic compound SOMALOY 500. Considering that the shapes of the low frequency hysteresis loops of this material and loops of the ferrite used in our experiments are alike, we can conclude that our data are not in contradiction with published ferromagnetic vector measurements. It should be noted that magnetization data presentation as \mathbf{B} - \mathbf{H} loci brings not enough information for permeability determining because generally vectors \mathbf{B} and \mathbf{H} are not parallel (see arrows on Fig.5) and it is difficult to put into correspondence points of the same time moment on \mathbf{B} and \mathbf{H} curves having no reference. From the other side, a given dependence of permeability on components of magnetic field strength is sufficient for reconstruction of \mathbf{B} - \mathbf{H} loci for soft magnetic materials.

IV. CONCLUSION

It is experimentally demonstrated that influences of collinear and orthogonal components of a magnetic field strength on the ferrite magnetic permeability measured in given direction are different.

The difference is highly pronounced at orthogonal field strength approaching to saturating values typical for hysteresis loop of the material.

Using measured permeability dependence on collinear and orthogonal components of the field tension the \mathbf{H} - \mathbf{B} loci corresponding to \mathbf{B} -vector rotation are reconstructed and compared with published ones. It can be seen from the comparison that reconstructed curves are qualitatively similar to published ferromagnetics vector testing data.

REFERENCES

- [1] Hord, W.E., Jr. ; Boyd, C.R. Simultaneous Dual-Polarization Ferrite Phase Shifter, *Microwave Symposium Digest, 1986 IEEE MTT-S International* , DOI:10.1109/MWSYM.1986.1132293 , 1986 , P.: 727-730.
- [2] Vasilenko, O.N., Kostin, V.N. The topography of the field and flux inside and above the surfaces of ferromagnetic plates during their contact and contactless magnetization, *Russian Journal of Nondestructive Testing* Volume 49, Issue 9, September 2013, Pages 510-518
- [3] Yu. E. Adam'yan, E. A. Vyrva, S. I. Krivosheev, and V. V. Titkov. Diffusion of a Pulsed Field and Electromagnetic Forces in Ferromagnets /*Technical Physics*, 2013, Vol. 58, No. 10, pp. 1397-1403.
- [4] Youguang Guo, Jianguo Zhu, Haiyan Lu, Zhiwei Lin, Shuhong Wang and Jianxun Jin. 3-D Vector Magnetic Properties of SMC Material for Advanced Field Analysis of SMC Machine / *2008 Australasian Universities Power Engineering Conference (AUPEC'08)* Paper P-079.
- [5] E. Cardelli, A. Fabaa. Vector hysteresis measurements of not oriented grain SiFe steels by a biaxial hall sensors array/ *Physica B*,435,(2014), pp. 34-39.
- [6] Hans Vande Sande, François Henrotte, Herbert De Gerssem, and Kay Hameyer. An Effective Reluctivity Model for Nonlinear and Anisotropic

- Materials in Time-Harmonic Finite Element Computations/ *IEEE TRANSACTIONS ON MAGNETICS*, VOL. 41, NO. 5, MAY 2005..
- [7] Botcharov, Yu.N., Efimov, I.P., Krivosheev, S.I., Shneerson, G.A. Transient processes and energy balance in inductive energy storage including ferromagnetic opening switch. *12th IEEE International Pulsed Power Conference*; Monterey, CA, USA; ; 27 June 1999 through 30 June 1999; Code 56431, *Digest of Technical Papers-IEEE International Pulsed Power Conference*, Volume 2, 1999, Pages 1250-1253.
- [8] Yongjian Li, Qingxin Yang, Jianguo Zhu, Youguang Guo. Magnetic Properties Measurement of Soft Magnetic Composite Materials Over Wide Range of Excitation Frequency / *IEEE TRANSACTIONS ON INDUSTRY APPLICATIONS*, VOL. 48, NO. 1, JANUARY/FEBRUARY 2012// DOI 10.1109/TIA.2011.2175677.



Yuri Eduardovich Adamian

Born: September 10, 1955, Tashkent, USSR
Education: Ph.D (Candidate of Technical Sciences), 2000.
Research Interests: Electrical physics, pulse power applications, power electronics.
Current Position: Associated Professor at the “High Voltage Engineering, Electrical Insulation and Cable Technology” department in the St.-Petersburg State Polytechnical University from 2000 till now

Conference activity: International Megagauss Conferences, Pulse Power Conference, Electromagnetic Compatibility conferences, NonDestructive Testing conferences and others



Sergey Ivanovich Krivosheev

Born: October 17, 1954, Leningrad, USSR.
Education: Ph.D (Candidate of Technical Sciences), 1996; Doctor of Science in Technical Engineering, 2006.
Research Interests: Electrical physics, super-high magnetic fields, mechanics of solids, fracture dynamics, pulse power applications.

Current Position: Head of Pulse Power Technology Laboratory, Professor at the “High Voltage Engineering, Electrical

Insulation and Cable Technology” department in the St.-Petersburg State Polytechnical University from 2006 till now.

Conference activity: International Megagauss Conferences, Pulse Power Conference, Electromagnetic Compatibility conferences, NonDestructive Testing conferences and others

Continuous Health-monitoring for early Detection of Patient by Web Telemedicine System

Hafez Fouad , hafez@eri.sci.eg

Microelectronics Dept., Electronics research Institute, Cairo, Egypt

ABSTRACT—Continuous Monitoring of vital signs of a patient by Wireless Sensor network (WSN) can help in diagnosis and can monitor patient's history in routine life activities to provide accurate diagnosis. Doctors can check the complete details of patients from remote location and can recommend a suitable medication. The main purpose of this technology is to reduce the load at hospitals and provide efficient healthcare facility remotely. To monitor the patients in their natural environments is not practical when devices or sensors are connected through a wire that is why we use Wireless body area network (WBAN) to carrying out daily activities through unobtrusive and contented way. In these networks various sensors are attached on clothing or on the body or even implanted under the skin. The wireless nature of the network and the wide variety of sensors offer numerous new, practical and innovative applications to improve health care and the Quality of Life. Using a WBAN, the patient experiences a greater physical mobility and is no longer compelled to stay in the hospital. This technology can provide very cheaper, easier and quick respondent history of patient. This paper discusses the architecture of (WBAN), and its position between different technologies. The paper also introduces the web portal telemedicine solution, and the implementation of telemedicine monitoring system using Wireless Body Area Networks.

KEYWORDS—Health Monitoring system, Telemedicine, Wireless Body Area Networks (WBAN), Body sensor network (BSN).

1. INTRODUCTION

The aging population in many developed countries and the rising costs of health care have triggered the introduction of novel technology-driven enhancements to current health care practices. Recent advances in electronics have enabled the development of small and intelligent bio-medical sensors which can be worn on or implanted in the human body. These sensors need to send their data to an external medical server where it can be analyzed and stored. Using a wired connection for this purpose turns out to be too cumbersome and involves a high cost for deployment and maintenance.

This work was supported in part by the Electronics Research institute in EGYPT under Grant (sponsor and financial support acknowledgment , www.eri.sci.eg).

Hafez Fouad Author is with the Electronics Research institute since 1994, (corresponding author phone: 202-333-10503; fax: 202-333-69738; e-mail: hafez@eri.sci.eg).

However, the use of a wireless interface enables an easier application and is more cost efficient [1]. The patient experiences a greater physical mobility and is no longer compelled to stay in a hospital. This process can be considered as the next step in enhancing the personal health care and in coping with the costs of the health care system. Where eHealth is defined as the health care practice supported by electronic processes and communication, the health care is now going a step further by becoming mobile. This is referred to as mHealth [2]. In order to fully exploit the benefits of wireless technologies in telemedicine and mHealth, a new type of wireless network emerges: a wireless on-body network or a Wireless Body Area Network (WBAN). This term was first coined by Van Damet al. in 2001 [3] and received the interest of several researchers [4-8].

Wireless Body Area Networks (WBAN) has emerged as a key technology to provide real-time health monitoring of a patient and diagnose many life threatening diseases. WBAN is a communication network composed of wireless sensor devices operates in close vicinity to, on, or inside a human body to acquire critical data for remote monitoring by health care providers. IEEE 802 has established a Task Group called IEEE 802.15.6 for the standardization of WBAN. The purpose of the group is to establish a communication standard optimized for low-power in-body/on-body nodes to serve a variety of medical and non-medical applications.

2. SYSTEM ANALYSIS AND DESIGN

2.1. Wireless Sensor Networks

Body area network (BAN), is also called Body sensor networks (BSN) and wireless body area network (WBAN). it is being very popular in society because patient's data monitoring is a leading issue for health & disease management, when patient enters the hospital, doctors & paramedical staff question him about symptoms and try to find the actual symptoms through different tests and prolonged stay at hospital, now the patient is equipped with different sensors, all these are connected by wires, it

is very uncomfortable situation. The core concept behind Wireless body area networks is to remove all wires connecting sensors on the patient and developing wireless network between sensors. All these devices are connected without cables and without reducing patient comfort. Moreover, patient could be monitored remotely. Doctors are mostly interested in diagnostic of cardiogram, blood pressure, oxygen saturation, sugar level and cancer, which can be measured using a number of sensors nodes attached to the patient [1,7]. The goal of e-health approach is to empower the citizen to fight against diseases and reduce the logistic constraints for patients and doctors. This technology has potential to revolutionize the health care diligence by providing real time patient monitoring capabilities to the health care professionals, Implanted wireless body area networks (IWBN) have emerged as an important and growing area of research [4-8].

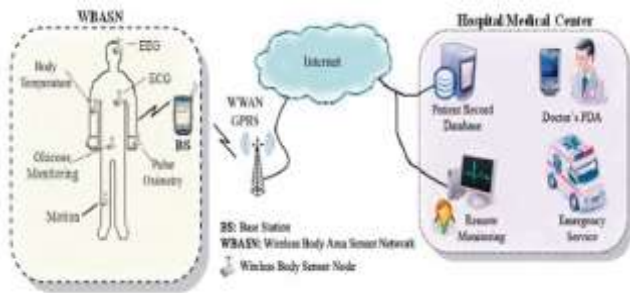


Figure.1 WBASN as an example of WSN [10].

2.2. Architecture of Wireless Body Area Network

A Wireless Body Area Network consists of small, intelligent devices attached on or implanted in the body which are capable of establishing a wireless communication link. These devices provide continuous health monitoring and real-time feedback to the user or medical personnel. Furthermore, the measurements can be recorded over a longer period of time, improving the quality of the measured data [12].

In order to realize communication between these devices, techniques from Wireless Sensor Networks (WSNs) and ad hoc networks could be used. However, because of the typical properties of a WBAN, current protocols designed for these networks are not always well suited to support a WBAN. The following table illustrates the differences between a Wireless Sensor Network and a Wireless Body Area Network:

Challenges	Wireless Sensor Network	Wireless Body Area Network
Scale	Monitored environment (meters / kilometers)	Human body (centimeters / meters)
Node Number	Many redundant nodes for wide area coverage	Fewer, limited in space
Result accuracy	Through node redundancy	Through node accuracy and robustness
Node Tasks	Node performs a dedicated task	Node performs multiple tasks
Node Size	Small is preferred, but not important	Small is essential
Network Topology	Very likely to be fixed or static	More variable due to body movement
Data Rates	Most often homogeneous	Most often heterogeneous
Node Replacement	Performed easily, nodes even disposable	Replacement of implanted nodes difficult
Node Lifetime	Several years / months	Several years / months, smaller battery capacity
Power Supply	Accessible and likely to be replaced more easily and frequently	Inaccessible and difficult to be replaced in an implantable setting
Power Demand	Likely to be large, energy supply easier	Likely to be lower, energy supply more difficult
Energy Scavenging Source	Most likely solar and wind power	Most likely motion (vibration) and thermal (body heat)
Biocompatibility	Not a consideration in most applications	A must for implants and some external sensors
Security Level	Lower	Higher, to protect patient information
Impact of Data Loss	Likely to be compensated by redundant nodes	More significant, may require additional measures to ensure QoS and real-time data delivery
Wireless Technology	Bluetooth, ZigBee, GPRS, WLAN, ...	Low power technology required

Table.1 Schematic overview of differences between Wireless Sensor Networks and WBANs

2.3. Wireless Body Area Network Devices

Generally speaking, two types of devices can be distinguished: sensors and actuators. The sensors are used to measure certain parameters of the human body, either externally or internally. Examples include measuring the heartbeat, body temperature or recording a prolonged electrocardiogram (ECG). The actuators (or actors) on the other hand take some specific actions according to the data they receive from the sensors or through interaction with the user. E.g., an actuator equipped with a built-in reservoir and pump administers the correct dose of insulin to give to diabetics based on the glucose level measurements. Interaction with the user or other persons is usually handled by a personal device, e.g. a PDA or a smart phone which acts as a sink for data of the wireless devices.

There are three kinds of devices used in wireless body area network which are described as following:

(Wireless) Sensor node: A device that responds to and gathers data on physical stimuli, processes the data if necessary and reports this information wirelessly. It consists of several components: sensor hardware, a power unit, a processor, memory and a transmitter or transceiver [13].

(Wireless) Actuator node: A device that acts according to data received from the sensors or through interaction with the user. The components of an actuator are similar to the sensor's: actuator hardware (e.g. hardware for medicine administration, including a reservoir to hold the medicine), a power unit, a processor, memory and a receiver or transceiver.

(Wireless) Personal Device (PD): A device that gathers all the information acquired by the sensors and actuators

and informs the user (i.e. the patient, a nurse, a GP etc.) via an external gateway, an actuator or a display/LEDS on the device. The components are a power unit, a (large) processor, memory and a transceiver. This device is also called a Body Control Unit (BCU) [14], body gateway or a sink. In some implementations, a Personal Digital Assistant (PDA) or smart phone is used. It provides suitable graphic or audio interface to client and transfer health related data to medical server through internet, wimax, volte or mobile telephone networks.

Many different types of sensors and actuators are used in a WBAN. The main use of all these devices is to be found in the area of health applications. In the following, the term nodes refer to both the sensor as actuator nodes. The number of nodes in a WBAN is limited by nature of the network. It is expected that the number of nodes will be in the range of 20-50 [15, 16].

The data rates for the different applications are given in Table (2) and are calculated by means of the sampling rate, the range and the desired accuracy of the measurements [17,18].

Application	Data Rate	Bandwidth	Accuracy
ECG (12 leads)	288 kbps	100-1000 Hz	12 bits
ECG (6 leads)	71 kbps	100-500 Hz	12 bits
EMG	320 kbps	0-10,000 Hz	16 bits
EEG (12 leads)	43.2 kbps	0-150 Hz	12 bits
Blood saturation	16 bps	0-1 Hz	8 bits
Glucose monitoring	1600 bps	0-50 Hz	16 bits
Temperature	120 bps	0-1 Hz	8 bits
Motion sensor	35 kbps	0-500 Hz	12 bits
Cochlear implant	100 kbps	-	-
Artificial retina	50-700 kbps	-	-
Audio	1 Mbps	-	-
Voice	50-100 kbps	-	-

Table.2 Examples of medical WBAN applications [15-18, 21]

An example of a medical WBAN used for patient monitoring is shown in Figure (2). Several sensors are placed in clothes, directly on the body or under the skin of a person and measure the temperature, blood pressure, heart rate, ECG, EEG, respiration rate, SpO₂-levels etc. Next to sensing devices, the patient has actuators which act as drug delivery systems. The medicine can be delivered on predetermined moments, triggered by an external source (i.e. a doctor who analyzes the data) or immediately when a sensor notices a problem.

One example is the monitoring of the glucose level in the blood of diabetics. If the sensor monitors a sudden drop of glucose, a signal can be sent to the actuator in order to start

the injection of insulin. Consequently, the patient will experience fewer nuisances from his disease. Another example of an actuator is a spinal cord stimulator implanted in the body for long-term pain relief [19].

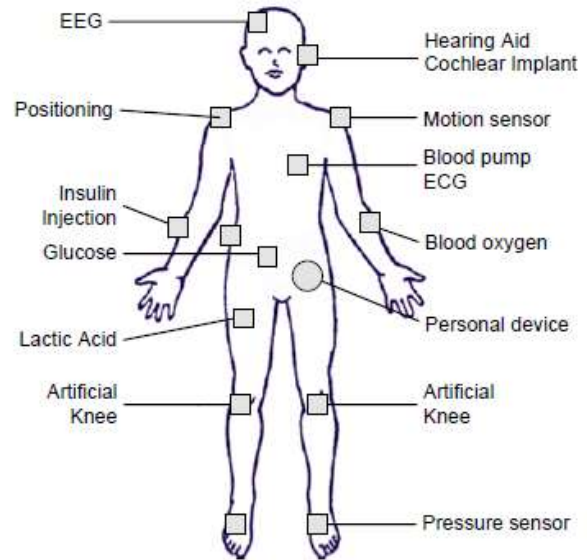


Figure.2 Example of patient monitoring in a Wireless Body Area Network [15]

A WBAN can also be used to offer assistance to the disabled. For example, a paraplegic can be equipped with sensors determining the position of the legs or with sensors attached to the nerves [20]. In addition, actuators positioned on the legs can stimulate the muscles. Interaction between the data from the sensors and the actuators makes it possible to restore the ability to move. Another example is aid for the visually impaired.

An artificial retina, consisting of a matrix of micro sensors, can be implanted into the eye beneath the surface of the retina. The artificial retina translates the electrical impulses into neurological signals. The input can be obtained locally from light sensitive sensors or by an external camera mounted on a pair of glasses [21].

2.4. Positioning WBANs between technologies

In order to have clear understanding, we propose the following definitions: intra-body communication and extra-body communication. An example is shown on Figure (3).

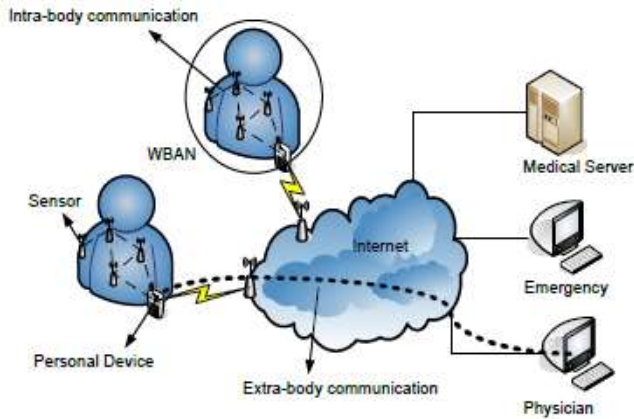


Figure.3 Example of intra-body and extra-body communication in a WBAN.

The former controls the information handling on the body between the sensors or actuators and the personal device [23-26], the latter ensures communication between the personal device and an external network [27], [28-30]. Doing so, the medical data from the patient at home can be consulted by a physician or stored in a medical database. This segmentation is similar to the one defined in [30] where a multi-tiered telemedicine system is presented. Tier 1 encompasses the intra-body communication, tier 2 the extra-body communication between the personal device and the Internet and tier 3 represents the extra-body communication from the Internet to the medical server. The combination of intra-body and extra-body communication can be seen as an enabler for ubiquitous health care service provisioning. An example can be found in [31] where Utility Grid Computing is combined with a WBAN. Doing so, the data extracted from the WBAN is sent to the grid that provides access to appropriate computational services with high bandwidth and to a large collection of distributed time-varying resources.

To date, development has been mainly focused on building the system architecture and service platform for extra-body communication. Much of these implementations focus on the repackaging of traditional sensors (e.g. ECG, heart rate) with existing wireless devices. They consider a very limited WBAN consisting of only a few sensors that are directly and wirelessly connected to a personal device. Further they use transceivers with a large form factor and large antennas that are not adapted for use on a body.

In Figure (4), a WBAN is compared with other types of wireless networks, such as Wireless Personal (WPAN), Wireless Local (WLAN), Wireless Metropolitan (WMAN) and Wide Area Networks (WAN) [42]. A WBAN is operated close to the human body and its communication

range will be restricted to a few meters, with typical values around 1-2 meters. While a WBAN is devoted to interconnection of one person's wearable devices, a WPAN is a network in the environment around the person. The communication range can reach up to 10 meters for high data rate applications and up to several dozens of meters for low data rate applications.

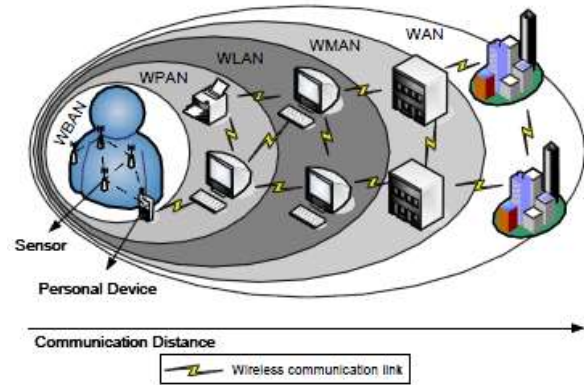


Figure.4 Positioning of a Wireless Body Area Network in the realm of wireless networks.

2.5. Web Portal Telemedicine System

Telemedicine enables the remote delivery of patient care using integrated health information systems and telecommunication technologies and allows scientists, physicians and other medical professionals around the world to serve more patients. The healthcare servers keep electronic medical records of registered users and provide different services to patients, medical consultants and informal caregivers. The patient's consultant can access the data from office via internet and examine the patient's history, current symptoms and patient's response to a give treatment. Once WBAN network is configured, the healthcare server manages the network, taking care of channel sharing, time synchronization, data retrieval and processing [22].

For patients to use these services he must register on our healthcare server; Ain Medical portal (www.ainmedical.com), and insert his/her medical history (all personal information, radiograph and tests). The system Requirements is the registration of a new user as Patient which allows him to become a member of the AinMedical's portal with Pre-condition having a valid email address to complete registration. AinMedical portal sends message to the patient to activate his/her account. A Message is also sent to AinMedical's Administrator (new Patient has been registered), AinMedical presents welcome

page for New Patient and provide link to login his account. As indicated in figure (5).

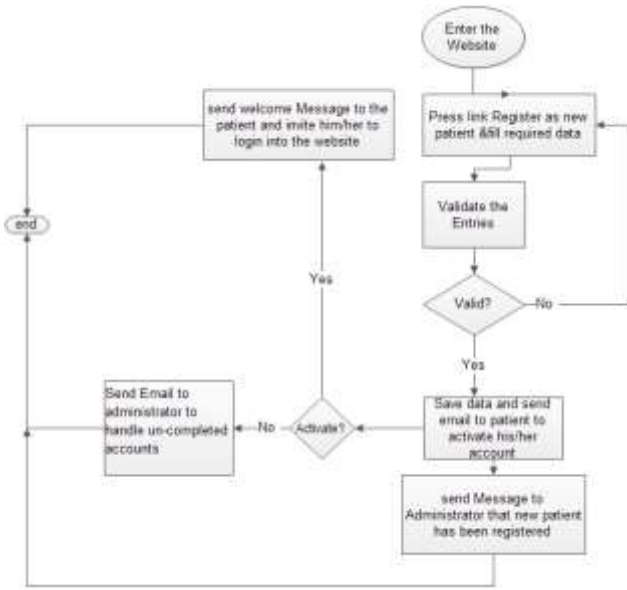


Figure.5 Patient Registration

Portal's patient needs to add his basic information. The patient enter to Telemedicine link, then user press "Add/View medical history", and select the needed link to review/add data for (basic information, diseases, symptoms ,pharmaceuticals, surgeries, sensitivities, radiograph, tests).

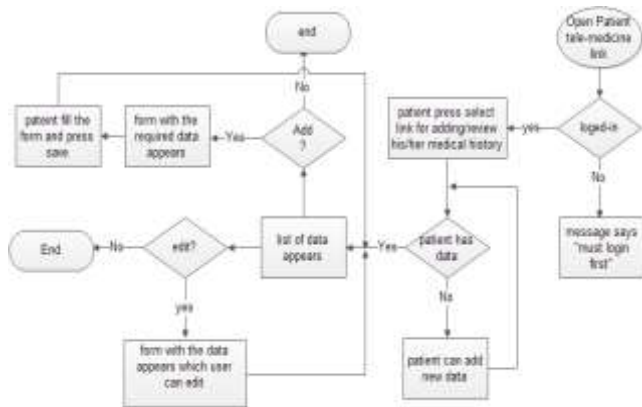


Figure.6 Patient add basic information & medical history

If Portal's patient needs to use telemedicine services and make booking, this requires the patient to review doctor list or search doctors. The patient press "book now" which beside the doctor he needs, fills the form of booking and selects the time and press send. The request will be sent and the payment taken from patient credit.

If Portal's patient needs to review his booking list. the patient enter to Telemedicine link, then user press

"booking data" link & review his booking list. If the conversation with doctor done, patient can review the prescription and required radiograph & tests.

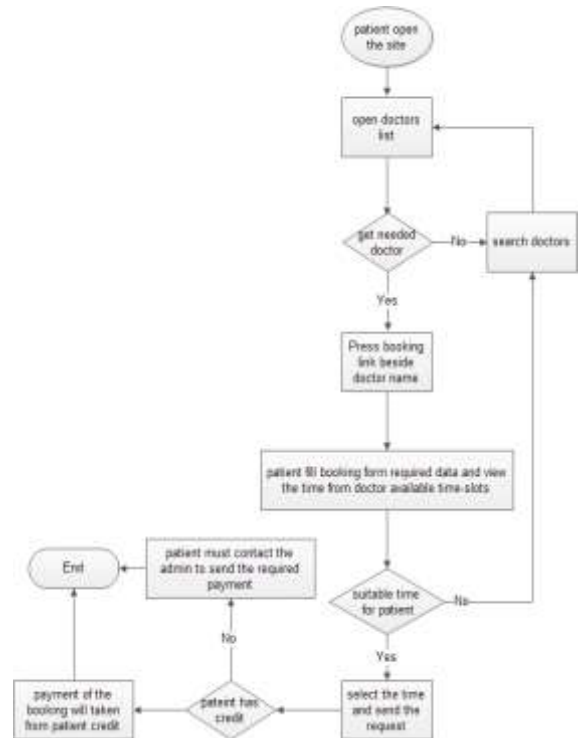


Figure.7 Patient reviews his booking list

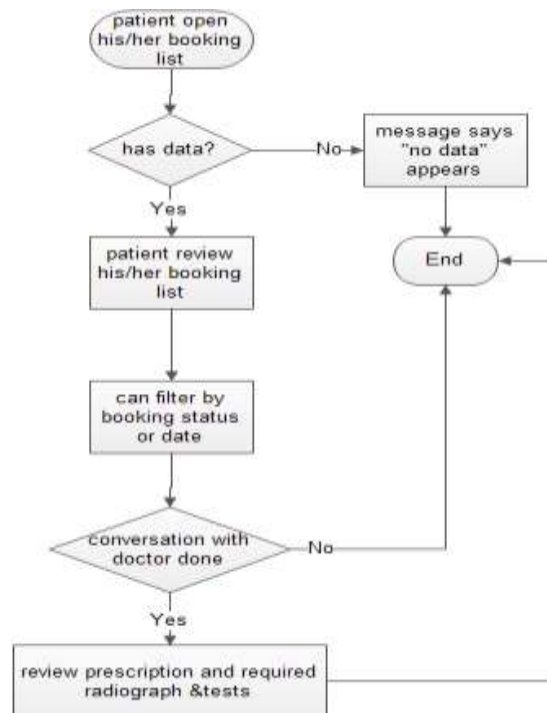


Figure.8 Patient makes booking

The patient can reserve an appointment with any doctor regardless his position through Ain Medical portal and a sample of the video conference between the doctor and patient in figure (9). The patient will use wireless sensor devices to acquire different data (to take prearrangement measures to control the following diseases: Blood pressure, Heart Attack, Diabetes, Glucose Level & many others) for remote monitoring by the doctor such that he could diagnose diseases.



Figure.9 Video conference between the doctor and patient through Ain Medical Portal

The complete telemedicine system process with its steps appears in Figure (10).



Figure.10 Telemedicine system process between the doctor and patient through Ain Medical Portal

Figure (11) shows an example of Ain Medical Web Telemedicine monitoring system. There are 2 graphics on each side. The first graphic shows real-time values of the received data from the selected sensor as a function of time. Maximum and minimum values are shown as dashed lines in same graphic. The second graphic, which is located under the first, displays average values belonging to the selected sensor as a bar graph according to the input value and unit (daily, weekly, monthly). For example, the second graphic on the right side in shows the average

value of the sensed body temperature as a function of the last 5 weeks. This feature provides doctors with useful information about patients.

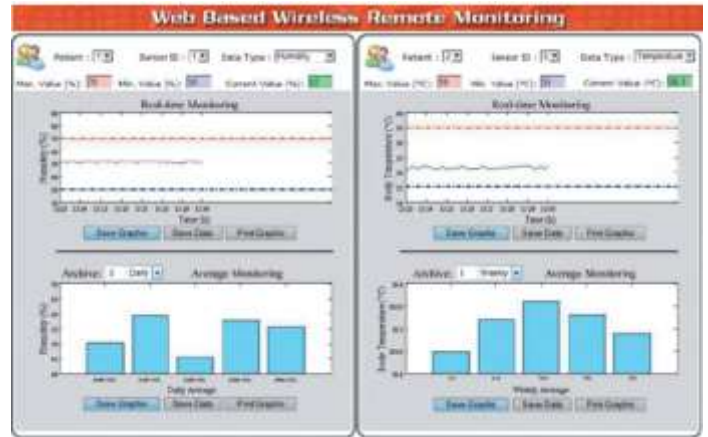


Figure.11 Web-based Telemedicine monitoring system

There is an additional important feature, such as the ability to save graphics and sensed data, and then print them. These properties make it possible to report on patient health information. Thus, medical professionals can detect vital sign variations with long-term health monitoring.

2.6. Telemedicine Hardware requirements

As discussed before, the patient can reserve an appointment with any doctor through Ain Medical portal and make the video conference with the doctor. The patient will use wireless sensor devices to acquire different data for remote monitoring by the doctor such that he could diagnose diseases as shown in Figure (8). The following points determine the needs in a Telemedicine Setup:

- High quality video which leads to a great patient experience.
 - Doctor not restricted to a room, can be located anywhere with his laptop and internet.
 - Integrated with patient hardware such as digital stethoscope, BP, ECG etc -much more than just a video conferencing experience.
 - Integrated with a teleradiology platform enabling Xrays/CT's etc of patient to be transmitted to the treating doctor.
 - Works on Low bandwidth (512 kbps), ideal for rural area.
- There are two types of hardware devices required of BAN.
- Wearable devices are used on the body surface of human.
 - Medical Implanted devices are inserted inside human body.

In wireless body area network, wearable systems for incessant health monitoring are a key technology in helping the transition to more pre-emptive and affordable healthcare. They allow monitoring the diagnostic status of patient and providing feedback to maintain an optimal health status and provide her /his better healthcare.

WBAN traffic is divided in three categories

- **Normal traffic** is the data traffic which we use to monitor the normal condition of patient without any criticality and on demand events.
- **On demand traffic** is initiated by the doctor or consultant to acquire certain information for diagnostic purpose.
- **Emergency traffic** is initiated by nodes when they exceed a predefined threshold and should be accommodate immediately. Such type of traffic is totally unpredictable.

This technology includes unobtrusive & routine health monitoring of patient, and treatment of many other diseases. All data collected through body network coordinator.

3. CONCLUSION

The patient can reserve an appointment with any doctor through Ain Medical portal and make the video conference with him. The patient will use wireless sensor devices to acquire different data for remote monitoring by the doctor such that he could diagnose diseases. Wireless body area network is integrated into telemedical system that promises inexpensive, unobtrusive and ambulatory monitoring during the routine activities. It has the potential to provide a better and less expensive alternative for rehabilitation healthcare and may provide benefit to patients, physicians, and society through continuous monitoring.

A WBAN is expected to be a very useful technology with potential to offer a wide range of benefits to patients, medical personnel and society through continuous monitoring and early detection of possible problems.

4. FUTURE WORK

To make this technology ubiquitous and affordable, a number of challenging issues should be resolved, such as system design, configuration and customization, seamless integration, standardization, further utilization of common off-the-shelf components, security and privacy, and social issues.

REFERENCES

[1] Erik Karulf, 2008, Body Area Networks (BAN)

[2] Moshaddique Al Ameen, Jingwei Liu, Sana Ullah, Kyung Sup Kwak, 2011, A Power Efficient MAC Protocol for Implant Device Communication in Wireless Body Area Networks, The 8th Annual IEEE Consumer Communications and Networking Conference - Smart Spaces and Personal Area Networks

[3] E. Monto´n, J.F. Hernandez, J.M. Blasco, T. Herve´, J. Micallef, I. Grech, A. Brincat and V. Traver, 2008, Body area network for wireless patient monitoring, Spain.

[4] Hoi-Jun Yoo, KAIST, Daejeon, 2011, Body Area Network: Technology, Solutions, and Standardization, Korea.

[5] Arif Onder ISIKMAN_, Loris Cazalony, Feiquan Chenz, Peng Li, 2011, Body Area Networks, Sweden.

[6] ANN-KRISTIN KOCK, 2010, Medical Body Area Networks, University of Luebeck.

[7] Faculteit Wetenschappen, 2011, Reliable and Energy Efficient Protocols for Wireless Body Area Network, University, Antwerpen.

[8] Fariborz Fereydouni_Forouzandeh, 2010, Ultra Low Energy Communication Protocol for Implantable WBSN, Concordia University, Canada.

[9] H.Baldus, 2004, Reliable Setup of Medical Body Sensor networks, Philips Research Laboratories, Germany.

[10] Chris Otto, Aleksandar, Corey Sanders, 2006, system architecture of a wireless body area sensor network for ubiquitous health monitoring, University of Alabama in Huntsville

[11] A. Akyildiz et al, "A Survey on Sensor Networks", IEEE Communications, pp.102-114, August 2002

[12] S. Park and S. Jayaraman, "Enhancing the quality of life through wearable technology," IEEE Engineering in Medicine and Biology Magazine, vol. 22, no. 3, pp. 41-48, May/June. 2003.

[13] I. F. Akyildiz, W. Su, Y. Sankarasubramaniam, and E. Cayirci, "A survey on sensor networks," IEEE Communications Magazine, vol. 40, no. 8, pp. 102-114, Aug. 2002.

[14] R. Schmidt, T. Norgall, J. Mörtsdorf, J. Bernhard, and T. von der G"un, "Body area network ban/a key infrastructure element for patient-centered medical applications." Biomedizinische Technik. Biomedical engineering, vol. 47, no. 1, pp. 365-368, 2002.

[15] C. Otto, A. Milenkovic, C. Sanders, and E. Jovanov, "System architecture of a wireless body area sensor

- network for ubiquitous health monitoring," *Journal of Mobile Multimedia*, vol. 1, no. 4, pp. 307-326, 2006.
- [16] T. Zasowski, F. Althaus, M. Stager, A. Wittneben, and G. Troster, "UWB for noninvasive wireless body area networks: channel measurements and results," in *Ultra Wide-band Systems and Technologies, 2003 IEEE Conference on*, Nov. 2003, pp. 285-289.
- [17] T. Penzel, B. Kemp, G. Klosch, A. Schlogl, J. Hasan, A. Varri, and I. Korhonen, "Acquisition of biomedical signals databases," *IEEE Engineering in Medicine and Biology Magazine*, vol. 20, no. 3, pp. 25-32, May-Jun. 2001.
- [18] S. Arnon, D. Bhastekar, D. Kedar, and A. Tauber, "A comparative study of wireless communication network configurations for medical applications," *IEEE [see also IEEE Personal Communications] Wireless Communications*, vol. 10, no. 1, pp. 56{61, Feb. 2003.
- [19] E. Krames, "Implantable devices for pain control: spinal cord stimulation and intrathecal therapies," *Best Practice & Research Clinical Anaesthesiology*, vol. 16, no. 4, pp. 619-649, December 2002.
- [20] H.-B. Li, K.-i. Takizawa, B. Zhen, and R. Kohno, "Body area network and its standardization at IEEE 802.15.MBAN," in *Mobile and Wireless Communications Summit, 2007. 16th IST, Budapest, Hungary, Jul. 2007*, pp. 1-5.
- [21] L. Theogarajan, J. Wyatt, J. Rizzo, B. Drohan, M. Markova, S. Kelly, G. Swider, M. Raj, D. Shire, M. Gingerich, J. Lowenstein, and B. Yomtov, "Minimally invasive retinal prosthesis," in *Solid-State Circuits, 2006 IEEE International Conference Digest of Technical Papers*, Feb. 2006, pp. 99-108.
- [22] B. Gyselinckx, R. Vullers, C. V. Hoof, J. Ryckaert, R. F. Yazicioglu, P. Fiorini, and V. Leonov, "Human++: Emerging technology for body area networks," in *Very Large Scale Integration, 2006 IFIP International Conference on*, Oct. 2006, pp. 175{180.
- [23] B. Latr_e, B. Braem, I. Moerman, C. Blondia, E. Reusens, W. Joseph, and P. Demeester, "A low-delay protocol for multihop wireless body area networks," in *4th Annual International Conference on Mobile and Ubiquitous Systems: Networking & Services, 2007, Workshop PerNets, Philadelphia, PA, USA, 6-10 August 2007*, pp. 479-486.
- [24] T. Watteyne, S. Aug_e-Blum, M. Dohler, and D. Barthel, "Anybody: a self-organization protocol for body area networks," in *Second International Conference on Body Area Networks (BodyNets), Florence, Italy, 11-13 June 2007*.
- [25] D. Takahashi, Y. Xiao, F. Hu, J. Chen, and Y. Sun, "Temperature-aware routing for telemedicine applications in embedded biomedical sensor networks," *EURASIP Journal on Wireless Communications and Networking*, vol. 2008, no. Article ID 572636, 2008, 11 pages.
- [26] A. Ylisaukko-oja, E. Vildjiounaite, and J. Mantyjarvi, "Five-point acceleration sensing wireless body area network - design and practical experiences," *iswc*, vol. 00, pp. 184-185, 2004.
- [27] E. Jovanov, A. Milenkovic, C. Otto, and P. C. de Groen, "A wireless body area network of intelligent motion sensors for computer assisted physical rehabilitation," *Journal of Neuro Engineering and Rehabilitation*, vol. 2, no. 1, pp. 16-23, March 2005.
- [28] N. T. Dokovski, A. T. van Halteren, and I. A. Widya, "Banip: Enabling remote healthcare monitoring with body area networks," in *FIDJI 2003 International Workshop on Scientific Engineering of Distributed Java Applications, Luxembourg, ser. Lecture notes in Computer Science, N. Guelfi, E. Astesiano, and G. Reggio, Eds., vol. 2952/2004. Heidelberg: Springer Verlag, 2004*, pp. 62-72.
- [29] K. E. Wac, R. Bults, A. van Halteren, D. Konstantas, and V. F. Nicola, "Measurements-based performance evaluation of 3g wireless networks supporting m-health services," in *Multimedia Computing and Networking 2005*. Edited by Chandra, Surendar; Venkatasubramanian, Nalini. *Proceedings of the SPIE, Volume 5680*, pp. 176-187 (2004)., S. Chandra and N. Venkatasubramanian, Eds., Dec. 2004, pp. 176-187.

Hafez Fouad, Author, he received his BSc. degree in Electronics and communications engineering in 1993, EGYPT and received his M.Sc. and Ph.D. degrees from Ain Shams University in 2001 and 2008. His Ph.D. is dedicated to Performance Optimization of CMOS RF Power Amplifiers for Mobile Communication systems. The M.Sc. is dedicated to Design and Optimization of Silicon RF Front-ends For Mobile Communication Systems. He is a researcher at the Electronics Research Institute (ERI), Ministry of Scientific Research since 1994, Cairo, Egypt. His current research interests are Telemedicine Systems, wireless sensors network, Bioelectronics, Bioinformatics and their applications.

The electromagnetics foundation of circuits revisited

Massimo Ceraolo - University of Pisa Italy

Abstract—It is as pillar of electromagnetics knowledge that the Maxwell’s equations describe in a very comprehensive way all electromagnetic phenomena and therefore can be in principle be used as the mathematical basis for any analysis involving systems subject to these phenomena.

In normal research and engineering practice, however, such systems are very often modeled as “circuits”, whose behavior is described by Kirchhoff’s laws instead of Maxwell’s. All physicists and electrical engineers profoundly know that the two equation sets are equivalent, but, in author’s knowledge, no systematic effort has made to evaluate and make explicit the relationship between them.

This paper tries to fill this knowledge gap, and to draw a clear link between the electromagnetism foundation (Maxwell’s equations) and the circuitual approach.

Keywords—Circuit analysis, Kirchhoff equations, Maxwell equations

I. Nomenclature

B	magnetic flux density (or magnetic induction)
D	electric flux density
E	electric field
J	current density field (or areic current field)
J_d	displacement current density field (or areic displacement current field)
H	magnetic field
ϵ	dielectric constant
σ	electric conductivity
μ	magnetic permeability
ψ	flux linkage
c	charge density (or volumic charge)

AC or a.c. Alternating Current

DC or d.c. Direct Current

EMF ElectroMotive Force

KVL: Kirchhoff’s Voltage Law

KCL: Kirchhoff’s Current Law

II. Introduction

DURING past centuries the electromagnetism theory has seen the basic laws first (such as Gauss’s, Ampère’s, Faraday’s, Ohm’s) to be discovered in an integral, macroscopic way, then to be expressed in a differential form that, while having as a consequence the integral versions from which they derive, are useful extensions of them. The most important effort in this rationalization of the basic laws was from Maxwell, and therefore the resulting equations are called Maxwell’s equations (in differential form).

The author is with The University of Pisa (phone: -393409173634, massimo.ceraolo@unipi.it)

Rather independently the basic circuit laws, known as Kirchhoff’s Current Law and Kirchhoff’s Voltage Law, have been postulated and widely used.

Kirchhoff’s laws are applicable to circuits, which are an abstraction widely used to study complex systems in a much easier way than directly applying to them the Maxwell’s differential, or even integral, equations.

The two approaches, however, have remained neatly distinct, so that it is not always clear what is the rationale behind the postulation of Kirchhoff’s laws in circuits, or, equivalently, what are the hypotheses that allow a physical, three-dimensional, system to be modeled and studied as a circuit (governed by Kirchhoff’s laws) [1 to 7].

This paper was therefore conceived with the purpose of (at least partially) filling the knowledge gap between electromagnetics and circuit theory, so that the relation of the two approaches is clarified.

A. Graphical conventions

This paper deals with the possibility to analyze spatial systems, containing conductors and the surrounding environment (air, dielectrics), by means of equivalent *circuits*, that are composed by blocks representing individual devices of the given system, and connector lines, among block.

It will be shown that circuit connector wires have an idealized behavior, and therefore are logically very different from physical conductors.

To ease understanding of the paper this logical distinction is made evident by the use of different symbols, as shown in fig. 1.

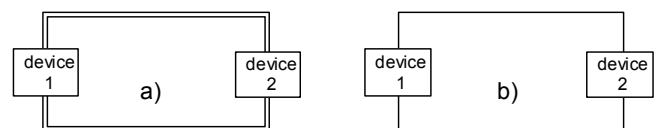


Fig. 1 Graphical convention adopted for conductors:

a) devices connected by real-life conductors

b) devices connected by idealized wires

B. Maxwell’s and other relevant electromagnetism equations

Although very well known, here the four Maxwell’s equations are reported in their differential form, so that they constitute an easy reference when reading of the remainder of the paper. The symbols are those reported in sect. I, and used throughout the paper.

$$\begin{cases} \nabla \times \mathbf{E} = -\frac{\partial \mathbf{B}}{\partial t} \\ \nabla \cdot \mathbf{D} = c \\ \nabla \times \mathbf{H} = \mathbf{J} + \frac{\partial \mathbf{D}}{\partial t} = \mathbf{J} + \mathbf{J}_d \\ \nabla \cdot \mathbf{B} = 0 \end{cases} \quad (1)$$

In addition to Maxwell’s equations the pointwise Ohm’s and continuity equations are reminded, because of their importance for the paper¹:

$$\mathbf{J} = \sigma \mathbf{E} \quad (2)$$

$$\nabla \cdot \mathbf{J} = -\frac{\partial c}{\partial t} \quad (3)$$

In case of systems where it is known that all quantities are constant, Maxwell’s equations become:

$$\begin{cases} \nabla \times \mathbf{E} = 0 \\ \nabla \cdot \mathbf{D} = c \\ \nabla \times \mathbf{H} = \mathbf{J} \\ \nabla \cdot \mathbf{B} = 0 \end{cases} \quad (4)$$

and continuity equation becomes:

$$\nabla \cdot \mathbf{J} = 0 \quad (\text{Error! Bookmark not defined.})$$

III. Distributed systems and circuits

Electromagnetism studies electrostatic (i.e. related to effects of the presence of charge in given portions of space) and electrodynamic, or magnetic (i.e. related to moving charges) phenomena.

It extends to phenomena related to interaction of the previous two, since in time-varying systems they are closely related to each other.

The use of Maxwell’s equations or other electromagnetism tools either in integral or differential form has proven too demanding to analyze systems composed by different electromagnetic subsystems.

Consider the simple system shown in fig. 2.

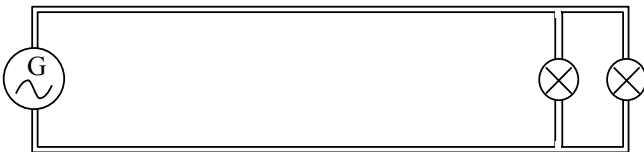


Fig. 2: A simple electromagnetic system.

It is formed by an electric sinusoidal generator feeding two lamps with the interposition of a couple of wires, which are

represented “thick”, because in a physical system they have not only a length but also a width.

Obviously, the analysis of this system would be greatly simplified if, instead of having to analyze simultaneously the whole system using Maxwell’s equations (differential equations to be applied at any point of space taking into account all boundary conditions), it would be possible to write independent equations of the involved individual, lumped, components and linking them by some additional congruence equations.

This approach can be referred to, for the time being, as the *circuit* or *circuital* approach.

A qualitative analysis of fig. 2 shows that the generator connects with the lamps by long wires, while short connections are present at the two horizontal sides of the system. Therefore a hypothetical approximation of the system of fig. 2 could be as shown in fig. 3 a): the connections are shown using thin wires, to evidence their connecting role, while the parts of the original system to be modeled individually are enclosed in boxes or circles. In fig 3 b) a further evolution of the system is reported, in which the components are substituted with symbols indicating specific mathematical modeling of the considered components: ideal resistors for line and loads, ideal generator for the generator.

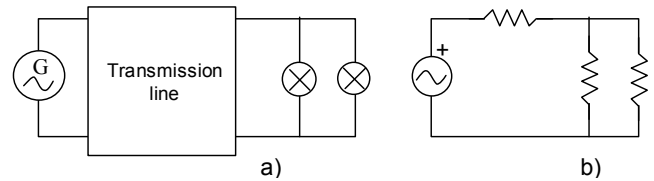


Fig. 3: Circuital approximation of system of fig. 2.

So the Circuital approximations of figure 3 are composed only by *circuit elements* (generator, lamps or resistors, transmission line box) and *ideal wires*. All physicists and electrical engineers already know very well that this “lumpization” of electromagnetic systems constituted by components joined by conductor wires is possible, but rarely the rationale behind this conversion is investigated.

In the following sections it is shown that the conversion of spatially-distributed physical systems into circuits is possible, under certain hypotheses, which also determine the choice on how to make the transformation, and with some limitations.

In search of the implementation of the conversion into circuit of any system governed by the electromagnetism equations, better is to start with the simplest case, i.e. when all quantities do not vary with time. By traditional nomenclature these systems are referred to as “direct current” systems.²

¹ The continuity equation is not independent of Maxwell’s equations: it can be easily derived taking the divergence of both members of the third of (1), and introducing c in the result taking it from the second one.

² Better name would have been “constant operation systems” or “steady-state systems”.

IV. Applicability of Kirchoff's Current Law in d.c. circuits

Consider a region of space, able to exchange charge between its interior and exterior. In case we want to analyze a system by means of the technique of conversion into a circuit, it is rather obvious that this charge exchange occurs only by means of discrete "channels" constituted by the wiring entering the surface, while charge exchange in regions not occupied by wires is neglected.

Therefore it is reasonable to put forward the following:

ASSUMPTION 1: any charge flow is neglected anywhere outside circuit elements, except than within conductor wires.

Consider the region of space V surrounded by surface S (fig. 4 a)).

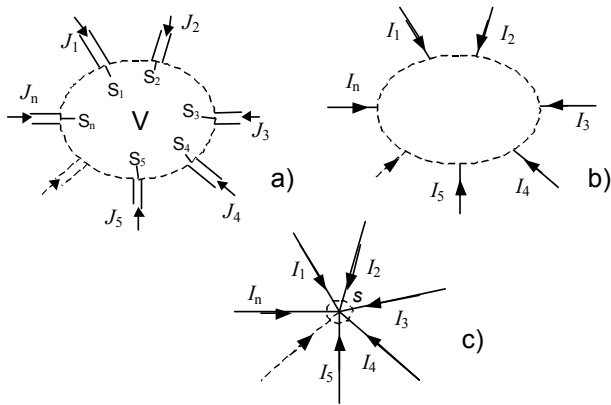


Fig. 4: A confined region of space (a) that can bring to a *generalized node* (b) and a *node* (c).

In the drawings of fig. 4 all the conductor wires converging into the volume V are considered (and shown).

Let us now consider the continuity equation (3)

$$\nabla \cdot \mathbf{J} = -\frac{\partial c}{\partial t}$$

where c is the spatial charge density, or charge per unit of volume.

Since by hypothesis we are "in d.c." that means that in the considered systems all quantities are constant, also charge density is constant and therefore in this case the continuity equation becomes the (4). Integrating through the volume V around the nodes or generalised nodes considered, it is:

$$\int_V \nabla \cdot \mathbf{J} \, dv = \int_S \mathbf{J} \cdot d\mathbf{s} = 0 \tag{5}$$

Using Assumption 1 conductive currents are possible only within wires. So the integral of (5) is simplified since \mathbf{J}_t is non-zero only through S_k , that are the intersections of S with conductor wires:

$$\int_S \mathbf{J} \cdot d\mathbf{s} = \sum_{k=1}^n \int_{S_k} \mathbf{J} \cdot d\mathbf{s} = \sum_{k=1}^n (-I_k) = 0 \quad \text{where} \quad I_k = \int_{S_k} \mathbf{J} \cdot d\mathbf{s}$$

Thus:

$$\sum_{k=1}^n I_k = 0$$

That is KCL for the region V .

Fig. 4 b) shows another representation of the same system of fig. 4 a). In the symbology of this paper, however, there is a logical distinction between the two: the thin wires of fig. 4 b) are idealized wires, based on special assumptions. At this point of the paper, the only assumption beyond the symbol of idealized wires is Assumption 1.

Obviously enough, the demonstration proposed, referred to the scheme of fig. 4 a), contained what is normally called in circuit terminology a "generalised node", is applicable also in the scheme of fig. 4 c) containing a conventional node: it is just necessary to consider a tiny surface S around the connection of some wires.

CONCLUSION 1: in a physical system operating in DC for which Assumption 1 is applicable the KCL applies.

V. Applicability Kirchoff's Voltage Law in d.c. circuits

Consider the system displayed in fig. 5.

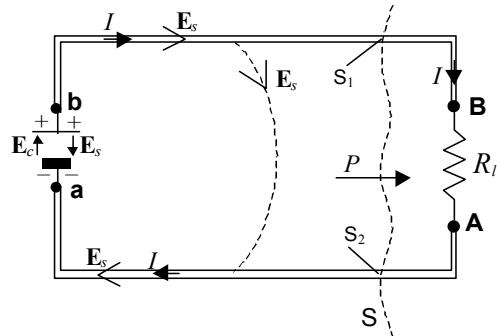


Fig. 5: Basic system with charge flow and chemical and electrostatic fields.

It is composed by an electrochemical battery (at the left side of the figure) connected through physical wires to a load resistor R_l at the right side³.

Let us first imagine that there is some positive charge in the upper terminal of the battery and an equal amount of negative charge in the lower one. These charges would create an electric field \mathbf{E}_s in the space around them: inside conductors it is longitudinal, while outside it has a different orientation (one possible force line is shown dashed in figure), but has no relevance for analysis of DC systems since by effect of Assumption 1, charge movement is allowed only within conductor wires.

Any individual charge present in the conductors (i.e. an

³ The dashed line called "S" and the names around it are non significant here and will be discussed in sect. **Error! Reference source not found.**

electron) would then circulate in the conductor loop of the system, and finally offset the initial charge accumulated at the two battery terminals, and so in a very rapid time the conductor loop would be neutral and no more charge could flow.

During this flow, the energy received by the charge by effect of acceleration due to \mathbf{E}_s is dissipated during the transit, by effect of the energy dissipation occurring during charge movement in conductor materials, i.e. where Ohm's law applies.

The thing is that the battery is able to cause continuous charge flow in the circuit. Although the actual behavior of an electrochemical battery is very complex, it can be modeled for the purposes of this study as a system able to "pump" charges pushing them from its negative electrode towards its positive one by means of an inner electric "chemical" field \mathbf{E}_c that this way lets charges flow. Any charge looping in the system of fig. 5, obtains energy when it goes through the battery, by combined effect of \mathbf{E}_c and \mathbf{E}_s , which is later and delivered (dissipated) when the charge flows through the external circuit.

The energy supplied by \mathbf{E}_c to the charge equals the energy dissipated during the flow. Since in the entire loop \mathbf{E}_c has a net contribution to the work transferred to the charge, it is a non-conservative field.

Therefore analysis of this circuit can be made starting from the supposed simultaneous presence of electrostatic, conservative (\mathbf{E}_s) and chemically induced, non-conservative (\mathbf{E}_c) fields in the battery:

$$\mathbf{E}_t = \mathbf{E}_s + \mathbf{E}_c \quad (6)$$

The charge movement in the loop is determined by the presence of the whole field \mathbf{E}_t , not only \mathbf{E}_s ; therefore the Ohm's law is to be written:

$$\mathbf{E}_t = \rho \mathbf{J}$$

and, taking the loop integral of both sides:

$$\oint \mathbf{E}_t \cdot d\mathbf{l} = \oint \rho \mathbf{J} \cdot d\mathbf{l} \quad (7)$$

The left part of (7) is:

$$\oint \mathbf{E}_t \cdot d\mathbf{l} = \int_a^b \mathbf{E}_c \cdot d\mathbf{l} \quad (8)$$

because of the conservativity of \mathbf{E}_s , and the absence of \mathbf{E}_c outside the battery.

The integral of right part of (7) may be computed neglecting the resistance of conductor wires in comparison to battery and load resistances:

$$\begin{aligned} \int_a^b \rho \mathbf{J} \cdot d\mathbf{l} + \int_b^B \rho \mathbf{J} \cdot d\mathbf{l} + \int_B^A \rho \mathbf{J} \cdot d\mathbf{l} + \int_A^a \rho \mathbf{J} \cdot d\mathbf{l} &\cong \\ \cong \int_a^B \rho \mathbf{J} \cdot d\mathbf{l} + \int_B^A \rho \mathbf{J} \cdot d\mathbf{l} &= (R_B + R_l)I \end{aligned} \quad (9)$$

while the latter equality is justified by the relations, for both resistive components:

$$\int \rho \mathbf{J} \cdot d\mathbf{l} = \int \rho(l)J(l)dl = \int \rho(l) \frac{I}{S(l)} dl = I \int \rho \frac{dl}{S(l)} = RI$$

where it has been exploited that, as a consequence of the continuity equation, current I does not depend of the integral variable l .

Substituting (8) and (9) into (7) gives:

$$V_e = \oint \mathbf{E}_c \cdot d\mathbf{l} = (R_B + R_l)I \quad (10)$$

where the quantity V_e , defined by means of \mathbf{E}_c , is called "electromotive force" (EMF) of the circuit (subscript e stands for electromotive)⁴.

Equation (10) is a usual expression of Ohm's law for one-loop system, and may be considered to be the result of application of KVL to the circuit of fig. 6, that assumes the role of equivalent circuit of system of fig. 5.

The utilization of KVL in this circuit is now validated by means of the Maxwell's and Ohm's equations.

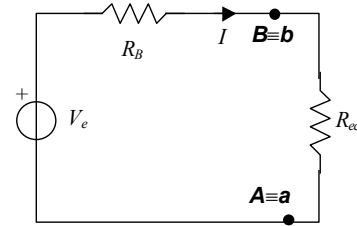


Fig. 6: Equivalent circuit of the system shown in fig. 5.

Although rather obvious, it is important to stress that the result obtained is not just linked to the presence of an electrochemical battery: several possibilities exist to create devices that in its inside "pump" changes from its negatively charged terminal to its positively charged one, so that charges can move through the external circuit forced to do that by the electric field created in the conductor by the charges located at the terminals of the pumping devices.⁵

Let us now consider a more complicated electric system (circuit), shown in fig. 7.

It contains several loops, resistors and several batteries. Moreover, it is not electrically isolated from the outside world: because of the connections at the corners of its loops.

In the whole system considered, including the parts not shown in figure, there exists in principle a field \mathbf{E}_s caused by the charge accumulated at all the battery terminals (considering also those outside the shown part of the system), and the corresponding current density field $\mathbf{J} = \sigma \mathbf{E}_s$, where, obviously, any point of space has a \mathbf{E}_s , \mathbf{J} , σ of its own.

However, because of Assumption 1, there is no interest in considering the fields present outside the conductor wires.

The direction of electric and current density fields inside the conductor is parallel to their axes, but its orientation is not known a priori (this lack of knowledge has prevented the possibility of reporting the vector arrows in the figure).

In the figure three possible loops may be considered: L1, L2 and L3. Let us concentrate, without loss of generality, to loop

⁴ The term electromotive force is maintained for its worldwide use; it is however apparent that it is partially confusing, since the quantity to which it refers is not a force in the physical sense.

⁵ Significant sources of constant electromotive force are fuel cells, photovoltaic cells; electric machines operating as source are sources of time varying electromotive forces.

L1.

If in the system shown in fig. 7 a generic charge q goes along loop L1, the work of the electrostatic field \mathbf{E}_s on it is null, because of the conservative nature of the electrostatic field.

Consequently, the analysis carried out with system of fig. 5 can be repeated for any loop of fig 7. The Ohm's law gives:

$$\oint_{L1} \mathbf{E}_t \cdot d\mathbf{l} = \oint_{L1} \rho \mathbf{J} \cdot d\mathbf{l} \quad (11)$$

The left part of (11) is:

$$\oint_{L1} \mathbf{E}_t \cdot d\mathbf{l} = \int_{a1}^{b1} \mathbf{E}_{c1} \cdot d\mathbf{l} + \int_{a2}^{b2} \mathbf{E}_{c2} \cdot d\mathbf{l} \quad (12)$$

because of the conservativity of \mathbf{E}_s .

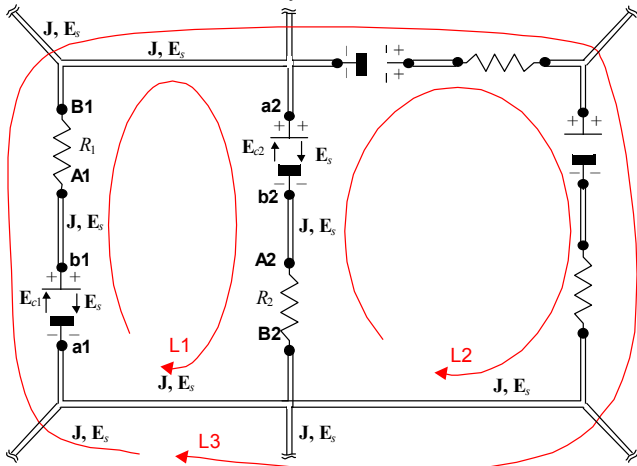


Fig. 7: A multiple-loop, multiple source, multiple resistor system.

Again, the integral of right part of (11) may be computed neglecting the resistance of conductor wires in comparison to battery and load resistances:

$$\oint_{L1} \rho \mathbf{J} \cdot d\mathbf{l} = (R_{B1} + R_1)I_1 + (R_{B2} + R_2)I_2 \quad (13)$$

where I_1 and I_2 can both be computed as $\oint_S \mathbf{J} \cdot d\mathbf{S}$ using any cross section of the system branches containing R_1 and R_2 respectively.

The above analysis perfectly replicates that made for the simpler case of fig. 5; therefore if the following definitions are adopted:

$$V_{e1} = \left| \int_{a1}^{b1} \mathbf{E}_{c1} \cdot d\mathbf{l} \right| = \int_{a1}^{b1} \mathbf{E}_{c1} \cdot d\mathbf{l} \quad V_{e2} = \left| \int_{a2}^{b2} \mathbf{E}_{c2} \cdot d\mathbf{l} \right| = - \int_{a2}^{b2} \mathbf{E}_{c2} \cdot d\mathbf{l}$$

the loop L1 of the system of fig. 7 can be studied as reported in the upper part of fig. 8, and the entire system of fig. 7 can be studied using the equivalent circuit shown in the bottom part of fig. 8.

At this point a more general result is obvious:

in any loop of any DC circuit the sum of all electromotive forces (integrals of inner, non conservative fields) equals the sum of all resistances multiplied by the correspondent currents. (14)

Although in the DC systems electromotive forces have a

very different physical interpretation than voltages across resistors, as shown above, (14) can be expressed in a more general form:

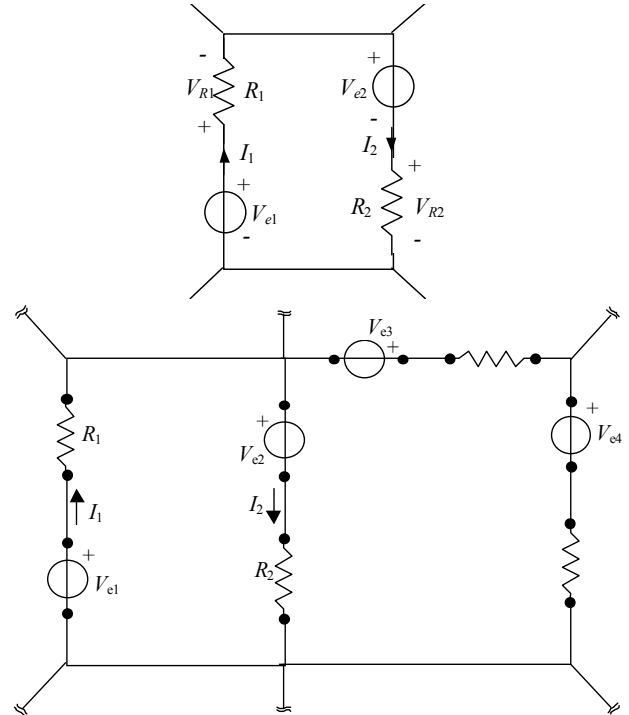


Fig. 8: Equivalent of loop L1 of the system shown in fig. 7 (top) and of the full system of fig. 7 (bottom).

if any loop is gone through in a clockwise direction (or, equivalently in counter clockwise direction) the sum of all voltages rises (or, equivalently, the sum of all voltage drops) is zero. (15)

Statement (15) is the well known KVL. Although it has been derived considering the fields inside the conductors, it assumes a form that is immediately usable in circuits, to state useful relations between circuit quantities.

The KVL can be seen to be *the circuital version of conservativity of electrostatic field.*

Indeed it states that any loop implies null voltage sum, which is the equivalent of the notion that any circuit integral of elementary work of electrostatic field is null. Furthermore it is also equivalent to state that in any circuit is possible to define a definite voltage value for any node, a fact that again recalls the correspondent characteristic of electrostatic (or any conservative field).

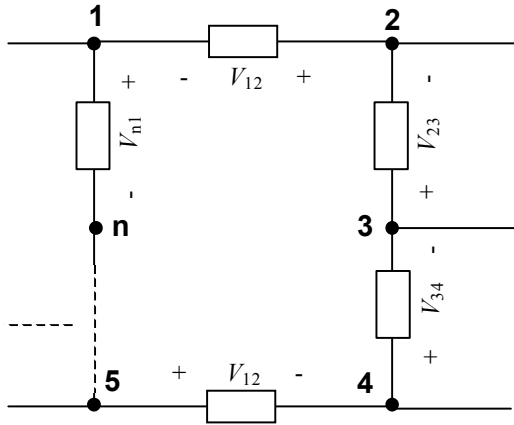


Fig. 9: One-loop, multiple-resistor circuit.

The equivalence of KVL and possibility to define given potentials to circuit nodes can be easily shown considering fig. 7, where different lumped components (having arbitrary inner behavior) are connected to each other in a loop inserted in a larger circuit (in the most general case any node may have a wire connected with it and with other electric circuit components).

The voltages across their terminals are named after the terminals themselves, and they are considered according to the polarity references (positive voltage rises) shown in fig. 7.

If a voltage can be defined for each node, then, considering that the $(n+1)$ th node is indeed the 1-st node, it is:

$$\sum_{k=1}^n V_{k,k+1} = \sum_{k=1}^n (V_{k+1} - V_k) = \sum_{k=2}^n V_k + V_1 - \sum_{k=1}^n V_k = 0$$

Let us summarize the procedure followed in this paragraph:

- it has been seen that the current continuously flowing in a simple DC circuit is consequence of the presence of a non-conservative field in one or more “forcing” component; as a consequence of this field, the terminals of the component wherein this field is present are able to remain differently charged;
- the charge difference at the terminals of a forcing component causes the presence of electrostatic field in the conductors outside it, whose potential difference at these terminals is equal to its electromotive force;
- this electrostatic field is obviously conservative and so voltages across circuit terminals are independent of the path considered, and thus a potential can be defined for each node
- the presence of node potentials is necessary and sufficient condition for the KVLs

The gist of this process is: forcing components determine an electrostatic (conservative) field in the conductors outside them, so potentials of individual circuit points can be defined and therefore the KVL applies.

This works in any case, if we consider that the circuits are totally separated from the outside world, except from interactions that may occur inside circuit elements (such as in the bat-

tery of figure 7)

Therefore the following is put forward:

ASSUMPTION 2: any interaction of the considered physical circuit with the outside world is made only inside circuit elements. No interaction with wires and space between wires is supposed to occur.

Then, the following conclusions can be made

CONCLUSION 2: in a physical system operating in DC for which Assumption 2 is applicable, the KVL applies.

CONCLUSION 3: in a physical system operating in DC for which Assumptions 1 and 2 are applicable, the KCL and KVL apply, and therefore it can be studied as a circuit.

VI. Extension of Kirchhoff's laws to time-variable circuits

In the previous paragraphs it was seen that in circuits operating with constant quantities, that by tradition are called DC circuits, the KVL is a direct consequence of the electrostatic field present in the circuit, and KCL is a consequence of continuity equation.

In this section, these concepts will be tried to expand also in the case of time varying circuits.

A. Extension of Kirchhoff's Current Law

Let the divergence to be taken of eq (1.3) be taken:

$$\nabla \cdot (\mathbf{J} + \mathbf{J}_d) = \nabla \cdot \mathbf{J}_t = \nabla \cdot \nabla \times \mathbf{H}$$

Where $\mathbf{J}_t = \mathbf{J} + \mathbf{J}_d$ is the total current density, sum of current density (areic current) and displacement current density (areic displacement current). Thus:

$$\nabla \cdot (\mathbf{J} + \mathbf{J}_d) = 0 \tag{16}$$

Equation (16) is an equivalent, alternative, expression of the continuity equation (3).

If applied to any closed surface S in space, crossing circuit wires and/or passing between capacitor armatures, and the volume $V(S)$ contained by S , (16) says that:

$$\int_{V(S)} \nabla \cdot \mathbf{J}_t dv = \int_S \mathbf{J}_t \cdot d\mathbf{s} = 0 \tag{17}$$

When a circuit is involved, the main dynamic phenomena are confined within components that are connected by wires, having a somehow idealized behavior. To make (17) adequate for circuits, the following assumption is made:

ASSUMPTION 3: the displacement current $\partial \mathbf{D} / \partial t$ is neglected anywhere, outside circuit elements.

Note that this is independent from Assumption 1, that referred to conduction, not displacement currents.

By Assumptions 1 and 3 conductive currents are possible only within wires and displacement currents only through ca-

capacitor armatures. So the integral of (17) is simplified since only through surfaces S_k \mathbf{J}_t is non-zero, where S_k are the intersection of S with conductor wires or capacitors .

$$\int_S \mathbf{J}_t \cdot d\mathbf{s} = \sum_{k=1}^n \int_{S_k} \mathbf{J}_t \cdot d\mathbf{s} = \sum_{k=1}^n I_k = 0$$

that is the KCL.

The concept is exemplified in fig. 10, where the sums are to be performed with k going from 1 to 6 (left-side circuit) or 1 to 7 (right-side circuit).

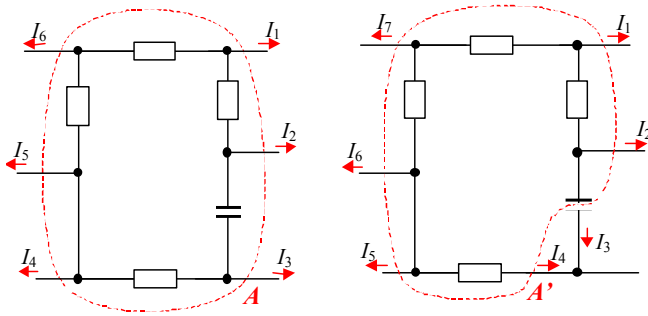


Fig. 10: Sample surfaces A and A' showing continuity equation and KCL in a sample circuit.

CONCLUSION 4: in a physical system for which Assumptions 1 and 3 are applicable, the KCL applies.

B. Circuits and metacircuits

Let us now try to use the theory introduced up to know in a system composed three subsystems: two of them are endowed with a couple of terminals that are the only way to interchange conductive current with the outside world, and do not allow exchange of displacement currents (these will be called *lumped components*). These are connected to a *distributed system*, wherein conductive and displacement current circulate.

To fix ideas, let the two lumped components be a generator of sinusoidal EMF (just as the one used in the first example) and a ohmic resistor, while the distributed system is a transmission line constituted by two conductors and the surrounding space (top of fig. 11).

In a system of this kind it may be unacceptable to neglect the effects of the magnetic field trough the loop created by the three subsystems; a case where the need to take it into account is particularly evident is when the resistance at the receiving end is null.

In this example, where the transmission line has a much greater length than the distance between the two conductors, it is reasonable to assume that the magnetic field in the loop can be assumed in shape as equal the magnetic field created by to wires of indefinite length, and that the effects of the magnetic field in space between the transmission line and the lumped components can be neglected. Finally, it can be assumed that the magnetic induction between the two conductors is due only to the current flowing in the conductors themselves.

Under these hypotheses, the behavior of the transmission line can be described using equations that do not involve

knowledge of what happens outside it, and there fore can be substituted by a lumped component (block “L” in bottom-left part of fig. 11).

The part of the circuit inside L is governed by (1.1), and its integral consequence, the Faraday’s law; therefore the system of fig. 11 is described by:

$$v = (R + R_L)i(t) + v_B(t) \tag{18}$$

where:

$$v_B(t) = \frac{d\psi}{dt} = L \frac{di}{dt}$$

and L , self-inductance of the circuit, is the proportionality coefficient between current and the flux linkage it creates.

Rather obvious, (18) can be interpreted as the KVL of the circuit reported in the bottom-right part of fig. 11, from which, then, $i(t)$. can be determined when $v(t)$ is known, and vice-versa.

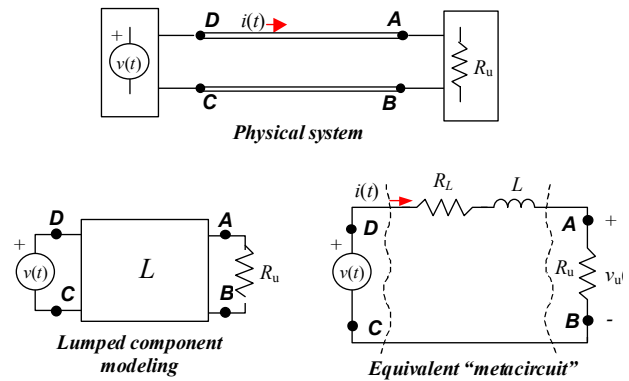


Fig. 11: Conversion of a system operating with time-varying quantities into a circuit. Case 2: presence of a magnetically-significant double-bipole.

It is by now not demonstrated whether the circuit of fig. 11 is adequate for evaluation of other voltages, such as for example $v_{AD}(t)$ or $v_{AC}(t)$.

Indeed it cannot be used for this purpose, simply because the Faraday’s EMF of loops containing simultaneously a point from the couple C-D and one from the couple A-B does depend on the loop geometry, because of the non-conservativity characteristic of the magnetic field.

This can be visualized clearly considering for example a measuring system of voltage v_{AD} in the physical system (fig. 12). It is apparent that any change of the position of a voltmeter that would be intended to measure v_{AD} would change the area of the loop composed by the conductor AD and the measuring wire, and therefore the electromotive force generated according to the Faraday’s law.

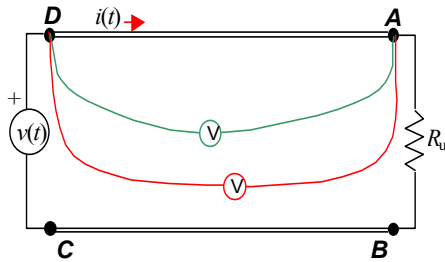


Fig. 12: Different measuring loops create different visualizations on the voltmeter V.

Without having the ambition to have analyzed in this example the problem of conversion into a circuit of a system having terminals spatially distant from each other (in the example terminals D and C are distant from A and B), it is felt safe enough to draw the following general conclusion from the example:

- in general it is not possible to determine a circuit completely equivalent to this kind of system
- a circuit can be determined that has a behavior equivalent to the given system, when used only for separate determination of electrical quantities in the two ends of the given system. We call *metacircuit* this special version of circuit.

VII. Summarizing concepts

We can resume what has been obtained in this paper as follows:

- Assumptions 1 and 2 allow physical system operating in DC to be treated as circuit, for which KCL and KVL are assumed to be valid.
- Assumptions 1 to 4 allow a physical system to be treated as circuit, for which KCL and KVL are assumed to be valid.

Therefore can now say that:

under precisely stated assumptions, a system, which is composed by circuit elements and conducting wires, can be analysed by means of the mathematical-graphical tool called circuit. For them KCL and KVL are postulated to be valid.

Circuit elements are subsystems that have electrical interaction to the rest of the system only through their terminals).

In the case of transmission lines, for which assumption 4 is unrealistic, *metacircuits* can be used, that operate as ordinary circuits, with the additional limitation that they must not be used to determine voltage across circuit sections at the two ends of the line.

The approach described can be extended to other systems such as those containing transformers, electric machines, multipoles, etc.; however such a comprehensive analysis is out of the scope of this paper.

The general approach presented in the paper has been adopted in book [8].

VIII. Conclusion

This paper had the purpose of showing the correspondence of the analysis of physical systems by means of the Maxwell's equations and by means of their circuital approximations.

Clear hypotheses that allow physical systems to be analyzed as circuits have been introduced, discussed and applied in examples.

It has been shown that while systems operating in D.C. can be easily formulated in such a way that the conversion into circuits is adequate for computation purposes, those operating in A.C. have important limitations in this respect.

The approach proposed is clarifying and useful also for teaching, and has been adopted in book [8].

references

- [1] Fawwaz T. Ulaby: Fundamentals of Applied Electromagnetics Prentice Hall, ISBN 0132413264.
- [2] Martin A. Plonus: "Applied Electromagnetics", Mc Graw-Hill International Editions, ISBN 0-07-050345-1.
- [3] C. Alexander, M. Sadiku: Fundamentals of Electric Circuits, Mc Graw-Hill, ISBN 13-9780073301150.
- [4] W. H. Hayt, J. Kemmersly: "Engineering Circuit Analysis, Mc Graw-Hill, ISBN 13-9780073366616.
- [5] C. R. Paul, S. A. Nasar, L. E. Unnewehr: "Introduction to electrical Engineering" Mc Graw-Hill Inc, ISBN 0-07-011322-X.
- [6] Mulukutla S. Sarma: Introduction to Electrical Engineering, Oxford University Press, ISBN 0-19-513604-7.
- [7] G. Rizzoni, Fundamentals of Electrical Engineering", Mcgraw Hill book, ISBN-13: 978-00733803377.
- [8] M. Ceraolo and D. Poli: "Fundamentals of Electric Power Engineering – from Electromagnetics to Power Systems", IEEE-Wiley 2014, ISBN 978-1-118-67969-2.

Disturbances Applied to Axis of Telescope Installed on the Deck of a Ship

S. A. Tushev¹, V. N. Drozdov²

Department of Electrical Engineering and Precision Electromechanical Systems

ITMO University

197101, Saint-Petersburg, Kronverkskij Ave., 49

RUSSIAN FEDERATION

¹tushev.sergei@gmail.com, ²drozdovuprint@rambler.ru

Abstract— The existing solutions in the field of trajectory measurement telescopes installed on a deck of the ship require a gyro-stabilized platform. However, gyro-stabilized platform has low dynamic characteristics, which influence on the precision of measurements. Therefore, it is necessary to develop a control system without a stabilizing device in which the ship motions are compensated by a precision electric drive. Among others, this purpose includes the problem of investigation of disturbances applied to axis of telescope's mount.

The mathematical model of telescope electric drive reference is built with six kinds of ship motions. It is used to simulate dynamic disturbances.

The authors have studied parameters of disturbances applied to telescope axis for the target motion path family in a wide range of angular coordinates.

The proposed mathematical model allows assessing parameters of dynamic disturbances caused by ship motions. It could be used for mounts of telescopes with different configuration. The article is helpful for students, specialists and developers of precision electric drives, especially of sea-based telescopes.

Keywords— pitching, precision electric drive, dynamic disturbances, sea-based telescope.

I. INTRODUCTION

THE telescope mount is installed on the deck of the ship without gyro-stabilized platform. There are ship motions with certain parameters in the area, where the telescope is planned to be used. It is assumed that the control system of electric motor drive of telescope should provide the specified accuracy in spite of ship motions. Ship motions compensation is provided by electric motor drive without additional device [1, 2].

Following main types of disturbing external influences are applied to the axis of telescope mount:

- frictional torque;
- wind torque;
- axis imbalance torque;
- ship motions torque.

External disturbance is an important factor that reduces the pointing accuracy of telescope, which depends on its magnitude, frequency and non-linearity. Any disturbance torques applied to the axis reduces the maximum motor dynamic torque, which limits implemented acceleration of the telescope. This, in turn, reduces the allowable range of the object's coordinates, in which continuous monitoring is possible [3].

One of the objectives of a telescope control is to reject external influences to ensure the specified accuracy. To assess the impact of these disturbing torques on the pointing accuracy it is necessary to consider them in detail and execute mathematical modeling [4].

II. TYPES OF DISTURBANCES

A. Frictional torque

Friction torque is reactive torque and occurs predominantly in the bearings of axis supports of telescope mount. It can be decomposed into two components - dry friction and viscous friction. Dry friction is constant in magnitude, but depends on the sign of the velocity and is always directed opposite to the motion. It is determined according to the formula:

$$M_{st} = |M_{st\max}| \cdot \text{sgn } \omega,$$

where $M_{st\max}$ - magnitude of friction torque, ω - axis velocity [5].

Fig. 1 shows a mechanical load characteristic of the dry friction torque (M - torque, ω - velocity). Typically, the coefficient of static friction is greater than the coefficient of rolling friction, as indicated by the dashed line.

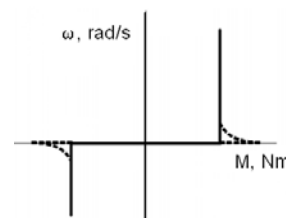


Fig. 1. Dry friction torque

Primarily, viscous friction torque is caused by internal friction in the axis of the bearing lubrication. It is linearly dependent on the axis velocity according to the formula:

$$M_{vf} = k\omega,$$

где k - coefficient of proportionality between the viscous friction torque and speed of rotation [6].

In real systems dry friction torque prevails over the other components, and at the same time has a high degree of non-uniformity due to the characteristics of bearings used.

Fig. 2 shows the dependence of dry friction torque of the azimuthal coordinate on the real system. At the $+80^\circ$ point resistance torque becomes two times greater than at the -80° point.

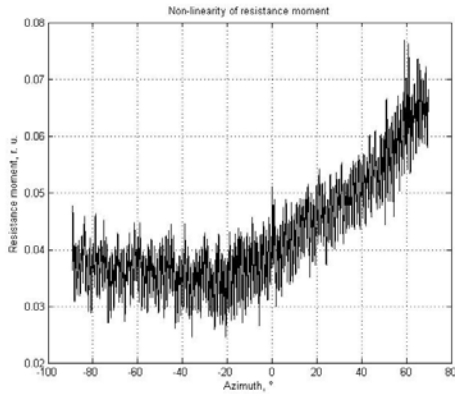


Fig.2. Friction torque at different azimuth angles

High requirements to the drive tracking accuracy are presented mainly at low and extra low speeds. Contribution of viscous friction is irrelevant at these speeds, and it could be neglected when control system is synthesized [7, 8].

B. Wind torque

A wind load torque is random and is given by the spectral density of the harmonic components. The initial phase of the components is defined as a random variable with uniform probability density function in range $\pi \leq \varphi_k \leq \pi$.

In practice, often the wind load torque is assessed by its maximum amplitude. When designing a control system it is modeled as an active static moment, which does not depend on direction of axis rotation [9, 10].

C. Axis imbalance torque

If an axis of telescope is not balanced, the center of mass of this axis does not match with the geometric center of mass. This leads to an additional imbalance torque determined as multiplication of force of gravity and shoulder, depending on the location of the center of mass, Fig. 3 a):

$$M_{nb}(\alpha) = F_g l_{AB} \sin(\alpha),$$

where F_g - gravity force applied to the center of mass of axis, l_{AB} - shoulder of the force of gravity, α - angle between force of gravity and its shoulder.

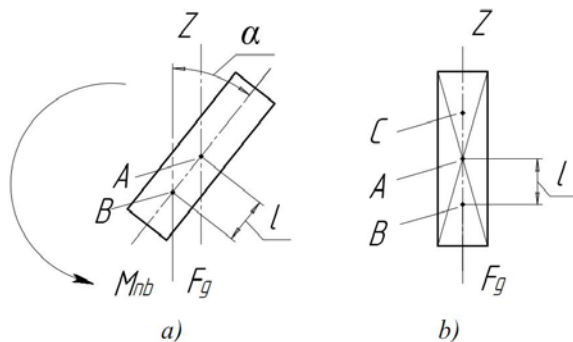


Fig.3. Imbalance torque of elevation axis

If the resistance torque is less than the torque of imbalance, the axis of telescope will try to take the position of equilibrium. In this position, the angle between shoulder AB and F_g is set to zero and, respectively, the imbalance moment also becomes equal to zero, Fig. 3 b). If balancing load is put to the point C , the center of gravity will shift to the geometric

center of mass. This eliminates the imbalance of axis over the entire range of possible positions.

When not enough balanced telescope mount is in the "standing point" mode, the moment of imbalance depends only on the current angular position of the axes in the fixed coordinate system. If the axes of the device are fixed, the moment of imbalance is variable and depends on the current level of ship motions, since the position of the axes of the telescope relative to the ground is also changing.

Imbalance torque is removable using a system of balancing masses. It is necessary to ensure that the amount of imbalance torque does not exceed the dry friction torque. In this case, it could be neglected during the simulation [11].

D. Ship motions torque

Ship motions have a multifaceted effect on the control system of the telescope. In particular, rotational kinds of ship motions cause occurring of additional dynamic disturbances on the axis of the telescope.

Parameters of ship motions corresponding to the area, where the telescope is used, are shown in Table I.

TABLE I.
PARAMETERS OF SHIP MOTIONS

Kind of motion	Amplitude	Period, sec
Roll	10 °	12
Pitch	3 °	7
Yaw	5 °	15
Heave	4 m	9
Surge	3.5 m	10
Sway	3.5 m	13

In case of alt-azimuth mount, due to the presence of the variable component of the moment of inertia of azimuth (AZ) axis, dynamic disturbance torque depends on the yaw level and on the position of the elevation (EL) axis:

$$M_{Daz} = J_{az}(\alpha_{el}) \frac{d^2 \varphi}{dt^2},$$

where φ - current yaw angle, $J_{az}(\alpha_{el})$ - moment of inertia of AZ axis in dependence of current α_{el} .

Dynamic disturbance torque, applied to the EL axis, depends on pitching and roll level. It also depends on current AZ position, since this determines the angle between the coordinate axes and the projection of the EL axis on the horizontal plane:

$$M_{Del} = J_{el} \left(\frac{d^2 \psi}{dt^2} \cos \alpha_{az} + \frac{d^2 \theta}{dt^2} \sin \alpha_{az} \right),$$

where θ - current roll angle, ψ - current pitching angle, J_{el} - moment of inertia of EL axis, α_{az} - current AZ axis angle.

III. MATHEMATIC MODELING OF DISTURBANCES

The parameters of each type of ship motions are different and depend on the position of the axes of the telescope. So, dynamic disturbances should be modeled at various object coordinates. The range of variation of the azimuth angle of object is from 0° to 90°, and if the elevation angle of object is from 0° to 75°. Upper limit is 75°, because there is significant acceleration on AZ axis caused by ship motions at this value

of the elevation, which energy subsystem of the telescope cannot fulfill [11].

Moment of inertia of the azimuthal axis generally depends on the position of the elevation axis, so that investigation of perturbations of the azimuthal axis is held in two versions - with and without consideration of variable moment of inertia. The elevation axis of telescope is represented in the form of hollow tube. Thus, dependence of moment of inertia of the azimuthal axis from position of the elevation axis is determined by formula:

$$J_{az}(\alpha_{el}) = \cos^2 \alpha_{el} + \frac{6r^2}{3r^2 + l^2} \sin^2 \alpha_{el},$$

where J_{az} – relative moment of inertia, divided by the moment of inertia at elevation position 0° , α_{el} – elevation axis angle, r – tube radius, l – tube length. Mathematical modeling of the system is performed for the parameters listed in Table II.

TABLE II.

PARAMETERS OF SYSTEM		
Parameter	Symbol	Value
AZ moment of inertia (EL 0°)	J_{az0}	1600, kg·m ²
AZ moment of inertia (EL 90°)	J_{az90}	1400, kg·m ²
EL moment of inertia	J_{el}	200, kg·m ²
EL tube length	L_{el}	4, m
EL tube diameter	D_{el}	1, m

The block diagram of the model of disturbances is in Fig. 4.

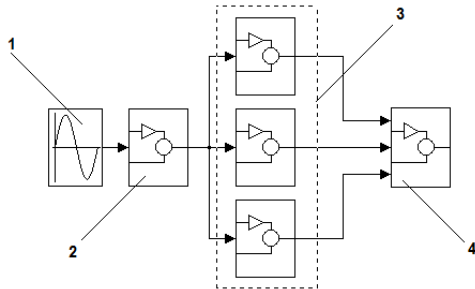


Fig 4. Block diagram of the model of dynamic disturbances: 1 - block of ship motions parameters; 2 - reference signal block; 3 - block forming a dynamic disturbance torques for the azimuthal and elevation axis; 4 - acquisition data unit.

Block of ship motions parameters outputs six signals corresponding to each kind of motion.

The reference block generates a task for both axes according to given parameters of marine pitching. Even when object is not moving, reference signal is complex, with a plurality of harmonic components.

The block forming disturbing effect determines the magnitude and character of change of disturbances on the axes caused by ship motions.

The data acquisition block saves maximum, minimum and average values of dynamic disturbances.

In general, dynamic disturbance torque depends on all three types of rotational pitching. However, it could be done simplification for alt-azimuth mount, ignoring changes in the position of axes under the influence of ship motions. Then the dynamic disturbances for azimuthal axis depend on the yaw

axis and disturbances for elevation axis depend on roll and pitching.

For the system, excluding the variable moment of inertia, average and maximum values of dynamic torques do not depend on the considered range of the object coordinates and is equal 15.5 Nm and 24.5 Nm respectively.

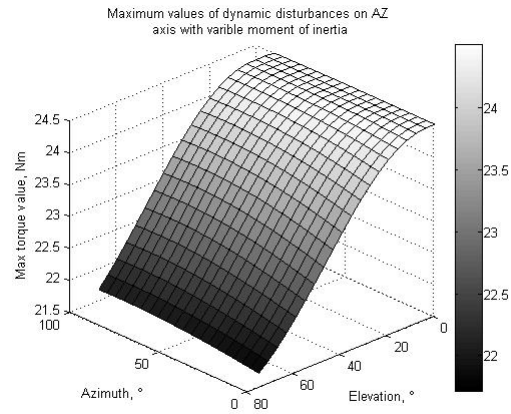


Fig 5. Maximum values of disturbing dynamic torques on azimuthal axis with variable moment of inertia.

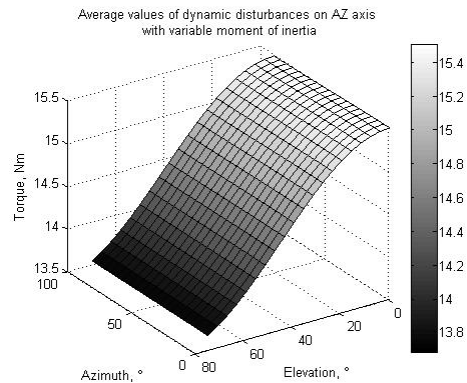


Fig 6. Average values of disturbing dynamic torques on azimuthal axis with variable moment of inertia.

Maximum and average surfaces of the dynamic disturbing torques caused by ship motions with taking into account variable moment of inertia of azimuth axis depending on the position of the elevation axis are shown in Fig. 5 and Fig. 6. Analysis of the graph shows that the maximum and average values are different for various object coordinates. Maximum dynamic torque is 24.5 Nm at EL position 0° and slowly decreases with increasing EL up to 21 Nm. Average torque is in the range of 13.5 - 15.5 Nm.

Surfaces of dynamic disturbances on elevation axis are shown in Fig. 7 and Fig. 8. Analysis of the graphs shows that the maximum disturbing torque is 12.7 Nm at an azimuth of about 45° , dropping at an azimuth of 0° and 90° . Average dynamic moment is about 5 Nm in the whole range of the coordinates of the observed object.

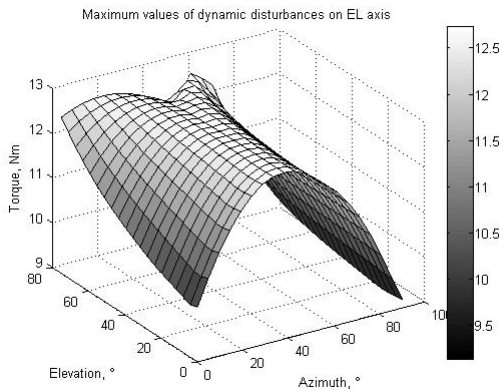


Fig 7. Maximum disturbing dynamic torques on elevation axis with variable moment of inertia.

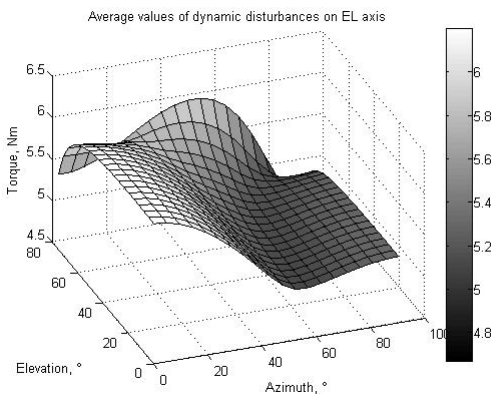


Fig 8. Maximum disturbing dynamic torques on elevation axis with variable moment of inertia.

For the telescope mount with parameters given in Table I, the maximum values of disturbances parameters are 24.5 Nm and 12.7 Nm for the azimuth and elevation axes, respectively. If it is taken into account, that moment of inertia is various, than disturbing dynamic torque reduces by 15% when the elevation is about 90° .

The studied object is designed to work with dry friction torque of 50 Nm and wind load with amplitude of 60 Nm. Moment of imbalance elevation axis of the telescope is limited to 20 Nm. Thus, additional dynamic disturbance corresponds to the magnitude of imbalances, and does not exceed the dry friction torque. When modeling, additional disturbances can be ignored, or they could be limited with their maximum values on top.

IV. FURTHER RESEARCH

In further research it is planned to synthesize a control system of electric drive of axes of the telescope on the deck of a ship, which is able to compensate the effects of ship motions on the reference signal and disturbances. Different mathematical models of control system of the telescope will be discussed: as a constant moment of inertia of the azimuthal axis, as well as variable moment of inertia, depending on the position of the elevation axis.

V. CONCLUSION

In the study of disturbances were given approximate

maximum values of dry friction torque, torque of unbalance and wind torque. Mathematical modeling of dynamic disturbances allows us to estimate the maximum and average values of these perturbations and compare them with other disturbing influences. This comparison allows us to conclude that the additional dynamic disturbances caused by rolling of the ship, may be excluded from taken into account when modeling the control system. Their values are negligible in comparison to dry friction torque and wind torque. The proposed model for calculation of dynamic disturbances, caused by ship motions, may be used for other sea-based telescope mounts installed without gyro-stabilized platform.

ACKNOWLEDGMENT

This work was financially supported by Government of Russian Federation, Grant 074-U01.

REFERENCES

- [1] A.P. Balkovoi, A.V. Kostin, A.S. Myagkikh, O.A. Tolstykh, V.K. Tsatsenkin, S.F. Yakovlev "Design of direct linear drives for manufacturing", *Russian Electrical Engineering*, 2013, Vol 7(84), pp. 363-369.
- [2] C. Ren, Liuzhao, Songlibin, Yiqiang, K. Chen, Z. Zhang "Design and simulation of the direct drive servo system", *Proceedings of SPIE - The International Society for Optical Engineering*, 2010.
- [3] D.A. Subbotin, S.Y. Lovlin, M.H. Tsvetkova "Identifying dynamic model parameters of a servo drive", *Manufacturing Engineering, Automatic Control and Robotics: Proceedings of the 14th International Conference on Robotics, Control and Manufacturing Technology (ROCOM '14) - 2014*, No. 32/1/1, pp. 50-57
- [4] D.A. Subbotin, S.Y. Lovlin, M.H. Tsvetkova "Two-mass mathematical model of magnetoelectric converter for reversible scanning device", *Manufacturing Engineering, Automatic Control and Robotics: Proceedings of the 14th International Conference on Robotics, Control and Manufacturing Technology (ROCOM '14) - 2014*, No. 32/1/1, pp. 11-14
- [5] H.S. Sarhan, R.H. Issa, M.A. Alia, I.K. Al-Abbas "Precision speed control of DC motor drive system", *International Review of Automatic Control*, Volume 5, Issue 5, September 2012, pp. 673-676.
- [6] M.S. Worthington, T.A. Beets, J.H. Beno, J.R. Mock, B.T. Murphy, B.J. Southa, J.M. Good "Design and development of a high precision, high payload telescope dual drive system", *Proceedings of SPIE - The International Society for Optical Engineering*, Vol. 7733, Issue PART 1, 2010.
- [7] M.-Y. Chen, J.-S. Lu "High-precision motion control for a linear permanent magnet iron core synchronous motor drive in position platform", *IEEE Transactions on Industrial Informatics* Volume 10, Issue 1, February 2014, Article number 6461410, pp. 99-108.
- [8] N.A. Smirnov, S.A. Tushev "Two Methods of Fault Detection in the PMSM Electric Drive IGBT-Based Inverter", *Manufacturing Engineering, Automatic Control and Robotics: Proceedings of the 14th International Conference on Robotics, Control and Manufacturing Technology (ROCOM '14) - 2014*, No. 32/1/1, pp. 140-146
- [9] R. Terec, V. Chindris, L. Szabo, Rafajdus. "Position sensing system for switched reluctance motor control", *Proceedings of 9th International Conference, ELEKTRO 2012*, pp. 266-269.
- [10] S. G. Voronin, D. A. Kurnosov, A. S. Kul'mukhametova. "Vector control of permanent-magnet synchronous motors", *Russian Electrical Engineering*, October 2013, Volume 84, Issue 10, pp. 581-585.
- [11] S.A. Tushev, V.N. Drozdov, N.A. Smirnov "The Ship Motions Effect on the Position Reference of Telescope's Axis Installed on the Deck of a Ship", *Manufacturing Engineering, Automatic Control and Robotics: Proceedings of the 14th International Conference on Robotics, Control and Manufacturing Technology (ROCOM '14) - 2014*, No. 32/1/1, pp. 194-199

Voice analysis for detecting persons with Parkinson's disease using MFCC and VQ

A. Benba, A. Jilbab, A. Hammouch

Abstract— In order to improve the assessment of speech disorders in the context of Parkinson's disease, we have collected 34 sustained vowel / a /, from 34 subjects including 17 Parkinsonian patients. We subsequently extracted from 1 to 20 coefficients of the Mel-Frequency Cepstral Coefficients (MFCCs) from each subject. The frames were compressed using vector quantization, with six Codebook sizes. We used a leave-one-subject-out (LOSO) validation scheme and the Support Vector Machines (SVM) classifier with its different types of kernels, (i.e.: RBF, Linear and polynomial). After viewing the obtained results, we proceeded to a bench of 100 trials. The best average result obtained was 82% using the codebook size of 1.

Keywords—Voice analysis, Parkinson's disease, MFCCs, Vector quantization. LOSO, SVM.

I. INTRODUCTION

THE assessment of the quality of speech, and the identification of the causes of its degradation based on phonological and acoustic cues have become major concerns of clinicians and speech pathologists. They have become more and more attentive to techniques or methods external to their domain, which might provide them additional information for the diagnosis and the assessment of neurological diseases. As is known, Parkinson's disease (PD) is one of these neurological disorders. It causes different symptoms during its course and it influences the system which controls the execution of learned motor plans such as walking, talking or completing other simple tasks [1] [2] [3]. PD generally affects people whose age is over 50 years and causes voice deterioration in approximately 90% of patients [4]. For these people, physical visits for diagnosis, monitoring and treatment are not practical [5] [6].

In the case of the assessment of speech disorders in Parkinson's patients, clinicians and the speech pathologists have adopted subjective methods based on acoustic cues to distinguish different disease states. In order to develop more objective assessments, recent studies use measurements of voice quality in time, spectral and cepstral domains [7] to detect voice disorders. These measurements includes fundamental frequency of vocal oscillation (F0), absolute

sound pressure level, jitter (which represents pitch perturbations), shimmer (which represents amplitude perturbations), and harmonicity (which represents the degree of acoustic periodicity) [1] [8] [9].

In this study we focused on the measurements in cepstral domain by applying Mel-Frequency Cepstral Coefficients (MFCCs) which have been traditionally used in speaker identification applications [10]. The automatic assessment of speech disorders in patients with Parkinson's disease using the Mel-frequency cepstral coefficient (MFCC) was first proposed by Fraile et al [11] [12]. During the last few years, the use of the MFCCs has been extended to speech quality assessment for clinical applications [10]. We have extracted MFCCs from the speech signals provided in a database and used vector quantization for feature compression. We then used a LOSO validation scheme with SVM for feature classification in order to discriminate patients with Parkinson's disease from healthy subjects.

This paper is organized as follows: the subject database is described in section II. The MFCC processes and vector quantization are presented successively in section III and IV. The methodology of this research is presented in section V. The results and discussion are presented in Section VI and conclusion in Section VII.

II. DATA ACQUISITION

Dysarthria is the set of speech disorders associated with disturbances of muscular control of the speech organs. Dysarthria includes all malfunctions related to breathing, phonation, articulation, nasalization and prosody. These indications can be measured and detected by analyzing various features of voice. The data collected in the context of this study belong to 17 Parkinsonian patients (6 female, 11 male) and 17 healthy individuals (8 female, 9 male). Voice signals were recorded through a standard microphone at a sampling frequency of 44,100 Hz using a 16-bit sound card in a desktop computer. The microphone was placed at a 15 cm distant from subjects and they were asked to say sustained vowel /a/ at a comfortable level.

All the recordings were made in stereo-channel mode and saved in WAVE format; acoustic analyses were done on these recordings. All the voice samples were collected by Mr. M. Erdem Isenkul of Department of Computer Engineering at Istanbul University, Istanbul, Turkey.

A. Benba, A. Jilbab, A. Hammouch are with the Electrical Engineering Department, Research team in computer and telecommunication, Research Laboratory in Electrical Engineering (LRGE), ENSET Rabat, Mohammed V University, Rabat, Morocco (e-mail: achraf.benba@um5s.net.ma; a_jilbab@yahoo.fr; hammouch_a@yahoo.com).

III. MFCCS PROCESSES

Our first aim was to transform the speech waveform to some type of parametric representation for further analysis and processing [13]. The speech signal is a slow time varying signal which is called quasi-stationary [13]. When it is observed over a short period of time, it appears fairly stable [13]. However, over a long period of time, the speech signal changes its waveform. Therefore, it should be characterized by doing short-time spectral analysis [13].

The computation of the MFCCs is based on a Mel-scale. This scale approximates the frequency perception of the human ear [14]. It was designed in such a way that 1000 Hz corresponds to 1000 Mel. The Mel scale is approached by a bank of (15-30) triangular filters spaced linearly up to 1 kHz and logarithmic above 1 kHz [15]. The process of computing the MFCCs is shown in Figure 1 and described in the next paragraphs.

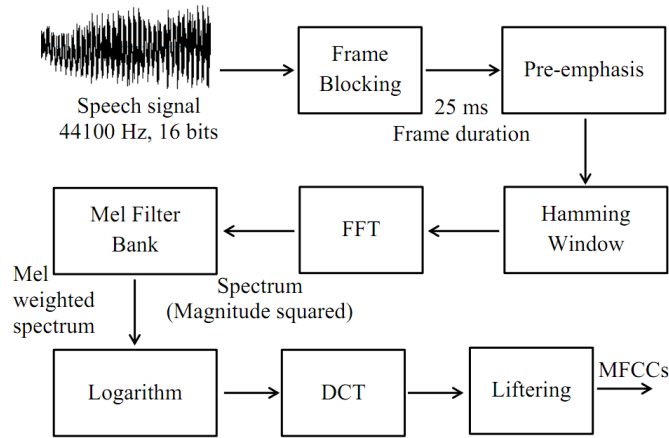


Fig. 1 Block diagram of Mel frequency cepstrum coefficients (MFCCs) extraction

A. Framing

The analysis of the speech signal over a long time periods shows that the speech waveform is not stationary [13]. Therefore, it is necessary to proceed with the technique of short time analysis. Generally, within the interval of 10 to 30 ms, the speech signal can be considered stable [13]. The rate of movement of the speech articulators is limited by physiological constraints [13]. For this reason, the analysis of speech signal is done within uniformly spaced time intervals or frames of typical duration (from 10 to 30 ms) [13]. In frame blocking, the speech signal is divided into frames of N samples. Adjacent frames should be separated by M ($M < N$) [13] [15].

B. Pre-emphasis

In this step, we increase the energy in the speech signal, by emphasizing the higher frequencies [15]. For that we apply the first order difference equation to the samples $\{s_n, n = 1, \dots, N\}$ [14]:

$$s'_n = s_n - k \cdot s_{n-1} \quad (1)$$

Where k is the pre-emphasis coefficient. It should be within the range of $0 \leq k < 1$ [14]. In this study we used a pre-emphasis coefficient of $k = 0,97$.

C. Hamming windowing

Since the speech signal is a real signal, it is finite in time; thus, a processing is only possible on finite number of samples [14]. To this end, the next step of MFCC process is to window each frame. The aim of this step is to reduce signal discontinuities, and make the ends smooth enough to connect with the beginnings [14]. This was done by using a window to taper the signal to zero in the beginning and in the end of each frame, by applying the following formula to the samples $\{s_n, n = 1, \dots, N\}$ [14]:

$$s'_n = \left\{ 0,54 - 0,46 \cdot \cos\left(\frac{2\pi(n-1)}{N-1}\right) \right\} \cdot s_n \quad (1)$$

D. Fast Fourier Transform (FFT)

The next processing step is to convert each frame of N samples from time domain into frequency domain by applying the Fast Fourier Transform (FFT) [13]. We used the FFT because it is a fast algorithm the implement the Discrete Fourier Transform (DFT) [13]. As known, the DFT is defined on the set of N samples (S_n) as follow [13]:

$$S_n = \sum_{k=0}^{N-1} s_k e^{-2\pi jkn/N}, \quad n = 0, 1, 2, \dots, N-1 \quad (1)$$

E. Filter bank analysis

Psychophysical studies have shown that human ear resolution of frequencies does not follow a linear scale across the audio spectrum [14]. Thus, for each frequency measured in Hz, a subjective pitch is measured on the Mel scale. Figure 2 represents the general form of the filter bank. As can be seen, the Mel-frequency scale is linearly spaced below 1000 Hz and logarithmic above 1000 Hz and the filters have a triangular shape [15].

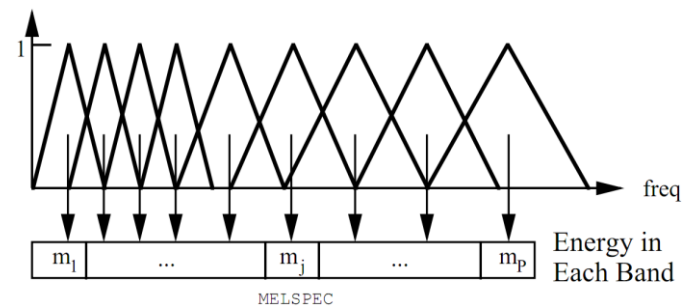


Fig. 2 Mel-Scale Filter Bank [14]

To calculate a Mel for a given frequency, we use the following approximate formula [14]:

$$Mel(f) = 2595 \cdot \log_{10} \left(1 + \frac{f}{700} \right) \quad (1)$$

F. Logarithm / DCT

In this step, the Mel-Frequency Cepstral Coefficients (MFCCs) are computed from the log filter bank amplitudes (m_j) through the Discrete Cosine Transform (DCT) [14]:

$$c_i = \sqrt{\frac{2}{N}} \sum_{j=1}^N m_j \cdot \cos \left(\frac{\pi i}{N} (j - 0,5) \right) \quad (1)$$

Here, N is the number of filter bank channels.

G. Liftering

The principal advantage of cepstral coefficients is that they are uncorrelated [14]. However, the problem with them is that the higher order cepstra are quite small [14], as shown in Figure 3. Hence, it is important to re-scale the cepstral coefficients to have quite similar magnitudes (Figure 4) [14]. This is done by liftering the cepstra according to the following formula [14]:

$$c'_n = \left(1 + \frac{L}{2} \cdot \sin \left(\frac{\pi \cdot n}{L} \right) \right) \cdot c_n \quad (1)$$

Where L is the Cepstral sine lifter parameter. In this work, we used $L=22$.

IV. VECTOR QUANTIZATION

Vector quantization (VQ) is a lossy data compression [10]. The main idea of this method is to take a large number of feature vectors and reduce it to a smaller group of feature vectors, which represent the centers of gravity of the distribution.

The VQ technique consists of extracting a small number of the most representative features to characterize different subjects.

Here VQ is used to reduce the number of frames of the MFCC in order to have only the most significant vectors which represent the center of gravity of the distribution of other MFCC frames. During this study, we have made tests using codebook sizes of 1, 2, 4, 8, 16 and 32 [15]. Figure 5 represents the first 13 MFCCs extracted from one PD subject, with data compression using a codebook size of 8, which gives us the 8 most significant frames representing the center of gravity of the distribution of other MFCC frames.

V. METHODOLOGY

The first step in this study was to build a database containing voice recordings of normal subjects and Parkinsonian patients. Ultimately, we were able to collect 17 voices from both groups. This gave us 34 records. These recordings were made via a standard microphone at a sampling rate of 44100 Hz. All participants were invited to pronounce the vowel / a / at a comfortable level.

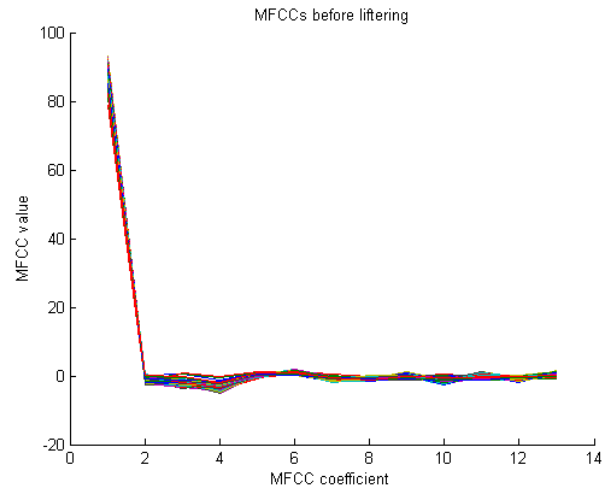


Fig. 3 MFCCs of PD subject before liftering

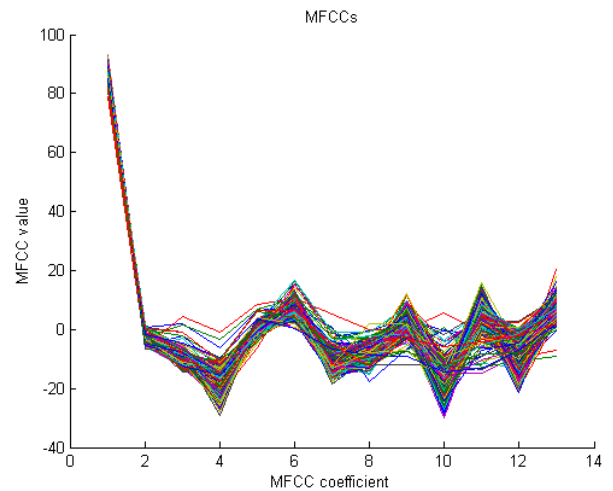


Fig. 4 MFCCs of PD subject after liftering

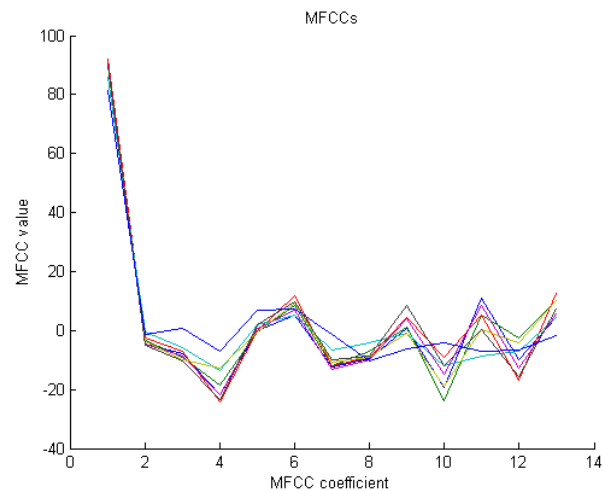


Fig. 5 MFCCs of PD subject using a codebook size of 8

All the algorithms were executed on a desktop computer with a Core (TM) 2 Quad CPU and a processing speed of 2.33 GHZ.

We then extracted from each voice sample, cepstral coefficients of the MFCCs. The number of coefficients extracted ranged from 1 to 20. We proceeded in this way to get the optimal number of coefficients needed for the best diagnostic accuracy.

The MFCC extracted from each sample contains a large number of frames which require extensive processing time for classification and prevents making the correct diagnostic decision. To overcome this problem, we used a method of lossy data compression known as vector quantization (VQ). The detailed description of this method has been made in section IV. As we know, VQ compresses the data according to the number of Codebooks. In this study we have used six codebooks of size 1, 2, 4, 8, 16 and 32. We applied this method over 20 MFCCs that have already been extracted from each voice sample, and which contains from 1 to 20 coefficients per subject. This makes a total of 120 (6 * 20) extraction operations per subject.

To train and validate our classifier, we used a method of classification called leave-one-subject-out (LOSO), that is, we left out all the compressed frames of the MFCCs of one individual to be used for validation as if it were an unseen individual, and trained a classifier on the rest of the compressed frames of other subjects [6]. We used the LOSO method of classification iteratively for each coefficient per subject until all 20 coefficients per subject for the six different codebooks size. In this study, we used the SVM classifier with its different types of kernels, i.e.; RBF, Linear and polynomial.

During the test phase, we noticed that the obtained results when using a Codebook size of 1 are not stable. Unlike the other Codebook sizes, namely 2, 4, 8, 16 and 32, the compression of the MFCC frames using a codebook size of 1, did not always give the same location of the centroids of the clusters forming the compressed MFCC. Therefore, every time we redid the test, we will not get the same classification results. To assess how the results change, we used a test-bed (100 times). This test-bed allows us to obtain the minimum, maximum and average value of the diagnostic results for Parkinson's disease.

We made a test-bed of 100 times, for the codebook size of 1, 2, and 4. As already mentioned, the results obtained using a codebook of size higher than 1 are stable, nonetheless we did the test on the other codebook sizes to get an idea of the variation in execution time and to be sure that the results remained the same. The thing which kept us from applying the test-bed on the codebook size of 8, 16 and 32 is the duration of a single test execution. As can be seen in Table II for a single test using a codebook size of 8, we need 2186.56 seconds. To do a test-bed 100 times, we need about 60 hours. Using the codebook size of 16 and 32 would take much more time. For a single test using a codebook size of 16 we need 5.31 hours and with a codebook size of 32 we need 22 hours. It is not practical to apply a test-bed if we already know that the results will remain the same even after 100 trials.

VI. DISCUSSION

Based on previous results, it is clear that when we use a larger codebook size, the accuracy of diagnosis decreases (Table I), and the time required for processing becomes longer (Table II).

The extracted MFCC from each subject contains in addition to the number of coefficients used, many frames with different values. The use of a large number of frames leads us to a variety of results, often very close to the extracted values from other subjects (PD and Normal). This similarity of results between different subjects prevents making the correct diagnostic decisions.

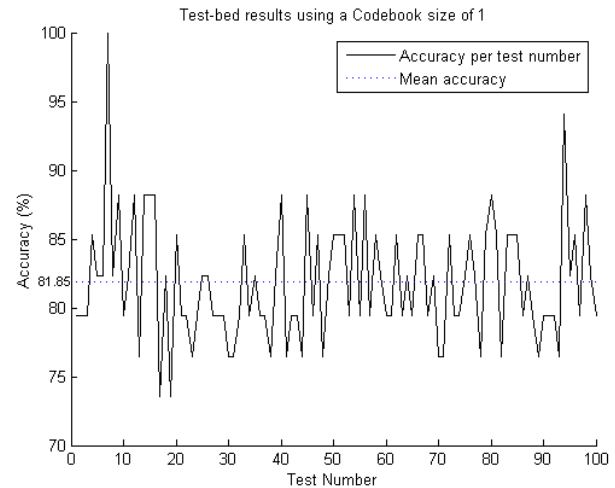


Fig. 6 The test-bed results using the codebook size of 1

TABLE I
CLASSIFICATION RESULTS FOR DIFFERENT CODEBOOK SIZES

Codebook sizes	Max Accuracy (%)	Min Accuracy (%)	Mean Accuracy (%)
1	100	73.5294	81.8529
2	70.5882	70.5882	70.5882
4	71.3235	71.3235	71.3235
8	69.8529	69.8529	69.8529
16	70.2206	70.2206	70.2206
32	67.6471	67.6471	67.6471

TABLE II
EXECUTION TIME OF THE CLASSIFICATION PROGRAM FOR DIFFERENT SIZES OF THE CODEBOOK

Codebook sizes	Max Time (second)	Min Time (second)	Mean Time (second)
1	172.9370	148.5731	154.4807
2	184.6522	168.3178	169.3411
4	347.8085	316.7237	324.9651
8	2186.565767	2186.565767	2186.565767
16	1.9118e+04	1.9118e+04	1.9118e+04
32	7.9210e+04	7.9210e+04	7.9210e+04

In other words, assuming that the frames are in the form of points distributed in space, increasing the number of frames causes an interference between these points. Therefore, the task of the classifier, to find a hyper plane able to separate perfectly the two classes (Normal and PD), will be very difficult, if not impossible.

The test-bed results using the codebook size of 1 are represented in Figure 6. A maximum classification accuracy of 100% was achieved using the first 13 coefficients of the MFCC as shown in Table I and Table III, by linear kernel SVMs. From the Table I, it is clearly observable that, even the minimum accuracy achieved using the codebook size of 1, remains better than the results obtained using other codebook sizes. As seen from the same table a mean classification accuracy of 82% was achieved using a codebook size of 1.

TABLE III
THE COEFFICIENTS OF THE MAXIMUM AND THE MINIMUM ACCURACY & SVM
KERNELS OF THE MAXIMUM ACCURACY

Codebook sizes	Max accuracy coefficient	Min accuracy coefficient	Kernels
1	13	3 2 4 5 7 10	Linear
2	8 9 10	8 9 10	Linear
4	5	5	Linear
8	8	8	Linear
16	8	8	Linear
32	15	15	Linear

VII. CONCLUSION

Dysarthria symptoms associated with Parkinson's disease do not appear abruptly. It is a slow process whose early stages may go unnoticed. To enhance the assessment of Parkinson's disease we collected a variety of voice samples from different subjects during the pronunciation of sustained vowel /a/. The extracted MFCCs from different participants contain many frames which take maximum processing time in the classification process, and prevent making accurate diagnosis. For this reason we have compressed the extracted MFCCs using vector quantization with different codebook sizes. After doing the tests we observed that the obtained results using a codebook size of 1 were not stable. To evaluate on how the results change, we proceeded to a bench of 100 trials. The compression of the MFCC using Vector Quantization with the codebook size of 1 has shown to be a good parameter for the detection of voice disorder in Parkinson's disease, showing a mean classification accuracy of 82%.

ACKNOWLEDGMENT

The authors would like to thank Mr. Erdem Isenkul of Department of Computer Engineering at Istanbul University, Mr Thomas R. Przybeck and Mr. Daniel Wood from United States Peace Corps Volunteers (Morocco 2013-2015), and all of the participants involved in the data collection process.

REFERENCES

- [1] M. A. Little, P. E. McSharry, E. J. Hunter, L. O. Raming, "Suitability of dysphonia measurements for telemonitoring of Parkinson's disease." *IEEE Trans. Biomed. Eng.* 2009.
- [2] L. Ishihara, C. Brayne, "A systematic review of depression and mental illness preceding Parkinson's disease," *Acta Neurol. Scand.* Apr 2006. 113(4):211-20.
- [3] J. Jankovic, "Parkinson's disease: clinical feature and diagnosis," *J. Neuro. Neurosurg. Psychiatry.* 79:368-376, 2008. doi:10.1136/jnnp.2007.131045.
- [4] S. B. O'Sullivan, T. J. Schmitz, "Parkinson disease," *Physical Rehabilitation, 5th ed.* Philadelphia, PA, USA: F. A. Davis Company, 2007, pp. 856-894.2007, pp. 856-894.
- [5] D. M. Huse, K. Schulman, L. Orsini, J. Castelli-Haley, S. Kennedy, G. Lenhart, "Burden of illness in Parkinson's disease," *Mov. Disord.* 20:1449-1454, 2005. doi:10.1002/mds.20609.
- [6] B. E. Sakar, M. E. Isenkul, C. O. Sakar, A. Sertbas, F. Gurgun, S. Delil, H. Apaydin, O. Kursum, "Collection and analysis of a Parkinson speech dataset with multiple types of sound recordings," *IEEE Journal of Biomedical and Health Informatics*, Vol. 17, no. 4, July 2013.
- [7] U. k. Rani, M.S. Holi, "Automatic Detection of Neurological Disordered Voices Using Mel Cepstral Coefficients and Neural Networks," *2013 IEEE Point-of-Care Healthcare Technologies (PHT)*, Bangalore, India, 16 - 18 January, 2013.
- [8] M. A. Little, P. E. McSharry, S. J. Roberts, D. A. Costello, I. M. Moroz, "Exploiting nonlinear recurrence and fractal scaling properties for voice disorder detection." *Biomed. Eng. Online*, 2007.
- [9] D. A. Rahn, M. Chou, J. J. Jiang, Y. Zhang, "Phonatory impairment in Parkinson's disease: Evidence from nonlinear dynamic analysis and perturbation analysis." *J. Voice.* 21:64-71, 2007.
- [10] T. Kapoor, R. K. Sharma, "Parkinson's disease diagnosis using Mel-frequency cepstral coefficients and vector quantization," *International Journal of Computer Application*, Vol. 14, no. 3, Jan. 2011.
- [11] R. Frail, JI. Godino-Llorente, N. Saenz-Lechon, V. Oasma-Ruiz, C. Fredouille, "MFCC-based remote pathology detection on speech transmitted through the telephone channel," *Proc Biosignals*, Porto, 2009.
- [12] A. Jafari, "Classification of Parkinson's disease patients using nonlinear phonetic features and Mel-frequency cepstral analysis," *Biomed. Eng. Appl. Basis Commun*, Vol. 52, no. 4, 2013. Available: <http://www.worldscientific.com>
- [13] Ch. S. Kumar, P. R. Mallikarjuna, "Design of an automatic speaker recognition system using MFCC, Vector Quantization and LBG algorithm," *International Journal on Computer Science and Engineering*, Vol. 3, no. 8, 2011.
- [14] S. Young, G. Evermann, T. Hain, D. Kershaw, X. Liu, G. Moore, J. Odell, D. Ollason, D. Povey, V. Valtchev, P. Woodland, "The HTK Book (for HTK Version 3.4)," Copyright. 2001-2006, Cambridge University Engineering Department.
- [15] J. Martinez, H. Perez, E. Escamilla, M. M. Suzuki, "Speaker recognition using mel frequency cepstral coefficients (MFCC) and Vector Quantization (VQ) techniques," *IEEE Electrical Communications and Computers*, Cholula, Puebla, Feb 2012, pp. 248-251.

Hand gesture recognition using 1\$ and background subtraction algorithms

Hazem Khaled¹, E. M. Saad^{1,2,3}, S. Sayed¹, Hossam Ali¹

¹Department of Electronics, Communications and Computers Engineering, Helwan University, Cairo, Egypt

²Department of Electronic and Electrical Engineering, University College London, UK

³Egyptian Computer Emergency Response Team (EG-CERT), National Telecom Regulatory Authority (NTRA), Cairo, Egypt

eng.hazemkhaled@gmail.com

elsayedmos@hotmail.com

sgaber@egcert.eg

hosam_ib_ali@yahoo.com

Abstract—The traditional 2D HCI inputs like keyboard, mice or joysticks are not enough to convey the latest technology. Instead of that there are many devices that can sense body positions, hand gestures, voice recognizer, facial expressions recognizer and many other aspects of human actions that can be used as inputs and that make the interaction between user and computer more powerful and natural. This paper proposes a system for Human Computer Interaction using real-time video streaming that depend on hand gesture detection by removing the background using average background algorithm and a 1\$ algorithm for hand's template matching then translate every hand gesture to commands that control robot movements.

INTRODUCTION

In the present day hand gesture based human computer interface is one of the most important methodologies to allow computers to visually recognize hand gestures in real time. Gestures are the physical movements of fingers, hands, arms or body that carry special meaning that can be translated to interaction with the environment . The traditional 2D HCI inputs like keyboard, mice or joysticks are not enough to convey the latest technology. Instead of that there are many devices that can sense body positions, hand gestures, voice recognizers, facial expressions recognizer and many other aspects of human actions that can be used as inputs and that make the interaction between user and computer more powerful and natural. Gesture recognition has many applications as:

- 1) Communication tool between hearing impaired.
- 2) Controlling virtual reality applications.
- 3) Lie detection.
- 4) Medical Applications.

There are many ways to handle gesture recognitions [1] including mathematical models based on hidden Markov chains [2] or approaches based on soft computing [3]. Hand gesture recognition techniques can be divided into two main categories: appearance based approaches and 3D hand model based approaches [4]. Appearance based approaches depend on features that have been extracted from the model image to model the hand appearance then compare all input frames from video streaming with the extracted features to detect correct

gesture. Three dimensional model depends on 3d hand model that can project many 2D hand gestures models which can be compared with all input images to detect the current 2D hand gesture. Generally appearance based approaches performance is better than 3D hand models performance in real time detection but three-dimensional hand model-based approaches offer a rich description that potentially allows a wide class of hand gestures [4].

Both hand shape and skin color are very important features that commonly used in hand gestures recognition [6-8]. Color based models facing problem of extracting region of interest from the entire frame and it fail if many objects have color similar to the hand and it is very sensitive to the lighting variations. Shape based model as 1\$ algorithm can be used to detect hand gestures [9]. Most of the shape descriptors are pixel based and the computational complexity is too high for real-time performance. But the 1\$ algorithm is very straight forward with low computational complexity algorithm that can be used in real time detection. The training time is too low compared with Viola-Jones method [5] and the detection rate is very high with accuracy 98 %.

This paper proposes a system for hand gesture detection by removing the background using average background algorithm [11] and a 1\$ algorithm [9] for hand's template matching then translate every hand gesture to commands that control robot movements.

SYSTEM OVERVIEW

Fig. 1 shows the block diagram of the proposed system that can be divided into two main stages:

- 1) Create model for background to remove all static objects that reside in the background then get the region of interest that contains hand gesture.
- 2) Compare the current hand gesture with the trained data using 1\$ algorithm and translate the detected gesture to a command that will control robot movements in the virtual world at the Webots simulator.

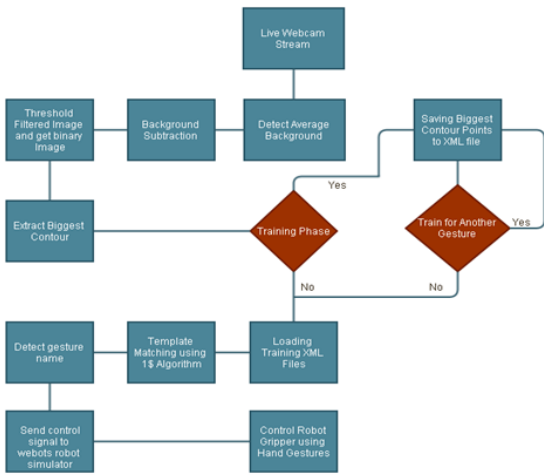


Figure 1. Proposed system block diagram

The first contribution in the paper is the conversion of I1\$ algorithm from hand writing detection algorithm to hand gesture detection algorithm. This leads to results and detection rate up to 98 %.The Second contribution is the utilization of background removing algorithm with the I1\$ algorithm to get the maximum throughput.

BACKGROUND SUBTRACTION ALGORITHM

The technique used to remove background [11] by isolating movable objects from the whole image and consider the static objects as a part from the background. This technique can be implemented by creating a model for the background and update it continuously to take in account the changes of light or the new added static objects. This model is considered as reference that will be subtracted from the current frame to detect the movable objects. There are many algorithms [14 - 16] that can be used to subtract background but any algorithm must contain the following features:

- 1) Support multilevel illumination.
- 2) Detect all moving object at different speeds.
- 3) Consider any resident object as part of background as soon as possible.

Steps of background subtraction algorithms follow the simple stages that are defined as shown in Fig. 2.

In the preprocessing stage the spatial smoothing [17] is used to reduce the noise that can be generated from the web camera or from the changes of whether conditions in outdoors camera. Modeling background stage is the main stage of the background subtraction. In [10] the background modeling algorithms are classified into two main types:

- 1) Recursive.
- 2) Non recursive.

Recursive models use buffer for storing all previous frames and estimate the background from the temporal variation of each pixel in the buffer. Non recursive algorithms don't depend on the previous frames such as frame differencing, median

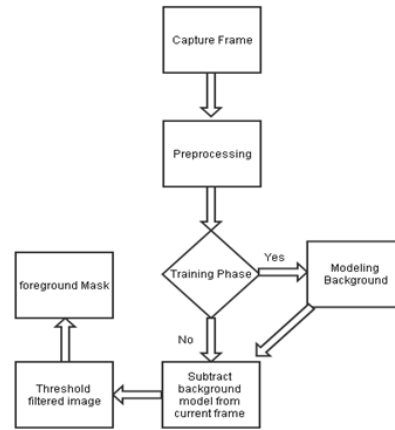


Figure 2. Background subtraction algorithm flowchart



Figure 3. Background subtraction algorithm outputs

filter and linear predictive filter. Non recursive models require storage less than recursive model but a temporal error occurs in the background model and takes longer time than recursive models.

To model the background the average filter is used [11]. Average filter will create an initial background from the first N frame as shown in (1), as an experiment N = 20 is taken. The moving areas are obtained by subtracting the current frame from the average background as shown in (2).

To get better result a threshold filter is applied on the difference image to create a binary image as shown in (3). Threshold = 50 because the background color model is brighter than human skin. The average background's pixels are updated using the equation (4) to remove any noise or any static objects, where alpha is used to control the speed of updating process in other words controls how quickly the average background is updated by the current frame. Alpha values varies from 0 to 1.The value 0.001 is used to decrease learning speed. The steps of hand extraction are shown in Fig. 3.

$$Avg(x,y) = \frac{1}{N} \sum_{i=1}^N Frame(i)(x,y) \tag{1}$$

$$\Delta Avg(x,y) = | Frame(x,y) - Avg(x,y) | \tag{2}$$

$$Bin(x,y) = \begin{cases} 1 & \Delta Avg(x,y) > Threshold \\ 0 & Otherwise \end{cases} \tag{3}$$

$$Avg(x,y) = \alpha \cdot Frame(x,y) + (1 - \alpha) \cdot Avg(x,y) \tag{4}$$



Figure 4. Extraction of biggest contour

CONTOUR EXTRACTION ALGORITHM

The contour is a curve that connects all points surrounding specific part of an image that has the same color or intensity. To identify hand gestures we detect the contours of all objects that exist in the threshold image as shown in Fig. 4 and select the biggest contour that has the biggest calculated area that represent the hand's area . To find the contour Suzuki's algorithm [12] is used .we approximate the filtered contour points to another contour that has fewer numbers of points. The contour approximation is the process of finding key vertex points [13] to speed up calculations and it consumes low memory size.

TEMPLATE MATCHING ALGORITHM

This algorithm is mainly used in hand writing recognition [5] by comparing the stored template with the user input, the hand's contour can be treated using this algorithm because it supports many features as:

- 1) Scaling independent.
- 2) Rotation Independent.
- 3) Doesn't require complex mathematical equations
- 4) High detection rate.
- 5) Allow user to train any number of gestures.
- 6) Low resources consumption.

In this paper this algorithm [5] is used to compare the saved contour templates and the biggest extracted contour from the current frame to get the best matching template and detect the user gesture. The algorithm is based on four main stages:

- 1) Rebuilding the point path : This feature makes the comparison operation independent of the number of points that have been saved in template contour at the training phase. Before comparison operation the algorithm rebuilds any stored contour template with M points to another contour that is defined with N equal spaced points. When the value of N is too low that makes high loss of precision, while using N too high that take too long time for comparison so the best value of N should be $32 \leq N \leq 256$. N = 80 is used .Fig. 5 shows different set of hands with different point paths.
- 2) Rotation Based on indicative angle :In this stage the indicative angle the angle between the center point of the gesture and the first point of the gesture is calculated , rotating the gesture until angle = 0 degree. Fig. 6 shows the hands with different angles.
- 3) Scale and Translate :At this step the algorithm scales all gestures to standard square .The scaling is non-uniformly and is applied on all candidates C and all

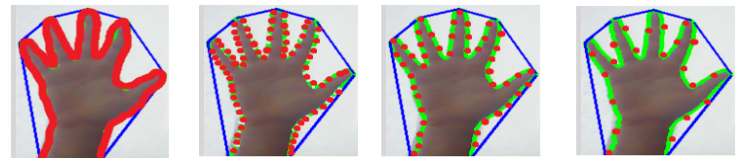


Figure 5. Hand with different point paths

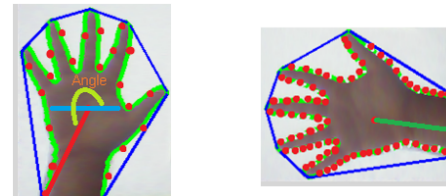


Figure 6. Hand template rotation

templates T. After scaling operation each gesture will be translated due to reference point , to simplify all operations , all points are translated to origin point $(x,y) = (0,0)$.

- 4) Find optimal angle for best matching :At these stages all templates and all candidates have been rebuilt, rotated, scaled and translated. The candidate C will be compared to each template Ti using the following equation (5) to find distance d between corresponding points (Euclidean Distance).The template with least distance is chosen.

$$D_i = \frac{\sum_{k=1}^N \sqrt{(C_x[k] - T_x[k])^2 + (C_y[k] - T_y[k])^2}}{N} \quad (5)$$

EXPERIMENTAL RESULTS

The detection speed of the 1\$ algorithm reaches (0.04) min per gesture and the error rate increases if the background has objects with many edges or darker than skin color as shown in Fig. 8. In the experiments five gestures are used to control robot movements as shown in Fig 7. The proposed system is implemented in C# and tested with Webots simulator virtual environment with boeobot robot as shown in Fig 10 on AMD Quad-Core processor (FX 4-Core Processor Black Edition, 3.8 GHz).

Gesture name	Detection speed (ms)	Testing data	Throughput
Forward	420	100	100
Backward	540	100	100
Stop	430	100	100
Right	435	100	100
Left	450	100	93

Table I
TESTING RESULTS

Gesture name	Proposed Algorithm	Reference Algorithm
Forward	100	100
Backward	100	80
Stop	100	50
Right	100	60
Left	93	90

Table II
TESTING RESULTS

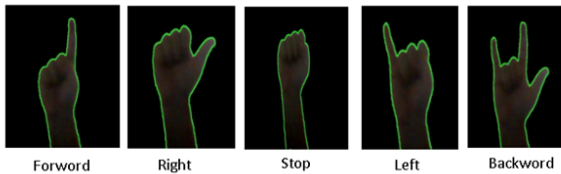


Figure 7. Gesture commands

The testing video stream was grabbed from a Web camera with a resolution of 320×240. The detection algorithm is connected to Webots robot simulator using socket programming and control the movements of the robot in the virtual environment as shown in Fig. 9. Table 1 shows the accuracy of hand gesture detection. The following link shows the algorithm implementation <http://goo.gl/4nVPw8>. Table 2 shows the comparison between the proposed algorithm and the algorithm used in [18].

CONCLUSION

In this paper an efficient hand gesture recognition algorithm is presented. This algorithm uses the background subtraction algorithm and the 1\$ algorithm as a gesture recognizer. That should provide an effective mechanism for recognizing hand gestures with different scaling and rotation. Such a hand gesture recognition system provides a robust solution in two real-life HCI applications, which can also be applied to many other hand gesture based HCIs.

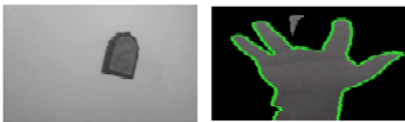


Figure 8. False positive detection



Figure 9. Webots virtual environment

REFERENCES

- [1] V. I. Pavlovic, R. Sharma, and T. S. Huang, "Visual interpretation of hand gestures for human computer interaction," *IEEE Trans. Pattern Anal. Mach. Intell.*, vol. 19, no. 7, Jul. 1997, pp.677–695.
- [2] L. R. Rabiner, "A tutorial on hidden Markov models and selected applications in speech recognition," *Proc. IEEE*, vol. 77, no. 2, Feb. 1989, pp. 257–285.
- [3] S. Mitra and T. Acharya, "Data Mining: Multimedia, Soft Computing, and Bioinformatics". New York: Wiley, 2003.
- [4] H. Zhou and T. S. Huang, "Tracking articulated hand motion with Eigen dynamics analysis," in *Proc. Int. Conf. Comput. Vis.*, 2003, vol. 2, pp.1102–1109.
- [5] Qing Chen, Nicolas D. Georganas, "Hand Gesture Recognition Using Haar-Like Features and a Stochastic Context-Free Grammar", *IEEE TRANSACTIONS ON INSTRUMENTATION AND MEASUREMENT*, VOL. 57, NO. 8, AUGUST 2008.
- [6] L. Bretzner, I. Laptev, and T. Lindeberg, "Hand gesture recognition using multiscale color features, hierarchical models and particle filtering," in *Proc. 5th IEEE Int. Conf. Autom. Face Gesture Recog.*, 2002, pp.405–410.
- [7] C.W. Ng and S. Ranganath, "Gesture recognition via pose classification," in *Proc. 15th ICPR*, 2000, vol. 3, pp. 699–704.
- [8] Nasser H, Dardas and Nicolas D. Georganas, "Real-time hand gesture detection and recognition using Bag-of-Features and Support Vector machine techniques," in *Proc. IEEE Trans. on Ins. and Mes.*, 2011, Vol. 60, No. 11, pp. 3592-3607.
- [9] Wobbrock, J.O., Wilson, A.D. and Li, Y. (2007). " Gestures without libraries, toolkits or training: A \$1 recognizer for user interface prototypes. Proceedings of the ACM Symposium on User Interface Software and Technology (UIST '07). Newport, Rhode Island (October 7-10, 2007). New York: ACM Press, pp. 159-168.
- [10] Elhajian, S., K. El-Sayed and S. Ahmed. 2008. "Moving object detection in spatial domain using background removal techniques ". *Recent Pat on Computer Sci.*, 2008, 1(1): 32-54.
- [11] Han-Sung Park, Kang-Hyun, "Real-Time Hand Gesture Recognition for Augmented Screen using Average Background and CAMshift", *The 19th Korea -Japan Joint Workshop on Frontiers of Computer Vision*, 30 Jan 2013 - 1 Feb 2013 , pp.18-21.
- [12] Satoshi Suzuki, Keiichi Abe, "Topological structural analysis of digitized binary images by border following", *Computer Vision, Graphics, and Image Processing*, Volume 30, Issue 1, April 1985, Pages 32-46.
- [13] David Douglas & Thomas Peucker, "Algorithms for the reduction of the number of points required to represent a digitized line or its caricature", *The Canadian Cartographer* 10(2) (1973), pp.12–122.
- [14] Y. Benezeth, B. Emile, and C. Rosenberger. "Comparative study on foreground detection algorithms for human detection". *International Conference on Image and Graphics*, 2007, pp.661–666.
- [15] T.H. Chalidabhongse, K. Kim, D. Harwood, and L. Davis. "A perturbation method for evaluating background subtraction algorithms". *International Workshop on Visual Surveillance and Performance Evaluation of Tracking and Surveillance*, 2003.
- [16] S.C.S. Cheung and C. Kamath. "Robust background subtraction with foreground validation for urban traffic video". *EURASIP Journal on Applied Signal Processing*, 14, , 2005, pp.2330–2340.
- [17] James C. Church, Yixin Chen, and Stephen. "A Spatial Median Filter for Noise Removal in Digital Images", *IEEE*, 2008, pp.618- 623.
- [18] Hazem Khaled Mohamed, S. Sayed, El Sayed Mostafa, Hossam Ali, "Hand gesture recognition using average background and logical heuristic equations", *international journal of computers and technology (IJCT)*, Vol 11 - No 5, 2013, pp.2634-2640

In-circuit Emulation of Memory Fault Injection

Olga V. Mamoutova, Oleg V. Nenashev, and Alexey S. Filippov

Abstract—This paper addresses a problem of fault injection for embedded memory blocks in Systems-on-Chip. A novel approach of automated instrumentation for FPGA-based emulation is presented. The approach uses processor-driven saboteurs as fault-injection agents, and utilizes multilevel model of instrumented design, combining information from high level hierarchical description and low-level synthesized netlist. Presented proof of concept shows low hardware and engineering effort overheads of the approach.

Keywords—Automated instrumentation, embedded memory, fault injection, hardware reengineering, SEU.

I. INTRODUCTION

POSSIBILITY of single and multiple event upsets (SEU) is one of the main threats against availability of modern circuits [1]. SEU effect appears as a flip of value (1 to 0 or 0 to 1) in one or several adjacent memory bits, being completely recovered by next write operation. Fault injection techniques as a part of reliability design address the SEU problem and consist in intentional introduction of faults into the system and observing the following reaction [2]. Fault injection can be used for location of reliability bottlenecks, classification of occurring faults, validation of error-mitigation techniques, and evaluation of error rates.

Emulated (or emulation-based) fault injection uses FPGA as a device model, allowing execution of system test workload in real time. This becomes particularly important for errors in memory, because such errors can stay unnoticed for a while and therefore require long-run experiments.

In our work we focus on *instrumentation* approach to emulated fault injection, which is a modification of device under test (DUT) in order to embed fault injection components, and specifically *saboteurs* (an additional component to be inserted into the split of connection between original components). With this approach FPGAs can be programmed with an instrumented version and then exercised under control of a host computer. On RTL-ready stage of design there are two alternatives to emulated fault injection: partial runtime reconfiguration (PRTR) of a programmable

chip, which is limited to selected range of FPGA devices, and simulation, which can not be used for long runs. Out of all options instrumentation is the most versatile.

Instrumentation of DUT is a creative custom-tailored process [3], and as a result many different methods have been suggested over the time. Although a lot of existing methods provide error injection into flip-flops, only few provide support of error injection into memory blocks [4]. The problem of memory fault injection is that usually original design does not provide access to a single cell of embedded memory arrays, apart from the regular device operation. Hence a significant amount of additional hardware should be added to the system under test.

This paper presents a new convenient instrumentation flow, which offers low hardware and design time overhead for memory instrumentation. This flow produces an instrumented version of SoC with embedded memory blocks, which can be used for upset-like fault injection experiments. On the hardware side the approach utilizes a concept of processor-driven saboteurs [5]. On the instrumentation side the main idea is to use hierarchical netlist-based model of device in order to perform the device analysis and transformation. Reasons behind selection of the model are that modification of original code in hardware description language (HDL) can be time-consuming, difficult to automate, and original behavioral descriptions may not contain memory components, which will be synthesized in final device. The selected multi-level model eliminates these difficulties. At the same time, opposed to traditional netlist, the model still allows selective instrumentation of only examined device parts, because it provides information about original design hierarchy. This paper also presents a developed extension of existent reengineering tool called PHRT for automated implementation of the presented approach. We illustrate the effectiveness of suggested approach with some quantitative estimates, using OpenRISC1200-based system as an example.

II. HARDWARE SUPPORT OF FAULT INJECTION

The problem of memory fault injection is that original designs usually do not provide an access to a single cell in embedded memory arrays, apart from the regular device operation. Hence the following requirements have been set for saboteurs: ability to target memory blocks of SoC and a minimal hardware overhead, which means no memory duplication and no additional memory port.

Suggested memory block instrumentation is the following: target memory is disconnected from its original interface and a

O. V. Mamoutova is with the Department of Computer Systems & Software Engineering, Saint-Petersburg State Polytechnical University, St. Petersburg 194021 Russia (phone: +7 (812) 297-42-18; fax: +7 (812) 297-42-18; e-mail: mamoutova@kspt.icc.spbstu.ru).

O. V. Nenashev is with the Department of Computer Systems & Software Engineering, Saint-Petersburg State Polytechnical University, St. Petersburg 194021 Russia (e-mail: nenashev@kspt.icc.spbstu.ru).

A. S. Filippov is with the Department of Computer Systems & Software Engineering, Saint-Petersburg State Polytechnical University, St. Petersburg 194021 Russia (e-mail: filippov@eda-lab.ftk.spbstu.ru)

saboteur is placed into the resulting gap. Saboteur muxes a regular memory interface and fault injection interface. Through the fault injection interface a control unit starts a read-modify-write procedure. We chose an embedded processor of DUT itself as a control unit for all saboteurs, thus utilizing a processor-driven embedded testing paradigm [5]. In this way a fault injection experiment can be programmed as any other software for the processor. More details about processor-driven fault injection for memory blocks can be found in [6] and at [7].

Since the fault injection operation into on-chip memory requires only several clock cycles, process of fault injection can be transparent for current workload. Moreover, the processor acts as control logic for fault injection process, and we achieve significant circuit area savings in terms of fault injection environment.

III. HYBRID DEVICE REPRESENTATION MODEL

Manual device instrumentation can be highly time-consuming and error-prone. Not surprisingly, most of existing instrumentation methods perform automated modification of source code in hardware description language (HDL), but such approach has several downsides. The major one is that HDL description does not always comply with final results of memory synthesis due to optimizations. Second is a possible struggle with connection of the fault injection agent to the processor interface through multiple levels of design hierarchy, which significantly increases transformation complexity. Third downside is that presence of various high-level HDLs and design flows leads to high engineering costs in case of development of flexible instrumentation tool.

In order to overcome all these issues we suggest instrumentation on the lower level of design by using a post-synthesis structured netlist-based model of device. It contains information about original hierarchy of design, which allows working only with a certain part of DUT. It also contains all instances of synthesized embedded memory, which otherwise demand extra efforts to identify them in behavioral descriptions from RTL code. Lastly it provides flat space for signal routing while instrumentation.

This hybrid device model is based on low-level hierarchical netlists, and at the same time it supports high-level features from regular HDLs like groups, inheritance, generics, conditional generation, etc. This model has proven its compatibility with most of popular netlist and HDL file formats (EDIF, VHDL, Verilog and SystemVerilog). Model is independent of initial descriptions, hence the resulting implementation of the proposed instrumentation algorithm becomes applicable to any input DUT description. More details about hybrid model can be found in [8].

IV. AUTOMATED DUT INSTRUMENTATION

Automation of our approach is based on Programmable Hardware Reengineering Toolkit (PHRT) [8]. PHRT has been selected, because its internal hybrid device model meets all

forementioned requirements and also provides extendable framework for automation of desired reengineering tasks. The tool is intended to become open-source and free to use in the middle-term perspective.

User-specific reengineering algorithms can be implemented in PHRT in the form of Java plug-ins or Tcl scripts. Plug-ins extend PHRT for user-specific tasks, development flows, software and hardware infrastructure. Typical PHRT applications are reliability design, evaluation-driven optimizations, built-in self-test insertion, etc. Combination of the framework core and custom plug-ins forms a specialized tool for user-specific applications. PHRT can be integrated with existing EDA tools from 3rd-party hardware design vendors.

Current PHRT version provides plug-ins for the following operations:

- import/export of EDIF, VHDL and XML data;
- basic transformations: creation and removal of elements, renaming, properties access, etc.;
- connection of elements on different hierarchy levels;
- analysis: area estimations, timing analysis, etc.;
- integration with Quartus II: project import/export, partial synthesis of generic and behavioral VHDL components.

PHRT does not provide the desired memory fault injection functionality “out of the box”, hence the presented work demanded development of a new PHRT plug-in called `memfault_inject`. All transformations are automated and are driven by a short script in Tcl. Fig. 1 depicts an overview of implemented reengineering flow.

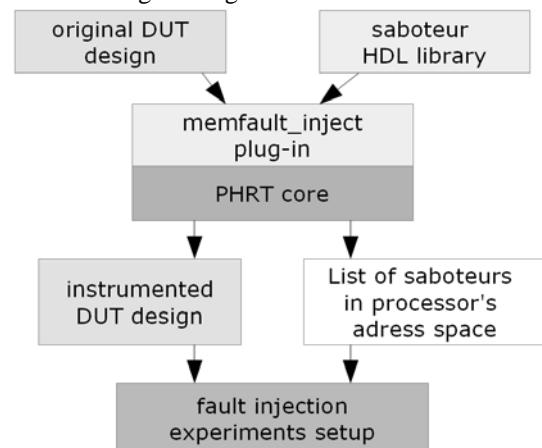


Fig. 1. Overview of DUT reengineering flow for the proposed memory fault injection approach

Process starts from the synthesis of an original design in QuartusII, producing a netlist with low-level structural description. Then, PHRT imports this netlist and creates a hybrid model using both netlist and original HDL description.

Then, `memfault_inject` plug-in performs device modification. This plug-in uses a source VHDL code of fault-injection saboteur and contains functions, which provide insertion of the saboteur into certain memory interface. Since VHDL source code has generic parameters, it cannot be used

in PHRT “as is”. PHRT performs dynamic synthesis of the saboteurs — it invokes Quartus II IDE and then imports the resulting netlist for saboteur with specified values of parameters. Then the algorithm instruments memory blocks and connects saboteurs to the processor. The last step is a saboteur list generation, which contains saboteur addresses in a processor’s address space. These addresses are later used in fault-injection software.

All transformations are driven by a short Tcl script, which searches for memory blocks using basic PHRT functions and then generates list of memory blocks to be instrumented. This list is a required input for further steps. At the end PHRT produces a list of assignments to use in CPU-based memory tests in order to inject errors into the specified memory block.

V. RESULTS

This section provides evaluation results for the prototype, which is based on Altera FPGAs. An open-source soft processor core OpenRISC1200 and several other systems on chips served as reference designs.

A. Efficiency Evaluation

The reference design has been instrumented in the following ways: manual instrumentation of one memory block, automated instrumentation of a single memory block and the whole system. Automated instrumentation has been performed with PHRT as described in previous sections.

Device modifications lead to the slight difference of the maximum clock frequency (Fmax) in cases, when the memory lays on the system clock’s critical path. Unmodified design, which went through PHRT import/export procedure, also differs in Fmax from original design due to different input formats and optimization results. Obtained Fmax evaluations show a 7% speed reduction in the worst case. Being compared to speed of simulated fault injection, this reduced speed is still several orders of magnitude greater. Therefore this reduction does not affect the main advantage of emulated fault injection the execution speed of experiments and long-run workload execution ability.

Hardware utilization metrics show that none of tested designs requires additional embedded memory resources. However, saboteurs require additional memory registers and combinatorial circuits. For example, manual instrumentation of all memory blocs in OpenRISC1200 core utilized 210 FPGA logic cells LCELL, including 37 one-bit registers. The same automated instrumentation utilized 63 LCELLs, including 82 registers. Such a difference in resource utilization can be explained by peculiarities of the developed PHRT-plugin prototype, which places additional latches on address and data buses of a processor. In future works the effectiveness of automated fault injection flows can be improved.

B. Benchmarks

A custom benchmark has been constructed as a simple memory test, which sequentially performs read-modify-check operations to all bits of instrumented memory blocks. Results

proved applicability of proposed memory instrumentation approach and PHRT-based solution to real applications.

In addition to custom benchmarks several standard benchmarks from EEMBC suite have been used in order to validate correctness of performed device transformations [9]. Benchmark runs showed that automated instrumentation of the OpenRISC-based device does not corrupt its functionality.

We don’t consider full verification of the processor’s core at the current stage. Such verification could be performed by external EDA tools during transformation in PHRT.

VI. CONCLUSIONS

Achieved results prove the applicability of the proposed approach for evaluation of memory’s SEU resistance in real designs like Systems on chip. The approach decreases resource overheads during the DUT instrumentation, but at the same time it retains applicable performance metrics compared to other approach. The usage of a hybrid device representation model and a generic hardware reengineering framework also allows achieving the better flexibility of the approach, because it can be integrated with other memory testing and verification techniques.

Further work is currently being carried out in order to perform examination of other existing processor cores with built-in fault-tolerant memory. Such survey would provide comparison of different memory architectures under real workloads and SEU profiles. Another goal is to develop reliability benchmark that collects fault statistics and calculates distribution of SEUs and probabilities of the memory error. It would allow assessing multiple memory architectures and selecting solution with the best performance.

REFERENCES

- [1] M. Nicolaidis, *Soft errors in modern electronic systems*, Springer, 2011.
- [2] J. Arlat, A. Costes, Y. Crouzet, J.-C. Laprie, and D. Powell, “Fault injection and dependability evaluation of fault-tolerant systems,” in *IEEE Trans. Computers*, vol. 42, 1993, pp. 913–923.
- [3] A. Benso, S. DiCarlo, “The art of fault injection,” in *J. of Control Engineering and Applied Informatics*, vol. 13, 2011, pp. 9–18.
- [4] M. Portela-Garcia, M. Garcia-Valderas, C. Lopez-Ongil, and L. Entrena, “A new approach to accelerate SEU sensitivity evaluation in circuits with embedded memories,” in *Proc. SPIE VLSI Circuits and Systems IV*, vol. 7363, 2009.
- [5] M. Psarakis, D. Gizopoulos, E. Sanchez, and M. S. Reorda, “Microprocessor software-based self-testing,” in *Design & Test of Computers*, vol. 27, 2010, pp. 4–19.
- [6] O.V. Mamoutova, “Processor-driven emulated upset-like fault injection for memory validation,” in *Humanities and Science University J.*, №5, 2011, pp. 185–193.
- [7] https://github.com/Mamoutova/memory_fault_injection
- [8] O. Nenashev, “An Extensible Framework for Automated Hardware Reengineering of Complex Systems-on-Chip,” in *Humanities and Science University J.*, №5, 2011, pp. 194–202.
- [9] J.A. Poovey, M. Levy, S. Gal-On, and T. Conte, “A benchmark characterization of the EEMBC benchmark suite,” in *IEEE Micro*, vol. 29, 2009, pp. 18–29.

Distress Situation Detection Based Data Fusion Analysis for HSH

Mohamed Fezari, Leila Abdoune

Computer Science Department Faculty of Engineering,
Badji Mokhtar Annaba University, Algeria
mohamed.fezari@univ-annaba.dz
lilouchetoday@yahoo.fr

Ali Al-Dahoud,

AFculty Of IT , AL-Zaytoonah University Amman
Amman, Jordan
aldahoud@zuj.edu.jo

Abstract— To improve the work presented in [2] and [18] we included in this work a microcontroller system based on ARDUINO-UNO to collect data from different sensors installed in a habitat. Microphones were used for Activity and distress situation detection of habitant by analyzing sounds within the House. It is an improvement of precedent work on HSH (Health Smart Home). It uses the constructed corpus of everyday life sounds, then a system for separation and classification of audio sources in a habitat; and an application of tele-monitoring the data and alerting elderly or disabled person on situation. We included a microcontroller system based on Arduino-Uno and some interesting sensors for security and comfort of habitant, the hardware module transmit the information to the central unit via an Xbee module. Finally we implemented a Graphic used Interface based on simple features for classification of seven type of home sounds. The obtained results are very encouraging.

Keywords- health smart home; DTW classifier, wireless icrophone; arduino-uno micorsystem.

I. INTRODUCTION

Home activity detection is an active research area [2, 3, 4, 5, 6] but despite this, it has not yet reached a satisfactory performance, or resulted in a standard methodology [1]. Among the objectives of this area we quote: recognition of distress situations for the elderly or disabled people in their habitats with the aim of their surveillance. The help of elderly and disabled people from a remote location with the use of information and communication technologies and artificial intelligence techniques and tools is part of what we call "Health Smart Homes" (HSH). Several tools were used to meet this objective such as infrared sensors, cameras and microphones, but given the high cost of these tools, the large number of these sensors and the need for interaction research tends towards the use of the audio channel. We cite as an example the system AUDITHIS [1] which allows the analysis of sound and speech in the HIS from 8 microphones.

The whole idea of our work is the realization of a system of classification and separation of audio sources in a habitat for an application of tele-monitoring of the elderly or disabled people. However, several problems have arisen [4], such as the choice of parameters, choice of classification methods, sound quality (presence of noise), volume of information (several signals

from different channels are acquired simultaneously), presence of noise, signals from other sensors

In this paper, we first presented the key concepts of the research area, and then we presented works and projects that address recognition of activities and detection of distress situations in a HSH. After that, we have described the overall system architecture and its main modules. Finally, we studied the different sounds used in a tele-monitoring application from which we are inspired to create our database, then we designed a sound classifier interface based on DTW and classical features, finally some tests were done to get idea on accuracy of the features and classifier selected..

II. RELATED WORKS TO ACTIVITIES AND DETECTION OF DISTRESS SITUATIONS

Recognition of activities and distress situations are made through the information provided by the sensors installed in the HSH. A popular trend is to use the maximum of sensors to acquire more information. An opposite trend is to use the minimum amount of sensors [1] in such a way to design the most powerful system possible and at lower prices. In this section, we present a series of works that deal with the recognition of the activities and the detection of distress situations and their application in health smart homes.

Maunder et al. in [7] who built a database of sounds of daily life acquired by two microphones in a kitchen. They tried to differentiate between sounds such as telephone, a cup falling, drop a spoon, etc. Another group in [8] collected sounds in an office environment and tried unsupervised algorithms to classify the sounds of everyday life at work. The work presented in [9] is to recognize the distress situations at home in embedded situations using hardware at affordable prices (with standard sound cards and audio microphones). Another trend [10] is to perform speech synthesis, speech recognition, and the construction of a coherent dialogue with the person. Such research has applications in robotics, the aim is then to accompany the person and reduce loneliness.

The CARE project [15], with the use of many sensors (localization, temperature ...), allows the recognition of activities: "going the toilet" and "Exit the apartment." In Britain, [16] created a model that distinguishes the work of preparing a hot or cold beverage with health activities based on

the theory of evidence. [17] Presents the selection and arrangement of a set of sensors (infra-red detectors, door switches, microphones...) in an apartment, to classify a set of seven activities of daily living: rest, dress, casual, dining, communication, hygiene and disposal. [18] Uses microphones to detect a special distress: the fall. The solution is based on floor vibration and acoustic sensing, and uses a pattern recognition algorithm to discriminate between human or inanimate object fall events.

III. PROPOSED SYSTEM DESIGN



Fig. 1. Case of Home sound detection

In [11,12,16,21], Fleury, Vacher, Istrate and Al. have defined six categories of sounds except the speech: human sounds which are related to the person, objects and supplies manipulation linked to the activity of the person, outside sounds, devices sounds, sounds of running water; this particular category provides interesting information on activities such as disposal, hygiene, meal preparation. The last category of sounds is other non home activity sounds. Examples of each category are described in the table below, we considered some useful sound in our case under cotes.

In the Framework of the RESIDE-HIS project sounds are divided into two categories [13]: *Useful Sounds* (impulsive and short) as: Falling objects, broken glass, door slamming, etc., and *environmental noise* (long and stationary) as: the flow of water, hair dryer, electric shaver, etc.

Istrate in [14], for example, achieved a database of everyday life sounds for an application of telemonitoring of elderly and disabled people in a habitat. Its methodology for achieving this database is based on the one used in the speech database with regard to labeling and description files. The sound database is composed of: 15% of sounds recorded in the studio, 15% of the sounds recovered from a CD of effects for films [24] and 70% of sounds coming from the CD "Sound scene database in Real Acoustical Environments" (RWCP) laboratory ATR [24]. In [22], the authors have defined seven

classes of sound: door slamming, broken glass, ringing phone, footstep sounds, screams, sounds of dishes, door lock. The corpus contains both the sounds associated with distress situations such as broken glass, falling objects, screaming, but also the usual sounds like the sounds of footsteps, door slamming, and sounds of dishes. The database must also contain the environmental sounds, such as TV, radio, hair dryer, water flow, considered as noise [14].

TABLE I. SOUNDS CATEGORIES IN A HABITAT

Sound category	Examples
Human sounds	Cough, gargle, sigh, singing, whistling, wiping, "talking", "cry"
Objects and supplies manipulation	Search a bag, Manipulation of the chair, handling a tray, sounds of footsteps, falling objects, sound of paper
Devices sounds	phone ringing, beep, TV, "washing machine", "radio"
Sounds of running water	Handwashing, sink drain, flush, water flow
Outside sounds	thunder, rain, "wind", "cars", "Adhan"
Other sounds	Industry sounds, factory machine, volcano., "road congestion"

Everyday life sounds database of [14] consists of the following sounds: stapler sounds, clapping, moving the chair, human sounds (sneezing, yawning, laughing, snoring, coughing), opening a pressure vessel, crease or decryption of paper, footstep sounds, punch sounds, slamming different doors (entrance door, cabinet, refrigerator), electric shaver, hair dryer, door lock, dishes, chair and book fall, screams, water flow in sink, shower and glass, ringtones, health smart home background noise.

IV. DATABASE CREATION

A. Description of the Sound Database

Sounds may be speech or everyday life sounds. In order to create our database, we have divided everyday life sounds into two categories:

- **Normal Sounds** (related to usual activities): ex. door slam, door lock, opening door, phone ringing, footstep sounds, and sounds of dishes.
- **Critical sounds** (possibility of existence of a of distress situation): ex. broken glass, falling objects, screaming.

Normal sounds are divided into two categories too:

- **Useful sounds:** which may help us to detect distress situation when combined with other information.
- **Disturbing sounds:** considered as noise, like television and radio sounds.

As it is described in [14], and as presented in our work in [2] and [18], a part of our DB (database) is obtained by recording different types of sounds; a second part is obtained from commercial CDs, the third part by extracting sound from mp3 or videos and movies files. The last part will

be recovered from existing DBs like the ones created in [1,14,13].

The list of sounds we need for our application is summarized in the table 2.

B. The Recording Parameters

We chose a sampling frequency of 44.1 KHz to faithfully reproduce the signal after digitization. We chose the ". Wav" format for sound files because it is a standard format, and can be read by various software, in addition to that its conversion to other formats is easy [14].

The signal to noise ratio SNR of the recordings takes several values that vary between 10 and 40 to 70 dB. The length of the sound files is 20s. This length was chosen taking into account the maximum length of sounds to be treated and seeing that the initialization time for some algorithms is ≈ 5 s [14]. The figures: 2.a. and 2.b below, illustrates examples of some recorded sounds using Matlab environment.

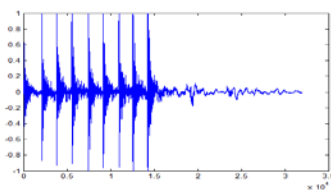


Figure 2.a Temporal evolution cknocking at door

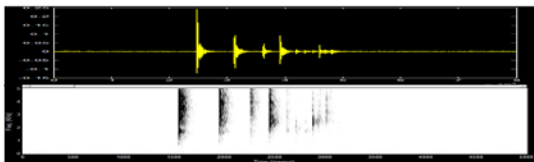


Figure 2.b: Temporal evolution and spectrogram of falling object

V. SYSTEM ARCHITECTURE

The proposed solution is based on: a) Home sound acquisition and analysis.

b) security and comfort situation sensors signals processed by Arduino-uno.

c) the fusion of both information will provide Security and some comfort for habitant

V.I Home sound Analysis: An application of sound recognition is composed of two main modules: the extraction module of the most relevant acoustic parameters of the processed signal which are features, and the recognition module that associates the sound with the corresponding class (most likely); it is the identification phase of the input sound. The main rooms are equipped with wireless microphones as shown in figure 1. the signals are sent to central unit that processes the sounds.

Our home sound analysis system is composed of three subsystems:

- The first subsystem deal with the detection of sounds in noise and their separation (SD) (mixture of sounds); input for the second subsystem.
- Features extraction: gets the mean parameters from segment of the processed sound signal.
- The third one is the classifier, which is DTW with Euclidean distance to classify the sounds resulted from the first subsystem.

The implementation of such a system requires first the construction of an everyday life sound database. For pattern recognition systems, there are always standard databases for the assessment of proposed systems. However, the construction of everyday life sound database in real conditions (environmental noise) is largely less explored.

In effect, sounds acquired by the acquisition system and from different sources are acquired together. If we consider the number of microphones installed in the apartment is n , then we have n sound sources in a time t and therefore the information gained may be the same but with a variation in the signal power (e.g. the object falling sound in the kitchen can be acquired simultaneously by all microphones of the apartment: bathroom, living room, etc. but the sound of the fall in the kitchen is the strongest) and this if we consider that there is no noise in the apartment, or several sounds can be acquired simultaneously, e.g. TV sound in the sitting-room, the flow of water in the bathroom with the cough sound of the habitant. It is therefore important to identify the sound to take into account i.e. choose the sound the most provider of information.

A. Detection & Separation: The SD implemented is based on analysis of crossing zero points and energy of the signal, the linear prediction mean square error computation helps in limiting the beginning and the end of a word; this makes it computationally quite simple.

B. Features Extraction: The parameter extraction block analyses the signal, extracting a set of parameters with which to perform the recognition process. First, the signal is analysed as a block, the signal is analysed over 20-mili seconds frames, at 256 samples per frame. Five types of parameters are extracted: Normalized Extremes Rate with Normalized Zero Crossing Rate (CZEXM), LPC coefficients (Ai), Energy Segments (ES) and Cepstral parameters (Ci) [14]. The LPC coefficients are produced from (1) and (2) equations :

$$x(n) = \sum_{i=1}^p \alpha_i x_{n-i} \quad (1)$$

$$H(z) = \frac{1}{1 + \sum_{i=1}^p \alpha_i z^{-i}} \quad (2)$$

These parameters were chosen for computational simplicity reasons (CZEXM, ES), robustness to background noise (12

Cepstral parameters) and robustness to speaker rhythm variation [15].

C. *Classification*: Dynamic Time Warping algorithm (DTW) [15], linear DTW with Euclidian distance (DTWE) is an algorithm that calculates an optimal warping path between two time series. The algorithm calculates both warping path values between the two series and the distance between them.

Suppose we have two numerical sequences (a_1, a_2, \dots, a_n) and (b_1, b_2, \dots, b_m) . As we can see, the length of the two sequences can be different. The algorithm starts with local distances calculation between the elements of the two sequences using different types of distances. The most frequent used method for distance calculation is the absolute distance between the values of the two elements (Euclidian distance). That results in a matrix of distances having n lines and m columns of general term:

$$d_{ij} = |a_i - b_j| \quad i=1..n \text{ and } j=1..m \quad (3)$$

Starting with local distances matrix, then the minimal distance matrix between sequences is determined using a dynamic programming algorithm and the following optimization criterion:

$$a_{ij} = d_{ij} + \min(a_{i-1,j-1}, a_{i-1,j}, a_{i,j-1}), \quad (4)$$

where a_{ij} is the minimal distance between the sub-sequences (a_1, a_2, \dots, a_i) and (b_1, b_2, \dots, b_j) .

A warping path is a path through minimal distance matrix from a_{11} element to a_{nm} element consisting of those a_{ij} elements that have formed the a_{nm} distance.

The global warp cost of the two sequences is defined as shown below:

$$GC = 1/P \sum_{i=1}^P W_i \quad (5)$$

where w_i are those elements that belong to warping path, and p is the number of them .

V.II Arduino-Uno and Senosrs for security and Confort: this part is composed of a microcontroller system based on Arduino-uno (composed of Atmel microcontroler) that provides : digital and analog I/O, USB interface, I2C and RS232 serial communication, large capacity for program memory , timers and WDT) , a set of sensors to detect flood , temperature inside and outside and intrusion sensors and a wireless transmission module Xbee. The overall harware part is illustrated in figure 3 [19] [20].

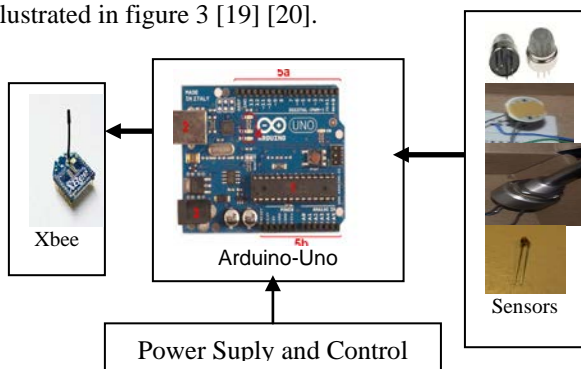


Fig 3. Electronic design of the node with all the necessary elements.

A) *LM75*: as temperature sensor: The LM75 is a temperature sensor, Delta-Sigma analog to digital converter, and digital over-temperature detector with I2C interface. The host can query the LM75 at any time to read temperature. The LM75's 3.0V to 5.5V supply voltage range, low supply current, and I2C interface make it ideal for a wide range of applications. These include thermal management and protection applications in personal computers, electronic test equipment, and office electronics.

B). *SHT21* as humidity sensor: The extremely small SHT21 digital humidity and temperature sensor integrates sensors, calibration memory and digital interface on 3 x 3 mm footprint. Additionally the humidity sensor provides electronic read-out of tracking information. This sensor reflows humidity and temperature sensor against external impact and leads to an excellent stability against aging, shock and volatile chemicals. Output : I²C digital, PWM, SDM/analog Volt , interface, RH operating range : and RH response time: 8 sec (tau63%).

C) *GP2Y1010AU0F* : is a dust sensor by optical sensing system. An infrared emitting diode (IRED) and an phototransistor are diagonally arranged into this device. It detects the reflected light of dust in air. Especially, it is effective to detect very fine particle like the cigarette smoke. In addition it can distinguish smoke from house dust by pulse pattern of output voltage. direct current 20 mA, output I2C.

D) *Transmitter Xbee*: The Xbee module type “OEM Xbee” were selected as radio frequency transmitter of the node , it swell suited for the design of WSN since it is in standard ZigBee/IEEE 802.15.4., the module can reach a distance of 1000 meters with baud rate 250 Kbps an it has a sensitivity of -92dbm.

VI. TESTS ON THE HSH

To test the sound analysis and classification we developed a GUI called HSH interface. The HSH interface is presented in figure 4, it is composed of 3 main figures: loading and fixing sound file, temporal and spectral signal of the sound file then classification for segment sound file. The interface has been tested with different sound from CDs and real sounds. The tests were' done on the seven sounds (Adhen, screaming, telephone, dishes, door open/close, normal speech, dropping objects) with 20 repetitions. And results are presented in figures 4 and 5. From the results in fig 8, we noticed a mice classification between “adhen” and “normal speech” also between “dishes” and “drop objects”.

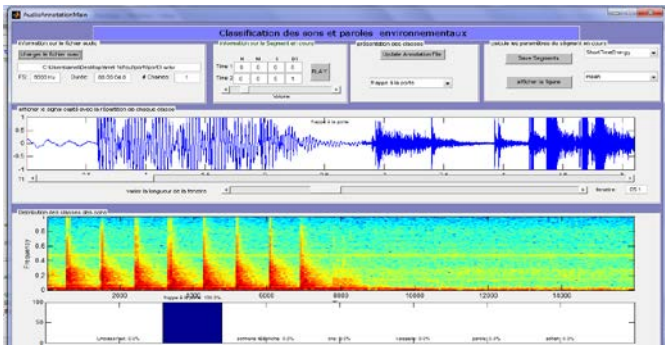


Figure 4. Figure. Illustration of the three main parts if the GUI

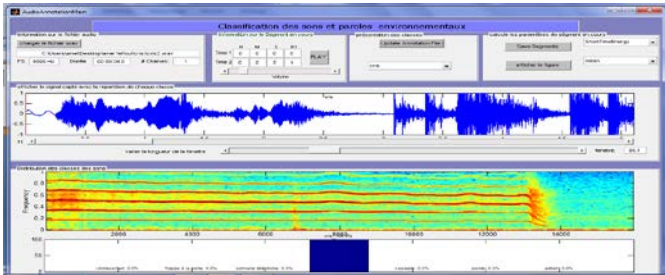
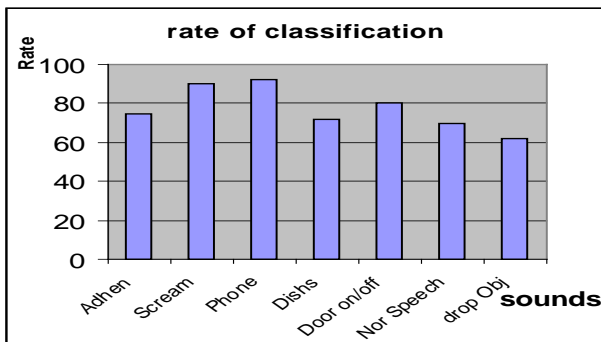


Figure 5.. test on screaming sound, show good classification.



VII. CONCLUSION

In this paper, we presented various works related to recognition of activities and detection of distress situations. Subsequently, we described the existing databases created to validate systems of tele-monitoring of elderly or disabled people via the detection of distress situations.

We have designed a system to detect and analyze home sounds then classify them normal or hazardous, the system can recognize some of the sounds to make the home "Health Smart homes", we also have used classical features and a basic classifier DTW then we designed a GUI interface, we added a hardware node based on Arduino-uno microcontroller to get other information from other sensors. The data fusion from arduino subsystem and Home sounds allow the central unit to inform the inhabitant or security members of the situation within the house.. The results obtained are very promising; we intend to include more nodes based on arduino in different room so that we can get a local wireless sensors network WSN. WSN

with microphones, accelerometers and other sensors to improve our HSH system design is in our perspectives.

REFERENCES

- [1] M. Vacher., A. Fleury., F. Portet, J.-F. Serignat, N. Noury .Complete Sound and Speech Recognition System for Health Smart Homes: Application to the Recognition of Activities of Daily Living. Dans New Developments in Biomedical Engineering, Domenico Campolo (Ed.) (2010) pp. 645 -- 673 - <http://hal.archives-ouvertes.fr/hal-00422576>.
- [2] L. Abdoun, M. FEZARI," Detection and Classification of Abnormal Sounds in a Habitat", in Proceedings of STA'2011 inter. Conf. on Science and Tech. of Automation Control. Sousse, Tunisia 2011.
- [3] S. Dalal, M. Alwan, R. Seifrafi, S. Kell & D. Brown. A rule-based approach to the analysis of elders' activity data: detection of health and possible emergency conditions, AAAI 2005 fall symposium, workshop on caring machines: AI in eldercare.
- [4] F. Duchêne , C. Garbay, & V. Rialle. Learning recurrent behaviors from heterogeneous multivariate time-series. Artificial Intelligence in Medicine 39: 25–47. 2007.
- [5] T. Duong , D. Phung, H. Bui, & S. Venkatesh. Efficient duration and hierarchical modeling for human activity recognition, Artificial Intelligence 173(7–8): 830–856. 2009.
- [6] A. Fleury. Détection de motifs temporels dans les environnements multi-perceptifs – Application à la classification des Activités de la Vie Quotidienne d'une Personne Suivie à Domicile par Télémedecine., PhD thesis, University Joseph Fourier, Grenoble. 2008.
- [7] D. Maunder, E. Ambikairajah, J. Epps, & B. Celler. Dual-microphone sounds of daily life classification for telemonitoring in a noisy environment, Proc. 30th Annual International Conference of the IEEE-EMBS 2008, pp. 4636–4639.
- [8] A. Harma, M. McKinney & J. Skowronek. Automatic surveillance of the acoustic activity in our living environment, Proc. IEEE Int. Conference on Multimedia and Expo ICME 2005, pp. 634–637.
- [9] D. Istrate, M. Vacher, & J.-F. Serignat, Embedded implementation of distress situation identification through sound analysis, The Journal on Information Technology in Healthcare 6(3): 204–211. (2008).
- [10] S.-y. Takahashi, T. Morimoto, S. Maeda, & N. Tsuruta, Dialogue experiment for elderly people in home health care system, Text Speech and Dialogue (TSD) 2003.
- [11] M. Vacher. "Analyse sonore et multimodale dans le domaine de l'assistance à domicile". Mémoire HDR, Octobre 2011.
- [12] A. FLEURY, M. VACHER, F. PORTET, P. CHAHUARA, N. NOURY. "A Multimodal Corpus Recorded in a Health Smart Home" Multimodal Corpora : Advances in Capturing, Coding and Analyzing Multimodality, LREC, 18-21 May 2010, Malta, pp. 99-105. 105. 99-105.
- [13] E. Castelli, M. Vacher, D. Istrate, L. Besacier, J. F. Sérignat, "Habitat Telemonitoring System Based on the Sound Surveillance", "1st International Conference on Information Communication Technologies in Health, Greece , 141-146, July 2003.
- [14] D. M. Istrate. "Détection et reconnaissance des sons pour la surveillance médicale". Thèse INPG, spécialité SIPT de l'Ecole Doctorale EEATS, Grenoble, 16 décembre 2003.
- [15] T Wang and V. "Robust Voicing estimation with DTW", Proceedings IEEE ICASSP'98, pp.533-536,May 1998.
- [16] A. Fleury, N. Noury, M. Vacher. Application des SVM à la classification des Activités de la Vie Quotidienne d'une personne à partir des capteurs d'un Habitat Intelligent pour la Santé, hal-00422566, version 1 - 7 Oct 2009.
- [17] D. Litvak, Y. Zigel, & I. Gannot. Fall detection of elderly through floor vibrations and sound, Proc. 30th Annual Int. Conference of the IEEE-EMBS 2008, pp. 4632–4635. 2008.
- [18] L. ABDOUN, M. FEZARI," A sound Database For Health Smart Home", pp.96, IeeeXplore conference, World Congress on Computer Application and Information Systems, WCCAIS'2014. ISBN: 978-1-4799-3350-1. Hammamet Tunisia, Jan-2014.
- [19] Yu, L.Y.; Wang, N.; Meng, X.Q. Real-time forest fire detection with wireless sensor networks. 2005 International Conference

- on Wireless Communications, Networking and Mobile Computing Proceedings, Wuhan, China, 2005, 1-2, 1214-1217.
- [20] Datasheet Arduino-uno 2014. <http://arduino.cc/fr/Main/Reference>
- [21] M. Vacher, F. Portet, A. Fleury, and N. Noury. "Development of audio sensing technology for ambient assisted living : Applications and challenges". International Journal of E-Health and Medical Communications, 2(1) :35–54. 2011.
- [19] D. ISTRATE, M. VACHER, E. CASTELLI, C.-P. NGUYEN. "Sound Processing for Health Smart Home". 2nd International Conference on Smart homes and health Telematics, Singapour, 15-17 septembre 2004, 8 p.
- [20] R. Harper. Inside the smart home. Springer, London, 2003.
- [21] M. Fezari et All, « *Human Machine Interface Communication System for Guiding a Colony of Mobile Robots in a Working Space* », in *Proceedings of ICIST- 2012, Tunisia* ,(2012)
- [22] Partnership, R. W. C. (1998-2001). CD – Sound scene database in real acoustical environments. <http://tosa.mri.co.jp/sounddb/indexe.htm>.
- [23] Stäger, M., Lukowicz, P., Tröster, G.: Power and accuracy tradeoffs in sound-based context recognition systems. Pervasive and Mobile Computing, vol. 3 (3), pp. 300–327. (2007).
- [24] Wang, J. C., Lee, H. P., Wang, J. F., Lin, C. B.: Robust Environmental Sound Recognition for Home Automation. Automation Science and Engineering, IEEE Transactions on, vol. 5 (1), pp. 25–31, Jan. 2008.

New Method Based on a Speech Processing Algorithm for Cochlea Implants using IIR Filters

Hajer Rahali, Zied Hajaiej, Nouredine Ellouze

Abstract—In this paper we present the conception and the implementation of a speech processing interface for cochlea prosthesis. This module is based on a numerical speech processing algorithm which models the infected ear and generates the stimulus signals for the cilia cells (brain). This interface uses a Gammachirp filterbank based on IIR filters. The central frequencies and ERB bands are computed with Glasberg and Moore models; however stimulus signals are selected after a spectral energy analysis of each channel. To validate our work, we tested it on vowels then on several words pronounced by different speakers. The results demonstrated a degree of discrimination and interferences between different sounds especially in multi speaker environment.

Keywords—Gammachirp filterbank, impulsive noise, cochlea.

I. INTRODUCTION

Speech is a natural and flexible mode of communication for humans. It is very efficient, for transmission of information; conversational speaking rates can be as high as 200 words per minute. And for reception of information, has others advantages as well. Speech recognition is today a quite common element in our lives. Cellular phones, computers, telephone services and many more products use speech recognition. An important drawback affecting most of the speech processing systems is the environmental noise and its harmful effect on the system performance. The presence of noise normally degrades the performance of speech recognition; therefore it is very important that a speech recognizer in some way deals with possible noise. A large amount of work has therefore been spent in this area and there exists a lot of technique that improves the speech recognizer's performances in noisy conditions. Most hearing deficiencies of the human auditory system affect the internal ear (cochlea) and requires a specific cochlea implant. It is based on the conversion of the vocal message in electric impulses to the stimulation of the nerve cells. This prosthesis is composed of on a speech processing module which models and replaces the internal ear for transmission, wave generation and signal reception [1]. Many studies developed auditory models which were inserted and used in the speech processing algorithms such as Flanagan model which is based on the physiological data measured by

Bekesy, and a mathematical-computational model for the auditory mechanism. This model is divided into two parts, one comprising the middle ear and the other the basilar membrane. In this work, a new approach for speech analysis based on gammatone and gammachirp decomposition is shown. The sounds are added to the word with different signal-to-noise (12 dB, 6 dB, 3 dB, 0 dB and -3 dB). The evaluation is done on the TIMIT database.

This paper is organized as follow the first section is to define the gammachirp filter, the second section presents the speech processing algorithm and the third section shows experimental result and conclusion.

II. GAMMACHIRP FILTER

The gammachirp filter is used in the psychoacoustic research as a reliable model of cochlear filter. The gammachirp filter is defined in the time domain (impulse response function) as:

$$g_c(t) = a^{n-1} \exp(-2\pi b \text{ERB}(f_r) t) \exp(j2\pi f_r t + j c \ln t + j c \phi). \quad (1)$$

Figure 1 shows the representation of the temporal response of the Gammachirp filter.

Where time $t > 0$, a is the amplitude, f_r is the asymptotic frequency and b are parameters defining the envelope of the gamma distribution. C is a parameter for the frequency modulation or the chirp rate, ϕ is the initial phase, and $\text{ERB}(f_r)$ represents the equivalent rectangular bandwidth of the filter, is given by the following relationship:

$$\text{ERB}(f_r) = 24.7 + 0.108 f_r. \quad (2)$$

The Fourier transform of the gammachirp in "equation 1" is derived as follows:

$$|G_c(f)| = \frac{a^{|\sigma(n+jc)|}}{\sigma(n)} * \frac{\sigma(n)}{\left[2\pi \sqrt{(b \text{ERB}(f_r))^2 + (f-f_r)^2}\right]^n} e^{c\theta}. \quad (3)$$

$$|G_c(f)| = a_\sigma |G_T| * e^{c\theta(f)}. \quad (4)$$

$$\theta(f) = \arctan\left(\frac{f-f_r}{b \text{ERB}(f_r)}\right). \quad (5)$$

Hajer Rahali, National Engineering School of Tunis (ENIT), Laboratory of Systems and Signal Processing (LSTS), BP 37, Le Belvédère, 1002 Tunis, Tunisie (e-mail: hajer.rahali@enit.mu.tn).

Zied Hajaiej, National Engineering School of Tunis (ENIT), Laboratory of Systems and Signal Processing (LSTS), BP 37, Le Belvédère, 1002 Tunis, Tunisie (e-mail: zied.hajaiej@enit.mu.tn).

Nouredine Ellouze, National Engineering School of Tunis (ENIT), Laboratory of Systems and Signal Processing (LSTS), BP 37, Le Belvédère, 1002 Tunis, Tunisie (e-mail: N.ellouze@enit.mu.tn).

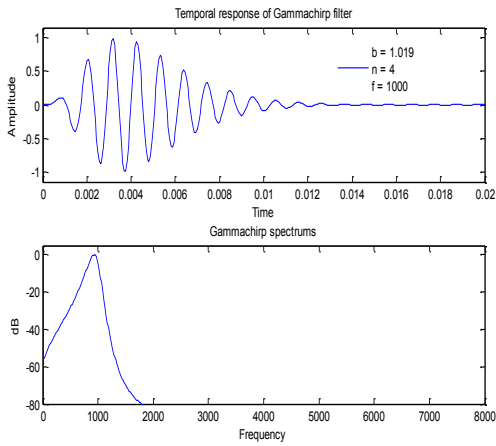


Fig. 1. Example of impulse response gammachirp

$|G_T(f)|$ is the Fourier magnitude spectrum of the gammatone filter, $e^{c\theta(f)}$, is an asymmetric function since is anti-symmetric function centered at the asymptotic frequency. The spectral properties of the gammachirp will depend on the $e^{c\theta(f)}$, factor; this factor has therefore been called the asymmetry factor. The degree of asymmetry depends on “c”. If “c” is negative, the transfer function, considered as a low pass filter, where c is positive it behave as a high-pass filter and if “c” zero, the transfer function, behave as a gammatone filter. In addition, this parameter is connected to the signal power by the expression, [2]:

$$C = 3.38 + 0.107 Ps. \quad (6)$$

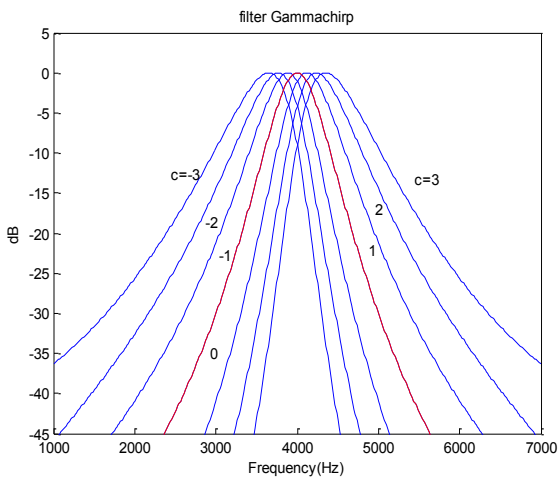


Fig. 2. Example of gammachirp spectrums for different values of C

III. CHARACTERISTICS OF THE GAMMACHIRP

The figure 3 shows a block diagram of the gammachirp filterbank. It is a cascade of three filterbanks: a gammatone filterbank, a lowpass-AC filterbank, and a highpass-AC filterbank. The output of the asymmetric compensation filterbank determines the asymmetric parameter c.

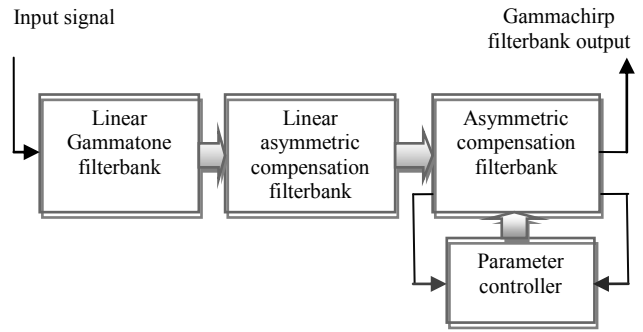


Fig. 3. Structure of the Gammachirp filterbank

Figure 4 shows the amplitude spectra of (a) the gammachirp and (b) the asymmetric function when the values of the chirp parameter c are integers between -3 and 3. Several characteristics are derived from this figure. Figure 4 (a) shows that the filter slope below the peak frequency is shallower than the slope it in the gammachirp when the parameter c is negative. The situation is the reverse when the parameter c is positive. The filter shape is symmetric when c is zero because it is the gammatone. The asymmetric function in fig. 4 (b) is an all-pass filter when c=0. This function is a high-pass filter when c>0, and a low-pass filter when c<0. The slope and the range of the amplitude increase when the absolute values of c increases. The filter shapes of the gammachirp in fig. 4 (a) reflect these characteristics.

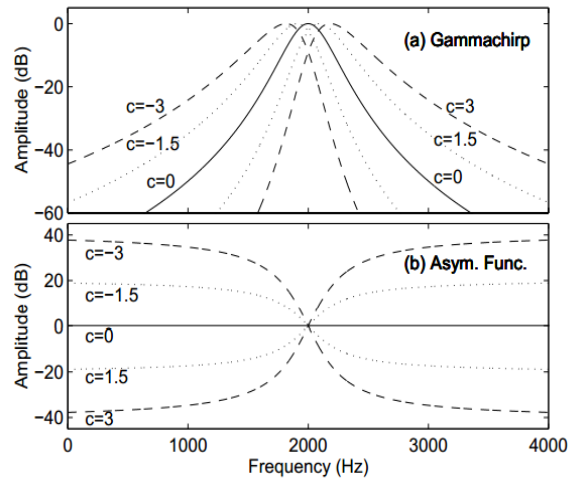


Fig. 4. Amplitude spectra of (a) a gammachirp filter and (b) an asymmetric compensation filter

IV. THE SPEECH PROCESSING ALGORITHM

In this paper, we present a new model that can replace the internal ear. The proposed modifications are presented in the following section. A schematic diagram of the proposed technique is shown in figure 5. In this proposed algorithm an application of pre-emphasis is applied to the speech signal. In the second step, the digitized noisy speech is segmented into overlapping frames, each of length 20 ms with 10 ms overlap, in speech processing a Hamming window is mostly used. Afterwards, the segmented signal is filtered using the non linear model of the external and middle ear which is given by the following analytical expression:

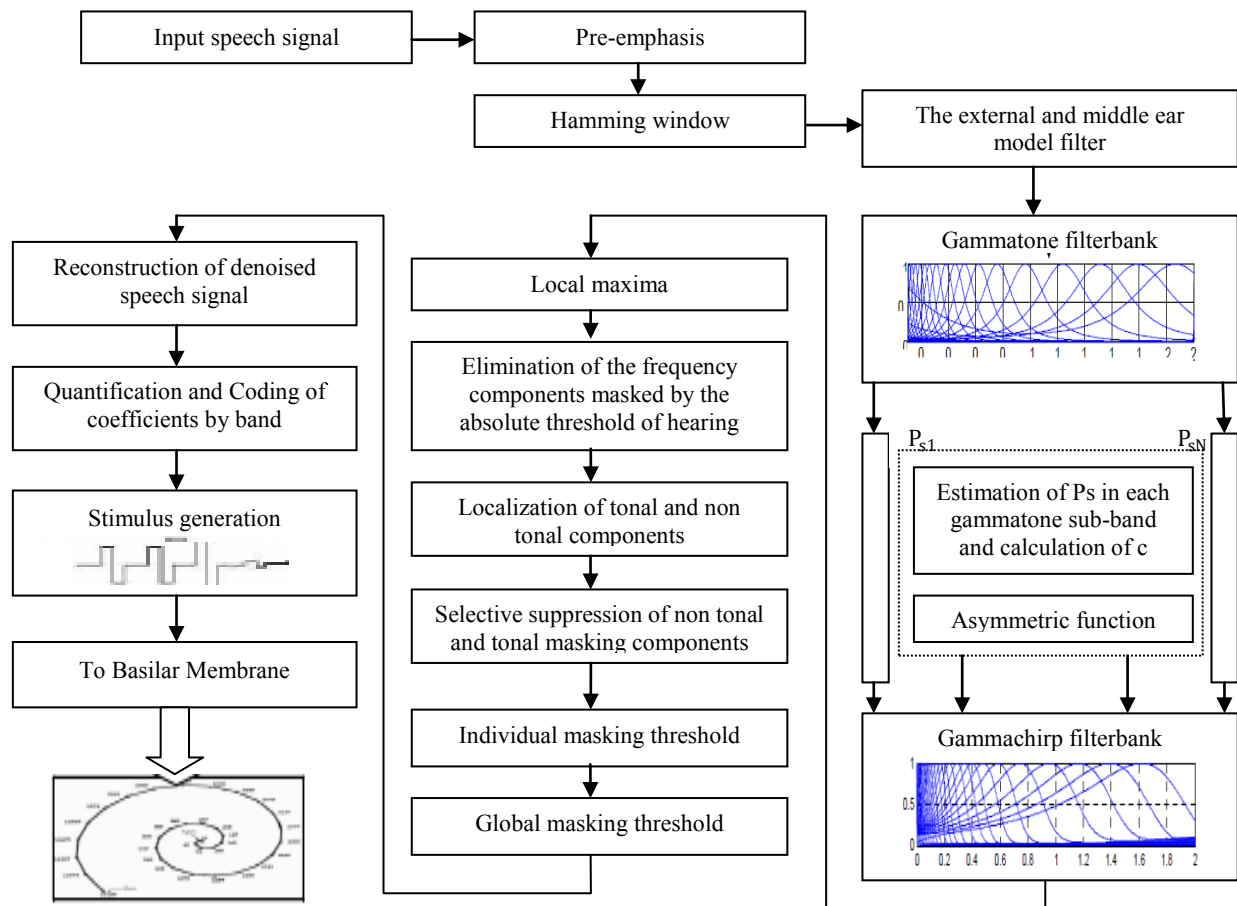


Fig. 5. The speech processing algorithm

$$H(f) = -2.184 * f^{-0.8} + 6.5 * e^{-0.6(f-3.3)^2} - 10^{-3} * f^{-3.6}. \quad (7)$$

The next processing step applies a filterbanks. Many different types of filterbanks exist but for this model features the gammachirp filterbank is used. The output signal of the outer and middle ear model filter is applied to a gammatone filterbank. On each sub-band we calculate the sound pressure level P_s (dB) in order to have the corresponding sub-band chirp term C . Those values of chirp term C corresponding to each sub-bands of the gammatone filterbank lead to the corresponding gammachirp filterbank. Each signal of the 16 outputs is analyzed in order to compute its energy and envelope. In the next stage, we calculate tonal and non tonal components. This step begins with the determination of the local maxima, followed by the extraction of the tonal components (speech) and non tonal components (impulsive noise), in a bandwidth of a critical band. If frequency exceeds neighboring components within a bark distance by at least 6 dB then it will be treated as “speech” otherwise it will be considered as “noise”. The selective suppression of tonal and non tonal components of masking is a procedure used to reduce the number of maskers taken into account for the calculation of the global masking threshold. The tonal and non tonal components remaining are those which are above the hearing absolute threshold. Individual masking threshold takes into account the masking threshold for each remaining component. Speech signals contain two types of information, time and

frequency. In time space, sharp variations in signal amplitude are generally the most meaningful features. In the frequency domain, although the dominant frequency channels of speech signals are located in the middle frequency region, different speakers may have different responses in all frequency regions [12].

Figure 6 represents the speech signal and its spectrogram of the vowel /a/ pronounced by a female speaker with impulsive sound “Door slams”. Figure 7 shows the frequency response of the gammachirp filterbank; in figure 8 we can observe the waveforms of the 16 filter bank output signals.

The spectral estimation of the filterbank output signals is used to extract the stimulus parameters which are: the excited electrodes (or channels) number and their order then the stimulation speed (or spikes) deduced from the channel amplitude or envelope. These parameters once normalized, will be quantized according to a uniform quantification before coding.

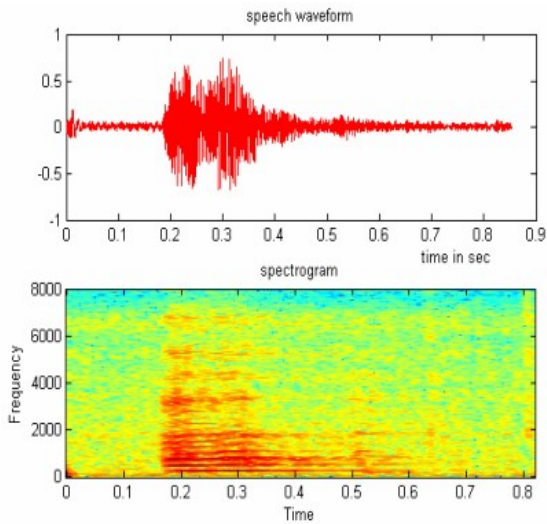


Fig. 6. The speech signal and its spectrogram of the vowel “a”: female sound with impulsive signal “Door slams” and SNR=12 dB

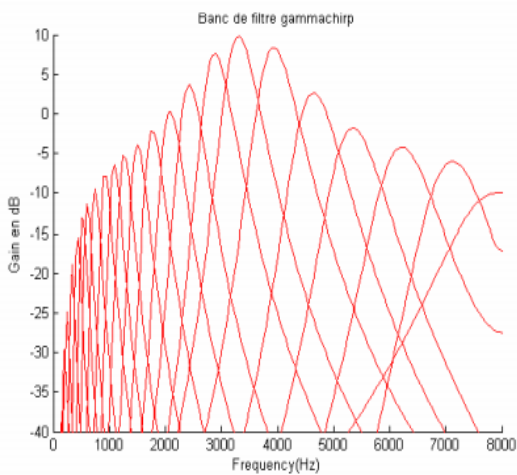


Fig. 7. Frequency response of the gammachirp filterbank

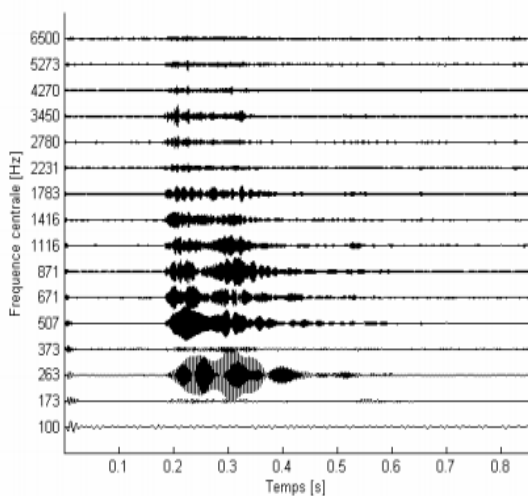


Fig. 8. Temporal responses of the filterbank outputs for the vowel “a”: female sound with SNR= 12 dB

The most significant bands are selected to be coded according to CIS strategy and then transmitted to the basilar membrane electrodes. In our study, we used an adaptive

coding method CIS based on the stimulation of a reduced number of electrodes (N) which present the high energies. The number N is determined by the spectral estimation of the outputs of this model.

V. SIMULATION RESULTS

We have integrated the algorithm of figure 6 in a Matlab speech processing program for evaluating and simulation of our coding strategy. As input speech, we used sounds from TIMIT database. These clean speech were contaminated with additive impulsive noise, in this paper contains 464 sounds of 3 different classes: 314 door slams, 88 glass breaks and 62 explosions. Tests were carried out at different SNR levels (12 dB, 6 dB, 3 dB, 0 dB and -3 dB).

Figures 9 and 10 illustrate respectively the output signal of this model temporal responses and its spectral energy (with 16 channels) of the vowels /a/, pronounced by a female voice with SNR=12 dB. We can observe that in the case of /a/ the maximum of energy is located at the 3rd channel with a variable energy distribution for the others channels.

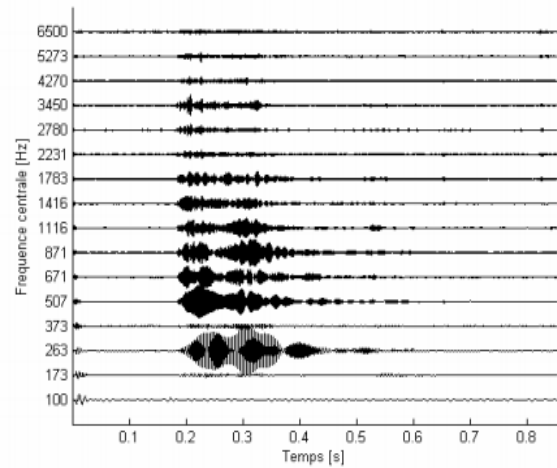


Fig. 9. The outputs of this algorithm for the vowel /a/ (N=16 channels)

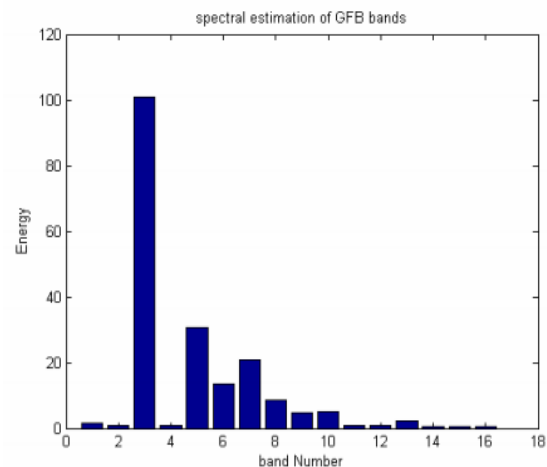


Fig. 10. Spectral estimation by band for the vowel /a/

The figure 11 represent the result of the sixteen channel energy coefficients calculated from vowels localized in several words and pronounced by the same female speaker. We can easily observe a similar localization of the similar processed speech around 3 or 4 channels. For example, the most energy channels (which will be selected and excited)

for the vowel /a/ in the words /dark/ and /had/ are the 4th, 5th and 6th channels. This little perturbation shows a certain overlap between certain vowels but this new model keeps a sufficient discrimination between them in multi and inter speaker environment.

The presented figures confirm these results since we see that each vowel is well localized in the selected stimulation channels.

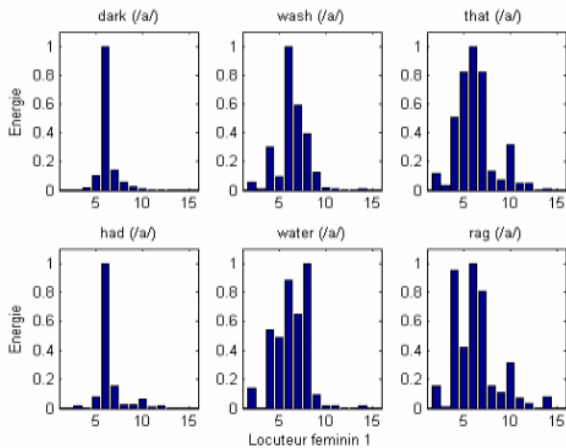


Fig. 11. Representation of the 16 channels energy parameters for the vowels /i/ and /a/ repeated by the same female speaker (in different words)

VI. CONCLUSION

This paper reviewed the background and theory of the gammachirp auditory filter proposed by Irino and Patterson. We have presented an approach of time-frequency analysis "auditory spectrogram" for speech. This takes account of characteristics of the ear. In this study, we presented a new implementation method of speech processing and coding which is intended for cochlea implants. This strategy is based on an adaptative parameters extraction of the speech signal. These three parameters are the number of the stimulation channels (3 to 5), their order and finally their stimulation rate (number of pulses per second). The first and second parameters are chosen after a spectral energy analysis by channel of the 16 filter bank output signals. However, the last parameter is chosen in function of the envelope and amplitude signal of every stimulated channel and the vocal and acoustic information. This technique is implemented and simulated under Matlab under several environments and speech database (TIMIT with several speakers and words). The several simulation results of stimulation channels and their interferences in different words, demonstrated a good discrimination between these information especially for vowels. This technique has the advantage to reduce the number of channels and to obtain best signal intelligibility.

REFERENCES

- [1] E. Zwicker, R.Feldkeller, "Psychoacoustique, l'oreille récepteur d'information", Masson Coll, 1981.
- [2] A.Ben Hamida, M.Samet, M.Benmessaoud, H. Ghriani, N. Lakhoua, M. Drira, J. Mouine, "Algorithme de traitement de la parole basé sur un banc de filtres numériques programmable dédié à la prothèse cochléaire " In proceedings of the Int. Electronic conf. JTEA, Tunis 1998.
- [3] A. B. Poritz, "Hidden Markov models: A guided tour", in Proc. of the IEEE Int'l. Conf. on Acoustics, Speech and Signal Processing (ICASSP '88), May 1988, pp. 7-13.

- [4] T. Irino, R. D. Patterson. Temporal asymmetry in the auditory system.J. Acoust. Soc. Am. 99(4): 2316-2331, April, 1997.
- [5] T. Irino, R. D. Patterson. A time-domain, Level-dependent auditory filter: The gammachirp. J. Acoust.Soc. Am. 101(1): 412-419, January, 1997.
- [6] T. Irinoet M. Unoki. An Analysis Auditory Filterbank Based on an IIR Implementation of the Gammachirp. J. Acoust. SocJapan. 20(6): 397-406, November, 1999.
- [7] Young S. J., Woodland P. C., Byrne W. J., "HTK. Reference Manual for HTK version 3.1", Décembre 2001.
- [8] T. Irino, R. D. Patterson. A compressive gammachirp auditory filter for both physiological and psychophysical data.J. AcoustSoc . Am. 109(5) : 2008-2022, may 2001.
- [9] J. O. Smith III, J.S. Abel. Bark and ERB Bilinear Transforms, IEEE Tran. On speech and Audio Processing, Vol. 7, No. 6, November 1999.
- [10] R. D. Patterson, I. Nimmo-Smith. Off-frequency listening and auditory-filter asymmetry, J. Acoust. Soc. Am., Vol. 67, No. 1, pp. 229-245, 1980.
- [11] B.R. Glasberg, B. C. J. Moore. Derivation of auditory filter shapes from notched-noise data, HearingResearch, 47, 103-198, 1990.
- [12] L. Bréhélin, O. Gasuel. Modèles de Markov cachés et apprentissage des séquences. Le temps, l'espace et l'évolutif en sciences du traitement de l'information, Éditions Cépaduès, pp. 407-421, 2000.
- [13] H. Hermansky. Perceptual Linear predictive (PLP) analysis of speech, J. Acoust. Soc. Am., Vol. 87, No. 4,pp. 1738-1752., April 1990.
- [14] T.Irino, T. and Unoki, M. (1998). "A time-varying, analysis/synthesis auditory filterbank using the gammachirp," IEEE Int. Conf. Acoust., Speech Signal Processing (ICASSP-98), 3653-3656.
- [15] University of Pennsylvania Linguistic Data Consortium. Darpa-timit: a multi speakers data base.
- [16] L.R. Rabiner. A tutorial on hidden Markov models and selected applications in speech processing. Proceedings of IEEE, 77(2):257-286, 1989.
- [17] J. W. Pitton, K. Wang, and B. H. Juang, "Time-frequency analysis and auditory modeling for automatic recognition of speech," Proc. IEEE, vol. 84, pp. 1199-1214, Sept. 1996.
- [18] O. Ghitza, "Auditory models and human performance in tasks related to speech coding and speech recognition," IEEE Trans. Speech Audio Processing, vol. 2, pp. 115-132, Jan. 1994.
- [19] Skowronski M. D. and Harris J. G., 2002, Increased MFCC filter bandwidth for noise-robust phoneme recognition, in Proc. ICASSP-02, Florida.

Management of a standardized Platform of Unified Medical History from Health Interoperability

- Case study Colombian Caribbean Islands system-

Fernando Prieto Bustamante, Yaneth P.Caviativa, Yoan Manuel Guzmán,

Abstract—In this article is presented the development and management process of standardized medical documents of a design platform as a proposal for the Sanity System of Colombian Caribbean islands system to which belongs the Archipelago San Andrés, Providencia and Santa Catalina Department; from the finding of own necessities of medical histories information system including, the communications protocol Health Level Seven (HL7), and facing the service inventory for XDS interaction, repository of documents and headers, design for the exchange of medical documents. Such purpose of architecture design linked to CDA (Clinical Document Architecture) should be oriented to the Colombian Caribbean islands system and respond to storage and communication services (SOA) of information, vigilance and control of user electronic information, from the presentation, business logic and repository of geographical data with health entities that the FOSYGA regulates as part of Colombian health system.

Keywords—E-Health, HL7, Interoperability, Management of medical documents.

F. Prieto is with Universidad Santo Tomás, Bogotá, Colombia. Phone number: +57 310 572 24 86 (e-mail: fernando.prieto@usantotomas.edu.co)

Y. Caviativa is with Universidad Manuela Beltrán, Bogotá, Colombia. Phone Number: +57 1 546 06 00 ext. 1151 (e-mail: janeth.caviativa@docentes.umb.edu.co)

Y. Guzmán is with Universidad Manuela Beltrán, Bogotá, Colombia. Phone Number: +57 1 546 06 00 ext. 1151 (e-mail: yoan.guzman@docentes.umb.edu.co)

It is impossible not to acknowledge the relations of information technologies that in direct and indirect way are associated with the development of knowledge and communicational processes in specific areas where knowledge appropriation becomes part of society and in clear ways encourage efficiency processes in a context. In this sense, in health care context, different forms of contribution to the concept of geolocation in this area, has been given from the design of geolocation platforms in charge of locating health centers. In some way, this has presented a problematic because of heterogeneity in platform design in which information is located, affecting not only financial corporations or producers, but also companies that have a common service and different places where to supply it. Thus, the presented subject can be seen not only in a national context, but also it can be seen in developed countries. Initiating discussions about communication standards between platforms so information becomes homogenous and updated for a real consult in different locations.

There is where HL7 under the use and develop of standards (ANSI, American National Standards Institute) provides an exhaustive framework and standards related to exchange, integration and reception of health electronic information that support the clinical practice, management and evaluation delivery of health services. This contextualization aims to apply these standards allowing understanding functioning and applicability in medical histories in Colombian Caribbean islands system developing an approximation to the improvement general system and standard handling in Colombia.

I. INTRODUCTION

II. THEORETICAL APPROACH

I A. Problem description

The design and implementation of a system for standard medical document management for Sanity System of

Colombian Caribbean islands system from Archipelago San Andrés, Providencia and Santa Catalina Department, consist in studying in detail information necessities that health institutions have, and the way they storage such information, so from HL7 standard becomes possible to establish the form in which information system of every institutions that conform the national health system, could be integrated and communicate, thanks to interface of interoperability that will be provided through the system platform. Additionally, and given the surveillance and control necessities by governmental entities, it is conceived as obligatory the fact of storing information of health system users and their respective medical histories, in centralized way in a server that is at hand for Social Protection Ministry and authorized people or entities.

B. Justification

Being Colombia referred in various investigations as part of health crisis system in Latinamerica region [1], establishing among them the lack of surveillance and control by the state as the greater criteria in lack of quality in health matters, allowing so that health service entities generate their own rules in a permissive way.

The biggest difficulty detected in the execution of state control, is an absent of a database that allows to know who are the affiliates and beneficiates of health system, and what services have been executed by any institution; so, validation times of presented complaints to Fosyga are reduced, and at the same time health services can be enjoyed without depending on having a regionalized model which do not allows national portability to the right of health [1].

This type of elements of identification and standardized findings in systematization of medical data, in many countries has allowed the improvement on the provision of health services at national level, by the integration of health information systems, which includes generation of Electronic Medical Histories (EMH) allowing developing an international coverage for users.

Under this interest scheme, the management of a standardized Platform of Unified Medical Histories from Health Interoperability will allow for institutions that count with heterogeneous information systems to communicate each other, making easier reference and counter reference processes, at the same time that users identification and services providing are more agile. On the other hand, given the centralization and systematization of data, communication errors will be reduced, information redundancy will be avoid, and government will be able to execute real control and verification of executed processes, giving more efficiency to collection and recollection processes of entities before the Fosyga.

Social Protection Ministry from resolution 1448 issued on 2006 in Law 1122 of 2007, initiates health institutions, universities and investigation groups efforts of expanding service providing system through telemedicine. About data standardization and communication between entities information systems of health sector, efforts have been isolated, which has not allowed to accomplish and real repercussion in health system for Colombia, even though the

existence of laws such as 1419 of 2010 [1] and 1438 of 2011 that stipulates as obligatory the efficiency and wide coverage in services provision, as well as the establishment and use of a single medical history. It is because of this reason that this project seeks to centralize information management for Social Protection Ministry, so the application of standards creates a direct effect in the whole country.

III. CONCEPTUAL FRAMEWORK

Before talking about the theoretical framework of implemented standard, it is important to make an introduction of the basic element of study, the evolution of patients' medical history and its passage to the technological world and data transmission via electronic ways.

With this concept, it can be said that is a non missing tool in diary labors of medics, internists, specialists, nurses, medical assistants and administrative staff. Concretely, it could be defined as a document that contains registered, clear, precise, detailed and ordered narrative of every data and knowledge, both personal and familiars, that are referred to a patient and that serve as base for the diagnostic of an illness or the opinion of his/her health state at the moment of consult.

Government has decreed through the Law 1419 of December 13th of 2010 [1], that all activity that is developed under the called Telesalud (telehealth), must fulfill principles of efficiency, universality, solidarity, integrity, unity and quality, among others. About the assurance and services providers, law stipulates that their portfolios must be expanded and offer telemedicine as a additional mode for the service provision. Moreover, to achieve a continuous improvement in the area, this law promotes investigation and education in technologies applied to health.

Besides the telemedicine promotion law, the Congress dictated as mandatory the use of an single electronic medical history for health institutions by Law 1438 of 2011 [3] since December 31th of 2013 (see transitory paragraph of article 112), and demands connectivity of health sector institutions, with the purpose of easing and making possible portability of services anywhere in the country.

In this way, and in concordance with the state necessities established by what is exposed in law, there are exposed the necessary themes to establish and clear context about topics or related issues with the project of Management of a standardized Platform of Unified Medical History from Health Interoperability - Case study Colombian Caribbean Islands system-

A. Collection and recollection process

In Colombia, exists an entity called FOSYGA (Solidarity and Guarantee Fund, for its initials in spanish) by which the government guarantee attention and care for its citizens before emergency events, due to car accidents, terrorism, naturalcatastrophes and other events that are stipulated in Law 100 of 1993 [4]. The functioning of this entity is based in two (2) procedures, which description can be found in article 7 of 1281 Decree of 2002 [5], known as collection and recollection. Collection occurs when a Health Provider Institution (HPI or IPS for its initials in spanish) presents a bill

to the corresponding Health Promoter Entity (HPE or EPS for its initials in spanish) to which attended user was affiliated, or to the FOSYGA when user belongs to subsidized regime. Additionally, when some service is vital for a patient, and it is not covered by the POS or subsidized regime, the user could present a protection claiming his/her right. If this protection is sanctioned on his/her favor, then the HPE will cover the costs for a certain amount, and the rest of the financial obligations would be responsibility of FOSYGA.

Recollection corresponds to bills passed by the HPE (of subsidized or contributive nature) to FOSYGA, claiming money devolution for payments done to the HPI after the provision of any health services and medications not included in the POS [7]. In the occurrence of a collection or recollection, it is imperative the delivery of supports which show that effectively a health service has been provided. These supports consist in the delivery of bills and individual registries corresponding to consults, procedures, urgency services, hospitalization, medicaments [6], all of which must be delivered in a term of six (6) months since the service provision.

B. Reference and counter reference system

Reference process consists in translating a user from one health provider entity to another, with the implication that the remittent professional must attach a reference format identifying the user in adequate way, and attaching a resume of his medical history, and a description of treatments and exams that has been done to him/her. Similarly, the motive and type of service that the patient requires must be specified. According to the benefit plan for the health services provision [8], reference and counter reference system was created with the ultimate goal of guaranteeing an adequate service provision to the patients when a HPI does not possess the physical resources for his/her care.

C. Standard CEN EN13606

This normative, initially recognized as European normative by the European Committee of Normalization, and afterwards as international standard by the Standardization International Organization, also known as CEN/ISO EN13606, corresponds to the established standard to define architecture or structure of Electronic Health Record (EHR), in order to achieve communication between systems that require to exchange patients information; ergo, those systems in which this standard is implemented, will reach a semantic interoperability, preserving the meaning of each elements [9]. Experience in the implementation of previously defined standards, gave the sufficient maturity so in the development of EN13606 standard was taken into account the fact that medical information systems turn out to be of high maintenance and become obsolete quickly, due to the complexity of medical information, heterogeneous data types and the fact that medical knowledge presents a continuous actualization [10]. According to the definition of the dual model, with its architecture two elements conforms it, the Reference Model that gives structure to EHR information through entities, and in which medical data is stored; and the

Archetypes Model in which are defined and related the entities of the Reference Model, which correspond to concepts of medical domain [9].

About Reference Model, EN13606 standard, disposes that any noting that is wished to place in an EHR must belong to any of the sets, that have been defined there, such as: folder, composition, section, entry, cluster, element [11] [12].

As was said previously, knowledge model is conformed of archetypes. These archetypes, which are no other than representations of concepts that are handled in medical domain, conform the ontology of the system to which they are developed; because besides of giving structure to EHR information, also establish the relation that exists between the different entities of Reference Model [10]. Archetypes are integrated of three (3) elements [11]:

- Header: contains an archetype identifier and author information.
- Definition: corresponds to the concept or entity description serving of the other entities of Reference Model.
- Ontology: describes entities used in the definition.

Fig. 1 corresponds to a mind map of archetype for a bone exam:

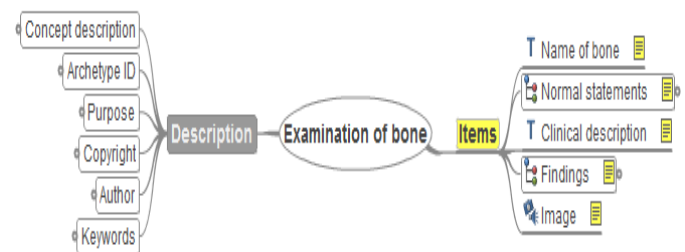


Fig. 1. Mind map of an archetype¹

D. HL7 Standard (Health Level 7)

The HL7 standard was defined by the Fund with the same name, which has dedicated since its foundation to create standards for health sector.

In a beginning, HL7 Foundation was dedicated to elaborate messages specifications for information sending between health institutions. Over time, and observing that institutions which wanted to establish communication had to invest high quantities of money to add modules or redesign their systems (due to they did not counted with a standard to define events and elements related to patients),HL7 started with the task of

¹ Taken from OpenEHR, Clinical Knowledge Manager. Disponible en la URL: <http://www.openehr.org/knowledge/> generating standards not only for communication but for medical information structure. That was how HL7 V2 was born. Afterwards, due to a lack of a clear implementation model, the foundation defined the HL7 V3 standard, which avoids divagation of the designer between the wide quantities of possibilities that V2 allowed. In this way, in year 2004 was

accomplished the generation of a clear standard of easy implementation and management [13]. In fig. 2 is shown the timeline corresponding to HL7 standard evolution.

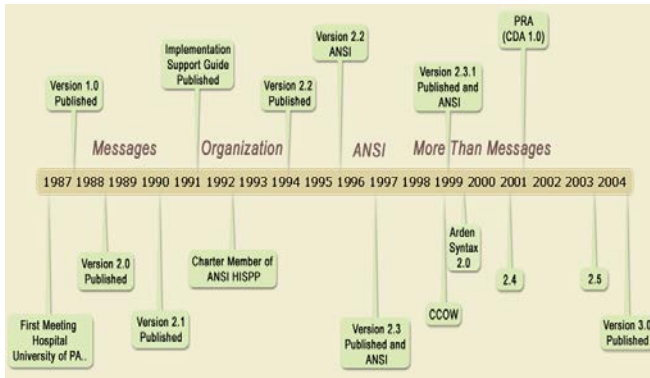


Fig. 2. HL7 standard evolution²

As it can be observed in fig. 2, it was on year 2001 when HL7 foundation released their first version of CDA HL7 standard (Clinical Data Architecture), in which was defined the structure of electronic medical documents. For version number 3 of HL7 standard, as the same as EN1606, was found the necessity of adding a Reference Model named RIM (Reference Information Model), which corresponds to semantic representation of elements and information contained in medical messages.

It is important to take into account that HL7 Reference Model does not define the structure of electronic medical documents, this is a function of the CDA HL7; but there must be clarity about the relation that exists between RIM and CDA, because tags that are used in XML documents of the CDA are defined in the RIM, so that every version of the CDA is directly related to the corresponding RIM, from which it takes the types that are necessary for every specification of parameters of the document to define, and with them constructs what is known as redefined reference model or RMIM [14].

In HL7 Reference Model exists three superior types for definition of medical domain: event (act), number of participants in the event (role), and involved subject in the event (entity) [15] [16].

E. Relation between HL7 and EN13606

HL7 and EN13606 standards have different origins, while HL7 surged as a standard for communication of medical data,

²Image taken from Introduction to Health Level Seven (HL7).History of HL7. 2007. Disponible en la URL: http://www.hl7.org/documentcenter/public_temp_CCB1EE66-1C23-BA17-0C50E3F5C517F93F/training/IntroToHL7/player.html

EN13606 have always been funded in development of a documentation structure, but at present, both chase the same objectives: achieve semantic and functional interoperability between different informatics systems of health sector institutions. Nowadays, in Europe, EN13606 standard has been implemented in various countries, while in United States

of America the utilized standard is HL7. Being this world such a globalized one, it has also been necessary to establish communication between heterogeneous systems about the standard. So that it is necessary to clarify similarities and differences between both. In the first place structural models are different but have their correspondence, as can be seen in fig. 3.

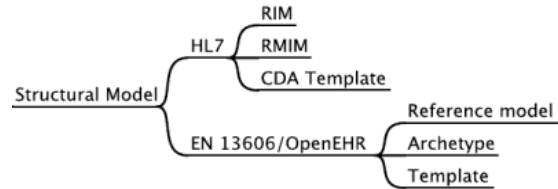


Fig. 3. Structural Model of HL7 and EN13606 [15]

About Reference Model, EN13606 covers the same domain as HL7, but Reference Model of EN13606 provides a structure based on the structure that traditionally has been used in medical documents. It is for this reason, that in the work of implementing a standard in many institutions, has been opted by working with EN13606 terms and subsequently map them to the GL7-RIM domain [15].

F. Medical History Characteristics

A medical history must fulfill a series of basic components: exact, accessible, organized, confidential, secure, legible and complete. And should fulfill the following parameters so it is taken into account as a medical document [17]:

- Integrity: medical history of a user should gather information of scientific, technical and administrative aspects related to health care in phases of encouragement, health promotion, specific prevention, diagnostic, treatment and illness rehabilitation, addressing it as a whole in its biological, psychological and social aspects, and relating it with personal, familiar and community dimensions.

- Sequentiality: register of health services provision should register in the chronological sequence in which the care occurred. From archivist point of view, medical history is an expedient that in a chronological way should accumulate documents relative to the provision of health services given to the user.

- Rationality: it is the application of scientific criteria in the filling and register of health actions given to a user, so that it is evident in a logical, clear and complete way, the procedure that was executed in the health conditions of the patient or diagnostic.

- Availability: it is the possibility of using the medical history at the time it is needed, with the limitations that the law imposes.

-Pertinence: it is the filling of care registers of medical history, simultaneously or immediately after that the provision of the service is given.

G. Interoperability between health institutions

It is the interconnection of different health institutions departments between them and it is and necessity nowadays. Overtime in Latinamerica are more implementations of pictures archives systems (PACS), of radiology information (RIS) and laboratory (LIS), and electronic clinic histories (ECH), connected to administrative systems (HIS) and patient administration (ADT). This interconnection through diverse levels demands the use of informatics standards; for example, DICOM, HL7, etc. Institutions must require, when acquiring an informatics solution, compatibility with different standards, and in this order they should know in what they are about.

Standards are protocols used by software industry to facilitate interoperability and/or integration. They can be found in different communication layers: data transportation, which allows to transport messages with any semantic: XML, XML-HTTP, etc; messaging: HL7; pictures: DICOM; vocabulary, which allows defining specific controlled vocabulary for each domain: laboratory, pathological anatomy, images diagnostic, nursery, procedures, etc.; document marking, to differentiate the distinct types of document that can be exchangeable and its possible content; communications, for example, wiring, TCP/IP, routers, etc. [18].

H. HL7 standards for interoperability

HL7 V2.x: the last version is v2.7 of 2008, but the most used in interdepartmental interhospital messaging are 2.3, 2.4 y 2.5, with a high level of penetration in market by suppliers of software and users (hospitals, providers, etc.). It is weak for regional implementations, with a bigger ambiguity, because requires of negotiation site by site and an implicit data model. As examples of utilization are LIS to HIS, LIS to BILLING, HIS to RIS, ADT broadcast. Among their domains are patient admission, laboratory, radiology, orders, interconsult and shifts.

HL7 V3 – Regional Level Messaging. Latest version is Normative 2010, available exclusively with syntaxes XML.

HL7 CDA R2 – Medical Documents. It is the standard for medical document exchanges instead of messages. The latest version is Normative 2005, CDA R2; CDA R3 is in discussion [19].

IV. MODELING

The system must start from an architecture oriented to sirveces that are directly linked to CDA (Clinical Document Architecture), for this it becomes necessary as first measure an

inventory of services empowered for the consult of medical register of patients, exposing solely proper capacities of the information consolidation and consult process in the context of specific information.

Similarly, it is proposed and proper service inventory for the interaction with XDS repository of documents and headers design for medical documents exchange in conformity with HL7 standard, lastly, it is defined a specific service inventory to the context of identification and access to demographic information of patient PIX.

The consumer layer must provide the service set that allows the visualization of local HIS consult (Hospitable Information System), administrative web client consult, and regulators entities consult.

Business process layer is compound by a series of service inventories such as patient consult, HCE consult, indicators information consult. So it, surgery services, reference counter reference, hospitalization, urgencies and admissions.

Services layer contains user applications, password, admission, alert generations, authorizations, informed consent.

System layer contains XDS, CDA, PIX repositories. Each of the repositories named in the system layer has its own sub layer system for architecture generation. To these layers it is added one more layer called service components, which is in charge of the whole process of authentication, data access, security, tracing, and user permissions.

V. RESULTS

The results that the execution of management of a standardized Platform of Unified Medical Histories from Health Interoperability - Case study Colombian Caribbean Islands system- would provide to the sanity system of Colombian Caribbean islands system in charge of Archipelago San Andrés, Providencia and Santa Catalina Department, and in future, to the country and society in general, would be focused on different fields:

The development of this proposal will allow to every entity that implements it to increase the incursion of new information and communication technologies improving responds timing to the user between different institutions. Helping to achieve an adequate management of electronic medical documents solving in that way one of the current shortcomings of the country at health level.

As an academic project, will allow the diminish of displacement of state entities to consult information about procedures, achieving that the governmental entities and health provider entities can enjoy of a more efficient service and gain access to services with a monitoring that assures quality of the required services.

Governmental entities as future users of this type of information system will perceive a higher saving in process generation as well as in budget of ICT system acquisition for this type of electronic management of document, since the development of this system will avoid expenses of time for the execution of procedures by technology without any contretemps, being operable from any mobile device with access to the platform.

VI. CONCLUSIONS

The investigation behind the platform design will allow knowing the problematic that many times is not taken into account, such as informatics in health. The selection of SOA architecture for transmission and reception of HL7 messaging is technological and strategically valid for health systems at international level, and adjusts to the necessities of management system of Colombian Caribbean islands system.

The comprehension executed with HL7 standard from independency of applications client-provider, will allow a quick development coupled to basic medical history and the diagnostics applied to it. The theme in health has many sections that are of great difficulty to address in only one proposal, nonetheless it is necessary this type of design and implementation proposal from management as a start of a complete investigation that can provide knowledge to this important subject for our country in themes of health, educations and environment.

HL7 standard is starting to grow in Colombia. Still, for being a private entity, different health providers institutions are implementing to their systems gradually, and at the moment, there are few that has adopted it by own initiative.

center information that are found in the server (health provider) developing their own client (user) by any mobile technology (access).

The main product in the development of this proposal will be a platform for management of unified medical history and health technological interoperability in archipelago of San Andres, Providencia and Santa Catalina Department.

The development of this platform will allow effective and transparent integration with general system of medical document consult, as well as will facilitate process of modification of user medical histories, collection, recollection, reference and counter reference.

Users will be benefit from agility in attention and absent of errors caused by transmission of medical information between institutions. Similarly they shall enjoy the portability of their health right, which assures them the attention independently of the place they are located. The conjunction between a hardware infrastructure of low cost, the integration of components of free software, the costs of telephonic services nowadays and a versatile and accessible application by the development of this platform, will allow the government to exercise control over health entities linked to the present project and besides, will count with reliable and fast communication tools when implementing HL7 protocol that will allow to verify collect and recollect data of these entities before FOSYGA.

REFERENCES

- [1] Crisis de la salud en Colombia. Declaración de Emergencia Social Económica. Noviembre de 2009. Sitio: Consultor salud. Carlos Felipe Muñoz Paredes. <http://www.consultorsalud.com/biblioteca/documentos/2009/Crisis%20de%20la%20Salud%20en%20Colombia%20emergencia%20social%202009%20Consultorsalud.pdf>
- [2] Ley 1419 de 2010 Lineamientos para el desarrollo de la telesalud en Colombia. <http://wsp.presidencia.gov.co/Normativa/Leyes/Documents/ley141913122010.pdf>
- [3] Ley 1438 de 2011. Reforma al sistema general de seguridad social en salud y otras disposiciones. <http://guajiros.udea.edu.co/fnsp/cvsp/ley1438.pdf>
- [4] Ley 100 de 1993. Creación del Sistema de Seguridad Social Integral. <http://www.colombia.com/actualidad/images/2008/leyes/ley100.pdf>
- [5] Decreto 1281 de 2002. Normas que regulan los flujos de caja y la utilización oportuna y eficiente de los recursos del sector salud y su utilización en la prestación. http://www.saludcolombia.com/actual/htmlnormas/Dec1281_02.htm
- [6] Resolución 3374 de 2000. Datos básicos que deben reportar los prestadores de servicios de salud y las entidades administradoras de planes de beneficios sobre los servicios de salud prestados. <http://www.fosyga.gov.co/LinkClick.aspx?link=MarcoNormativo%2FE%20CAT%2FResolucion+3374+de+2000.pdf&tabid=310&mid=598>
- [7] Glosario de Términos. FOSYGA. <http://www.fosyga.gov.co/AcercaDelFOSYGA/GlosariodeT%C3%A9rminos/tabid/324/Default.aspx>
- [8] Plan de Beneficios para prestación de servicios de salud. Anexo 20. Protocolo de referencia y contrarreferencia. http://www.contratos.gov.co/archivospuc1/DA/124004000/07-2-77212/DA_PROCESO_07-2-77212_124004000_242552.pdf
- [9] EN 13606 Association. The CEN/ISO standard. <http://www.en13606.org/>
- [10] Utilidad de los Arquetipos ISO 13606 para representar modelos clínicos detallados. Pablo Serrano, David Moner, Tomás Sebastián, José Maldonado, Rafael Navalón, Monserrat Robles, Ángel Gómez. INFOLAC2008-AAIM. <http://revistaesalud.com/index.php/revistaesalud/article/view/308/641>
- [11] EN 13606 Association. CEN/ISO EN 13606 Archetype Model. <http://www.en13606.org/>
- [12] Uso de la norma europea EN13606 en un sistema de historia clínica electrónica federada. José Alberto Maldonado Segura, Monserrat Robles Viejo, Pere Crespo Molina, Carlos Ángulo Fernández, Andrés SanchisEstruch, Alfonso Saura Herranz. <http://www.ibime.upv.es/bie/docs/I+S2005.pdf>
- [13] The HL7 Evolution. Comparing HL7 Version 2 to Version 3, Including a History of Version 2. CorepointHealth. 2010. Disponible en la URL: <http://www.corepointhealth.com/sites/default/files/whitepapers/hl7-v2-v3-evolution.pdf>
- [14] HL7 FAQs. Health Level Seven International. Disponible en la URL: <http://www.hl7.org/about/FAQs/index.cfm>
- [15] Principles of health interoperability HL7 and SNOMED. Tim Benson.
- [16] Chapter 7 The HL7 V3 RIM. Disponible en la URL: http://www.shopcreator.com/mall/Abiescouk/Downloads/chapter_7_the_hl7_v3_rim.pdf.
- [17] P. Marcia ,Q Jhon J., B María L, and A. Lilia E, "Análisis bajo el Estándar HL7 del Proceso de Referencia y Contrarreferencia en el Hospital San Rafael de Fusagasugá," FESALUD – Fundación para la eSalud, ISSN 1698-7969 Vol.6 N° 21, 2010
- [18] L.Grundel, "Introducción a HL7". Meeting HL7 Colombia. Marzo 2010. Pagina Web de consulta http://www.hl7.org.co/hl7_files/ivmeeting/CDAR2.pdf. Fecha de consulta noviembre 2011.
- [19] Interfaceware. "HL7 Resources. HL7 Standard Messages, segments, fields definitions". 2011, Pagiana web de consulta <http://www.interfaceware.com/hl7-standard/hl7-segments.html>, fecha de consulta febrero 2011

Now Social Protection Ministry has a project for the rest of institutions initiate this implementation and it becomes mandatory, since as a strategy and being an informatics solution it can be implemented an interface to access health

Authors Index

Abdoune, L.	108	Jilbab, A.	96
Adamian, Y. E.	72	Juarez, P. G.	48
Al-Dahoud, A.	108	Kalinin, M.	54
Ali, H.	101	Khaled, H.	101
Benba, A.	96	Kim, H.	68
Bustamante, F. P.	119	Konoplev, A.	54
Camacho, J. C.	48	Krivosheev, S. I.	72
Castillo, M. M. M.	48	Kwiatkowski, J.	58
Caviativa, Y. P.	119	Lampe, B. P.	27
Ceraolo, M.	84	Mamoutova, O. V.	105
Chernyshov, K. R.	21	Moskvin, D.	54
Chung, Y.-H.	68	Nawrat, A.	58
Cortes, J. I.	48	Nenashev, O. V.	105
Drozdov, V. N.	92	Pabon, L. D.	38
Ellouze, N.	114	Puig, N. I. P. de L.	48
Fezari, M.	108	Rahali, H.	114
Filippov, A. S.	105	Rodriguez, J. L. D.	38
Flores, J. E.	48	Rosenwasser, E. N.	27
Fouad, H.	76	Saad, E. M.	101
Garcia, A. P.	38	Sayed, S.	101
Gutierrez, J. E. M.	48	Sewaiwar, A.	68
Guzmán, Y. M.	119	Sobel, D.	58
Hajaiej, Z.	114	Tushev, S. A.	92
Hammouch, A.	96	Tutygin, V.	32
Jędrasiak, K.	58	Zegzhda, D.	54
Jharko, E. Ph.	62	Zvyagin, P. N.	45